Downloaded from orbit.dtu.dk on: Apr 25, 2024

DTU Library

Mechanisms of sulfur dioxide and sulfuric acid neutralization in lube oil for marine diesel engines

Lejre, Kasper Hartvig

Publication date:
2019

Document Version
Publisher's PDF, also known as Version of record

Link back to DTU Orbit

Citation (APA):
Lejre, K. H. (2019). *Mechanisms of sulfur dioxide and sulfuric acid neutralization in lube oil for marine diesel engines*. Technical University of Denmark.

General rights
Copyright and moral rights for the publications made accessible in the public portal are retained by the authors and/or other copyright owners and it is a condition of accessing publications that users recognise and abide by the legal requirements associated with these rights.

- Users may download and print one copy of any publication from the public portal for the purpose of private study or research.
- You may not further distribute the material or use it for any profit-making activity or commercial gain
- You may freely distribute the URL identifying the publication in the public portal

If you believe that this document breaches copyright please contact us providing details, and we will remove access to the work immediately and investigate your claim.

DTU Chemical Engineering
Department of Chemical and Biochemical Engineering

Mechanisms of sulfur dioxide and sulfuric acid neutralization in lube oil for marine diesel engines

PhD Thesis

by

Kasper Hartvig Lejre

Technical University of Denmark
Department of Chemical and Biochemical Engineering
CHEC Research Center
May 2019

Preface and acknowledgments

This thesis is the summary of three years of research, from October 2015 to December 2018, and is submitted in partial fulfillment of the requirements for the PhD degree. Besides the research, the requirements for completion of the PhD degree also include: taking courses, teaching, dissemination, and the public defense of this thesis. The work was conducted at the Technical University of Denmark (DTU) at the Department of Chemical and Biochemical Engineering in the research center Combustion and Harmful Emission Control (CHEC).

This thesis was funded by Innovation Fund Denmark as part of the SULCOR project (SULfuric acid CORrosion) which was a collaboration between DTU (Department of Chemical and Biochemical Engineering and Department of Mechanical Engineering) and MAN Energy Solutions. The financial support, under grant 4106-00028B, is gratefully acknowledged.

I would like to express my sincere gratitude to my main supervisor Søren Kiil and co-supervisor Peter Glarborg, for their continuous support and interest of my PhD study, for their patience, motivation, and immense knowledge. I would like to thank my co-supervisor Henrik Christensen for countless conversations and discussions, your guidance and constructive feedback have really helped me a lot. Philip Loldrup Fosbøl, I am thankful for our discussions and your important feedback. Stefan Mayer, thank you for your dedication to my work during the vast number of meetings over the years. You have really challenged me during our meetings and provided quality feedback for the project. Thank you, Dorthe Jacobsen and Svend Eskildsen for letting me borrow your titrator and for all our interesting discussions on lube oils, analysis methods, and safety. I would also like to thank the other PhD students and Postdocs within the SULCOR project. I will therefore like to thank Lars Kjemtrup, Henrik Lund Nielsen, Nikolas Karvounis, Rasmus Cordtz, and Kar Mun Pang for innumerable fruitful discussions and many fun conversations. I have learned a lot from working with you within the fields of engines, computational fluid dynamics, and corrosion. I would also like to thank the remaining core people of the SULCOR project, Anders Vølund, Jesper Schramm, and Jens Honore Walther for valuable inputs and discussions during all our meetings over the years.

I would like to thank the entire technical staff at CHEC and in particular Anders Kjersgaard and Malene Hessellund Dinesen for practical support and always being eager to help when needed.

My gratitude is also directed to Anders Larsen and Jakob Dan Nielsen from Q-Interline for support on how to analyze the lube oil samples by use of FTIR-ATR and to Anders Egede Daugaard, who provided access to the FTIR-ATR located at the Danish Polymer Center, DTU. Thank you, Soheila Ghafarnejad Parto for introducing me to the batch reactor setup, your help is really appreciated.

A tremendous thank you is dedicated to all my colleagues at CHEC for many good and fun moments, both professionally and socially. A special thank you goes to my friends, Anna Leth-Espensen, Magnus Zingler Stummann, Line Riis Christensen, and Steen Riis Christensen. I have really enjoyed your wonderful company since we all started at DTU 8 years ago. To my officemate throughout the PhD, Magnus Zingler Stummann: a special thank you for all the funny moments, for all the eaten “snegle”, for all the hours spent in the gym, and for always being ready to listen to lube oil-related issues. I cannot imagine a better officemate than you.

Finally, I would like to thank my family and Mia for your limitless and irreplaceable support and encouragement. To the love of my life, Mia: thank you for all the adventures, for always being there for me, for making me happy, and for listening on innumerable monologues concerning the PhD. I love you right up to the moon – and back.

Thank you,
Kasper Hartvig Lejre

Abstract

The maritime sector has seen notable changes in recent years, the most important being sailing at reduced speeds to save fuel, which has been possible due to the abundance of large vessels. This, combined with new engine designs and tunings for further fuel savings, has resulted in increased water and acid condensation onto the cylinder liner, promoting a combination of corrosion and wear, significantly reducing the liner lifetime. The condensing sulfuric acid (H_2SO_4) originates from the fuel bound sulfur. To counteract corrosion, the lubrication (lube) oil is formulated with additives ($CaCO_3$-based reverse micelles).

Nowadays, further engine improvements for better fuel efficiencies are desired, however, the effects on corrosive wear are difficult to predict. In addition, switching fuels frequently is being introduced driven by availability, price, and stricter regulations on emissions. To cope with legislation, either sulfur-poor fuel can be combusted or sulfur-rich fuel with subsequent treatment with an exhaust after-treatment technology. These improvements/changes put additional demand on lubricating the engine optimally because defective lubrication has severe consequences. To understand how to optimally lubricate the engines, knowledge on what happens to the sulfur-related species (SO_2 and H_2SO_4) in the lube oil film is required.

The work presented in this thesis is an investigation of the neutralization of SO_2(g) and H_2SO_4(aq) by reaction with $CaCO_3$(s) reverse micelles in a fully formulated lube oil. The reactions are studied individually and by experiments and mathematical modeling.

The first part of the thesis investigates experimentally the reaction between H_2SO_4 and $CaCO_3$ in lube oil in a mixed flow reactor (MFR) setup by varying the Ca/S molar ratio, H_2SO_4(aq) inlet concentration, residence time, and stirrer speed. The analysis methods applied were Fourier Transform Infrared (FTIR) spectroscopy and a titration method to quantify the conversion of $CaCO_3$ and H_2SO_4 at specific conditions. The results revealed that the first step of the reaction was emulsification of the H_2SO_4 into the lube oil followed by reaction between the solubilized H_2SO_4 droplets and $CaCO_3$ reverse micelles. For the residence times investigated, it was observed that the reaction between H_2SO_4 and $CaCO_3$ was significantly reduced when reaching a critically low Ca/S molar ratio. A certain degree of stirring was found to initiate and maintain the reaction. Also, no apparent effect of varying the residence time was observed. Diluting the inlet H_2SO_4

concentration led to a decreased conversion of $CaCO_3$, probably due to the introduction of a large amount of water, leading to poor solubilization of the H_2SO_4 droplets.

The second part of the thesis concerns mathematical modeling of the experimental MFR data for the reaction between H_2SO_4 droplets and $CaCO_3$ reverse micelles. It was difficult to identify conclusively the limiting step of the neutralization reaction, however, a quantitative description of the reaction rate and its temperature-dependency was determined. The validated mathematical model was used to predict conversion of H_2SO_4 in a lube oil for conditions relevant for a full-scale application. The calculations show that H_2SO_4 may interact with the cylinder liner surface regardless of how well-wetted the surface is.

The third and last part of this thesis describes a study of the mechanism underlying the reaction between gaseous SO_2 and $CaCO_3$ reverse micelles in lube oil in a pressurized stirred batch reactor setup. The first step of the mechanism is the absorption of gaseous SO_2 into the lube oil emulsion, followed by reaction with $CaCO_3$ reverse micelles. The reaction shows a dependence on the initial water concentration due to increased SO_2 absorption in the lube oil emulsion. The overall temperature dependence on the reaction was observed to be weak because the absorption of SO_2 decreases at increased temperature. It was also observed that $CaSO_3$ was initially formed, followed by formation of $CaSO_4$ at extended residence times and increased temperature. A mathematical model was derived and kinetic parameters were determined by fitting of the model to experimental data. The batch reactor model was used to predict the $CaCO_3$ conversion in a lube oil emulsion from SO_2 for worst-case conditions relevant for a full-scale application. The simulations revealed that consumption of $CaCO_3$ by SO_2 is insignificant in a two-stroke marine diesel engine application; the H_2SO_4-$CaCO_3$ reaction is much faster than the SO_2-$CaCO_3$ reaction.

The work contributes with insight on how H_2SO_4 is neutralized by $CaCO_3$ reverse micelles in the lube oil film and that SO_2 is not a concern with respect to $CaCO_3$ consumption. The tools developed can be used in models of complete two-stroke marine diesel engines, including estimation of the condensation rate of H_2SO_4 and the corrosion rate of the cylinder liner surface by unreacted H_2SO_4 in the lube oil emulsion, with the aim of determining optimal lubrication strategies.

Dansk Resumé

Den maritime sektor har gennemgået betydelige ændringer i de seneste år, hvoraf en af de vigtigste er at sejle med reducerede hastigheder for at spare brændstof, hvilket har kunnet lade sig gøre grundet overfloden af store containerskibe. Dette, kombineret med nye motordesign og justeringer for at spare yderligere brændstof, har resulteret i stigende kondensering af vand og syre på cylinderforingerne i motorerne, hvilket har fremmet en kombination af korrosion og slid. Dette har nedbragt levetiden af foringerne betydeligt. Den kondenserende svovlsyre (H_2SO_4) stammer fra svovlen som er bundet i brændslet. Derfor, for at modvirke korrosion, formuleres smøreolien med additiver ($CaCO_3$-baserede omvendte miceller).

Nu til dags ønskes endnu flere motorforbedringer for at øge brændselseffektiviteten yderligere, men indvirkningerne af disse, på korrosivt slid, er vanskelige at forudsige. Derudover, drevet af tilgængelighed, pris og strengere udledningsreguleringer, udskiftes det anvendte brændsel ofte i motoren. For at overholde lovgivningen, kan enten svovlfattige eller svovlrige brændsler forbrændes i motoren med efterfølgende behandling af udstødningsgassen. Disse ændringer/forbedringer sætter yderligere krav til optimal smøring af motoren, fordi en ufuldstændig smøring har alvorlige konsekvenser. Derfor, for at forstå hvordan motoren smøres optimalt, kræves der yderligere viden omkring, hvad der sker med de svovlrelaterede arter (SO_2 og H_2SO_4) i smøreoliefilmen.

Denne afhandling er en undersøgelse af neutraliseringen af SO_2(g) og H_2SO_4(aq) ved reaktion med $CaCO_3$(s) omvendte miceller i en fuldt formuleret smøreolie. Reaktionerne blev studeret individuelt ved forsøg og matematisk modellering.

Første del af afhandlingen er en eksperimentel undersøgelse af reaktionen mellem H_2SO_4 og $CaCO_3$ i smøreolie i en velomrørt reaktoropstilling ved at variere Ca/S molforholdet, indgangskoncentrationen af H_2SO_4(aq), opholdstiden samt omrøringshastigheden. De anvendte analysemetoder var Fourier Transform Infrarød (FTIR) spektroskopi og en titreringsmetode til at kvantificere omdannelsen af $CaCO_3$ og H_2SO_4 under specifikke forsøgsbetingelser. Resultaterne viste, at det første trin i reaktionen var emulgering af H_2SO_4 i smøreolien efterfulgt af reaktion mellem de emulgerede H_2SO_4 dråber og $CaCO_3$ omvendte miceller. For de undersøgte opholdstider blev det observeret, at reaktionen mellem H_2SO_4 og $CaCO_3$ var betydeligt reduceret, når et kritisk lavt Ca/S molforhold blev anvendt. Der blev ikke observeret nogen tilsyneladende

virkning af at variere opholdstiden. En vis grad af omrøring viste sig at igangsætte og opretholde reaktionen. Fortynding af indgangskoncentrationen af H_2SO_4 førte til reduceret omdannelse af $CaCO_3$, sandsynligvis på grund af tilsætningen af en stor mængde vand, hvilket resulterede i nedsat emulgering af H_2SO_4 dråberne.

Anden del af afhandlingen omhandler matematisk modellering af de eksperimentelle data fra den velomrørte reaktor for reaktionen mellem H_2SO_4 dråber og $CaCO_3$ omvendte miceller. Det var vanskeligt at bestemme det begrænsende trin i neutraliseringsreaktionen, dog blev den temperaturafhængige reaktionshastighed bestemt kvantitativt. Den validerede matematiske model blev brugt til at forudsige omdannelse af H_2SO_4 i en smøreolie under betingelser, der er relevante for en fuldskalaapplikation. Beregningerne viste, at H_2SO_4 muligvis interagerer med cylinderforingsoverfladen, uafhængigt af hvor godt befugtet overfladen er.

Tredje og sidste del af denne afhandling beskriver studiet af mekanismen, der danner basis for reaktionen mellem gasformig SO_2 og $CaCO_3$ omvendte miceller i smøreolie i en tryksat og omrørt batchreaktoropstilling. Det første trin i mekanismen er absorption af gasformig SO_2 i smøreolieemulsionen, efterfulgt af reaktion med de $CaCO_3$-baserede omvendte miceller. Reaktionen viser en afhængighed af den oprindelige vandkoncentration på grund af forøget SO_2 absorption i smøreolieemulsionen. Det blev observeret, at den overordnede temperaturafhængighed på reaktionen var svag, fordi absorptionen af SO_2 falder ved stigende temperatur. $CaSO_3$ blev dannet i begyndelsen af reaktionen, efterfulgt af dannelse af $CaSO_4$ ved længere opholdstider og stigende temperatur. En matematisk model blev udledt og kinetiske parametre blev bestemt ved at tilpasse modellen til de eksperimentelle data. Batchreaktormodellen blev anvendt til beregning af $CaCO_3$ omdannelse i en smøreolieemulsion fra reaktion med SO_2 under værst tænkelige betingelser, relevante for en fuldskalaapplikation. Simuleringerne viste, at forbruget af $CaCO_3$ fra reaktion med SO_2 er ubetydelig i en totakts dieselmotor og at H_2SO_4-$CaCO_3$ reaktionen er meget hurtigere end SO_2-$CaCO_3$ reaktionen.

Dette arbejde bidrager med indsigt i, hvordan H_2SO_4 neutraliseres af $CaCO_3$ omvendte miceller i smøreoliefilmen og at SO_2 ikke er et problem med hensyn til forbrug af $CaCO_3$. De udviklede værktøjer kan anvendes i modeller, som beskriver en komplet totakts dieselmotor, herunder estimering af kondensationshastigheden af H_2SO_4 og korrosionshastigheden af cylinderforingsoverfladen af det ikke-omsatte H_2SO_4 i smøreolieemulsionen med det formål at bestemme optimale smøringsstrategier.

Conference contribution and publications

Oral conference contribution

Kasper H. Lejre, Peter Glarborg, Henrik Christensen, Stefan Mayer, Søren Kiil, "*Reaction of sulfuric acid in lube oil: Implications for large two-stroke diesel engines*". Presented at The Internal Combustion Engines Fall Conference (ICEF2017), October 15-18, 2017, Seattle, Washington, USA.

Peer-reviewed article published in conference proceedings

Kasper H. Lejre, Peter Glarborg, Henrik Christensen, Stefan Mayer, Søren Kiil, "*Reaction of sulfuric acid in lube oil: Implications for large two-stroke diesel engines*". In *Large Bore Engines; Advanced Combustion*, Proceedings of the ASME 2017 Internal Combustion Engines Fall Conference, October 15-18, 2017, Seattle, Washington, USA, Paper ICEF2017-3580, DOI: 10.1115/ICEF2017-3580.

Peer-reviewed article published in journal

Kasper H. Lejre, Peter Glarborg, Henrik Christensen, Stefan Mayer, Søren Kiil, "*Mixed flow reactor experiments and modeling of sulfuric acid neutralization in lube oil for large two-stroke diesel engines*", Industrial & Engineering Chemistry Research, 2019, 58 (1), 138-155. DOI: 10.1021/acs.iecr.8b05808.

Article in preparation

Kasper H. Lejre, Peter Glarborg, Henrik Christensen, Stefan Mayer, Søren Kiil, "*Experimental investigation and mathematical modeling of the reaction between $SO_2(g)$ and $CaCO_3(s)$-containing micelles in lube oil for large two-stroke marine diesel engines*", To be submitted 2019.

Table of Contents

1 | Introduction

Approximately 90% of the world trade is transported by the international shipping industry[1] and the dominant propulsion technology in the modern ship propulsion market is the large, low-speed two-stroke diesel engine.[2,3]

In the latter part of the 2000s, high oil prices and the global economic recession forced ship operators to dramatically reduce operating costs, especially the fuel oil consumption, which constitutes the main expense of the ship operation.[4] The easiest way of reducing the fuel cost was to reduce the speed of the ships, also known as slow steaming.[5] By operating large container ships at 60-70% of their design speeds, reduction of up to 70% of the daily fuel consumption was achieved.[6] The enablement for the introduction of the slow steaming principle was overcapacity in the shipping market at that time due to a downturn in trade and delivery of newly build ships ordered before the economic crisis.[6] The total economic profit of increasing the slow steaming vessel fleet to maintain the vessel frequency is difficult to exactly assess, as it depends on many factors.[5] Addition of vessel that would otherwise have been idle allowed carriers to reduce the overcapacity because the lower speeds add to the voyage time.[6,7]

Along with the introduction of the slow steaming principle, the ship manufactures further optimized fuel efficiency in the low load range by introducing new engine designs and tunings.[8] The overall effect of slow steaming and engine modifications/improvements led to increased operating cylinder pressures and lower cylinder liner surface temperatures.[8] These changes in operating conditions resulted in increased water and acid condensation onto the cylinder liners and promoted a combination of abnormal corrosion and wear (called cold corrosion) of the cylinder liners and piston rings.[8–13] The condensing acid responsible for the observed cold corrosion is thought to be sulfuric acid (H_2SO_4), which originates from the preferred fuel used, heavy fuel oil (HFO).[14] The HFO is of very low quality and is basically a waste product from the oil refineries, containing a considerable amount of sulfur.[15] Because cold corrosion can develop within hours[16] and result in a high material loss rate (thereby significantly reducing the lifetime of the components),[8,13] it is crucial to mitigate the phenomenon. To hamper corrosion of the cylinder liners and piston rings, cylinder lubricants are fed to the engine, providing an oil film between piston rings and cylinder liners. The cylinder lubricant (lube) oils contain alkaline additives, for the purpose of mitigating the harmful effects from the combustion products, mainly condensing H_2SO_4.[14,17–20] The general, but rather obvious, recommendation is to limit cold corrosion by supplying sufficient alkaline additives to the cylinder liner (the amount of alkalinity is defined by the base number, BN: mg KOH per g oil), see Figure 1.1.

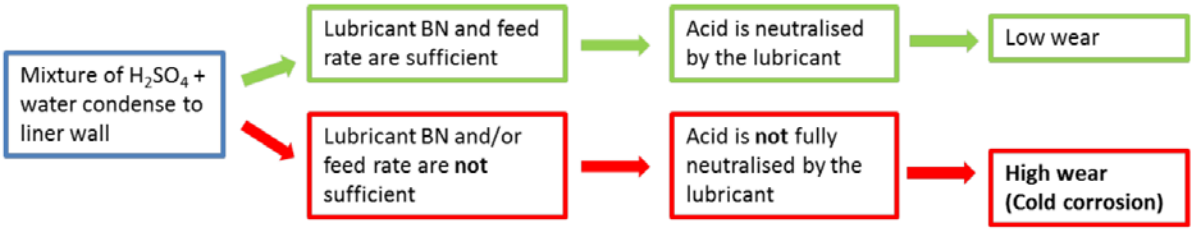

Figure 1.1. General recommendation to handle cold corrosion.[8]

In reality, the way of lubricating the engine optimally is a difficult task. Under-lubricating the cylinder liners lead to cold corrosion, whereas too much lube oil is expensive and may have severe, irreversible consequences, such as scuffing (direct metal to metal contact).[21] Actually, a controllable degree of corrosion (denoted "low wear" in Figure 1.1) is beneficial to maintain a sufficiently rough surface for better supporting an oil film.[19] Adding to the complexity of determining the optimal lubrication strategy is the newly and future actions related to emission legislation taken by the International Maritime Organization (IMO), which has defined regulations regarding overseas emission of sulfur oxides, see Figure 1.2.

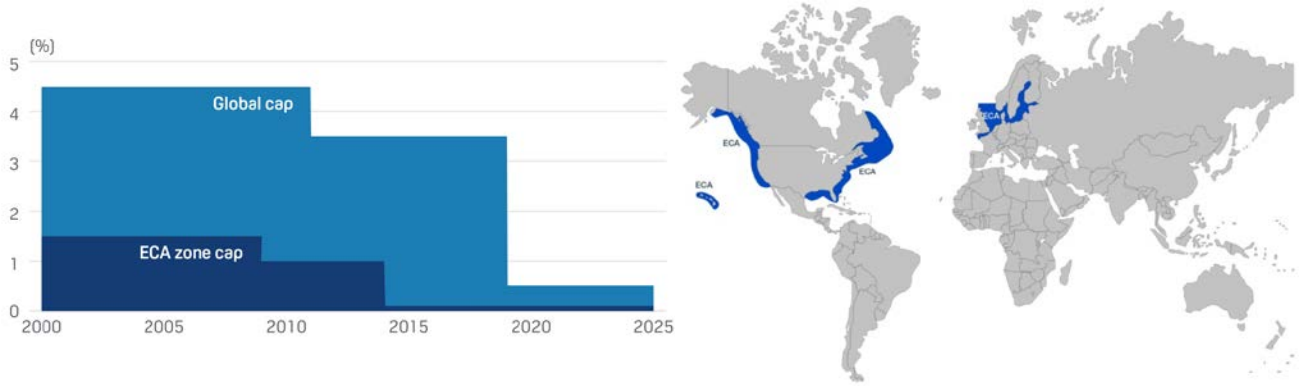

Figure 1.2. The sulfur limits defined in MARPOL Annex VI, regulation 14 (left)[22,23] and the present ECA zones within the blue areas (right).

The sulfur cap defined by IMO depends on whether a ship is operated within or outside a specific Emission Control Area (ECA) depicted in Figure 1.2. When operated within an ECA, a maximum of 0.1 wt.% sulfur is allowed in the burned fuel. A significant reduction in sulfur emission is enforced in 2020 by reducing the global sulfur cap from 3.5 to 0.5 wt.%. However, it is allowed to operate with higher sulfur content in the fuel if using an exhaust cleaning technology capable of reducing the emissions to an equivalent level to that of burning low-sulfur fuel.[16,23] Depending on price and availability, it may therefore be cost-effective to combust high sulfur fuels in the future, and even burning fuels with a sulfur content higher than today's limit of 3.5 wt.%.[16] Based on the global 0.5 wt.% sulfur cap enforced in 2020, MAN Energy Solutions expects that the high sulfur fuels will remain a significant part of the fuels burned after 2020; the price may probably be sufficiently low to support installation and operation of exhaust gas cleaning technologies.[16] Against this background, it may be profitable to change the fuel type with respect to sulfur content frequently. As a consequence, the lube oil dosing has to conform to maintain its performance with respect to low wear rates, outlined in Figure 1.3.

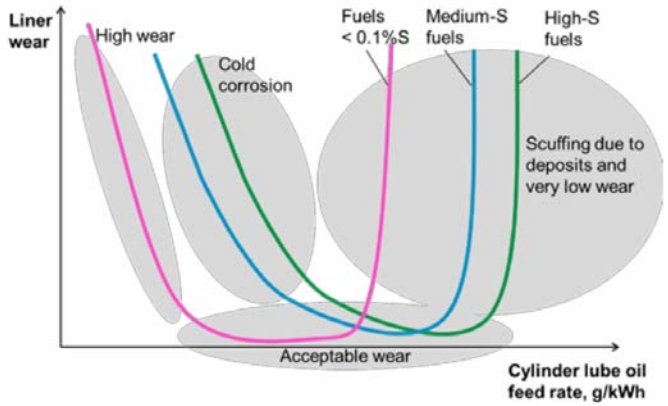

Figure 1.3. Liner wear as a function of cylinder lube oil feed rate for different sulfur-containing fuels. If the engines are not lubricated by an optimal feed rate of lube oil, scuffing or cold corrosion may occur giving high wear rates of the cylinder liners.[16]

Figure 1.3 only considers the interaction between sulfur content in the fuel, the lube oil feed rate, and wear rate. However, differences in operational conditions, ambient conditions, and engine configuration add to the complexity of setting up general recommendations for optimal lubrication dosage. Especially when trying to further optimize the performance of the engines for better fuel efficiencies, it is presently impossible to predict the exact effect on the sulfur chemistry in the hostile cylinder environment and how to best mitigate the harmful effects. What needs further investigation is a detailed physical and chemical understanding of the processes in the combustion chamber that govern the cold corrosion phenomenon, that is the formation of SO_3 and H_2SO_4, the simultaneous heat transfer and phase change of combustion gases in the turbulent boundary layer close to cooled combustion chamber walls, the diffusion of acid into the oil film, and the chemical reactions that takes place within the oil film and on the cylinder surfaces. With improved knowledge in these areas, it will be possible to guide the design process towards engine concepts with even lower fuel consumption without sacrifice to component lifetime and reliability. To gain a deeper understanding of the underlying processes occurring in the large two-stroke marine diesel engine with respect to sulfur corrosion, the research project SULCOR was initiated.

1.1 SULCOR – SULfuric acid CORrosion in large marine diesel engines

The overall objective of the SULCOR project was to identify the mechanisms and rate-limiting steps, as well as the impact of process parameters, on the sulfur-induced corrosion in marine diesel engines. By developing experimentally verified mathematical tools, sulfur corrosion was to be quantified. The hope was that this would allow MAN Energy Solutions to develop efficient tools for mitigating the corrosion problem and improve engine efficiency. The anticipated modeling tools in SULCOR included a multi-zone model to calculate the amount of H_2SO_4 condensing on the cylinder liner, a heat and mass transfer model for the turbulent boundary layer near the wall, a model for the physical/chemical neutralization of H_2SO_4 in the lube oil film, and a corrosive wear model of the cylinder liner wall. The anticipated result of the project was hoped to be a significant improvement of the ability to predict corrosion in large diesel engines for ship propulsion. These improvements will lead to faster development of these engines in the efforts to meet stricter regulations on fuels, fuel consumption, and emissions. The project was a collaboration between research groups at DTU Mechanical Engineering (2 PhD and 2 Postdoc) and DTU Chemical Engineering (2

PhD), together with MAN Energy Solutions. In addition, three international universities were involved in SULCOR, namely University of Southampton, Rostock University, and Lund University.

1.2 Aims of the present work

This PhD project constitutes a part of the larger SULCOR research project, focusing on the chemical/physical interactions taking place within the lube oil film on the cylinder liner, more specifically investigating the sulfur-related reactions with the alkaline additives in a fully formulated lube oil. The specific aims of this PhD project are summarized below:

- Mapping and quantification of acid generation, transport, and neutralization mechanisms *in* a fully formulated lube oil, by:
    - Constructing reactors to investigate the reactions between the sulfur-related components (SO_2 and H_2SO_4) and the alkaline additives in the lube oil and to verify the mathematical models derived.
    - Developing mathematical models to extract reaction kinetics of the acid neutralization reactions and to quantify acid conditions (such as acid concentration) in the lube oil at the oil-cylinder wall interphase as a function of various engine relevant input parameters such as temperature, flow of sulfur components to the oil phase, limestone content in the lube oil, and lube oil residence time.

1.3 Scientific hypotheses

Now follows the scientific hypotheses which were established based on an extensive literature study and carrying out preliminary experiments of the reaction between H_2SO_4 and lube oil.

- The neutralization reaction between H_2SO_4 and the alkaline additives (present as micelles) in lube oil is limited by a single rate-limiting step; micelle diffusion, micelle adsorption, chemical reaction, micelle desorption, or macromixing.
- The H_2SO_4 droplets get into the bulk of the lube oil film, eventually reaching the cylinder liner surface, by either:
    - Diffusion, or
    - Mixing by the piston rings
- The specific engine conditions will have a significant impact on the conversion rate of the acidic sulfur components.
- Different experimental setups can be used to individually investigate the sub-processes happening in a lube oil film.

- The SO_2 reacts with the alkaline additives in the lube oil in an engine due to the high partial pressure of SO_2 prevailing in the combustion chamber.

- Different analysis equipment can be used to accurately measure the BN and determine the reaction products in the lube oil.

- Modeling results can be used to estimate the acid concentration on the cylinder liner surface, which can be used in a model concerning the corrosive wear of the surface material.

1.4 Outline of this thesis

Each of the following chapters can be read separately. The experimental chapters (Chapters 3, 4, and 5) are manuscripts that are either published or prepared for submission and they are therefore introduced by a short literature section, resulting in some inevitable overlap. The content of each chapter is summarized below:

- **Chapter 2** is a literature review on the general concepts of a two-stroke marine diesel engine, the acid's way from fuel sulfur to condensing H_2SO_4 that corrodes the cylinder liners, the role of SO_2 on corrosive wear, and how corrosion is mitigated.

- **Chapter 3** consists of a published peer-reviewed conference article with the title "*Reaction of sulfuric acid in lube oil: Implications for large two-stroke diesel engines*", where the neutralization of H_2SO_4 in a fully formulated lube oil was investigated experimentally by use of a mixed flow reactor.

- **Chapter 4** is based on a published article with the title "*Mixed flow reactor experiments and modeling of sulfuric acid neutralization in lube oil for large two-stroke diesel engines*". The experimental work of this chapter expands the work and conclusions presented in Chapter 3. A mathematical model was also derived to extract kinetics for the neutralization mechanism and used to predict H_2SO_4 conversions at conditions relevant for a two-stroke marine diesel engine.

- **Chapter 5** consists of an article in preparation for submission with the title "*Experimental investigation and mathematical modeling of the reaction between SO_2(g) and $CaCO_3$(s)-containing micelles in lube oil for large two-stroke marine diesel engines*", where the reaction between SO_2 and the alkaline additives contained in the lube oil was investigated in a batch reactor setup at elevated pressures and temperatures. A mathematical model was derived and used to extract kinetics of the reaction. The model was finally used to determine the significance of SO_2 consuming alkaline additives at conditions relevant for a two-stroke marine diesel engine.

- **Chapter 6** revisits the scientific hypotheses in order to clarify whether each of the hypotheses was true or false.

- **Chapter 7** presents conclusions and suggestions for future work.

- **Appendix A** describes shortly preliminary lube oil investigations to determine the kind of alkaline additives formulated in the lube oil used for the experimental work of this thesis. Analysis methods include Fourier Transform Infrared Spectroscopy (FTIR), titration, gas analysis, Energy Dispersive X-Ray Fluorescence (ED-XRF), and Thermogravimetric Analysis (TGA).

- **Appendix B** is a short description of some preliminary computational fluid dynamics (CFD) simulation results that were carried out during this PhD.

- **Appendix C and D** contains supporting information for Chapter 4.

- **Appendix E** contains supporting information for Chapter 5.

References

(1) MAN Energy Solutions. Exhaust gas emission control today and tomorrow http://marine.man.eu/docs/librariesprovider6/technical-papers/exhaust-gas-emission-control-today-and-tomorrow.pdf?sfvrsn=22 (accessed Dec 3, 2018).

(2) Hemmingsen, C. S.; Ingvorsen, K. M.; Mayer, S.; Walther, J. H. LES And URANS Simulations of the Swirling Flow in a Dynamic Model of a Uniflow-Scavenged Cylinder. *Int. J. Heat Fluid Flow* **2016**, *62*, 213–223.

(3) Hengeveld, J.; Schenk, C.; Aabo, K. The Role of Temperature and Pressure in the Wear Processes in Low Speed Diesel Engines. **2000**.

(4) Bejger, A.; Drzewieniecki, J. Analysis of Tribological Processes Occuring in Precision Pairs Based on Example of Fuel Injection Pumps of Marine Diesel Engines. **2015**, *41* (113), 9–16.

(5) Wiesmann, A. Slow Steaming – a Viable Long-Term Option? *Wärtsilä Tech. J.* **2010**, No. 2, 49–55.

(6) Mander, S. Slow Steaming and a New Dawn for Wind Propulsion: A Multi-Level Analysis of Two Low Carbon Shipping Transitions. *Mar. Policy* **2017**, *75*, 210–216.

(7) Harrold, P. Lubricating Marine Crosshead Engines Operating at Reduced Load. *J. Japan Inst. Mar. Eng.* **2014**, *49* (1), 88–95.

(8) CIMAC Working Group 8 “Marine Lubricants.” CIMAC Guideline Cold Corrosion in Marine Two Stroke Engines. 2017.

(9) MAN Diesel & Turbo. Service Letter SL2014-587/JAP. 2014.

(10) García, L.; Gehle, S.; Schakel, J. Impact of Low Load Operation in Modern Low Speed 2-Stroke Diesel Engines on Cylinder Liner Wear Caused by Increased Acid Condensation. *J. JIME* **2014**, *49* (1), 100–106.

(11) Cordtz, R. L.; Schramm, J.; Rabe, R. Investigating SO_3 Formation from the Combustion of Heavy Fuel Oil in a Four-Stroke Medium Speed Test Engine. *Energy Fuels* **2013**, *27* (10), 6279–6286.

(12) Adamkiewicz, A.; Drzewieniecki, J. Operational Evaluation of Piston Ring Wear in Large Marine Diesel Engines. *J. Polish CIMAC* **2012**.

(13) Cordtz, R.; Mayer, S.; Eskildsen, S. S.; Schramm, J. Modeling the Condensation of Sulfuric Acid and Water on the Cylinder Liner of a Large Two-Stroke Marine Diesel Engine. *J. Mar. Sci. Technol.* **2017**, 1–10.

(14) Amblard, C. New Chemistry to Protect against Cold Corrosion in Marine Cylinder Lubricants. *J. Japan Inst. Mar. Eng.* **2015**, *50* (6), 54–62.

(15) Cordtz, R. The Influence of Fuel Sulfur on the Operation of Large Two-Stroke Marine Diesel

Engines. Ph.D. Dissertation, Technical University of Denmark, Kgs. Lyngby, 2015.

(16) Jacobsen, D. M. S.; Pedersen, J. M.; Svensson, J.; Mayer, S. Cylinder Lube Oil Experiences and New Development for the MAN B&W Two-Stroke Engines. In *28th CIMAC World Congress*; Helsinki, 2016.

(17) Golothan, D. W. Review of the Causes of Cylinder Wear in Marine Diesel Engines. *Inst. Mar. Eng. Trans.* **1978**, *90*, 137–163.

(18) Bovington, C. H. Friction, Wear and the Role of Additives in Controlling Them. In *Chemistry and Technology of Lubricants*; Mortier, R. M., Fox, M. F., Orszulik, S. T., Eds.; Springer Netherlands: Dordrecht, 2010; pp 77–105.

(19) Atkinson, D. Onboard Condition Monitoring of Cold Corrosion in Two-Stroke Marine Diesel Engines. *11th Int. Conf. Cond. Monit. Mach. Fail. Prev. Technol. C. 2014 / MFPT 2014* **2014**, *5* (2), 17–22.

(20) Marković, I.; Ottewill, R. H.; Cebula, D. J.; Field, I.; Marsh, J. F. Small Angle Neutron Scattering Studies on Non-Aqueous Dispersions of Calcium Carbonate - Part I. The Guinier Approach. *Colloid Polym. Sci.* **1984**, *262* (8), 648–656.

(21) Christensen, O. Cylinder Lubrication of Two-Stroke Crosshead Marine Diesel Engines. *Wärtsilä Tech. J.* **2010**, 39–48.

(22) S&P Global Platts. *The IMO'S 2020 Global Sulfur Cap: What a 2020 Sulfur-Constrained World Means for Shipping Lines, Refineries and Bunker Suppliers*; 2016.

(23) International Maritime Organization (IMO). Sulphur oxides (SOx) and Particulate Matter (PM) – Regulation 14 http://www.imo.org/en/OurWork/Environment/PollutionPrevention/AirPollution/Pages/Sulphur-oxides-(SOx)-%E2%80%93-Regulation-14.aspx (accessed Oct 22, 2018).

2 | Background

This chapter serves the purpose of introducing the reader to the two-stroke engine principle and the hostile environment prevailing in a cylinder liner with the focus on the sulfur chemistry from burning sulfur-containing fuels. This includes the formation of the corrosive acid species in the gas phase, condensation, neutralization mechanisms, wear mechanisms, and how to mitigate corrosive wear by use of lube oil.

2.1 The two-stroke engine principle

A central part of the reciprocating engine is the cylinder liner that forms the cylindrical inner part of the engine block in which the piston travels. The two-stroke principle is characterized by taking two piston strokes to complete each combustion cycle (converting the energy in the fuel to work). This means that the piston moves one time up and one time down the cylinder liner for each cycle and therefore the crankshaft must revolve once. The two-stroke cycle is illustrated in Figure 2.1 and consists of four major events: 1) compression, 2) injection, 3) combustion, and 4) scavenging.

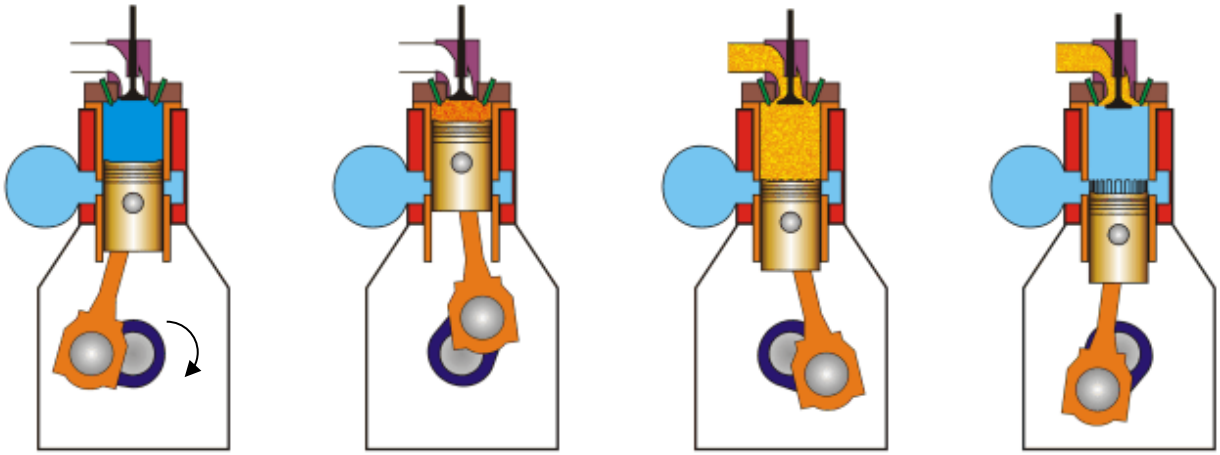

Figure 2.1. The two-stroke cycle illustrated by four still images: 1) compression, 2) fuel injection, 3) combustion, and 4) scavenging.[1]

The four major events occurring during a cycle are briefly described in the following:[1]

1) **Compression:** As the piston is moved upwards, the volume of the combustion chamber is decreased and the pressure and temperature increases. This happens after the closing of the exhaust valve and scavenging ports, which means that the combustion chamber is filled mainly with fresh air, but also with some residual combustion gas from the previous combustion cycle.

2) **Fuel injection:** Just before the piston reaches the top of the cylinder (known as top dead center, TDC), fuel injection starts. The fuel breaks into droplets which evaporate and mixes with the air followed by self-ignition and combustion of the fuel.

3) **Combustion:** Due to the occurring combustion, high pressure and temperature are evolved in the combustion chamber which forces the piston downwards (expansion stroke). The force of the downward movement of the piston is transferred into kinetic energy by rotation of the crankshaft.

4) **Scavenging:** Before reaching the bottom of the cylinder (known as bottom dead center, BDC), the exhaust valves open and the combustion gas begins to leave the cylinder. Shortly after, the piston uncovers the scavenge ports from which fresh, pressurized air enters the cylinder environment. The exhaust valves are still open and the fresh intake air therefore pushes the remaining combustion gas out of the combustion chamber. This is called ‘scavenging’. The piston then reaches BDC and begins to approach TDC once again. During the upward stroke, the scavenge ports are covered by the piston, closing off for the intake air and shortly after the exhaust valves also closes. The combustion chamber now mostly consists of fresh intake air and the compression stroke begins.

The two-stroke cycle illustrated in Figure 2.1 can also be presented as a function of the crank angle degree (CAD) in a timing diagram, see Figure 2.2. The combustion cycle consists of two strokes (up and down) and thereby one complete revolution of the crankshaft (360 degrees), i.e., TDC is located at 0 CAD and BDC is located at 180 CAD.

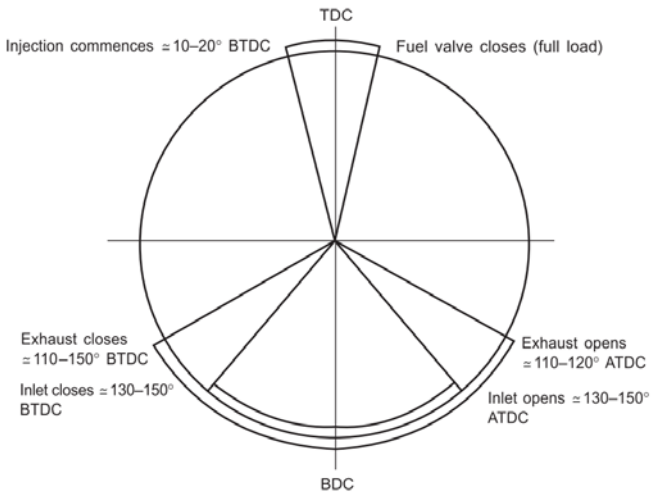

Figure 2.2. The two-stroke cycle as a function of the crank angle degree (CAD). The placement of the different events in the cycle is described relative to the top dead center position: after top dead center (ATDC) or before top dead center (BTDC).[2]

Figure 2.2 shows that the fuel is injected around 10-20 CAD BTDC followed by combustion and expansion of the combustion gas. Around 110-120 CAD ATDC, the combustion gas is exhausted and the scavenge ports open at around 130-150 CAD ATDC and close at around 130-150 CAD BTDC. Shortly after, at 110-150 CAD BTDC, the exhaust valves are closed and the compression stroke proceeds. The period from injection of the fuel to the exhaust valves open is the available timeframe for the acidic sulfur species to be formed and reach the lube oil film. After the opening of the exhaust valves, the combustion gas is ventilated and this removes the sulfur species formed from the gas phase. The acidic species are then present in the lube oil film as a minimum for the remaining part of the cycle, where they can react with the alkaline additives in the lube oil film or with the cylinder liner wall.

2.2 Sulfur chemistry in the gas phase

The main sulfur products from the combustion of sulfur-containing fuels are SO_2, SO_3, and H_2SO_4 according to the overall reactions shown below:[3]

$$\text{Fuel-S}_{(s)} + O_{2(g)} \rightarrow SO_{2(g)} \tag{2.1}$$

$$SO_{2(g)} + 1/2\, O_{2(g)} \rightarrow SO_{3(g)} \tag{2.2}$$

$$SO_{3(g)} + H_2O_{(g)} \rightarrow H_2SO_{4(g)} \tag{2.3}$$

$$H_2SO_{4(g)} \rightarrow H_2SO_{4(aq/l)} \tag{2.4}$$

The first step is oxidation of the sulfur in the fuel according to Eq. (2.1). For excess air combustion, as is valid for an engine application, the reaction is fast and the fuel sulfur is predominantly oxidized to SO_2 because local temperatures reach more than 2500 K.[3–6] A fraction of the SO_2 is then oxidized to SO_3 primarily in the temperature range from 1300 K to 2000 K during the expansion stroke,[5,7] up to 10% depending on species concentrations (SO_2, O_2, SO_3), temperature, and pressure (which are determined by the specific operating conditions of the engine such as load, sulfur content in fuel, and ambient conditions).[3,4,7] The SO_x reaction mechanism at combustion conditions has been investigated comprehensively over the years[6] and a detailed reaction mechanism has been proposed.[8] Formation of gaseous H_2SO_4 from Eq. (2.3) is favored when the temperature decreases further.[4,7] This happens very close to the cylinder wall, where a high temperature difference is present between the cylinder temperature and the cylinder liner temperature.[5] It is also in this narrow segment that H_2SO_4 condenses either as concentrated acid or diluted acid in water.[7]

Because it is impossible to track the formation rate of SO_x and H_2SO_4 practically during an expansion stroke, due to for instance the moving piston, the short residence time, etc., various models have been developed to describe this.[5,7,9–11] However, SO_2 to SO_3 conversion degrees have been measured experimentally in the exhaust.[4,5] Investigation of formation of gaseous SO_x and H_2SO_4 in the combustion chamber under large, two-stroke marine diesel engine conditions is scanty in the literature. Van Helden et al.[9] modeled corrosive wear due to H_2SO_4 on the liners, however, they assumed that all fuel sulfur was initially present as SO_2 and that 5% of the SO_2 was immediately converted to SO_3, i.e., no realistic evolution of the sulfur species was considered during the expansion stroke. Further, the developed model completely neglects condensation of H_2SO_4. The first numerical model considering the realistic formation of SO_x and H_2SO_4 during cylinder

expansion under large two-stroke marine diesel engine conditions was developed by Cordtz et al.[6,7,12] They derived a 0D multizone model which was able to predict realistic SO_2 to SO_3 conversion degrees. However, detailed information about temperature and combustion product distributions was absent. To provide a more detailed insight into the in-cylinder events happening during the expansion stroke, Pang et al. recently performed 3D Computational Fluid Dynamics (CFD) simulations.[5] They developed a skeletal hydrocarbon/sulfur reaction mechanism, reducing the SO_x mechanism from 18 species and 98 reactions[8] down to 4 species and 5 reactions. Kinetics of the H_2SO_4 formation reaction, Eq. (2.3), was taken from Reiner and Arnold.[13] The simulations were based on the conditions and dimensions of the MAN Energy Solutions 4T50ME-X research engine. The simulated SO_2 to SO_3 conversions under low load conditions were compared with measurements from engine tests and acceptable agreement was found. The CFD model was able to predict the spatial and temporal evolution of gaseous SO_x and H_2SO_4 in the combustion chamber in the range between 0 to 90 CAD ATDC. To better compare the effect of changing operating conditions, the averaged concentrations were calculated as a function of the CAD ATDC. An example is shown in Figure 2.3, where the effect of varying the sulfur content in the fuel was simulated.

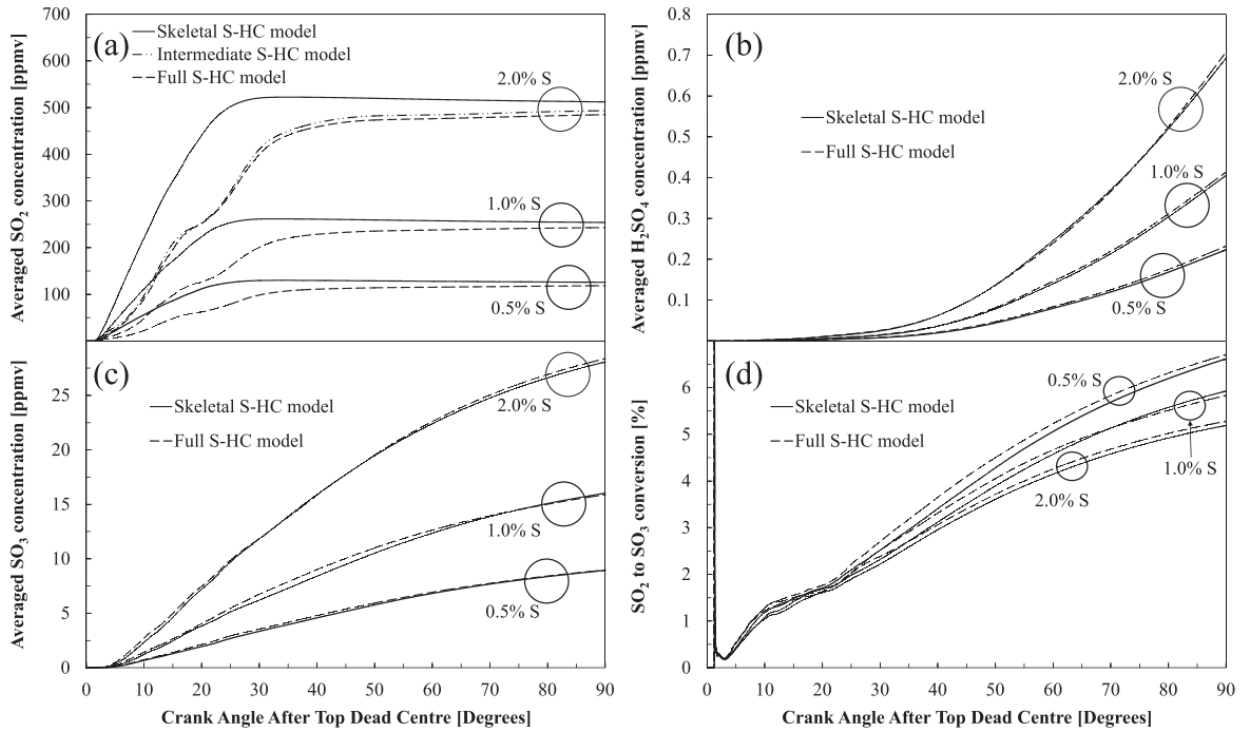

Figure 2.3. Temporal evolution of the (a) averaged SO_2 concentration, (b) averaged H_2SO_4 concentration, (c) averaged SO_3 concentration, and (d) SO_2 to SO_3 conversion for fuel sulfur contents of 0.5 wt.%, 1.0 wt.%, and 2.0 wt.%. The start of injection is at 1.2 CAD ATDC and end of injection is at 23 CAD ATDC for the specific simulations. Also, no water was initially present in the gas phase and the simulations were based on high load conditions.[5]

Figure 2.3 also shows the difference between the full sulfur-hydrocarbon (S-HC) model and the skeletal model. As expected, the averaged concentrations of SO_x and H_2SO_4 increase when the sulfur content in the fuel is increased. The SO_2 to SO_3 conversion degree decreases, when more sulfur is present in the fuel. The reason is that more radicals are present relative to the sulfur amount when decreasing the sulfur content in the fuel. Figure 2.3(a) reveals that the formation of SO_2 happens rapidly and is complete at 25 CAD ATDC for the skeletal S-HC model and around 35 CAD ATDC for the full S-HC model. Formation of SO_3 begins shortly after the SO_2 formation, and later (around 20 CAD ATDC), H_2SO_4 begins to form in the gas phase.

This is due to the gradually decreasing temperature in the combustion chamber due to cylinder expansion, gradually favoring formation of SO_3 and H_2SO_4. Therefore, it is expected that formation of gaseous H_2SO_4 will continue after reaching 90 CAD ATDC and eventually terminate when the exhaust valves open. Pang et al. further observe that H_2SO_4 is formed very close to the cylinder liner wall where the temperature is low relative to the bulk gas temperature and H_2SO_4 is mainly formed when the local temperature is less than 600 K. The distance from the wall, where H_2SO_4 begins to form, increases at increasing CAD ATCD due to the cylinder expansion (lower bulk gas temperature). This behavior is depicted in Figure 2.4, where the local H_2SO_4 concentration against the distance from the cylinder wall for different CAD ATDC is presented. The local computational cells are grouped, based on the local gas temperature.

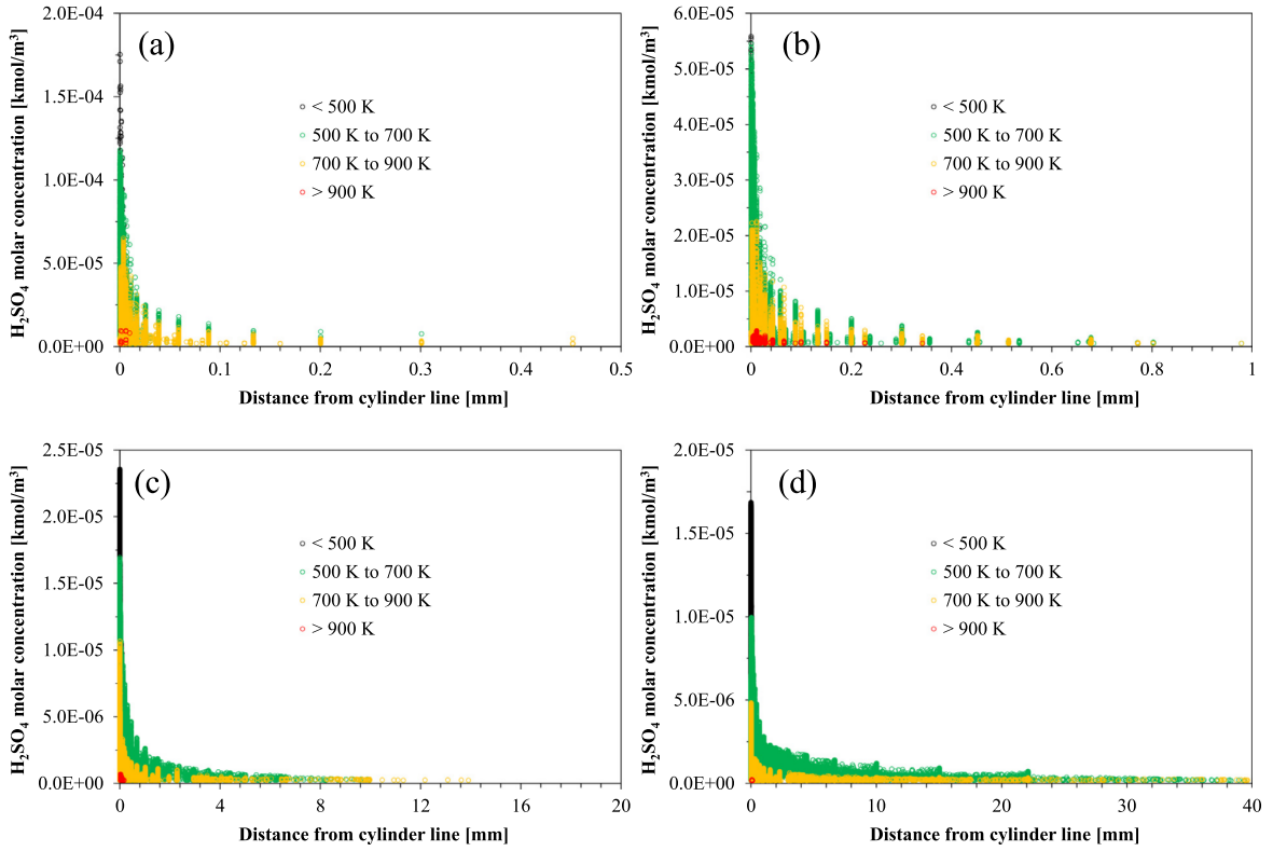

Figure 2.4. Local H_2SO_4 concentration against the distance from the cylinder liner wall at (a) 15, (b) 30, (c) 45, and (d) 60 CAD ATDC. The computational cells are grouped, based on the local gas temperature. The cylinder liner wall is fixed at 323 K for the simulations.[5]

Generally, Figure 2.4 shows that the H_2SO_4 concentration is highest near the cylinder wall where the temperature is low. At 15 CAD ATDC, Figure 2.4(a), H_2SO_4 is mainly found within 0.1 mm from the cylinder liner wall. During cylinder expansion, the distance, wherein H_2SO_4 is formed, increases. Further, Pang et al.[5] calculated dew point temperatures, indicating that H_2SO_4 condensation may already start at around 6 CAD ATDC, i.e., in the very top of the cylinder liner. The study by Pang et al. proves that H_2SO_4 is present very close to the cylinder liner wall during the expansion stroke and dew point calculations supported that H_2SO_4 may condense already in the very top of the cylinder. In practice, this is also the region, where the most corrosive wear is found.[14]

2.3 Models describing condensation of H_2SO_4 onto the lube oil film

Gaseous H_2SO_4 may condense on the cylinder liner wall if the local temperature is lower than the H_2SO_4 dew point temperature.[6] The dew point temperature of H_2SO_4 can be determined from a simple empirical formula that is a function of the partial pressure of gaseous water and H_2SO_4.[15] The formula predicts a high dependence on the H_2SO_4 concentration in the gas phase. Taking into account specific engine conditions, Hengeveld et al.[16] predicted H_2SO_4 dew point temperatures as high as 553 K when combusting 3.5 wt.% sulfur fuel and having a pressure of 180 bar in the cylinder. For typical practical engine operating conditions and burning sulfur-rich fuels, the temperature of the cylinder liner is typically below the theoretically determined H_2SO_4 dew point temperatures, thereby promoting the likelihood of H_2SO_4 condensation throughout the whole vertical direction of the cylinder liner.[17] The concentration of the condensing H_2SO_4 (diluted in water) depends on how far the cylinder liner temperature is from the dew point temperature of pure water. If below, highly diluted H_2SO_4 may condense.[6] However, such correlations are based on fully equilibrated systems, which may be far from accurate in an engine application where conditions are extremely dynamic. Therefore, to predict realistic condensation rates of H_2SO_4 onto cylinder liners, it is important to include the effect of e.g. mixing, residence time, local $SO_3/H_2O/H_2SO_4$ concentrations, and local temperature.

The first study quantifying condensation of H_2SO_4 in a large two-stroke marine diesel engine application was performed by Cordtz et al.[12] This work expanded on their earlier developed 0D multizone model,[6,7] by the implementation of a condensation model. The condensation model was based on prediction of dew point temperatures by a two-phase vapor-liquid equilibrium (VLE) model combined with a coupled mass and heat transfer model assuming a homogenous gas phase in the cylinder. The model applies a calibrated mixing factor to adapt the effect of mixing between the fresh air and combustion products on the condensation. Further, the model involves a realistic cylinder liner temperature profile under low load operation. Simulations quantify total H_2SO_4 condensation profiles along the vertical direction of the cylinder liner at EVO (Exhaust Valve Opening). The simulations revealed that a few milligrams of H_2SO_4 are condensing during one expansion stroke until reaching EVO, e.g., 2 mg H_2SO_4 condenses at 4 wt.% sulfur in the fuel. The model predicts that condensation of H_2SO_4 increases for increasing sulfur content in the fuel and for increasing mixing between the combustion products and intake air. Most of the H_2SO_4 and water condense in the upper segment of the cylinder liner. While simulated water condensation revealed high dependence on cylinder liner temperature and humidity of the intake air, the effect was negligible on the H_2SO_4 condensation. This means that highly diluted aqueous H_2SO_4 may condense in the upper part of the cylinder liner for a liner temperature profile in the lower range and for humidified intake air.

The lack of information regarding the spatial distribution of the condensation of H_2SO_4 and water and taking into account a realistic flow pattern with a heterogeneous gas phase, substantiated the work of Karvounis et al.[18] Their work originated and expanded the 3D CFD work performed by Pang et al.[5] (described shortly in the section above) by including the condensation process. Their condensation model was validated against experimental data concerning condensation of H_2SO_4 and water in a laminar pipe. Their CFD model offers assessment of the spatial and temporal evolution of H_2SO_4 and water condensation at the cylinder liners during the expansion stroke. An example of such an evolution is illustrated in Figure 2.5, where the spatial mass fractions of liquid H_2SO_4 and water in the unwrapped cylinder liner are shown at different CAD ATDC for a high load baseline case. Figure 2.5 reveals that both H_2SO_4 and water condense primarily around TDC

and that condensation of H_2SO_4 starts early in the combustion cycle, already around 15 CAD ATDC (Figure 2.5(b)), which is in agreement with the study by Cordtz et al.[12] In addition, the figure illustrates that the distribution of condensed H_2SO_4 and water varies quite a lot along the vertical direction of the cylinder liner wall, but also along the horizontal direction due to the complex behavior prevailing inside the combustion chamber.

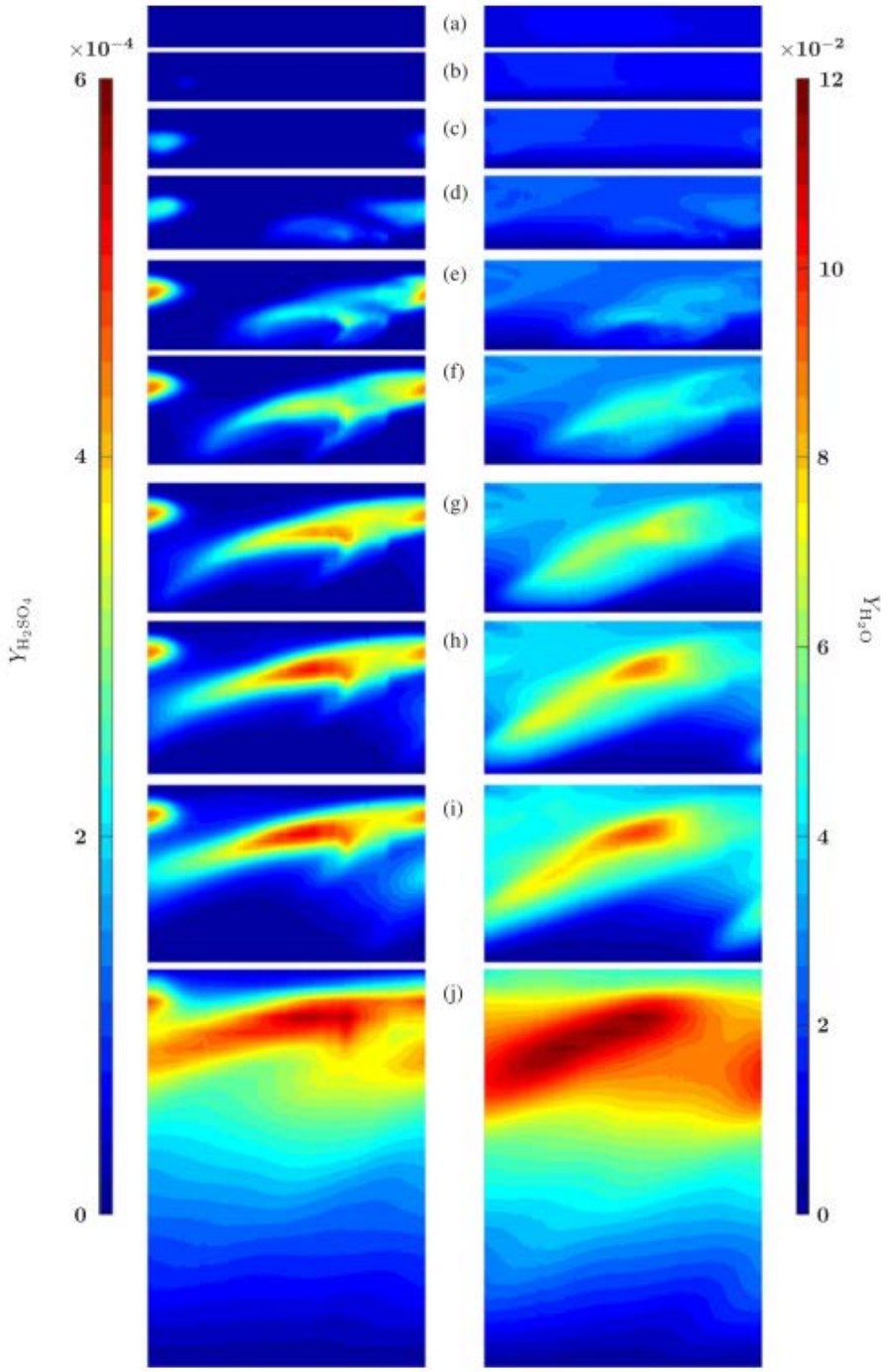

Figure 2.5. Mass fractions of liquid H_2SO_4 (left column) and water (right column) in the unwrapped cylinder liner lube oil film at (a) 10, (b) 15, (c) 20, (d) 25, (e) 30, (f) 35, (g) 40, (h) 45, (i) 50, and (j) 90 CAD ATDC. The simulations are carried out at specific baseline conditions: liner temperature = 323 K, sulfur in fuel = 2 wt.%, initial water content in gas phase = 0.5 wt.%, initial pressure = 152 bar, initial gas temperature = 924 K, engine speed = 123 rpm, and injected fuel mass = 44.6 g.[18]

Karvounis et al. also performed a parametric study, to investigate the effect of different operating conditions on the total condensed mass of H_2SO_4 and water at 90 CAD ATDC. This analysis yielded that increasing the sulfur content in the fuel, increased the total condensed mass of H_2SO_4, whereas the total condensed mass of water was unaffected. Increasing the humidity of the scavenge air, significantly increased condensation of water, whereas the effect on H_2SO_4 was not as pronounced. Increasing the cylinder liner temperature from 323 K to 523 K, resulted in a slight decrease in total condensed H_2SO_4, however, almost no water was condensing at 523 K. This is due to the wall temperature is far above the dew point temperature of water and just below the dew point temperature of H_2SO_4. The above observations are in general agreement with the work by Cordtz et al.[12] Increasing the lube oil film thickness decreased both the H_2SO_4 and water condensation with a higher dependence on condensation of water. For a low load case, the total condensed amount of H_2SO_4 and water decreased (29% and 15%, respectively, compared to the high load case). However, for the low load case, the injected fuel amount was reduced by around 50% which also halves the total amount of sulfur species present in the gas phase. The percentage of initial sulfur from the fuel ending up as condensed H_2SO_4 is therefore increased when decreasing the load. This is due to a lower piston velocity at low load which gives more time for condensation to happen. Lastly, the effect of initial pressure revealed a counter-intuitive behavior, where condensation of H_2SO_4 and water decreased at increasing pressure. However, this was attributed to the change in resulting flame size and flow in the cylinder.

The above section highlighted that condensation of H_2SO_4 and H_2O onto the lube oil film in an engine application is a complex phenomenon which depends on the dimensions and operating conditions of the specific engine such as cylinder liner temperature, cylinder pressure, local $H_2O/SO_3/H_2SO_4$ concentrations, and the time available under favorable condensation conditions. To hamper contact between H_2SO_4 and the cylinder liner material, the liner wall is lubricated with cylinder lube oil.

2.4 Lube oil formulation

The specific lube oil formulation should be able to uphold sufficient performance even though it is present in a very hostile environment, as outlined above. The main purposes of the formation of a lube oil film at the cylinder liner are the following:[2,19]

- Prevention of metal-metal contact between the cylinder liner and piston rings by spreading uniformly over the cylinder liner surface and forming a stable lube oil film.
- Prevent combustion gas from escaping to maintain the predefined internal pressure by providing a gas seal between the piston rings and cylinder liner.
- Neutralize the condensing H_2SO_4 to limit corrosion.
- Clean the cylinder liner and piston rings by the accumulation of combustion and neutralization products.

Fully formulated lube oils are therefore a complex formulation containing a lot of different components. The cylinder lube oils are based on a base oil where a specific additive package has been incorporated. For slow speed engines, paraffinic base oil is used because it has a good oxidation resistance, good thermal stability, low volatility, good demulsibility (prone to water contamination), and a high viscosity index (low change in viscosity with temperature).[20] The choice of the correct additive package is crucial to achieving a high performing lube oil which sufficiently fulfills the above-mentioned purposes. The additive package consists

of various components, each of them having specific properties and functions. The main types with the corresponding function are outlined below with a detailed focus on the detergents.[21,22]

2.4.1 Detergents

The function of the detergents is two-fold: (1) to suspend unwanted products which would otherwise deposit in the engine (called neutral detergents or soaps) and (2) supply the oil with alkalinity (called alkaline or overbased detergents) which can neutralize the condensing acids, mainly H_2SO_4, to prevent corrosion. The overbased detergents are simply neutral detergent complexes which surround and suspend alkaline particles in the oil, leading to large excess of alkalinity or base of the complex (thereof the term "overbased").[21,23] The structure of overbased detergents in lube oils are in the form of reverse micelles,[24–27] illustrated in Figure 2.6. Here, the neutral detergents consist of a hydrophilic head which is attached to a hydrophobic hydrocarbon tail (e.g. an alkyl). Typical components of the head group are sulfonates, phenates, and carboxylates with typically calcium as the counterion.[21,24,28] Based on molecular dynamics simulations of an overbased $CaCO_3$/calcium sulfonate reverse micelle, Tobias and Klein found that it is roughly spherical with an average diameter of the $CaCO_3$ core of 2.3 nm and a surfactant thickness of 0.9 nm, giving a total diameter of 4.1 nm.[24] Hudson et al.[29] reported core diameters of 1-10 nm and surfactant thicknesses of 1-5 nm, which gives total diameters of 3-20 nm. The detergents incorporating $CaCO_3$ are the most widely used[21] and the concentration of $CaCO_3$ in lube oil is also known as the base number, BN. The BN is defined as "the quantity of acid, expressed in terms of the equivalent number of milligrams of KOH required to neutralize all alkaline constituents in a one gram sample".[30]

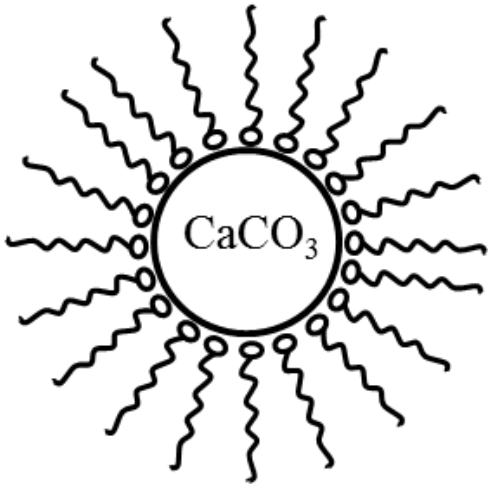

Figure 2.6. Representation of an overbased detergent reverse micelle.

2.4.2 Dispersants

Ashless dispersants have the same effect and structure as neutral detergents. They are used to clean the engine by solubilizing products, e.g. soot from the combustion, which would otherwise precipitate and possibly act as abrasive particles or disrupt the coherent lube oil film. A common component used for marine applications are of the type polyisobutylene-succinimide.[21]

2.4.3 Antioxidants

The antioxidants prevent oxidation, i.e. degradation, of the oil. This could otherwise result in the formation of acids (thereby corrosion or unnecessary consumption of BN), increased viscosity of the lube oil (increased friction between sliding parts, thus increased wear), or formation of insoluble products (such as abrasive particles, leading to increased wear).[31,32] Commonly, phenols, amines, dithiophosphate, and dithiocarbamates can be included in the lube oil formulations.

2.4.4 Corrosion inhibitors

The way of combating corrosion has already been outlined, however, (additional) additives are added to prevent rusting of the cast iron cylinder liners. These include neutral alkyl sulfonates, fosfates, amines, and alkyl succinic acids/esters. They have the function of forming a hydrophobic film on the liner surface to prevent water-metal contact, which eventually could lead to rusting.[21]

2.4.5 Anti-wear and extreme pressure additives

These are used to form a film on the highly loaded metal surface to prevent metal-metal contact, thereby limiting wear. Also, if the normal hydrodynamic lube oil film breaks down under high pressure and temperature. Commonly used additives for this purpose are: zinc dithiophosphates, dithiocarbamates (also used as antioxidants), sulfurized fatty acids, disulfides, and sulfurized alkenes.[21,33]

2.4.6 Pour-point depressants

Pour point is defined as the lowest temperature at which a lube oil will flow under specified conditions, i.e., defines the lowest temperature at which the lube oil is suitable.[2,33] The paraffinic base oil contains waxes, which at low temperature start to crystallize and agglomerate, which impede the oil flow. The additives help to lower the pour point by modifying the wax crystal structure in the paraffinic base oil, preventing the waxes to precipitate out of solution at low temperature. The additives are commonly polyalkylmethacrylates, alkyl naphthalenes, and alkylated wax.[21]

2.4.7 Anti-foam additives

The formation of foam in the lube oil film is undesirable because it among others hampers the lubrication and promotes oxidation of the lube oil. Common additives are silicone based oil insoluble additives which function by lowering of the surface tension of the foam bubbles to accelerate their collapse.[21,34]

2.4.8 Viscosity index improvers

To ensure optimal lubrication, the establishment of a so-called hydrodynamic lube oil film (from the Stribeck curve[35]) between the piston rings and cylinder liner is essential. A hydrodynamic lube oil film is characterized by complete separation between the two sliding surfaces resulting in low friction and minimal wear. The viscosity of the lube oil is an important parameter to achieve and maintain the hydrodynamic film.[35] This is a complicated matter because the viscosity of oil significantly changes with temperature. During engine start-up, the temperature is low and the viscosity is thereby high – and vice versa when the engine has been running for some time. Viscosity index improvers are therefore added to reduce the viscosity

at low temperatures and increase the viscosity at high temperatures. Typical viscosity index improvers are polymethacrylates, olefin copolymers, styrene-diene copolymers, and styrene-ester copolymers.[34] A typical viscosity grade of a cylinder lube oil is SAE50, having typical kinematic viscosities of $2.18 \cdot 10^{-4}$ m^2 s^{-1} at 40 ^oC and $1.9 \cdot 10^{-5}$ m^2 s^{-1} at 100 ^oC.[21]

2.5 The lube oil film environment

The present section shortly describes the environment of the lube oil film on the cylinder liner surface, specifically the temperature of the cylinder liner surface, the surrounding pressure, the lube oil thickness, the lube oil consumption, and the residence time of the lube oil in the engine. The lube oil used for a two-stroke marine diesel engine is not recycled and is supplied once into the piston ring pack every third to eighth revolution when the piston approaches TDC.[35] The lube oil is then moved up and down by the movement of the piston and becomes depleted by drainage in the lower part of the cylinder (the used oil is called drain oil).[36] The piston rings help to spread the lube oil throughout the vertical direction of the cylinder liner. Figure 2.7 shows a close-up of the cylinder liner-piston ring package environment. The lube oil is contained in the orifice between the cylinder liner surface and the end of the piston rings. The figure also illustrates the secondary (horizontal) movement of the piston, besides the primary (vertical) movement.

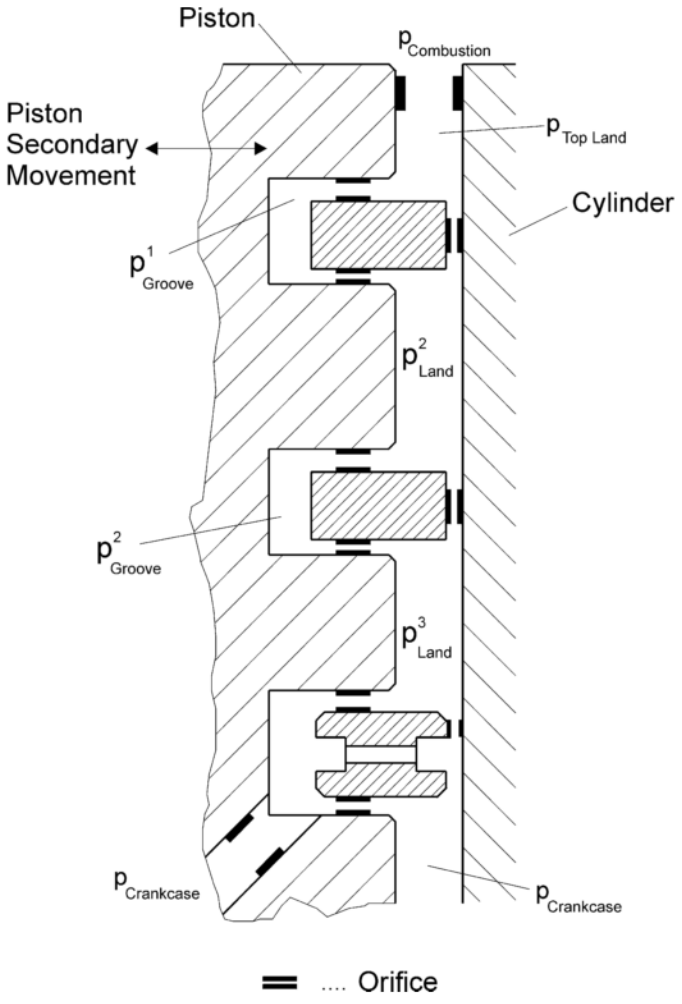

Figure 2.7. A close-up illustration of the cylinder liner surface-piston rings environment.[37]

2.5.1 Cylinder liner surface temperature and surrounding pressure

The cylinder pressure depends on the location of the piston during the combustion cycle. As stated earlier, the pressure has increased in recent years because of new engine designs and tunings to reduce the fuel consumption. This has reduced the maximum operating pressure gap between low and high load significantly.[17] It is reported that the maximum operating pressure can be as high as 200 bar, which occurs just after the fuel injection.[2,17,35] This means that the cylinder pressure is very high during the combustion phase when the piston is near TDC. Due to the rapid pressure evolution, the piston approaches BDC rapidly and the cylinder pressure decreases equivalently. After exhausting of the combustion gas, just prior to the piston approaching TDC again, the pressure is at its lowest which can be in the range of 10 bar.[11] With respect to the temperature, this is very dependent on the specific design of the engine and operating conditions.[17] The temperature is highest near TDC and lowest near BDC. The cylinder liner temperature is indeed highly dependent on the load. At high load, the cylinder wall temperature can be as high as 280 ^{o}C near TDC and 180 ^{o}C near BDC. At low load, the temperature at TDC can be in the range 150 ^{o}C and around 100 ^{o}C at BDC.[3,12,17,38]

2.5.2 Lube oil film thickness

The lube oil film thickness is mainly dependent on the viscosity, piston speed, geometry, and contact load between cylinder liner and piston ring.[32] Practically, the lube oil film thickness varies along the vertical direction of the cylinder liner, lowest near TDC,[39] having a minimum thickness in this upper part between 2-5 µm. At higher piston speeds, the thickness increases to around 10-12 µm.[40] Christiansen et al.[39] performed simulations showing that the oil film thickness can be as high as 45 µm. Recently, Ayranci and Akalin[41] used a reciprocating bench test rig to investigate the lube oil film thickness by use of laser-induced fluorescence (LIF) method. They found that high sliding speed and viscosity increases the lubrication whereas an increased load had the opposite effect, leading to metal-metal contact. Lube oil film thicknesses up to 20 µm were measured.[41]

2.5.3 Lube oil dosage

The lube oil is fed through so-called quills (bores) to uniformly distribute the lube oil film around the liner circumference.[3] The feed rate of the lube oil to the engine is primarily determined from the sulfur content in the fuel and a factor, called ACC factor with unit g/(kWh·wt.%S). Running on a 100 BN lube oil, the optimal ACC factor should be between 0.2 and 0.4 g/(kWh·wt.%S) and not take a value under 0.6 g/kWh. g/(kWh·wt.%S) (valid for newer engines).[42] The feed rate in grams per hour can then be calculated by multiplying the ACC factor with the sulfur content in the fuel and the produced energy of the engine (in kW). It is recommended that the lube oil feed rate is initially based on a high value of the ACC factor and is then gradually reduced until reaching an optimal lube oil feed rate with respect to minimal lube oil consumption and wear.[42] The ACC factor (and thereby the feed rate of the lube oil) can be reduced by increasing the BN of the lube oil equivalently.[3,38]

The optimal lube oil flow rate to the cylinder liner is highly dependent on the specific engine, ambient conditions, operating pattern, lube oil type, injection system, etc.[3,43] Therefore, it is recommended to perform a so-called cylinder lube feed rate sweep test, to determine the optimal ACC factor, in which the engine is operated for 24 hours on a specific lube oil feed rate followed by analysis of the drain oil. The lube oil feed

rate is hereafter decreased and a new test analysis of the drain oil is performed after 24 hours of operating at the specific feed rate. The complete test period can be 4 to 6 days and the engine operation must be kept as constant as possible.[42] The drain oil samples are analyzed for the total content of iron (both corrosive and abrasive iron) and BN. The optimal feed rate can then be determined by securing that drain oil samples are in the safe area (denoted 1) of Figure 2.8 when operating on high sulfur fuels. It is recommended that the BN (corrected for system oil dilution) is between 25 and 50, whereas the total iron content should be no higher than 200 mg kg^{-1}. If a too low value of BN is observed (2), cold corrosion may be an issue and more BN has to be supplied either by increasing the feed rate or increasing the BN of the oil. On the other hand, having a too large BN value (4), liner polishing may develop (explained in section 2.7.1). The lube oil feed rate can then be reduced or a lower BN oil can be used. Finally, if too much iron is measured in the drain oil sample (3), it may be due to "cat fines" (worn-down catalyst particles from the fuel oil, see section 2.7.1). Inspection of the fuel system is then required.[3,35,42]

The BN of the drain oil sample can be analyzed on-board by a pressure cell, otherwise, it can be analyzed in a laboratory by titration or infrared spectroscopy.[3,44] Different analysis techniques are also available for measuring iron, both abrasive/adhesive wear (magnetic iron) and wear due to corrosion (non-magnetic).[44] Besides this, visual inspections of e.g. the cylinder liner and piston rings should be carried out together with measuring physically the wear of the cylinder liner, piston rings, and piston ring grooves.[3,45]

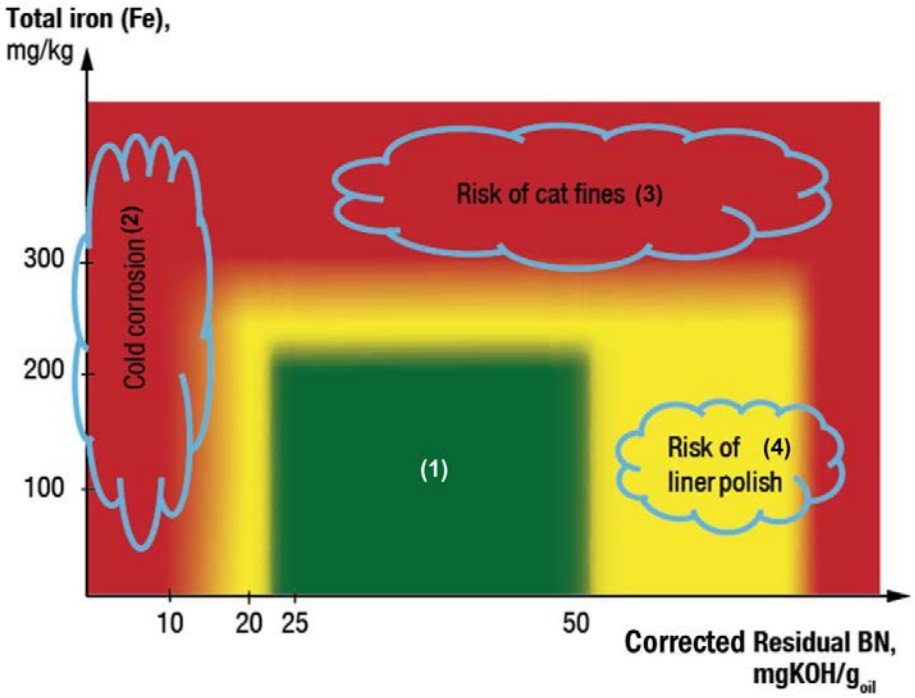

Figure 2.8. Interpretation of the drain oil sample analysis: (1) safe area, keep current operating conditions, (2) cold corrosion, increase lube oil feed rate or switch to a higher BN lube oil, (3) cat fines, inspect fuel centrifuge operation and cleanliness of the fuel, and (4) liner polishing, reduce the lube oil feed rate or switch to a lower BN lube oil.

2.5.4 Lube oil loss

When balancing the dosage amount of lube oil with the condensing H_2SO_4, it is important to establish whether there are other mechanisms which can lead to consumption of the lube oil. If this is the case, it has to be included in the balancing to ensure that sufficient alkaline additives (described in section 2.4.1) are

present at the cylinder liner surface to neutralize the condensing H_2SO_4. Herbst and Priebsch[37] stated that lube oil loss from the cylinder liner surface mainly happens by four mechanisms:

- Evaporation from the cylinder liner surface (depends on the temperature, pressure, and velocity of the combustion gas).
- Throw-off of accumulated oil above the top ring (uppermost ring of the piston ring package, depends on piston speed).
- Oil blow through the top ring end into the combustion chamber due to a reverse gas flow, which happens if the pressure in the second piston land exceeds the combustion gas pressure leading to a reversed flow carrying oil droplets.
- Oil scraping of the piston top land edge. During engine operation, the gap between the piston top land and cylinder liner gets rather low (decreases even further by deposit buildup and the secondary movement), possibly leading to direct contact, thus scraping off the lube oil film.

When the lube oil leaves the cylinder liner surface by one of the above mechanisms, it may reach the combustion chamber and thereby being combusted due to the higher temperature there.[35,36]

2.5.5 Lube oil residence time

The residence time of the lube oil in the engine determines for how long the lube oil should be functional with respect to minimizing wear of the cylinder liners and is an important parameter to consider when studying the neutralization and wear process in an engine. An average lube oil residence time can be derived from the lube oil film thickness, the feed rate, the stroke length, the cylinder liner diameter, and the load, see Figure 2.9.[14]

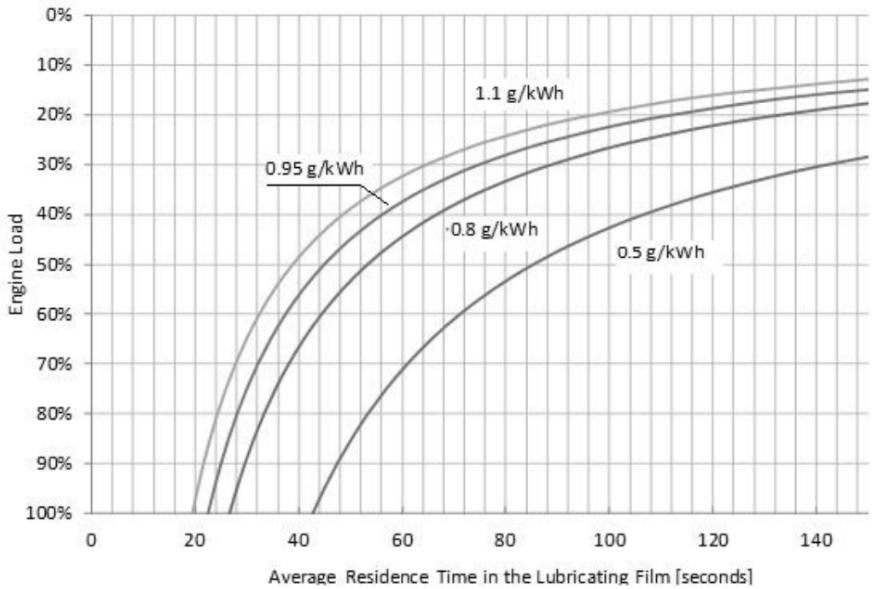

Figure 2.9. Calculated average residence times for a lube oil with an average lube oil thickness of 5 µm present at a cylinder liner with a diameter of 96 cm and having a stroke of 250 cm. The effect of engine load and lube oil feed rate are also shown in the figure.[14]

The average lube oil residence time is based on a uniform lube oil film thickness of 5 µm for a 250 cm stroke and 96 cm in diameter engine and is calculated as a function of the engine load and lube oil feed rate. This figure also explains part of the issue with respect to slow steaming (sailing at low load) and the resulting increase in corrosive wear: when e.g. the engine load is reduced from 90 to 30% at a feed rate of 0.8 g/kWh, then the residence time is increased from about 30 to 90 seconds, i.e., a factor of three. This means that the lube oil should be durable for much longer times. In addition, the effect of slow steaming is colder cylinder liner surfaces thus more H_2SO_4 is possibly condensing on the lube oil film.[14,46,47] However, when the load is decreased, the consumption of fuel is also decreased, thus having fewer sulfur species present in the system.

The actual residence time of the lube oil on the cylinder liners is difficult to exactly determine due to the reasons outlined in section 2.5.4, but also due to the highly dynamic environment of the cylinder system augmented by the moving piston. Nevertheless, Doyen et al.[48] used a tracer technology to determine the residence time of the lube oil in the research engine of Wärtsilä. A specific amount of tracer was injected at once and the accumulation in the drain was then monitored. They found that a part of the lube oil goes directly to the drain because it is scraped off the cylinder wall rapidly thus not being used for lubrication. Further, the major part of the tracer left the engine within half an hour, but 8-10% stayed in the engine significantly longer. This was attributed to lube oil accumulation in the piston grooves and/or the physical/chemical interactions occurring between the liner wall and lube oil.[48]

2.6 Neutralization of H_2SO_4 in cylinder lube oil

When H_2SO_4 condenses onto the lube oil film, it is crucial that it is neutralized before interacting with the cylinder liner wall, which eventually may result in corrosion of the wall material. For this purpose, the lube oils are formulated with alkaline additives (described in section 2.4.1) to handle the job. However, the amount of alkaline additives in the lube oil formulation (BN) is not necessarily equal to the performance of neutralizing the condensing H_2SO_4. The BN of a specific lube oil formulation only represents the potential of neutralizing the condensed H_2SO_4. Comparison of the neutralization rate for different commercial lube oil formulations with the same BN value has been reported in the literature. For instance, Wu et al. reported a factor of more than 2.5 (70 BN lube oils at room temperature) and Roman[49] reported a factor of up to 4 (70 BN lube oil at 353 K) between the fastest and slowest neutralization rate for different lube oil formulations having the same BN value.[50] Therefore, an increased understanding of how H_2SO_4 is neutralized by alkaline additives in the lube oil film may pinpoint how to optimize the lube oil formulation optimally to boost the neutralization rate.[24] Different investigations with this in mind have therefore been undertaken. Table 2.1 compactly presents a summary of the different research groups which experimentally has investigated the neutralization reaction with the aim of understanding the underlying neutralization mechanism.

Table 2.1. Historical overview of experimental investigations concerning the neutralization mechanism between acid droplets and alkaline additives in lube oil formulations.

Research group	Hosonuma and Tamura[51,52]	Roman[49]	Hone[28,53–56]	Papadopoulos[24,50,57–66]
Temperature (^oC)	25-80	80-120	10-30	23-170
Acid concentration (mol/L)	2.5-12.5 (H_2SO_4)	Concentrated (H_2SO_4)	0.1 (HCl and H_2SO_4)	H_2SO_4: 4.7-18 HNO_3: 4.4-15.6 CH_3COOH: 4.4-17.4 (Acid diameters: 70-200 µm)
Molar ratio of base and acid (mol/mol)	1-2	~0.5	~10	>>1 (order of magnitude: 100)
Oil type and base number (BN)	Diesel engine oil: 90 BN	Fully formulated experimental and commercial lube oils: 30-100 BN	Non-diluted base oil: 300 BN	Model oil: 30-75 BN Commercial cylinder oil: 70 BN Passenger car oil: 13 BN
Product location	Inside H_2SO_4 droplets	Solubilized in bulk or precipitates	In acid droplets	At oil/acid interface at oil side, inside acid droplets, inside reverse micelles, and no products observed
Experimental setup	Stirred batch reactor	Rotating batch reactor to study reaction in a thin oil film	Stopped-flow technique (study microemulsions, acidic droplets ~2 nm in diameter)	Capillary video-microscopy
Analysis method	Evolved CO_2	Evolved CO_2	Spectroscopy by monitoring the pH change	Visually
Mechanism of importance	Adsorption of $CaCO_3$ micelles	"Probability of contact"	Base transfer from micelles into acid droplets (not diffusion-controlled)	Adsorption of micelles onto acid droplets
Factors affecting the reaction rate	H_2SO_4 droplet size, $CaCO_3$ micelle size, ashless additives (indirectly)	H_2SO_4 droplets size, $CaCO_3$ micelle size, BN, temperature	Temperature, base concentration, the concentration of water droplets, type of solvent (hydrocarbon chain length)	Oil formulation (e.g. concentration of nonionic surfactants and type), temperature, acid droplet size, the likelihood of strong-stick collisions
Year	1984	1998	1999-2000	1999-2016

In the following, the most interesting results from the research groups will be outlined with a focus on describing the different proposed reaction mechanisms and which factors that affect the reaction rate of the neutralization reaction.

One of the earliest attempts to describe how H_2SO_4 and alkaline additives (also known as overbased detergents) in an oil media react, was proposed by Hosonuma and Tamura in 1984.[51,52] In a stirred batch reactor, they investigated the reaction between H_2SO_4 and overbased detergents in a diesel engine lube oil by monitoring the formed CO_2 from the reaction and by obtaining micrographs of the reacted lube oils. From the investigations, the neutralization model shown in Figure 2.10 was proposed. The neutralization model highlights that the alkaline additives are present as $CaCO_3$ reverse micelles and that the H_2SO_4 is emulsified into the lube oil and is stabilized by exchangeable surfactants molecules (so-called calcium sulfonate). Further, the $CaCO_3$ reverse micelles adsorb onto the H_2SO_4 droplet interface where the reaction takes place and the reaction product, calcium sulfate ($CaSO_4$), is located inside the H_2SO_4 droplet. Hosonuma and Tamura found that the reaction rate was increased with a decrease in H_2SO_4 droplet size and an increase in $CaCO_3$ particle size.

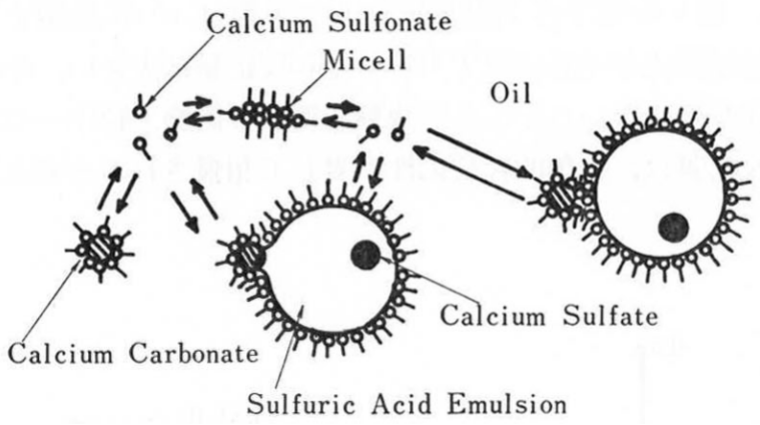

Figure 2.10. Proposed neutralization model for the reaction between emulsified H_2SO_4 and $CaCO_3$ reverse micelles, proposed by Hosonuma and Tamura.[52]

Roman[49] investigated the neutralization reaction in lube oil by use of a specially designed rotating vessel, wherein excess H_2SO_4 (compared to the molar $CaCO_3$ in the lube oil) was injected to react with the $CaCO_3$ overbased detergent additives in a thin lube oil film of about 100 µm. The pressure evolution from the produced CO_2 gas was monitored. This study showed that the neutralization reaction occurs in three stages by observing three different stages of the measured pressure profiles. The first stage is solubilization of H_2SO_4 in the lube oil film, where H_2SO_4 droplets are formed and stabilized by the excess detergent and dispersant molecules. This process was observed by a decrease in pressure and took up to six seconds, depending on the lube oil formulation and temperature. The solubilization time can double between one additive package and another. The second stage is illustrated in Figure 2.11 and deals with the fast reaction between solubilized H_2SO_4 droplets and $CaCO_3$ reverse micelles, observed by a rapid increase in pressure. The neutralization speed depends on the lube oil formulation, temperature, and BN value. As stated above, the magnitude of this stage can vary up to a factor of 4 for lube oils with equal BN but different formulation. Thirdly, when the relative concentration of H_2SO_4 droplets and $CaCO_3$ particles fall below a critical value, the pressure profile reached a plateau, thus the neutralization reaction was significantly reduced or quenched, even if H_2SO_4 droplets were still present. It was explained by reaching a critical number of H_2SO_4 droplets, thus decreasing the reaction rate significantly. This was also observed by Hone et al.,[28] who stated that the first 70% of the base particles in the oil is neutralized more rapidly than the last 30% for conditions where all base are neutralized. Roman[49] further proposed that the formed $CaSO_4$ from the reaction was solubilized into the bulk by the excess surfactants present in the lube oil, see Figure 2.11. For the temperature range investigated, 80-120 ^oC, Roman observed that a higher temperature resulted in lowering of the difference

between the neutralization rates of the different lube oil formulations. This behavior was also confirmed by Wu et al.[57] in the temperature range 25-55 °C. Roman further postulated that the neutralization reaction depends on the "probability of contact", which is lower at higher dilutions.[49] Whether this is translated to a diffusion- or adsorption-controlled (or something else) reaction is questionable.

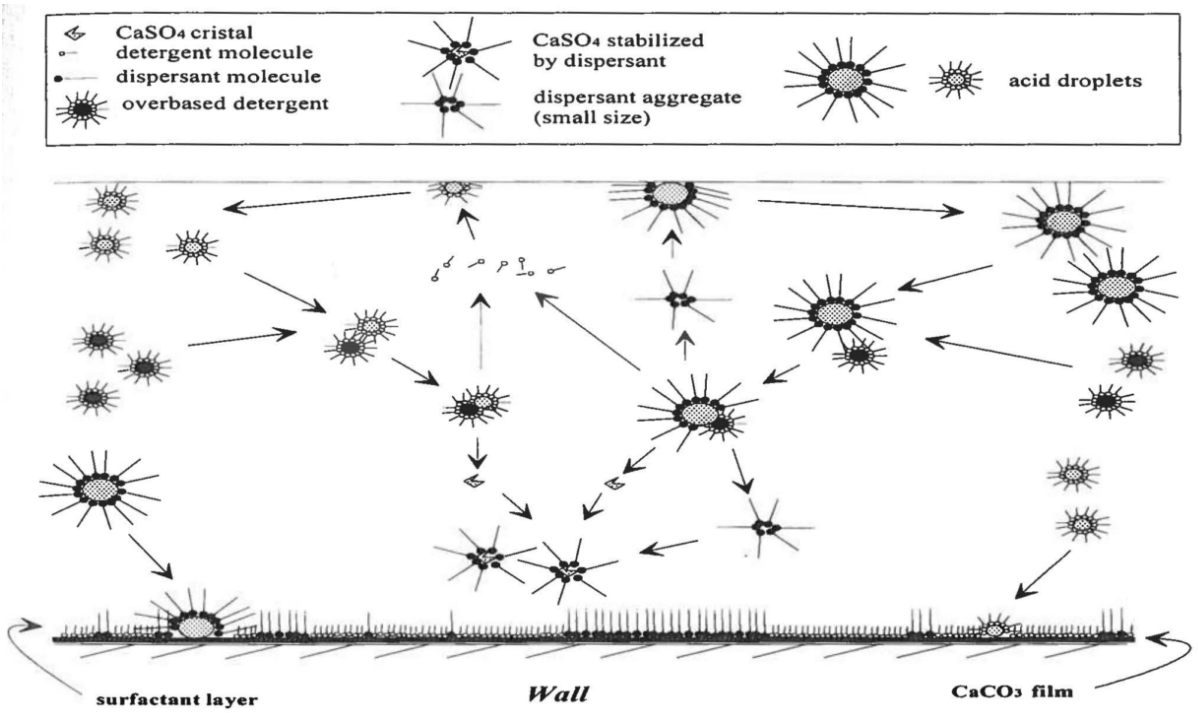

Figure 2.11. Illustration of the second stage (the fast neutralization reaction) of the reaction mechanism proposed by Roman.[49]

Hone et al.[28,53–56] used a stopped-flow method to investigate the reaction between nanometer-sized overbased additives and similar-sized acid droplets in model oils by monitoring the pH change, spectroscopically, accompanying the neutralization reaction. They suggested that the reaction between an emulsified acid droplet and an overbased detergent particle proceeds through the mechanism shown in Figure 2.12.

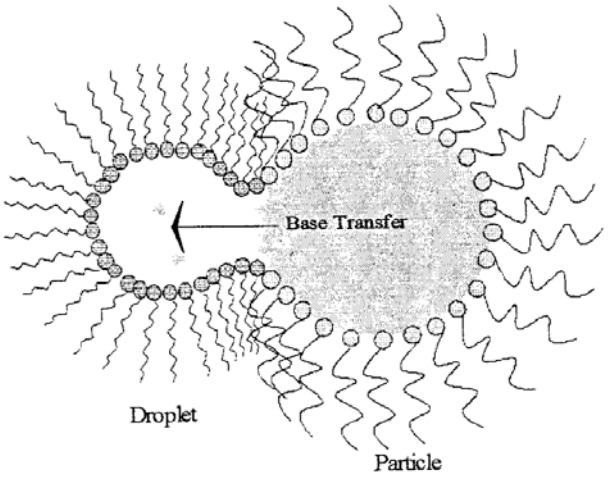

Figure 2.12. Illustration of the base-transfer channel mechanism between an overbased detergent particle and microemulsion droplet during an effective collision, proposed by Hone et al.[28]

Upon a successful "sticky" collision, the base is transferred from the overbased detergent particle into the aqueous acid core of the droplet where neutralization of the solubilized acid happens.[55] The work by Hone et al. is rather different from the work conducted within the field (see Table 2.1), more specifically with respect to the low acid concentration used (0.1 M) and the small size of the acid droplets (nanometer-sized). Nevertheless, they found that the reaction rate increased for increased overbased additive (i.e., $CaCO_3$) concentration, increased temperature (investigated in the range 10-30 ^oC), increased concentration of droplets (for a constant overall acid concentration), and increased hydrocarbon chain length of the solvent. Investigating the temperature dependency of the neutralization reaction, Hone et al. measured an activation energy of 54±2 kJ mol^{-1} and concluded that the reaction is not diffusion-controlled because these would have activation energies ~20 kJ mol^{-1}.[28]

The reaction between acid droplets and alkaline additives has over the years been extensively investigated using a capillary video-microscopy technique by the research group of Papadopoulos.[24,50,57–66] This technique allows a visual assessment of the shrinking of an acid droplet in an oil phase containing alkaline additives due to the neutralization reaction, specifically to measure the shrinking rate of the injected acid droplet. In their earlier work, the neutralization mechanism shown in Figure 2.13 was proposed.[24,50]
The interface of the much larger acid droplet (*S*) is shown as a plane in Figure 2.13. The first step (*step I*) of the mechanism is adsorption (a successful "sticky" collision) of a reverse micelle (M_1) on the acid-oil interface followed by transfer of acid and water into the core of M_1 where the neutralization reaction occurs (*step II*). The reverse micelle then desorbs (*step III*) and are now denoted M_2 which contains the reaction products. Another M_1 can then adsorb onto the acid-oil interface to repeat the neutralization mechanism. That the acid is transferred from the acid droplet to the reverse micelle contradicts the proposed base-transfer channel mechanism by Hone et al., where the base was transferred into the acid droplet.[28] In addition, Wu et al.[24,50] suggested that adsorption of the reverse micelle onto the acid droplet interface was the controlling step in the neutralization mechanism. It was further found that the shrinking rate (proportional to the reaction rate) increased for an increased BN of the lube oil. The reaction rate of acid neutralization was also found to depend on the specific formulation of the commercial lube oil, around a factor of 2.5 was found between the best and worst performing lube oil (with respect to shrinking rate). This is in agreement with the factor of 4 found by Roman.[49]

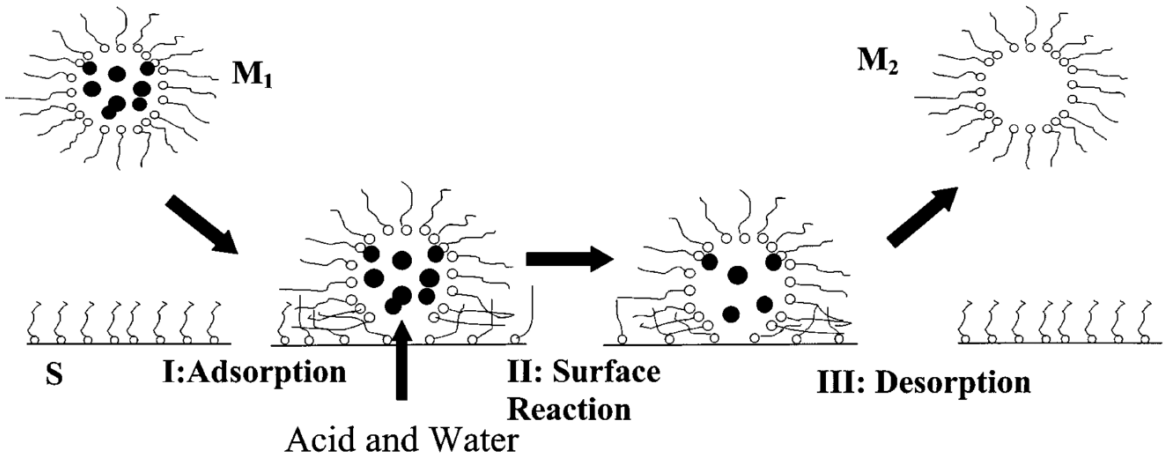

Figure 2.13. Neutralization mechanism between an acid droplet and an overbased detergent reverse micelle (M_1) proposed by Wu et al.[50]

Later, Fu et al.[60] observed four different reaction phenomena for the reaction between a H_2SO_4 droplet and $CaCO_3$-containing reverse micelles in different lube oil formulations (both commercial and model oils) in the temperature range 23-170 ^oC. The four different observations are summarized as: (1) $CaSO_4$ crystals and CO_2 gas were observed on the oil side of the oil/acid interface of the acid droplets (observed in the temperature range 25-170 ^oC), (2) crystals and gas bubbles were observed inside the acid droplet (110-170 ^oC), (3) no crystals, but gas bubbles were observed on the oil side of the acid/oil interface (23-27 ^oC), and (4) no reaction products were observed, but shrinking of the acid droplet was observed (23-170 ^oC). The first mentioned observed phenomenon is in agreement with the visual observations of Wu et al.,[24,50] whereas the second phenomenon agrees with the proposed neutralization mechanism of Hosonuma and Tamura[52] and Hone et al.[28] Phenomenon 3 or 4 may explain the proposed mechanism of Roman,[49] because he suggested that $CaSO_4$ crystals may solubilize into the bulk oil by the excess surfactants and detergents present in the lube oil formulation. Further, phenomenon 2 and 3 was observed in model oils whereas phenomenon 4 was observed in a commercial lube oil. This may augment that $CaSO_4$ formation at the oil/acid interface is not a hindrance for the neutralization mechanism in a commercial lube oil formulation, because these contain excess detergents and surfactants to solubilize the formed crystals. The four different observed phenomena were further divided into two types of reactions based on whether crystal formation was visually observed: strong/weak-stick collisions. The mechanism is illustrated in Figure 2.14 and is an extension of the proposed mechanism by Wu et al.[24,50] The crystal-observed reactions was proposed to consist of a high frequency of strong-stick collisions and the crystal solubilized reaction phenomena were explained to mainly consist of weak-stick collisions. For a strong-stick collision, the rigid structure of the reverse micelle is destroyed and the $CaCO_3$ is directly exposed to the acid. For a weak-stick collision, the rigid structure of the reverse micelle is maintained, thus neutralization proceeds through the transfer of acid from the acid droplet into the reverse micelle. Fu et al.[60] also found that crystal-observed reactions were faster than crystal-solubilized reactions (factor of ~2). Thus, the strategy of increasing the neutralization rate is to formulate the lube oils with as many surfactants as possible that enhance strong-stick collisions.[60]

In another study, Fu et al.[59] investigated the effect of temperature on the shrinking rate of a H_2SO_4 droplet in commercial lube oil formulations with a base number (BN) of 70. They were able to track the shrinking of the H_2SO_4 droplet over time and thereby calculate a shrinking rate. Constructing an Arrhenius plot of the measured temperature dependent shrinking rates, it is possible to calculate an activation energy of 52.8 kJ mol^{-1}, in great accordance with the value of 54±2 kJ mol^{-1} by Hone et al.[28] Fu et al.[61] also found that Ostwald ripening (growth of larger droplets at the expense of the smaller ones) could be an issue with respect to prolonging the existence of H_2SO_4 droplets in a lube oil film by diminishing the interfacial area of the droplets gradually.

Duan et al.[66] used Fourier Transform Infrared Spectroscopy (FTIR) and Nuclear Magnetic Resonance (NMR) spectroscopy to investigate the reaction between acetic acid and fully formulated passenger-car lube oil (base number of 13.1). Preparation time prior to obtaining the recorded spectra was around 30 seconds for FTIR and 2 min for NMR and included stirring of the batch emulsion. They concluded that the acetic acid was almost neutralized completely and the reaction was instantaneous for the conditions investigated. Besides using FTIR and NMR spectroscopy, video-microscopy was also used. Based on the experiments, they proposed a neutralization mechanism of overbased additives and acetic acid, describing that the reaction takes place at the oil/acid interface as well as in the bulk lube oil by diffusion of acetic acid in the lube oil. This is different from the reaction between overbased additives and H_2SO_4, which takes place exclusively at the oil/acid interface due to H_2SO_4 being insoluble in base oil.[66]

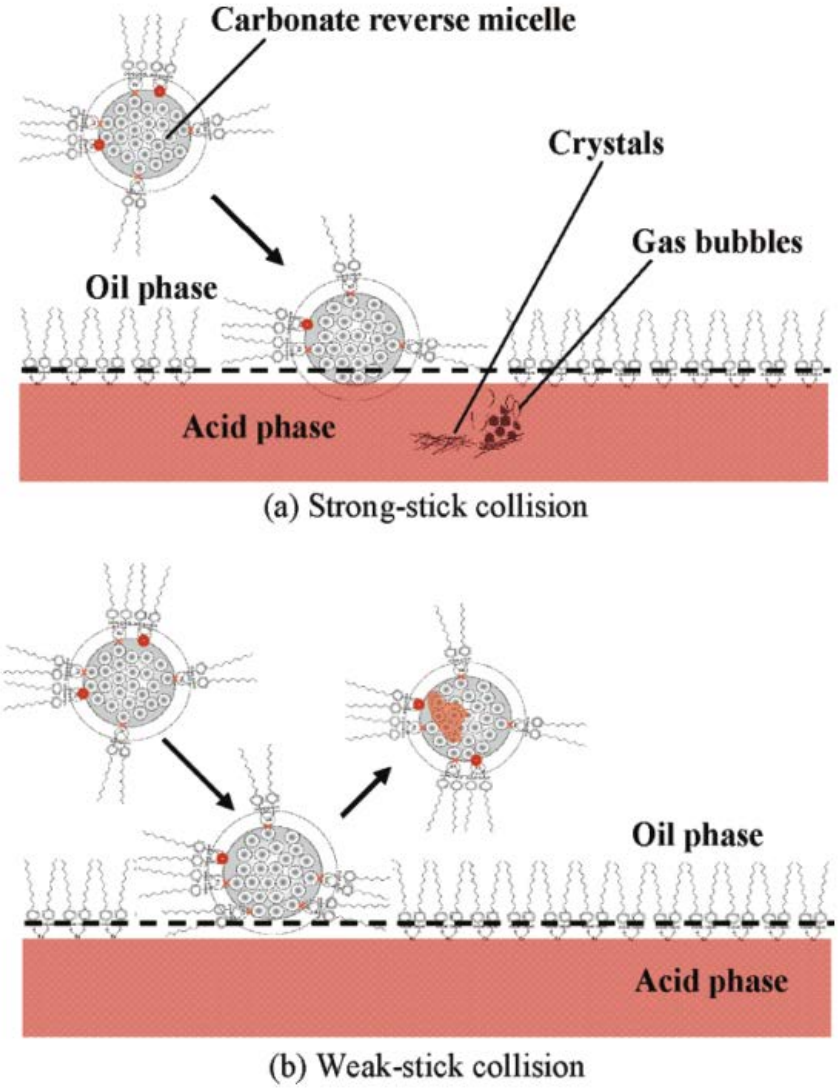

Figure 2.14. Illustration of the proposed strong/weak-stick collision mechanism by Fu et al.:[60] (a) strong-stick collision, where the base is directly exposed to acid. Here the rigid structure of the reverse micelle is destroyed at the interface, thus resulting in a fast reaction, which may have a chance to nucleate and grow crystals. (b) weak-stick collision, where the rigid structure of the reverse micelle is maintained before it desorbs back into the bulk lube oil. The reaction is dependent on the transfer of acid into the base core of the reverse micelle, thus resulting in a slow reaction and possible inability of nucleating and grow crystals.[60]

The above described proposed neutralization mechanisms between acid droplets and alkaline reverse micelles have dissimilarities, however, there is a joint consensus that a successful collision between the droplet and reverse micelle is a precursor for the reaction to occur. Wu et al.[24,50] even report that this may be the limiting step for a successful reaction. Even though the reaction has been investigated at rather different reaction conditions, it seems that the reaction rate is highly dependent on especially the specific lube oil formulation.[60] However, it was found that the higher the temperature, the lower the difference between lube oils of various formulations.[49,57,59] This may suggest that the neutralization efficiency of the commercial lube oils is optimized at realistic cylinder liner temperatures (>100 ^{o}C[12]). It has also been indicated that the

reaction between H_2SO_4 and alkaline additives is diffusion-controlled, having a reaction rate constant equal to $8.4 \cdot 10^{17}$ m^3 mol^{-1} s^{-1}.[9,10,67]

2.7 Wear mechanisms

When condensing H_2SO_4 is not neutralized in the lube oil emulsion immediately (or not fast enough), there is a risk that it reaches and corrodes the internal parts of the cylinder environment, most exposed are the cylinder liner surface and the piston rings. Augmented by the fast movement of the piston, the corroded material may be scraped off. If the material loss rate gets too high (MAN Energy Solutions recommends a maximum wear rate of 0.1 mm/1000 h[68]), then the cylinder liner and piston rings have to be replaced too often which is costly and time-consuming. Further, if an uncontrollable material loss rate is occurring for an extended period of time, it may eventually result in failure of the engine to operate (by the loss of operating pressure and prevention of formation of a lube oil film), which would be catastrophic. This combination of corrosion and wear (either abrasive or adhesive) is known as corrosive wear (or cold corrosion). These wear types are outlined below:[3,69]

2.7.1 Abrasive wear

Abrasive wear is occurring when a harder material is rubbing against a softer material, which then leads to a loss of material.[3,35] Two types of abrasive wear are sketched in Figure 2.15:[3,35] two-body abrasive wear and three-body abrasive wear.

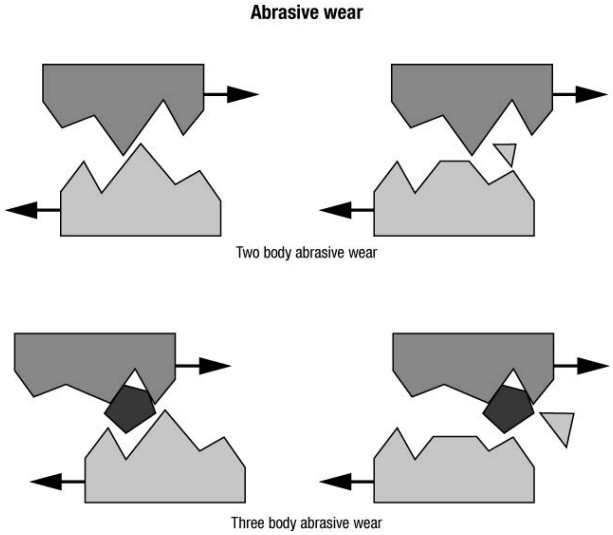

Figure 2.15. Illustration of the two types of abrasive wear: *upper*, two-body abrasive wear and *lower*, three-body abrasive wear.[35]

The two-body abrasive wear is when asperities of the harder material rub against/collide the softer material, leading to a material loss. The three-body abrasive wear includes a hard particle embedded between the cylinder liner and piston ring, which then leads to a loss of material.[70] The hard abrasive particles can originate from various sources, e.g. from the fuel oil (as small, worn down catalysts particles[71]), the lube oil (calcium deposits), or from scraped off piston material.[35,72] The latter means that abrasive wear can also be an effect of adhesive wear by the formation of abrasive particle. Abrasive wear may also lead to bore polishing (mirror-like appearance of the cylinder liner surface), e.g. by abrading of the cylinder liner surface

by calcium deposits (if e.g. over-lubrication occurs).[19] The cylinder liner surface can then not support a lube oil film, which may lead to adhesive wear and consequently scuffing[36] (described next).

2.7.2 Adhesive wear

Adhesive wear is when direct contact is established between the cylinder liner and piston ring because of lack of a lube oil film, leading to local (micro-)welding between the two surfaces. The results of local welding are a loss of material and formation of abrasive particles. The mechanism is sketched in Figure 2.16. The situation of not having a coherent lube oil film may be a result of insufficient lube oil dosage or inadequate cylinder liner surface roughness which then cannot support a lube oil film (the latter may be a result of abrasive wear). When adhesive wear is pronounced on a larger (macroscopic-)scale in the engine, it is commonly known as scuffing.[35]

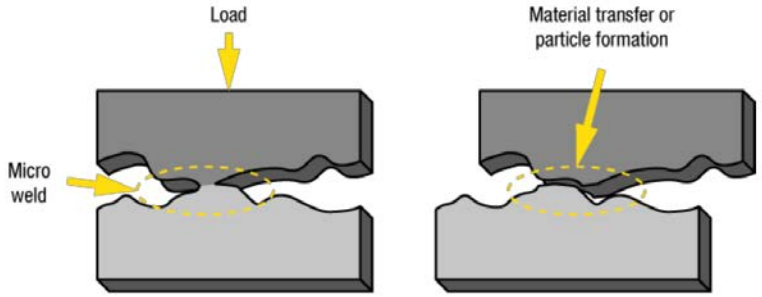

Figure 2.16. Illustration of adhesive wear.[35]

2.7.3 Corrosive wear

As stated, corrosive wear (or cold corrosion) is defined as loss of material when there is a combined effect of corrosion and wear (abrasive or adhesive). The cylinder liners are made out of cast iron,[45] which mainly consist of iron. When aqueous H_2SO_4 is present at the cylinder liner surface, iron is dissolved eventually forming iron oxide and iron sulfate mainly,[3,14,44,73–77] which normally act as a passive layer on top of the cylinder liner surface. However, the formation of a growing layer is continuously scraped off by the moving piston ring; see Figure 2.17(a).

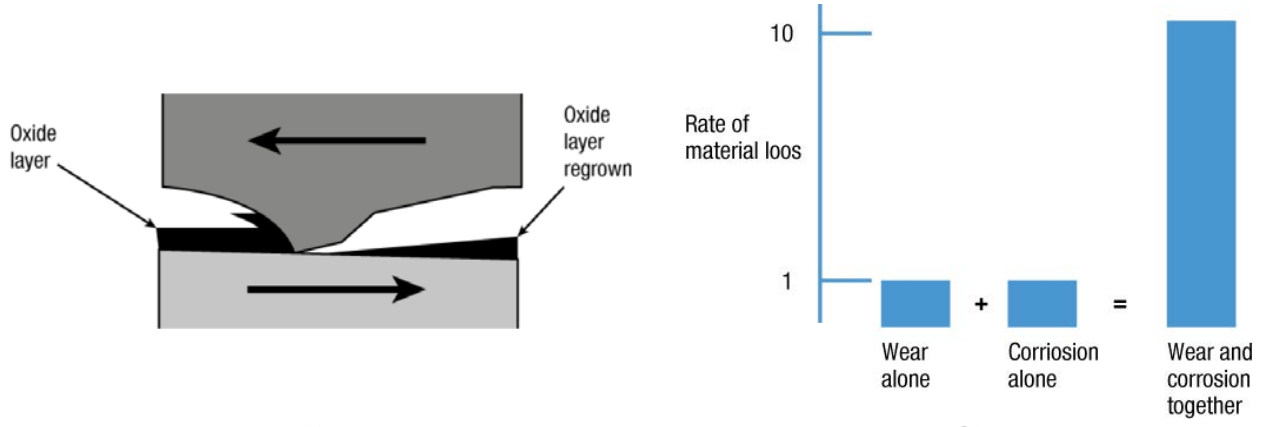

Figure 2.17. (a) Illustration of the protective oxide layer removal by the piston rings, which exposes the cylinder liner material for continuous corrosion. (b) arbitrary bar chart showing the combined effect of wear and corrosion on the rate of material loss compared to the individual contributions.[35]

Beneath the passive layer is then fresh iron which corrodes rapidly for continuous acid exposure. This means that the protective layer is continuously worn away by the piston rings, contributing to significant wear. The combined effect of wear and corrosion is therefore much higher than the sum of the individual contributions;[3,35,75,78] see Figure 2.17(b).

The electrochemical corrosion of iron by H_2SO_4 is a rather complex reaction mechanism. The first step is the dissolution of the iron by the dissociated protons from the aqueous acid:[79]

$$Fe_{(s)} \rightarrow Fe^{2+} + 2e^- \tag{2.5}$$

$$2H^+_{(aq)} + 2e^- \rightarrow H_{2(g)} \tag{2.6}$$

The further progress of the reaction mechanism and possible products depends on the local conditions. For instance, Fe^{2+} can combine with the salt of H_2SO_4, SO_4^{2-}, to form $FeSO_4$. However, if oxygen is present in the water, it is possible that the Fe^{2+} reacts further to Fe^{3+} and thereby Fe_2O_3, Fe_3O_4 (known as rust), etc. The resulting corrosion product can be a mixture of these precipitates.[79] In H_2SO_4-water solutions under static conditions, using a rotating disc electrode, Yahagi[75] found that the corrosion rate of cast iron peaked at around 20 wt.% H_2SO_4 and was non-existing at very high H_2SO_4 concentrations (>85 wt.%) at 23 °C. At low concentrations, an increase in H_2SO_4 concentration leads to an increase in corrosion rate. This is valid until a certain point (around 20 wt.% for the study by Yahagi), where the corrosion rate is significantly reduced for an increase in H_2SO_4 concentration. The reason is that the concentration of water decreases at increasing concentration of H_2SO_4 in the solution, thus decreasing the concentration of resulting protons, which are used to dissolve the iron.[79] In addition, it is reported that formation of a passive film is pronounced at higher H_2SO_4 concentrations,[80] which suppresses the dissolution of cast iron by limiting the diffusion of reactive species to and from the iron surface.[78,81] Rylands and Jenkinson[81] reported that it is the silicon compounds, present in the cast iron, which are mainly responsible for the formation of a protective film on the cast iron surface (iron oxide will also be protective, however). At increased H_2SO_4 concentration, the silicon-based film would grow more stable and more protective which increases the resistance of cast iron to H_2SO_4 attack.[81] Stott and Breakell[82] report that it is a hydrated $FeSO_4$ film that forms at the cast iron surface for more concentrated H_2SO_4 solutions during static corrosion tests (60 vol.% H_2SO_4 in water).[83]

The reciprocating pin-on-disc laboratory apparatus of Stott and co-workers[74,78,82,84–86] included the sliding of a pin (made of cast iron piston ring material), with different loads applied, against a disc (different cylinder liner cast irons) submerged in a stirred, temperature-controlled base oil/H_2SO_4 solution. The effects of varying different operating conditions were examined, including temperature, the load on the pin, acid concentration, surface treatment, and materials. They found that the wear rate increased for an increased temperature of the oil/acid emulsion and attributed this to mainly three things: (1) the viscosity decreases at increased temperature, which increases the metal-to-metal contact during sliding, (2) the dissolution rate of the iron increases with increasing temperature, and (3) the solubility of the protective corrosion products film increases at increased temperature.[84] Varying the roughness of the discs revealed that low wear was found for very smooth and very rough surfaces while the intermediate surface finish showed high wear. This was explained by very rough surfaces develop a protective film easily and very smooth surfaces develop an oil film easily.[85] When increasing the applied load on the pin, it was found that the total wear increased significantly, in agreement with the study by Yahagi.[75] However, the absolute value was higher for a more

diluted H_2SO_4 in the oil emulsion (10 vol.% acid in oil with acid concentrations of 10 and 40 vol.% in water).[85] This was attributed to the formation of an adherent, wear-protective corrosion product film at the more concentrated acid, which prevented metal to metal contact. Increasing the volume percentage of acid solution in oil (up to 40 vol.% acid in oil with the concentration of the acid in water of 10 vol.%) increased the total wear significantly. The reason was that increased acid content in the oil emulsion disrupted the oil film, enhancing the metal-metal contact and also the formation rate of the electrochemical products which then were removed rapidly away from the disc surface by the sliding pin.[74,86] When the acid in oil volume was 20 vol.%, the wear rates increased with increasing acid in water concentration. For 40 vol.% of acid in oil, the wear rates were very high and were reasonable independent of the acid in water concentration.[74] This was explained by disruption of the oil film, leading to long periods of metal-metal contact, when the acid in oil content was increased. These studies show that the resulting wear rate is a complex function of the local conditions prevailing between the sliding components, such as load, protective film formation, the degree of disruption of the oil film, temperature, surface roughness, specific material composition, aqueous content in oil, H_2SO_4 concentration, etc. The overall conclusion from these reciprocating pin-on-disc experiments was that corrosion has a significant contribution on the wear rate of cast iron under corrosive wear conditions. If no corrosion takes place, the mechanical wear alone is much less damaging and vice versa.[75,78] This is in agreement with Figure 2.17(b). By applying a specific load on the pin and adding carbon particles to the H_2SO_4 solution, Yahagi[75] found that this increased the wear rate significantly.

Amblard[31] presented results from corrosion experiments performed by submerging an iron plate into a stirred and heated lube oil volume followed by continuous H_2SO_4 addition by a syringe. The amount of total H_2SO_4 added over 1.5 hours corresponded to 90% conversion of the base number of the commercial lube oil. By measuring the weight loss of the iron plate, it was found that maximum corrosion (highest weight loss) occurred when using a 50% H_2SO_4 solution at 60 ^oC (investigated in the range 0-95% H_2SO_4, it is not stated whether this is weight or volume percent, however). Amblard attributed this to water having a shielding effect which reduces the contact between H_2SO_4 and the alkaline additives at low H_2SO_4 concentrations. At higher H_2SO_4 concentrations, the reaction between H_2SO_4 and the alkaline additives was so fast that the interaction between H_2SO_4 and iron was minimized.[31] The effect of temperature was investigated in the interval 40-100 ^oC, yielding that the highest wear occurred at 70 ^oC. Above this temperature, water began to evaporate thereby limiting the effect of H_2SO_4. The dosage rate of H_2SO_4 had no effect on the total mean weight loss, but the foam formation was increased. This could be an issue in practice because severe foam formation could disrupt the coherent lube oil film on the cylinder liner promoting corrosion.[31] The effect of using nitric acid and carboxylic acid instead of H_2SO_4 showed that these are minor contributors to corrosion compared to H_2SO_4.

2.8 The role of SO_2 in a diesel engine

So far, the above sections (and the relevant literature in general) have mainly been focused on how H_2SO_4 condenses onto the cylinder liner wall, how it reacts with the alkaline additives present in the lube oil film, and how H_2SO_4 reacts with the cast iron liner wall and affects corrosive wear. However, Figure 2.3 showed that SO_2 is in vast excess in the combustion chamber compared to SO_3 and H_2SO_4, around a factor of 20. Actually, it has been reported that SO_2 can be in molar excess compared to SO_3/H_2SO_4 by a factor in the range 10-40.[3,11] For the SO_2 to reach the bulk lube oil film, it has to be absorbed by the lube oil itself or by the condensing water droplets. Even though sulfur-induced corrosive wear has mainly been attributed to

H_2SO_4,[31] some research studies advocate that SO_2 can also contribute to $CaCO_3$ consumption and corrosive wear. These will be outlined below.

Nagaki and Korematsu[87–89] investigated the effect of EGR (Exhaust Gas Recirculation, i.e., recirculation a part of the exhaust gas into the combustion chamber, mainly done to reduce the combustion temperature and thereby reducing the formation of NO_x[3,90]) on the wear rate of the piston rings and cylinder liner. By recirculating a part of the gas, the SO_2 concentration in the combustion chamber is increased (nowadays, an internal scrubber is normally fitted together with EGR[3]). It was done by model simulations, but also experiments where both an actual exhaust gas was recirculated and by adding SO_2 to the intake air. Experiments, carried out in a single-cylinder four-stroke diesel engine, revealed that increasing the EGR rate and the SO_2 addition to the intake air increased the wear of the piston rings and cylinder liner. Nagaki and Korematsu advocated that the main cause of increased wear was related to the absorption of SO_2 in the lube oil. It proceeded through the following three steps: (1) SO_2 is absorbed by the lube oil film, (2) SO_2 forms H_2SO_4 and sulfates (e.g. $CaSO_4$) in the lube oil film, (3) these cause wear on the piston rings and cylinder liner. The increase in SO_4^{2-} concentration was also measured after 50 hours of operation (the lube oil is recirculated to the engine), showing no additional increase by adding SO_2 to the intake air, but more wear was measured.[89] This means that the alkaline additives were not consumed in an observable degree when adding SO_2 to the intake air, possibly contradicting the hypothesis that SO_2 reacts to H_2SO_4 or directly with the $CaCO_3$ to form $CaSO_4$.

Naegeli and Marbach[73] also investigated the effect of SO_2 on wear in laboratory engine setups. They found that less than 1% of the SO_2 was converted to H_2SO_4, and concluded that H_2SO_4 is unimportant with respect to the measured wear. They performed engine experiments, where sulfur was added in the fuel or as SO_2 in the intake air. It was concluded that the resulting corrosive wear was due to the formation of sulfurous acid (H_2SO_3) in the lube oil film which reacts with the cylinder liner wall (possibly also with the alkaline additives). Further, the effect of placing iron in aqueous solutions of SO_2 was investigated, yielding that the resulting corrosion product appeared to be a mixture of FeS, FeO, and Fe_2O_3. The following overall reaction was therefore suggested to happen:[73]

$$SO_{2(aq)} + 2H_2O_{(aq)} + 3Fe_{(s)} \rightarrow FeS_{(s)} + 2Fe(OH)_{2(s)} \tag{2.7}$$

Based on their study, they concluded that SO_2 is the principal cause of fuel sulfur-induced wear and deposit formation in diesel engines, which complements the conclusions of Nagaki and Korematsu and may explain why an increase in SO_4^{2-} concentration was not observed in their study.

From other research fields, it is found that SO_2 do react with $CaCO_3$ and iron. For instance, $CaCO_3$ is used to capture gaseous SO_2 in wet flue gas desulfurization (FGD) plants. The SO_2 is scrubbed from the flue gas by reacting with $CaCO_3$ in an aqueous slurry by the following reactions:[91,92]

$$SO_2 + H_2O \rightarrow H^+ + HSO_3^- \tag{2.8}$$

$$HSO_3^- \rightarrow H^+ + SO_3^{2-} \tag{2.9}$$

$$2HSO_3^- + O_2 \rightarrow 2H^+ + 2SO_4^{2-} \tag{2.10}$$

$$Ca^{2+} + SO_4^{2-} + 2H_2O \rightarrow CaSO_4 \cdot 2H_2O(s) \tag{2.11}$$

If the system is not saturated in O_2, the formation of $CaSO_3$ may happen:

$$Ca^{2+} + SO_3^{2-} + 1/2\,H_2O \rightarrow CaSO_3 \cdot 1/2\,H_2O(s) \quad (2.12)$$

If dissolved iron is present from Eq. (2.5), $FeSO_3/FeSO_4$ may be possible corrosion products from Eqs. (2.8)-(2.12).[93] Also, the reaction between humid SO_2 and $CaCO_3$ particles has been investigated (23-80 ^oC), finding that $CaSO_3$ and $CaSO_4$ were formed.[94–96] This shows that it is possible for $CaCO_3$ (in aqueous systems) to react with SO_2, forming $CaSO_3$ and/or $CaSO_4$. Absorption data of SO_2 in lube oil and water even confirms that it is possible for SO_2 to be present in the lube oil film emulsion (lube oil + water).[87,88,97,98]

With respect to the reaction between iron and aqueous SO_2, different studies, besides the study by Naegeli and Marbach, have been carried out. These find that aqueous SO_2 do react with iron to form corrosion products, such as $FeSO_3$, $FeSO_4$, and FeS, by different proposed reaction mechanisms.[93,99,100] It is also found that $FeSO_4$ can react with water and oxygen to produce FeOOH and H_2SO_4.[100] Thereby, H_2SO_4 is formed and can either react with the iron or the alkaline additives. Also, Fishman et al.[101] found that saturating a 35% H_2SO_4 solution with SO_2 increased the corrosion rate significantly (a factor of "several tens") compared to the case with no SO_2 in the H_2SO_4 solution.

To sum up this section, it was outlined that increased wear in laboratory diesel engines was observed when increasing the concentration of SO_2 in the combustion chamber. However, no increase of SO_4^{2-} was found, which may be due to the formation of corrosive H_2SO_3 (aqueous SO_2), which may also react with $CaCO_3$ to form $CaSO_3$. From other research fields, it is found that SO_2 and $CaCO_3$ do react and the same is valid for aqueous SO_2 and iron.

2.9 Practical cases on how to mitigate cold corrosion

Significant attention has been given to the solution of the cold corrosion issue. This has mainly been done by implementing various countermeasures such as decreasing the scavenge air temperature (to minimize the amount of water vapor entering the cylinder).[38] A very important step toward increasing the control of cold corrosion, has been the introduction of 100 BN lube oil (and 140 BN).[38] In the following, a practical case will be presented which shows the effect on the iron and BN content in the drain oil by changing the BN of the lube oil and the feed rate. Other practical cases can be also be found in the reference.[3]
Figure 2.18 shows the results of a sweep test performed on-board where half the engine was lubricated with 70 BN lube oil and the other half with 100 BN lube oil. The sulfur content in the fuel was 3% and the engine load was between 38-52% (but mostly at 39%). The figure shows both the measured iron concentration (mg/kg) and the BN in the drain oil samples at varying ACC factor. The figure reveals that for the 70 BN lube oil, an ACC factor larger than 0.31 g/(kWh·wt.%S) is needed to achieve an iron content lower than 200 mg/kg and a BN value larger than 20. For the 100 BN lube oil, an ACC factor of 0.20 g/(kWh·wt.%S) easily handles the limits. Thus the lube oil consumption can be reduced by approximately 35% and still achieve better protection. It is also shown that there is around 30 BN in difference between the two different lube oils for the same ACC factor (e.g. at 0.25 g/(kWh·wt.%S)), but the iron content is significantly decreased. This may mean that most of the corrosion is happening at a local spot on the cylinder liner where all the BN has been depleted with the 70 BN lube oil. Using the 100 BN lube oil then gives more protection in this exposed area, which decreases the corrosive wear significantly.

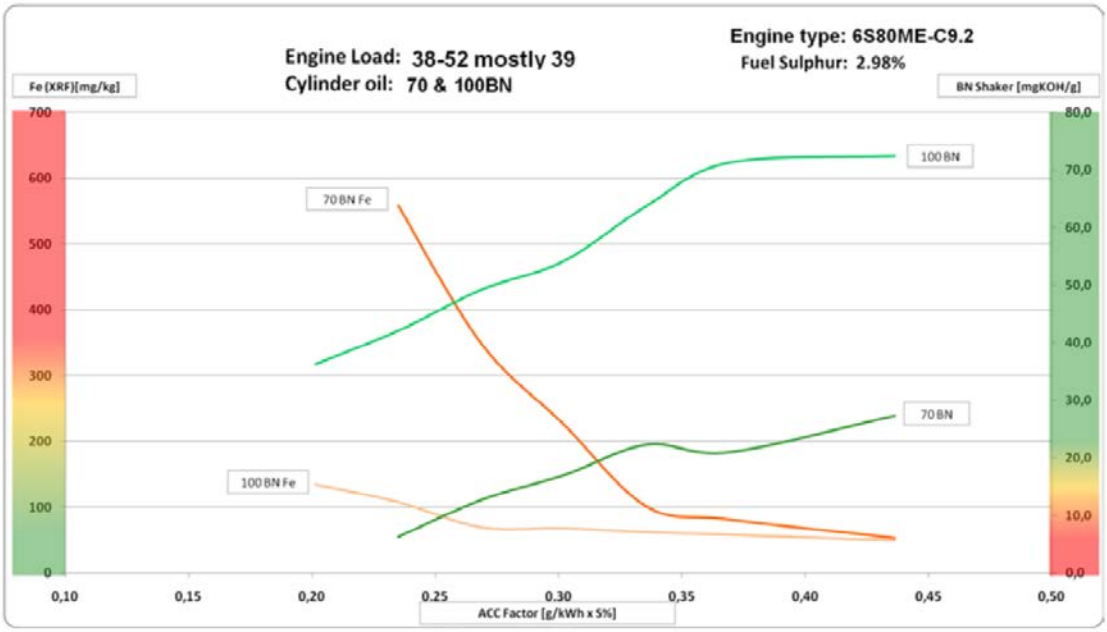

Figure 2.18. Drain oil data (iron content and BN) from an engine with a split lubrication system (half is lubricated with 70 BN lube oil and the other half with 100 BN lube oil). The iron content and BN are presented as a function of the ACC factor.[3]

Corrosive wear can also be reduced significantly by increasing the temperature of the cylinder liner surfaces, thereby decreasing the H_2SO_4 condensation rate.[3] The corrosive wear can also be decreased by optimizing the spatial lubrication. For instance, Jensen[68] reported that the maximum wear was decreased when injecting the lube oil 1/8 from TDC instead of 1/3 from TDC, but the average wear rate was more or less unaffected. Because the durability of the cylinder liner is determined from the maximum wear (0.1 mm/1000 h), the reduction in maximum wear rate increases the lifetime of the cylinder liners.[68] Because most wear is observed near TDC,[17] the results of Jensen may mean that it is due to starvation of BN at TDC and a way to decrease the wear is to supply more lube oil (BN) in the upper part of the cylinder liner. How to reduce wear is a very complex situation and a lot of different measures can be taken. This section only illustrated a handful of different approaches.

2.10 Concluding remarks

To better understand the very complex and dynamic environment prevailing inside a large two-stroke marine diesel engine, the different sub-processes occurring, concerning the sulfur-induced corrosive wear, needs to be studied separately. This literature review has focused on experimental and theoretical studies on the different sub-processes from the formation of sulfur oxides in the gas phase to the governing wear reactions on the cast iron with the focus on the components SO_2 and H_2SO_4.

The formation of the sulfur oxides (SO_x) in the gas phase and subsequent formation and condensation of H_2SO_4 during the combustion stroke has been quantified through 3D CFD modeling by which it is possible to quantify the effect of changed operating conditions on the condensation of H_2SO_4 on the cylinder liner surface. The condensation of H_2SO_4 is mainly dependent on the pressure in the cylinder, the cylinder liner surface temperature, the sulfur content in the fuel, and the amount of water present. The formation and

condensation of H_2SO_4 may happen immediately upon each other due to the small distance from the wall where H_2SO_4 is formed. The alkaline additives in the lube oil (mainly $CaCO_3$ reverse micelles) have the job of neutralizing the condensing H_2SO_4. The lube oil is a complex formulation of many components, each of which has a very specific task in the hostile environment on the cylinder liner surface. The reaction between H_2SO_4 and $CaCO_3$ has been investigated separately and various reaction mechanisms have been proposed in the literature. It is suggested that the reaction may be adsorption-/diffusion-controlled; however, quantification of the reaction is lacking which hinders quantification of the conversion degree at specific conditions. The reaction between H_2SO_4 and cast iron has been investigated in various laboratory setups, both with and without base oil. Generally, a higher H_2SO_4 concentration leads to increased corrosion and water has to be present in order to dissociate the H_2SO_4 sufficiently. However, when the H_2SO_4 concentration is high, a protective layer may be formed rapidly which hampers the further corrosion process. Nevertheless, the sliding motion of a piston ring may gradually remove the formed protective layer and facilitate further corrosion. Even though it was found that a high concentration of H_2SO_4 forms a wear-resistant protective corrosion product layer, the load in a real engine may be large enough to scrape off the layer. This would lead to a substantial wear rate of the cylinder liner and piston rings. Also, when a large fraction of H_2SO_4/water is condensing, it would increase the metal-metal contact between the piston ring and cylinder liner surface thus increase the wear rate. The role of SO_2 on consumption of $CaCO_3$ reverse micelles is presently also not clear. However, the SO_2 is greatly present close to the lube oil film and it is known from other research fields that SO_2 indeed do react with $CaCO_3$. From practice, it is found that the most severe corrosion is happening near TDC, this is in general agreement with the CFD simulations which showed that most of the water and H_2SO_4 are condensing in this upper region. This may lead to a molar excess of H_2SO_4 compared to $CaCO_3$ reverse micelles and H_2SO_4 can thereby react with the cast iron liner. With the high load of water also condensing near TDC, this further augments the corrosive wear. To combat corrosive wear practically, many parameters (such as operating conditions, engine design, and lube oil formulation) can be adjusted. However, investigating the effect of each parameter in practice on the corrosive wear is ineffective (time-consuming and expensive). To support the optimization process, development of modeling tools of the sub-processes leading to corrosive wear is required. This includes quantifying the chemical/physical interactions taking place in the lube oil film on the cylinder liner, more specifically investigating the sulfur-related reactions with the alkaline additives in fully formulated lube oil. The subsequent chapters of the thesis will focus on this matter.

References

(1) marinediesels.co.uk. The 2 Stroke Diesel Cycle http://www.marinediesels.info/ (accessed Nov 12, 2018).

(2) Woodyard, D. Pounder's Marine Diesel Engines and Gas Turbines. Eighth Edition.

(3) CIMAC Working Group 8 "Marine Lubricants." CIMAC Guideline Cold Corrosion in Marine Two Stroke Engines. 2017.

(4) Cordtz, R. L.; Schramm, J.; Rabe, R. Investigating SO_3 Formation from the Combustion of Heavy Fuel Oil in a Four-Stroke Medium Speed Test Engine. *Energy Fuels* **2013**, *27* (10), 6279–6286.

(5) Pang, K. M.; Karvounis, N.; Walther, J. H.; Schramm, J.; Glarborg, P.; Mayer, S. Modelling of Temporal and Spatial Evolution of Sulphur Oxides and Sulphuric Acid under Large, Two-Stroke Marine Engine-like Conditions Using Integrated CFD-Chemical Kinetics. *Appl. Energy* **2017**, *193*, 60–73.

(6) Cordtz, R. The Influence of Fuel Sulfur on the Operation of Large Two-Stroke Marine Diesel

Engines. Ph.D. Dissertation, Technical University of Denmark, Kgs. Lyngby, 2015.
(7) Cordtz, R.; Schramm, J.; Andreasen, A.; Eskildsen, S. S.; Mayer, S. Modeling the Distribution of Sulfur Compounds in a Large Two Stroke Diesel Engine. *Energy Fuels* **2013**, *27* (3), 1652–1660.
(8) Hindiyarti, L.; Glarborg, P.; Marshall, P. Reactions of SO_3 with the O/H Radical Pool under Combustion Conditions. *J. Phys. Chem. A* **2007**, *111* (19), 3984–3991.
(9) van Helden, A. K.; Valentijn, M. C.; van Doornt, H. M. J. Corrosive Wear in Crosshead Diesel Engines. *Tribol. Int.* **1989**, *22* (3), 189–193.
(10) van Helden, A. K. A Physico-Chemical Model of Corrosive Wear in Low Speed Diesel Engines, Report D-9. 1987, pp 1–16.
(11) Andreasen, A.; Mayer, S. PAPER NO.: 39 Modelling of the Oxidation of Fuel Sulfur in Low Speed Two-Stroke Diesel Engines. *CIMAC Congr. Bergen* **2010**, 12.
(12) Cordtz, R.; Mayer, S.; Eskildsen, S. S.; Schramm, J. Modeling the Condensation of Sulfuric Acid and Water on the Cylinder Liner of a Large Two-Stroke Marine Diesel Engine. *J. Mar. Sci. Technol.* **2017**, 1–10.
(13) Reiner, T.; Arnold, F. Laboratory Investigations of Gaseous Sulfuric Acid Formation via $SO_3+H_2O+M \rightarrow H_2SO_4+M$: Measurement of the Rate Constant and Product Identification. *J. Chem. Phys.* **1994**, *101* (9), 7399–7407.
(14) Hammett, J. Utilising the Latest Findings Engine Oil Stress from Field & Laboratory Engine Testing. *J. JIME* **2014**, *49* (3), 6–13.
(15) Verhoff, F. H.; Banchero, J. T. Predicting Dew Points of Flue Gases. *Chem. Eng. Prog.* **1974**, *70* (8), 71–72.
(16) Hengeveld, J.; Schenk, C.; Aabo, K. The Role of Temperature and Pressure in the Wear Processes in Low Speed Diesel Engines. **2000**.
(17) García, L.; Gehle, S.; Schakel, J. Impact of Low Load Operation in Modern Low Speed 2-Stroke Diesel Engines on Cylinder Liner Wear Caused by Increased Acid Condensation. *J. JIME* **2014**, *49* (1), 100–106.
(18) Karvounis, N.; Pang, K. M.; Mayer, S.; Walther, J. H. Numerical Simulation of Condensation of Sulfuric Acid and Water in a Large Two-Stroke Marine Diesel Engine. *Appl. Energy* **2018**, *211*, 1009–1020.
(19) Christensen, O. Cylinder Lubrication of Two-Stroke Crosshead Marine Diesel Engines. *Wärtsilä Tech. J.* **2010**, 39–48.
(20) Chevron. *Marine Lubricants Information Bulletin 13: Bright Stock*; 2013.
(21) Mortier, R. M.; Fox, M. F.; Orszulik, S. T. *Chemistry and Technology of Lubricants*, 3rd ed.; Springer Netherlands: Dordrecht, 2010.
(22) Liston, T. V. Engine Lubricants Additives: What They Are and How They Function. *Lubr. Eng.* **1992**, *48* (5), 389–397.
(23) O'Connor, S. P.; Crawford, J.; Cane, C. Overbased Lubricant Detergents – a Comparative Study. *Lubr. Sci.* **1994**, *6* (4), 297–325.
(24) Wu, R. C.; Papadopoulos, K. D.; Campbell, C. B. Visualization Test for Neutralization of Acids by Marine Cylinder Lubricants. *AIChE J.* **1999**, *45* (9), 2011–2017.
(25) Marković, I.; Ottewill, R. H.; Cebula, D. J.; Field, I.; Marsh, J. F. Small Angle Neutron Scattering Studies on Non-Aqueous Dispersions of Calcium Carbonate - Part I. The Guinier Approach. *Colloid Polym. Sci.* **1984**, *262* (8), 648–656.
(26) Marković, I.; Ottewill, R. H. Small Angle Neutron Scattering Studies on Non-Aqueous Dispersions of Calcium Carbonate. Part III. Concentrated Dispersions. *Colloid Polym. Sci.* **1986**, *264* (5), 454–462.
(27) Marković, I.; Ottewill, R. H. Small Angle Neutron Scattering Studies on Nonaqueous Dispersions of

Calcium Carbonate Part 2. Determination of the Form Factor for Concentric Spheres. *Colloid Polym. Sci.* **1986**, *264* (1), 65–76.

(28) Hone, D. C.; Robinson, B. H.; Steytler, D. C.; Glyde, R. W.; Galsworthy, J. R. Mechanism of Acid Neutralization by Overbased Colloidal Additives in Hydrocarbon Media. *Langmuir* **2000**, *16* (2), 340–346.

(29) Hudson, L. K.; Eastoe, J.; Dowding, P. J. Nanotechnology in Action: Overbased Nanodetergents as Lubricant Oil Additives. *Adv. Colloid Interface Sci.* **2006**, *123-126* (SPEC. ISS.), 425–431.

(30) ASTM International. ASTM 2896-11. Standard Test Method for Base Number of Petroleum Products by Potentiometric Perchloric Acid Titration. 2011.

(31) Amblard, C. New Chemistry to Protect against Cold Corrosion in Marine Cylinder Lubricants. *J. Japan Inst. Mar. Eng.* **2015**, *50* (6), 54–62.

(32) Buhaug, Ø. Deposit Formation on Cylinder Liner Surface in Medium-Speed Engines, Norwegian University of Science and Technology, 2003.

(33) CIMAC. Guidelines for Diesel Engines Lubrication: Lubricating Oil Degradation. 2004.

(34) Rizvi, S. Q. A. *A Comprehensive Review of Lubricant Chemistry, Technology, Selection, and Design*; ASTM International: West Conshohocken, PA, 2009.

(35) CIMAC Working Group 8 “Marine Lubricants.” CIMAC Recommendation 31: The Lubrication of Two-Stroke Crosshead Diesel Engines. 2017.

(36) Olander, P.; Eskildsen, S. S.; Fogh, J. W.; Hollman, P.; Jacobson, S. Testing Scuffing Resistance of Materials for Marine 2-Stroke Engines – Difficulties with Lab Scale Testing of a Complex Phenomenon. *Wear* **2015**, *340-341*, 9–18.

(37) Herbst, H. M.; Priebsch, H. H. Simulation of Piston Ring Dynamics and Their Effect on Oil Consumption. In *SAE Technical Papers*; 2000; pp 1–12.

(38) Jakobsen, S. B. Service Experience of MAN B&W Two Stroke Diesel Engines. In *28th CIMAC World Congress*; Helsinki, 2016.

(39) Christiansen, J.; Klit, P.; Volund, A.; Hwang, J.-H. Calculation of Oil Film Thickness from Damping Coefficients for a Piston Ring in an Internal Combustion Engine. In *Proceedings of the International Conference BALTTRIB’2007*; Kaunas, 2007; pp 162–167.

(40) Sautermeister, F. A.; Priest, M.; Lee, P. M.; Fox, M. F. Impact of Sulphuric Acid on Cylinder Lubrication for Large 2-Stroke Marine Diesel Engines: Contact Angle, Interfacial Tension and Chemical Interaction. *Tribol. Int.* **2013**, *59*, 47–56.

(41) Ayranci, Y. E.; Akalin, O. Continuous Lubricant Film Thickness Measurement Between Piston Ring and Cylinder Bore. *J. Eng. Gas Turbines Power* **2018**, *140* (7), 072802.

(42) MAN Diesel & Turbo. Service Letter SL2014-587/JAP. 2014.

(43) Jensen, T. Swirl Injection Lubrication Low Cylinder Oil Consumption without Sacrificing Wear Rates. *J. Japan Inst. Mar. Eng.* **2002**, *37* (2), 41–50.

(44) Atkinson, D. Onboard Condition Monitoring of Cold Corrosion in Two-Stroke Marine Diesel Engines. *11th Int. Conf. Cond. Monit. Mach. Fail. Prev. Technol. C. 2014 / MFPT 2014* **2014**, *5* (2), 17–22.

(45) Jacobsen, D. M. S.; Pedersen, J. M.; Svensson, J.; Mayer, S. Cylinder Lube Oil Experiences and New Development for the MAN B&W Two-Stroke Engines. In *28th CIMAC World Congress*; Helsinki, 2016.

(46) Harrold, P. Lubricating Marine Crosshead Engines Operating at Reduced Load. *J. Japan Inst. Mar. Eng.* **2014**, *49* (1), 88–95.

(47) Shell Marine. Superior Technology for Overcoming the Changing Challenges of the Sea. 2016.

(48) Doyen, V.; Drijfholt, R. K.; Delvigne, T. PAPER NO .: 61 Advanced Applied Research Unravelling

the Fundamentals of 2-Stroke Engine Cylinder Lubrication – an Innovative on-Line Measurement Method Based on the Use of Radioactive Tracers-. *CIMAC Congr. 2007, Vienna* **2007**.

(49) Roman, J.-P. New Method of Measurement in Thin Film of the Neutralization of Marine Lubricants for Low-Speed and Medium-Speed Diesel Engines. In *CIMAC Congress 1998, Copenhagen*; Copenhagen, 1998; pp 913–926.

(50) Wu, R. C.; Papadopoulos, K. D.; Campbell, C. B. Acid-Neutralizing of Marine Cylinder Lubricants: Measurements and Effects of Dispersants. *AIChE J.* **2000**, *46* (7), 1471–1477.

(51) Hosonuma, K.; Tamura, K. Acid Neutralization of Overbased Detergents (Part 1) Neutralization in the Test Methods of ASTM Base Number. *J. Japan Pet. Inst.* **1984**, *27* (2), 101–107.

(52) Hosonuma, K.; Tamura, K. Acid Neutralization of Overbased Detergents (Part 2) Neutralization with Sulfuric Acid Emulsion. *J. Japan Pet. Inst.* **1984**, *27* (2), 108–113.

(53) Galsworthy, J. R.; Glyde, R. W.; Diggs, N. Z.; Gorda, K. R.; Hone, D. C.; Robinson, B. H. Acid Neutralization Studies of Overbased Detergents: Mechanism and Impact of Detergent Structure. *Recent Adv. Chem. Lubr. Addit. ACS Symp. Prepr.* **1999**, *44* (3), 345–350.

(54) Galsworthy, J.; Hammond, S.; Hone, D. Oil-Soluble Colloidal Additives. *Curr. Opin. Colloid Interface Sci.* **2000**, *5* (5-6), 274–279.

(55) Hone, D.; Robinson, B.; Galsworthy, J.; Glyde, R. Colloidal Chemistry of Lubricating Oils. In *Reactions And Synthesis In Surfactant Systems*; Texter, J., Ed.; Surfactant Science; CRC Press, 2001; pp 385–394.

(56) Hone, D. C.; Robinson, B. H.; Steytler, D. C.; Glyde, R. W.; Cleverley, J. A. Acid-Base Chemistry in High-Performance Lubricating Oils. *Can. J. Chem.* **1999**, *77*, 842–848.

(57) Wu, R. C.; Campbell, C. B.; Papadopoulos, K. D. Acid-Neutralizing of Marine Cylinder Lubricants: Effects of Nonionic Surfactants. *Ind. Eng. Chem. Res.* **2000**, *39* (10), 3926–3931.

(58) Fu, J.; Lu, Y.; Campbell, C. B.; Papadopoulos, K. D. Optical Microscopy inside a Heating Capillary. *Ind. Eng. Chem. Res.* **2005**, *44* (5), 1199–1203.

(59) Fu, J.; Lu, Y.; Campbell, C. B.; Papadopoulos, K. D. Temperature and Acid Droplet Size Effects in Acid Neutralization of Marine Cylinder Lubricants. *Tribol. Lett.* **2006**, *22* (3), 221–225.

(60) Fu, J.; Lu, Y.; Campbell, C. B.; Papadopoulos, K. D. Acid Neutralization by Marine Cylinder Lubricants Inside a Heating Capillary: Strong/Weak-Stick Collision Mechanisms. *Ind. Eng. Chem. Res.* **2006**, *45* (16), 5619–5627.

(61) Fu, J.; Papadopoulos, K. D.; Lu, Y.; Campbell, C. B. Ostwald Ripening: A Decisive Cause of Cylinder Corrosive Wear. *Tribol. Lett.* **2007**, *27* (1), 21–24.

(62) Garcia-Bermudes, M. Study on the Neutralization Mechanism of Overbased Detergents and Their Formulates, Tulane University, 2013.

(63) Garcia-Bermudes, M.; Rausa, R.; Papadopoulos, K. Vertically-Oriented-Capillary Video-Microscopy: Drops Levitated by a (Reacting) Fluid. *Ind. Eng. Chem. Res.* **2011**, *50* (24), 14142–14147.

(64) Garcia-Bermudes, M.; Rausa, R.; Papadopoulos, K. Formation of Colloidal Shells on Acidic Droplets Undergoing Neutralization in Marine Diesel Engine Cylinder Oils. *Tribol. Lett.* **2013**, *51* (1), 85–92.

(65) Duan, Y.; Rausa, R.; Fiaschi, P.; Papadopoulos, K. D. Neutralization of Acetic Acid by Automobile Motor Oil. *Tribol. Int.* **2016**, *98*, 94–99.

(66) Duan, Y.; Rausa, R.; Zhao, Q.; Papadopoulos, K. D. Neutralization Mechanism of Acetic Acid by Overbased Colloidal Nanoparticles. *Tribol. Lett.* **2016**, *64* (8), 1–11.

(67) Schramm, J.; Henningsen, S.; Sorenson, S. C. Modelling of Corrosion of Cylinder Liner in Diesel Engines Caused by Sulphur in the Diesel Fuel. In *SAE Technical Paper*; SAE International, 1994; pp 1–10.

(68) Jensen, P. Lubtronic SIP Promise Remarkably Low Wear Rates with Low CLO Consumption. *CIMAC Congr. 2016, Helsinki* **2016**.
(69) Golothan, D. W. Review of the Causes of Cylinder Wear in Marine Diesel Engines. *Inst. Mar. Eng. Trans.* **1978**, *90*, 137–163.
(70) Bovington, C. H. Friction, Wear and the Role of Additives in Controlling Them. In *Chemistry and Technology of Lubricants*; Mortier, R. M., Fox, M. F., Orszulik, S. T., Eds.; Springer Netherlands: Dordrecht, 2010; pp 77–105.
(71) McGeary, T.; Chew, F.; Fogh, J. W. Investigations into Abrasive and Corrosive Wear Mechanisms of Pistons and Liners in Large Bore 2-Stroke Diesel Engine Cylinders. *24th CIMAC World Congr.* **2004**.
(72) Roman, J. (TOTAL L. New Chemistry Is a Key Factor for Future Cylinder Oils. *SNAME Conf. Houst.* **2012**, No. January.
(73) Naegeli, D. W.; Marbach, H. W. Role of Sulfur Oxides in Wear and Deposit Formation in Army Diesel Engines. Interim Report BFLRF No. 248, Contract No. DAAK70-87-C-0043. Southwest Research Institute: San Antonio, Texas, 1988.
(74) Stott, F. H.; Macdonald, A. G. The Influence of Acid Strength on the Corrosive Wear of Grey Cast Irons in Oil-Sulphuric Acid Mixtures. *Wear* **1988**, *122* (3), 343–361.
(75) Yahagi, Y. Corrosive Wear of Diesel Engine Cylinder Bore. *Tribol. Int.* **1987**, *20* (6), 365–373.
(76) McConnell, G.; Nathan, W. S. A Wear Theory for Low Speed Diesel Engines Burning Residual Fuel. *Wear* **1962**, *5* (1), 43–54.
(77) McGeehan, J. A.; Kulkarni, A. V. Mechanism of Wear Control by the Lubricant in Diesel Engines, No. 872029. In *SAE Technical Paper Series*; 1987; pp 1–14.
(78) Stott, F. H.; Breakell, J. E.; Newman, R. C. The Corrosive Wear of Cast Iron Under Potentiostatically-Controlled Conditions in Sulphuric Acid Solutions. *Corros. Sci.* **1990**, *30* (8), 813–830.
(79) Groysman, A. *Corrosion for Everybody*, 1st ed.; Springer Netherlands: Dordrecht, 2010.
(80) Maahn, E. Corrosion of Cast Iron in Concentrated Sulphuric Acid under Potentiostatic Conditions. *Br. Corros. J.* **1966**, *1* (9), 350–354.
(81) Rylands, J. R.; Jenkinson, J. R. The Corrosion of Heating Surfaces in Boiler Plants: Further Studies in Deposit Formation. *Proc. Inst. Mech. Eng.* **1948**, *158* (1), 405–425.
(82) Stott, F. H.; Breakell, J. E. The Influence of Corrosion on the Wear of Cast Iron in Sulphuric Acid Solutions. *Wear* **1989**, *135* (1), 119–134.
(83) Riggs, O. L. Sulfates in the Passive Iron Layer. *Corrosion* **1964**, *20* (9), 275t – 281t.
(84) Macdonald, A. G.; Stott, F. H. Effect of Temperature on the Corrosive Wear of Cast-Iron in Oil-Sulphuric Acid Environments. *React. Solids* **1987**, *4* (3), 237–249.
(85) Macdonald, A. G.; Stott, F. H. The Influence of Load and Surface Treatment on the Corrosive Wear of Cast Iron in Oil-Sulphuric Acid Environments. *J. Mater. Sci.* **1988**, *23* (2), 629–636.
(86) Macdonald, A. G.; Stott, F. H. The Corrosive Wear of Cast Iron in Oil-Sulphuric Acid Mixtures. *Corros. Sci.* **1988**, *28* (5), 485–501.
(87) Nagaki, H.; Korematsu, K. Relation Between Diffusion Process of Sulfur Oxides in Exhaust Gas into Oil Film and Wear of Cylinder Liner and Piston Rings in Diesel Engines. *SAE Pap.* **1991**.
(88) Nagaki, H.; Korematsu, K. Effect of Sulfur Dioxide in Recirculated Exhaust Gas on Wear within Diesel Engines - (Relationship between Wear and Amount of SO_2 Absorbed by Lubricating Oil Film). *JSME Int. J. Ser. B-Fluids Therm. Eng.* **1995**, *38* (3), 465–474.
(89) Nagaki, H.; Korematsu, K. Effect of SO_2 in Recirculated Exhaust Gas on Wear in Diesel Engine - (Effect of SO_2 Added to Intake Air on Wear). *JSME Int. J. Ser. B-Fluids Therm. Eng.* **1996**, *39*, 193–201.

(90) Lamas, M. I.; Rodríguez, C. G. Emissions from Marine Engines and NOx Reduction Methods. *J. Marit. Res.* **2012**, *9* (1), 77–82.
(91) Kiil, S. Experimental and Theoretical Investigations of Wet Flue Gas Desulphurisation. Ph.D. Dissertation, Technical University of Denmark, Kgs. Lyngby, 1998.
(92) Córdoba, P. Status of Flue Gas Desulphurisation (FGD) Systems from Coal-Fired Power Plants: Overview of the Physic-Chemical Control Processes of Wet Limestone FGDs. *Fuel* **2015**, *144*, 274–286.
(93) Xiang, Y.; Wang, Z.; Xu, C.; Zhou, C.; Li, Z.; Ni, W. Impact of SO_2 Concentration on the Corrosion Rate of X70 Steel and Iron in Water-Saturated Supercritical CO_2 Mixed with SO_2. *J. Supercrit. Fluids* **2011**, *58* (2), 286–294.
(94) Klingspor, J.; Karlsson, H. T.; Bjerle, I. A Kinetic Study of the Dry SO_2-Limestone Reaction at Low Temperature. *Chem. Eng. Commun.* **1983**, *22*, 81–103.
(95) Baltrusaitis, J.; Usher, C. R.; Grassian, V. H. Reactions of Sulfur Dioxide on Calcium Carbonate Single Crystal and Particle Surfaces at the Adsorbed Water Carbonate Interface. *Phys. Chem. Chem. Phys.* **2007**, *9* (23), 3011–3024.
(96) Al-Hosney, H. A.; Grassian, V. H. Water, Sulfur Dioxide and Nitric Acid Adsorption on Calcium Carbonate: A Transmission and ATR-FTIR Study. *Phys. Chem. Chem. Phys.* **2005**, *7* (6), 1266.
(97) Costa, D. L.; Underhill, D. Solubility and Reactivity of Sulfur Dioxide in Various Oils. *Am. Ind. Hyg. Assoc. J.* **1976**, *37* (1), 46–51.
(98) NIST Chemistry WebBook: https://webbook.nist.gov/chemistry.
(99) Johansson, L.-G.; Vannerberg, N.-G. The Corrosion of Unprotected Steel in an Inert-Gas Atmosphere Containing Water Vapour, Oxygen, Nitrogen and Different Amounts of Sulphur Dioxide and Carbon Dioxide. *Corros. Sci.* **1981**, *21* (12), 863–876.
(100) Allam, I. M.; Arlow, J. S.; Saricimen, H. Initial Stages of Atmospheric Corrosion of Steel in the Arabian Gulf. *Corros. Sci.* **1991**, *32* (4), 417–432.
(101) Fishman, V. A.; Dobrolyubov, V. V.; Smirnova, I. S.; Dubinin, V. G. Corrosion and Electrochemical Behavior of Cast Iron in Sulfuric Acid Solutions Saturated with SO_2. *Zhurnal Prikl. Khimii* **1974**, *47* (4), 926–929.

3 | Reaction of sulfuric acid in lube oil: Implications for large two-stroke diesel engines

Preceding work of this chapter can be found in Appendix A (lube oil analyses to determine and quantify the alkaline core of the overbased detergent) and Appendix B (investigation of the well-mixed lube oil film assumption by use of computational fluid dynamics simulations).

This chapter is a reprint of the published peer-reviewed conference article “Reaction of sulfuric acid in lube oil: Implications for large two-stroke diesel engines”, published in Proceedings of the ASME 2017 Internal Combustion Engines Fall Conference. The article is available under the following DOI: 10.1115/ICEF2017-3580.

Abstract

Slow-steaming operation and an increased pressure in the combustion chamber have contributed to increased sulfuric acid (H_2SO_4) condensation on the cylinder liners in large two-stroke marine diesel engines, thus causing increased corrosion wear. To cope with this, lube oils are formulated with overbased detergent additives present as $CaCO_3$ reverse micelles to neutralize the condensing H_2SO_4. In this present work, a mixed flow reactor (MFR) setup aims to investigate the neutralization reaction by varying Ca/S molar ratio, stirrer speed, H_2SO_4 inlet concentration, and residence time. Lube oil samples from the outlet of the MFR were analyzed by use of Fourier Transform Infrared Spectroscopy (FTIR) and a titration method. The MFR results indicate that the $CaCO_3$-H_2SO_4 reaction is very fast in a real engine, if the cylinder liner is well-wetted, the oil-film is well-mixed, and contains excess of $CaCO_3$ compared to the condensed H_2SO_4. The observed corrosion wear in large two-stroke marine diesel engines could consequently be attributed to local molar excess of H_2SO_4 compared to $CaCO_3$ reverse micelles on the cylinder liners.

Keywords: Corrosion, Lubrication, Neutralization, Mechanism

3.1 Introduction

Slow-steaming became popular during the recession in the last part of the 2000s. This meant that the large two-stroke marine diesel engines were now operated at a lower engine load in order to save fuel. To ensure optimal specific fuel oil consumption the engines were further optimized in this new part load range. This resulted in increased cylinder pressures and colder cylinder liners at part load among others. The lower liner surface temperature, in combination with an increased operating pressure, has led to increased water and acid condensation in the cylinder lube oil film on the cast iron liner surfaces.[1,2] This causes accelerated corrosion and wear of the liners and piston rings,[3] so-called cold corrosion. It is generally thought that the cold corrosion phenomenon originates mostly from corrosion by condensed sulfuric acid (H_2SO_4), due to the sulfur-rich fuel used in marine diesel engines.[4,5] The heavy fuel oil sulfur oxidizes to SO_2 from which only a few percents oxidize further to SO_3.[6] The SO_3 may react with water vapor to form gaseous H_2SO_4 that can condense, either as concentrated acid or as acid diluted in water, if the temperature locally is below the H_2SO_4 dew point.[7]

However, alternative explanations involving corrosion wear from SO_2 are also found. Neageli and Marbach[8] found that absorption of SO_2 in lube oil, followed by reaction with water, could lead to the formation of sulfurous acid (H_2SO_3), thus increasing corrosion wear. Nagaki and Korematsu[9–11] advocate that H_2SO_4 can form in the cylinder lube oil from SO_2, causing corrosion wear, by: (1) absorption of SO_2 by lube oil, (2) formation of H_2SO_4 in the lube oil film, and (3) wear on the piston rings and cylinder liner caused by H_2SO_4.

3.1.1 Mechanisms of neutralization

Commercial lube oils are typically formulated with overbased detergent additives present as reverse micelles[12] to neutralize H_2SO_4 in the lube oil film. The core of the reverse micelles consists primarily of calcium carbonate ($CaCO_3$), which has a diameter of between 4 and 14 nm. Together with the stabilizing surfactant monolayer, the overall diameter of the micelle is between 8 and 18 nm.[13] Reaction products from the neutralization mechanism between H_2SO_4 and $CaCO_3$ are $CaSO_4$, CO_2, and water according to the following reaction:

$$H_2SO_4\,(l) + CaCO_3\,(s) \rightarrow CaSO_4\,(s) + CO_2\,(g) + H_2O\,(l) \tag{3.1}$$

Hosonuma and Tamura[14] proposed the first neutralization mechanism between H_2SO_4 droplets and $CaCO_3$ by measuring the CO_2 gas produced from the reaction. Their neutralization model showed that the $CaCO_3$ particles and H_2SO_4 droplets are stabilized by surfactant molecules. The reverse micelles adsorb onto the oil/acid interface and react with H_2SO_4. $CaSO_4$ is formed inside the H_2SO_4 droplets. They found that the reactivity increased with decreasing size of the H_2SO_4 emulsion, larger base particle size, and the addition of ash-less dispersants. By use of a stopped-flow method, Hone et al.[15] proposed a base-transfer channel neutralization mechanism, where base transfer from the $CaCO_3$ reverse micelles into nanometer-sized, dispersed water/acid droplet in a model oil occurred, upon an effective collision, followed by acid neutralization in the acid droplet. They report that the neutralization reaction becomes faster at higher temperatures (studied in the temperature range 10-30^{o}C) and increasing concentration of overbased $CaCO_3$ particles. The neutralization mechanism between H_2SO_4 droplets and $CaCO_3$ reverse micelles has also been investigated extensively by a capillary video-microscopy technique,[13,16–23] investigating the shrinkage of acid

drops in different lube oils. Wu et al.[17] proposed an interfacial neutralization mechanism, Figure 3.1, between a nanometer-sized reverse micelle (RM) and a micrometer-sized acid drop.

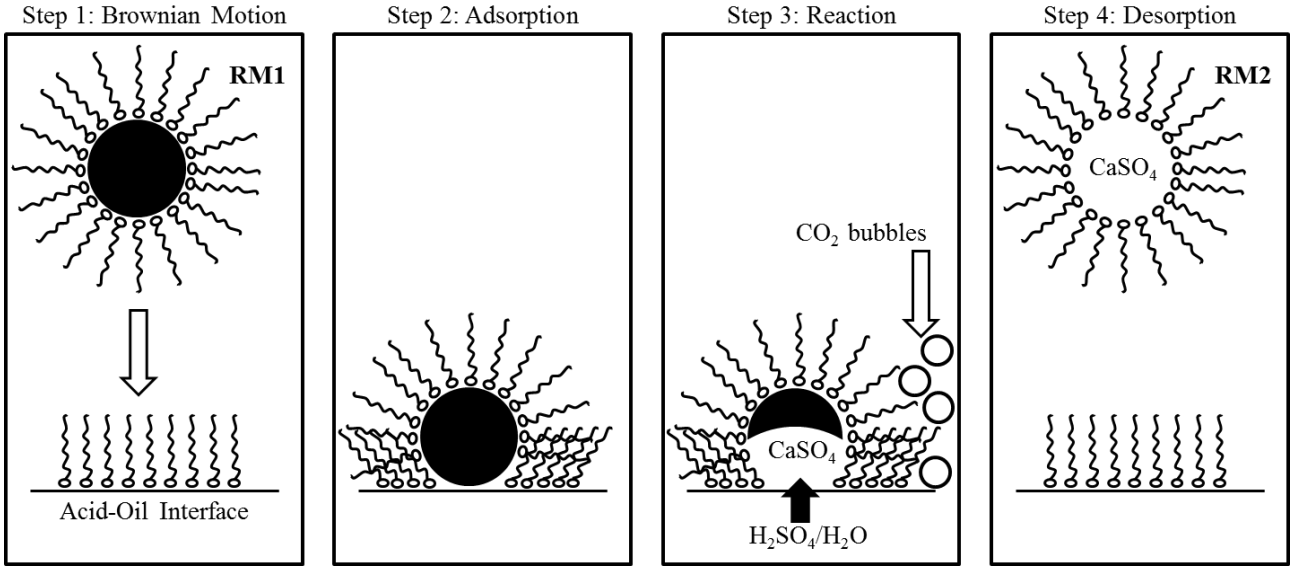

Figure 3.1. Neutralization mechanism between an acid droplet and $CaCO_3$ reverse micelle (adopted from Ref. 17).

Following diffusional approach by Brownian motion (step 1) of the micelle and a "sticky" collision, the second step is adsorption (step 2 in Figure 3.1) of an overbased reverse micelle (RM1) onto the acid/oil interface. A channel forms allowing the water and acid to enter into the micelle. The acid then reacts immediately with the $CaCO_3$ in the reverse micelle (step 3). After reaction, RM1 solubilizes the reaction products, becomes RM2, and desorbs back into the bulk oil (step 4). Another overbased reverse micelle can then adsorb onto the oil/acid interface, repeating the procedure. Wu et al. propose that the adsorption step (step 2 in Figure 3.1) is rate-limiting in the proposed interfacial neutralization mechanism, since the shrinking rate of the acid droplet increases as the concentration of $CaCO_3$ reverse micelles (BN) in the lube oil increases. However, their mechanism of the neutralization reaction was based on the fate of nitric acid droplets and not H_2SO_4 droplets in lube oil, since insoluble $CaSO_4$ was formed for the H_2SO_4-$CaCO_3$ reaction.[16,17] When H_2SO_4 was used instead of nitric acid, formation of needle-like $CaSO_4$ crystals was observed, which deposited at the H_2SO_4 droplet surface, eventually breaking down the droplet. This may slightly contradict with the proposed neutralization mechanism in Figure 3.1, i.e. the formed $CaSO_4$ deposits on the acid/oil interface on the oil side instead of being solubilized in the reverse micelles followed by desorption back into the bulk oil. Wu et al. suggest that the deposition of $CaSO_4$ crystals may inhibit further reaction between $CaCO_3$ reverse micelles and H_2SO_4 droplets.

Hosonuma and Tamura[14] found that the reaction products are formed inside the acid droplets, which agrees with the findings of Hone et al.[15] by their proposed base-transfer channel neutralization mechanism. Contrary, Wu et al.[17] advocate that it is the acid which is transferred to the overbased reverse micelles. However, there is a joint consensus that an effective collision between an overbased reverse micelle and an acid droplet is essential for the neutralization reaction to occur. Wu et al.[17] conclude in their study that the neutralization rate is independent of initial acid droplet size, whereas Hosonuma and Tamura[14] found a higher reactivity when decreasing the H_2SO_4 droplet size. Fu et al.[19] combine the two findings by suggesting that the neutralization rate is independent of droplet size until reaching a certain change point, where the acid droplet has shrunk to a certain size. After this point, the shrinking rate of acid droplets increases. This effect

was not observed by Wu et al. since they probably did not reach the change point in their study.[19] Also by use of capillary video-microscopy, Fu et al.[20] observed visually four different reaction behaviors between different cylinder lube oil formulations and H_2SO_4 droplets at temperatures in the range 25-170^oC: (1) $CaSO_4$ crystals and CO_2 gas bubbles were observed on the oil/acid interface on the oil side, (2) crystals and bubbles observed inside the acid droplet, (3) no crystals, but bubbles were found at the oil/acid interface on the oil side, and (4) no reaction products were observed. The first observation agrees with the results found by Wu et al.,[17] whereas the second observation may justify the neutralization mechanisms proposed by Hosonuma and Tamura[14] and Hone et al.,[15] which indicated that reaction products were found in the acid droplets.

To explain the different reaction behaviors, Fu et al.[20] introduced a strong-stick/weak-stick collision mechanism. A strong-stick collision is a result of direct exposure of the $CaCO_3$ core of the reverse micelles to the acid, thus destroying the rigid structure of the reverse micelles at the oil/acid interface. A weak-stick collision is where the rigid structure of the reverse micelles is maintained before desorbing back into the bulk oil and is dependent on the acid transfer into the core of the reverse micelle. A faster neutralization rate for a strong-stick collision is expected since the $CaCO_3$ is directly exposed to the acid. They further suggested that $CaSO_4$ crystal-growing reactions (reaction behavior 1 and 2) are a consequence of a higher frequency of strong-stick collisions occurring. This was supported by the fact that a higher shrinking rate of an acid droplet was found, when crystals were observed (~23 seconds to break down an acid droplet of 177 µm at 110-140^oC). The different observations of reaction products formation locations (reaction behavior 1 and 2) may be attributed to the use of different lube oil formulations, temperatures, and overbased detergents.[20] The study by Fu et al.[20] therefore indicates that increasing the neutralization reaction rate is a question of formulating cylinder oils which enhance the occurrence of strong-stick collisions.

The temperature dependence in the range 25-170^oC on the neutralization reaction was also investigated by Fu et al.[19] The neutralization rate increased around 1000 times at 170^oC, when comparing to the rate at 25^oC, which is a very notable effect. This effect was explained by a decrease of the time period that a base particle stays on the oil-acid interface of an acid droplet and increase of the frequency of effective collisions, thereby increasing the adsorption rate, thus increasing the neutralization reaction rate.

In the capillary video-microscopy technique investigations, great excess of $CaCO_3$ reverse micelles is found compared to H_2SO_4 on a molar basis.[20] This may not be representative for a large two-stroke marine diesel engine, where the molar ratio of H_2SO_4 and $CaCO_3$ is closer to stoichiometry.[1] Therefore, this study investigates if limitations are found for the oil-acid neutralization reaction at different molar ratios between H_2SO_4 droplets and $CaCO_3$ reverse micelles. In a large two-stroke marine diesel engine, roughly two different lube oil-H_2SO_4 interactions take place. (1) When the piston is at the top dead center (TDC) and moves downwards. Here, H_2SO_4 may condensate as a film on top of the lube oil film present at the cylinder liner. Since no mixing is occurring, transport of $CaCO_3$ micelles to the H_2SO_4 happens by diffusion. (2) When the piston moves towards TDC. Here, one important role of the piston rings is to spread and remove excess lube oil from the cylinder liner and combined with the high velocity of the piston, effective mixing of the condensed H_2SO_4 and lube oil, at the top of the piston, may be expected.

3.1.2 Aims of present work

The second H_2SO_4-lube oil interaction is investigated in this study, assuming that the high velocity of the piston contributes to a well-mixed lube oil-H_2SO_4 flow at the top of the piston. A mixed flow reactor (MFR) setup is therefore used to simulate the H_2SO_4-lube oil interaction at well-mixed conditions. The scope of this

paper is to investigate the neutralization reaction between H_2SO_4 droplets and $CaCO_3$ reverse micelles contained in a cylinder lube oil. This is done in a MFR setup by varying different operating conditions. The product samples are analyzed using Fourier Transform Infrared Spectroscopy (FTIR) and a potentiometric titration method to estimate the degree of conversion of H_2SO_4 droplets and $CaCO_3$ in the cylinder lube oil. The experimental results from the MFR setup can be used in the discussion of the problems found in a large two-stroke marine diesel engine.

3.2 Experimental section

3.2.1 Materials

The commercial lube oil used is obtained from Infineum with a base number (BN) value of 100 ± 2, which corresponds to (8.9 ± 0.18) wt.% $CaCO_3$.The BN is defined as the quantity of acid, expressed in terms of the equivalent number of milligrams of KOH, required to neutralize all alkaline constituents in one gram of sample.[24] The sulfuric acid is obtained from Sigma-Aldrich with a concentration of 95-98 wt.%. For calculations and experiments, an average concentration of 96.5 wt.% is used for the acid. For the potentiometric titration method, chlorobenzene, glacial acetic acid, and 0.1 M perchloric acid in glacial acetic acid are likewise received from Sigma-Aldrich.

3.2.2 Mixed flow reactor

To investigate the reaction between H_2SO_4 and the $CaCO_3$ contained in the lube oil, a mixed flow reactor (MFR) setup is used. The setup consists of three peristaltic pumps, which can provide flow rates between 7 µL/min and 380 mL/min depending on the type of tubing, a glass reactor (250 mL), and a motor-driven stirrer (stirrer speed up to 1200 rpm) as shown in Figure 3.2.

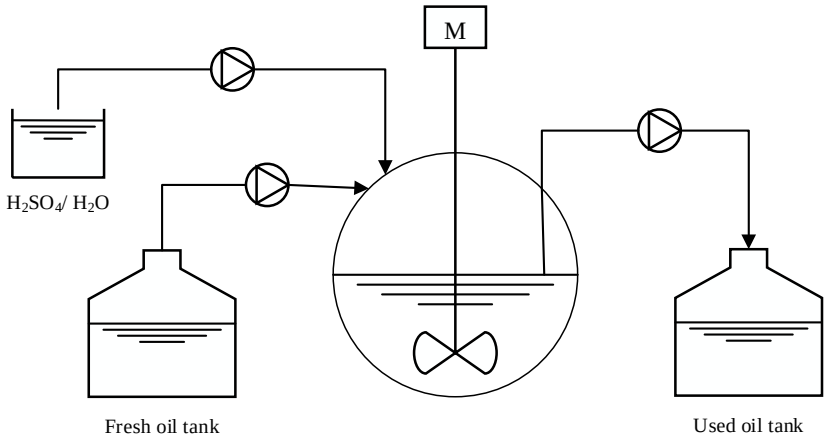

Figure 3.2. Schematic representation of the experimental setup.

The two inlet pumps supply the reactor with H_2SO_4/H_2O-solution as droplets and fresh 100 BN lube oil, respectively, whereas the third pump is an outlet pump controlling the level inside the reactor. A MFR is assumed to achieve perfect mixing, where the outlet composition is identical to the composition inside the reactor. The degree of conversion can then be studied inside the MFR by sampling and analysis of the outlet stream. The first step of the experimental procedure is feeding of H_2SO_4 solution as droplets and lube oil to the MFR, where the $CaCO_3$ in the lube oil reacts with H_2SO_4. A product sample is collected after five

residence times to make sure that steady state is reached.[25] Immediately after sampling, the sample is analyzed by an FTIR to estimate the conversion of the $CaCO_3$ in the lube oil (denoted 'fast analysis'). Practically this takes a couple of minutes and includes sampling, preparation of the sample, and measuring time. After additional stirring of the product sample to ensure complete reaction of H_2SO_4 droplets with $CaCO_3$, another IR spectrum is obtained (denoted 'complete conversion analysis'). By comparing these two results, it is possible to conclude whether all the added H_2SO_4 droplets have reacted with the $CaCO_3$ in the lube oil within the specified residence time in the MFR.

A range of different operating conditions are investigated, varying stirrer speed, H_2SO_4 concentration, residence time, and inlet $CaCO_3/H_2SO_4$ molar ratio. Typical operating conditions are: max stirrer speed (1200 rpm), concentrated H_2SO_4 droplets in the inlet stream, and a residence time in the reactor of about 3 minutes. However, the effect of a stirrer speed down to around 120 rpm, a residence time down to around 1 minute, and a H_2SO_4 concentration of 38.3 wt.% are also investigated. Lastly, $CaCO_3/H_2SO_4$ molar ratios in the inlet streams between 1 and 10 are investigated. A low ratio implies that more H_2SO_4 is fed to the MFR compared to the $CaCO_3$ in the lube oil (on a molar basis), resulting in a higher consumption of $CaCO_3$ at complete conversion of acid. When the ratio is 1, 100% conversion of the $CaCO_3$ in the lube oil is achieved at complete acid conversion.

3.2.3 Analysis methods

Fourier Transform Infrared Spectroscopy (FTIR) is used to analyze the product samples immediately after sampling. It is then possible to calculate how much of the inlet H_2SO_4 and $CaCO_3$ that have reacted within the residence time in the reactor. The measurements were done on a Thermo Scientific Nicolet iS50 FTIR-ATR (Attenuated Total Reflectance) spectrometer. The infrared spectra are recorded using a resolution of 4 cm^{-1} and 32 scans in the wavenumber range of 400-4000 cm^{-1}. The IR spectrum is unique for each chemical compound, making the approach applicable for identifying $CaCO_3$ and $CaSO_4$. To measure a concentration of $CaCO_3$ in the product lube oil sample a calibration curve is constructed, combining the peak height/area (output from an IR spectrum) to the concentration. A Mettler Toledo T50 potentiometric titrator is used for this purpose following the standard test method for measuring base number in lube oil, ASTM D-2896.[24] This analysis technique measures the concentration of $CaCO_3$ in a lube oil sample and the value is then converted to the unit of BN. The repeatability of the method showed a 2*s* (*s* = sample standard deviation) of less than ± 3 % from the mean, by measuring on fully formulated unused lube oil samples with base numbers in the range 6 to 100. This repeatability is consistent with that reported for the standard test method.[24] The calibration curve is constructed by mixing lube oil with H_2SO_4 in different ratios, i.e. from 10% to 90% conversion of the $CaCO_3$ in the lube oil. After stirring of the samples till complete conversion of the added H_2SO_4, they are analyzed in the titrator and then analyzed by FTIR. The resulting IR spectra are analyzed in OriginPro 2015, extracting peak height and peak area by defining the baseline as a straight line connecting the end points of the respective peak. The calibration curve is constructed based on the $CaCO_3$ peak, due to a better linear fit compared to using the $CaSO_4$ peak. The resulting calibration curve is shown in Figure 3.3 for the peak height of the $CaCO_3$ peak. Duplicate analyses are performed on each sample for the titrator method, i.e. the y-axis of Figure 3.3 is an average. The FTIR analyses are based on single measurements. To estimate the accuracy of the calibration curve, lube oil-H_2SO_4 samples are analyzed both by the titrator and the FTIR. The measured BN from the titrator is then compared to the BN calculated by the calibration curve (Figure 3.3). This analysis shows a difference of 2 BN (2*s*, *s* = sample standard deviation) between the two methods, i.e. roughly within the uncertainty of the titrator method. A similar result is found using the $CaCO_3$ peak area calibration curve. This means that the FTIR, by use of the calibration curve, can measure the concentration

of $CaCO_3$ (BN) in an unknown sample within ± 2 BN. The repeatability of the FTIR method lies within ± 1 % (2*s*), which is within the uncertainty of the calibration curve method. The experiments are carried out at ambient temperature and pressure, however, due to the heat of reaction between $CaCO_3$ and H_2SO_4 droplets, the temperature in the MFR increased till steady state. The difference in temperature did not influence the resulting IR spectra noticeably.

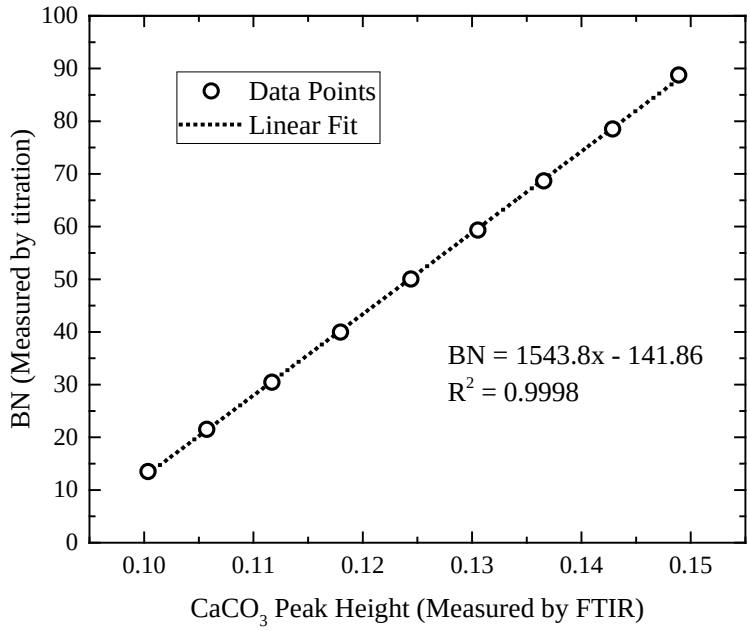

Figure 3.3. Calibration curve connecting the BN determined by the titrator with the peak height of the $CaCO_3$ peak measured by FTIR. The circles are measurements and the dotted line is a linear fit curve.

3.3 Results and discussions

A series of experiments was conducted in the MFR setup, varying the $CaCO_3/H_2SO_4$ (Ca/S) molar ratio in the inlet stream, residence time (τ), stirrer speed (N), and H_2SO_4 droplet concentration in the inlet stream, followed by analysis with the FTIR spectrometer. The experimental settings for each experiment are presented in Table 3.1.

Here, experiments 3-4 and 6-9 investigate the effect of residence time, 3 and 9-12 the effect of stirrer speed, 1-5 and 9 the effect of Ca/S molar ratio, and 4 and 13 the effect of concentration of inlet H_2SO_4. Figures 3.4, 3.5, 3.6, and 3.7 show results of the percentage conversion of $CaCO_3$ in the lube oil and H_2SO_4 as a function of the Ca/S molar ratio. The Ca/S molar ratio (x-axis of the figures) is calculated based on the inlet flow rates of H_2SO_4 and lube oil, respectively.

Table 3.1 Experimental settings for the lube oil-H_2SO_4 experiments in the MFR, varying $CaCO_3/H_2SO_4$ molar ratio (Ca/S), residence time (τ), stirrer speed (N), and H_2SO_4 concentration ($C_{H_2SO_4}$) in the inlet stream.

Exp. #	Ca/S (mol/mol)	τ (min)	N (rpm)	$C_{H_2SO_4}$ (wt.%)
1	9.18	3.3	1200	96.5
2	3.86	3.1	1200	96.5
3	2.12	3.1	1200	96.5
4	1.26	3.5	1200	96.5
5	1.11	3.0	1200	96.5
6	1.93	0.8	1200	96.5
7	1.38	1.9	1200	96.5
8	1.40	0.9	1200	96.5
9	2.08	2.5	1200	96.5
10	1.94	2.5	600	96.5
11	1.94	2.5	120	96.5
12	1.94	2.5	360	96.5
13	1.30	2.9	1200	38.3

Two measurements are made for each inlet flow, and an average is used to calculate Ca/S. The uncertainty of this procedure is not shown in the figures. The conversion of $CaCO_3$ in the lube oil is calculated as:

$$X_{CaCO_3}\,(\%) = \left(1 - \frac{BN_{outlet}}{BN_{inlet}}\right)\cdot 100\%, \tag{3.2}$$

where the BN of the outlet sample is measured and calculated by FTIR and use of Figure 3.3. The conversion of H_2SO_4 is calculated as:

$$X_{H_2SO_4}\,(\%) = \frac{\left(\frac{(BN_{inlet}-BN_{outlet})\nu_{oil}\rho_{oil}}{2M_{KOH}}\right)}{\left(\frac{\nu_{H_2SO_4}\rho_{H_2SO_4}w_{H_2SO_4}}{M_{H_2SO_4}}\right)}\cdot 100\%, \tag{3.3}$$

where the numerator is the molar flow of reacted H_2SO_4 in the MFR and the denominator is the inlet molar flow of H_2SO_4. The reacted molar flow of H_2SO_4 is calculated as the difference between the molar inlet $CaCO_3$ and outlet $CaCO_3$. The following parameters are used: volumetric flow rate (ν_i), density (ρ_i), the molar weight (M_i), and the weight fraction of H_2SO_4 in the H_2SO_4 inlet flow ($w_{H_2SO_4}$). The number '2' comes from the stoichiometry between the $CaCO_3$/KOH-H_2SO_4 reactions since the unit of BN is mg KOH per g sample.

The dotted line in the figures presents the conversion of $CaCO_3$ in lube oil, when the reaction between $CaCO_3$ and H_2SO_4 droplets is instantaneous and complete, i.e. all added H_2SO_4 has reacted since Ca/S > 1. For a Ca/S molar ratio of 4, the molar ratio between $CaCO_3$ and H_2SO_4 is 4. When all H_2SO_4 has reacted with $CaCO_3$, 25% conversion of the $CaCO_3$ in the lube oil is expected, as the dotted curve predicts. The

measured conversion of $CaCO_3$ in the MFR (denoted 'Fast Analysis' in figures) at specific conditions is then compared to this curve. If equal, within the uncertainties, it means that complete conversion between H_2SO_4 droplets and $CaCO_3$ has been reached in the MFR setup. The measured conversions of $CaCO_3$ in the lube oil in the MFR are presented by the squared symbols in Figures 3.4, 3.6, and 3.7. The circled symbols present the measured conversion of $CaCO_3$ in the lube oil sample at complete conversion (after additional reaction time with stirring of the samples). Ideally, the complete conversion measurements and the dotted curve should be equal to each other. When there is a difference between the complete conversion points (circles) and fast analysis point (squares), e.g. when Ca/S approaches 1, complete conversion of H_2SO_4 droplets was not achieved in the MFR. The numbers in the figures identify each experiment according to Table 3.1. The effects of varying the described parameters are discussed in the following sub-sections.

3.3.1 Experimental Uncertainty

The experimental uncertainty can be estimated by comparing experiments 3 and 9 (called experiment 3/9). Table 3.1 reveals minor differences in residence time and Ca/S molar ratio between the two experiments due to variations in the oil flow from day to day dependent of wear of tubing, among others. Average $CaCO_3$ conversions and $2s$ (s = sample standard deviation) for the fast and complete conversion analysis sample are calculated to be 46.51% ± 4.29% and 47.62% ± 3.40% with a Ca/S molar ratio of 2.10 ± 0.06. Average H_2SO_4 conversions and standard deviations for the fast and complete conversion analysis sample are found to be 97.74% ± 5.99% and 100.08% ± 4.06%, respectively. It is worth noting that the conversion of H_2SO_4 exceeds 100%, which is not possible. The reason is that a minor deviation on the Ca/S determination has a significant impact on the conversion calculation especially at lower Ca/S molar ratios. The two times sample standard deviations for experiment 3/9 are shown in Figures 3.4, 3.5, 3.6, and 3.7 as error bars.

3.3.2 Ca/S molar ratio

The effect of varying the Ca/S molar ratio in the range 9.18-1.11 is shown in Figures 3.4 and 3.5. Figure 3.5 shows the conversion of H_2SO_4 droplets as a function of Ca/S molar ratio. Data points for experiment 1 are not shown in Figure 3.5. The figures show that the conversions for the fast and complete analysis sample for experiments 1, 2, and 3/9 are equal to each other within the uncertainties. This means that all the H_2SO_4 droplets react with the $CaCO_3$ in the lube oil within the available residence time in the MFR. Contrary to this, for experiments 4 and 5 only 85.6% and 82.6%, respectively, of the available H_2SO_4 reacts with the $CaCO_3$. This indicates that the H_2SO_4-$CaCO_3$ total reaction rate slows down, when reaching a critically low Ca/S molar ratio value and becomes more pronounced when the Ca/S value is decreased further. The explanation for such an observation could be that the neutralization reaction is controlled by the rate of micelle adsorption (or desorption) onto the acid droplets. According to the Gibbs adsorption equation,[26] a decrease in surfactant (in this work a $CaCO_3$ micelle) concentration results in a decrease in adsorption. At decreasing Ca/S molar ratio, the concentration of $CaCO_3$ micelles decreases significantly compared to the H_2SO_4 droplets. The reduction in conversion of H_2SO_4 droplets at lower Ca/S ratios can therefore be explained by a decrease in adsorption rate of the $CaCO_3$ micelles on the H_2SO_4 droplet, thereby reducing the total reaction rate of $CaCO_3$ micelles. Wu et al.[17] also suggested that for an acid droplet (µm-sized) the adsorption of $CaCO_3$ micelles on the H_2SO_4 droplet interface is the controlling step in the neutralization reaction mechanism. The present study addresses further that the effect of reducing adsorption becomes noticeable at a Ca/S ratio lower than around 2 for the conditions studied.

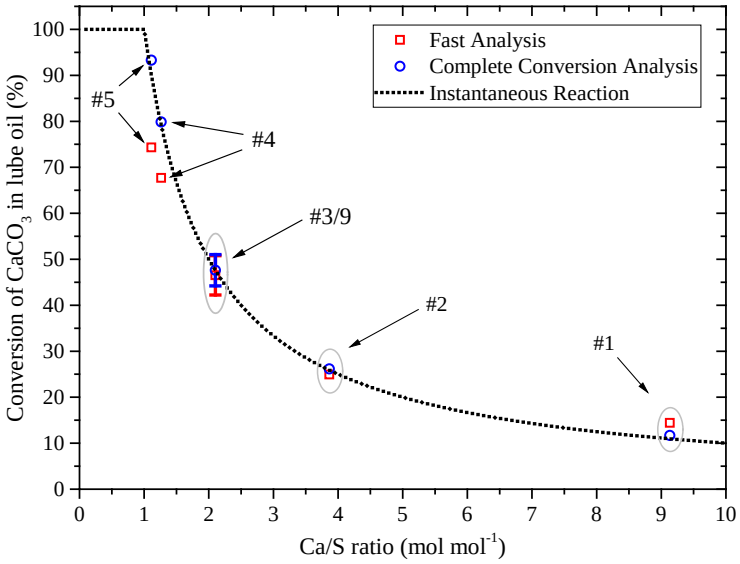

Figure 3.4. Effect of varying Ca/S molar ratio on the $CaCO_3$ conversion in the lube oil.

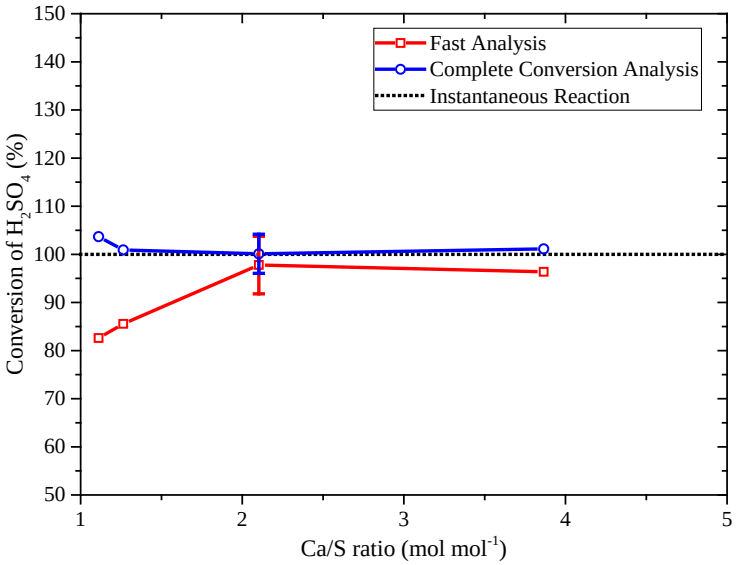

Figure 3.5. Effect of varying the Ca/S molar ratio on the H_2SO_4 conversion.

The observation that the H_2SO_4-consumption is diminished when the excess of $CaCO_3$ is reduced (corresponds to a lower Ca/S molar ratio) could also indicate that the reaction is mixing limited. Even though maximum stirrer speed is applied, it may be impossible to achieve perfect mixing. Therefore, when most of the H_2SO_4 droplets are converted, insufficient contact between H_2SO_4 droplets and $CaCO_3$ micelles may arise, having some local depletion regions with an excess of H_2SO_4 droplets in the lube oil compared to $CaCO_3$, resulting in incomplete reaction of the added H_2SO_4. Both explanations describe that the limiting factor is a reduced contact between $CaCO_3$ micelles and H_2SO_4 droplets at lower Ca/S ratio. The results suggest that by having a Ca/S molar ratio larger than around 2, complete conversion of H_2SO_4 droplets is obtained in the MFR.

3.3.3 Residence time

The effect of residence time was investigated at two different Ca/S molar ratios. Experiments 3/9 and 6 investigate the effect of residence time at Ca/S equal to around 2. Figure 3.6 shows that the data points for these experiments lie on the dotted curve. Complete conversion of the H_2SO_4 droplets was therefore obtained within the range of residence times (0.8-2.8 min). When the Ca/S molar ratio was decreased to 1.3-1.4 (experiments 4, 7, and 8), conversion of the H_2SO_4 droplets in the MFR was limited to 85.6-91.2%. By decreasing the residence time from 1.9 min to 0.9 min (experiment 7 and 8, respectively), only a very minor difference in the degree of conversion is found. Even though the residence time in experiment 4 is higher (3.5 min) than in experiment 7 (1.9 min) and 8 (0.9 min), a larger difference between the fast and complete conversion analysis data points is found. This is attributed to the lower Ca/S molar ratio in experiment 4 compared to experiment 7 and 8. Based on these results, we conclude that within the investigated range the residence time does not influence the $CaCO_3$-H_2SO_4 reaction. This illustrates that the reaction is very fast at well-mixed conditions. However, the $CaCO_3$-H_2SO_4 reaction becomes limited in the MFR at a Ca/S molar ratio somewhere between 1.4 and 1.9, as also shown in Figures 3.4 and 3.5.

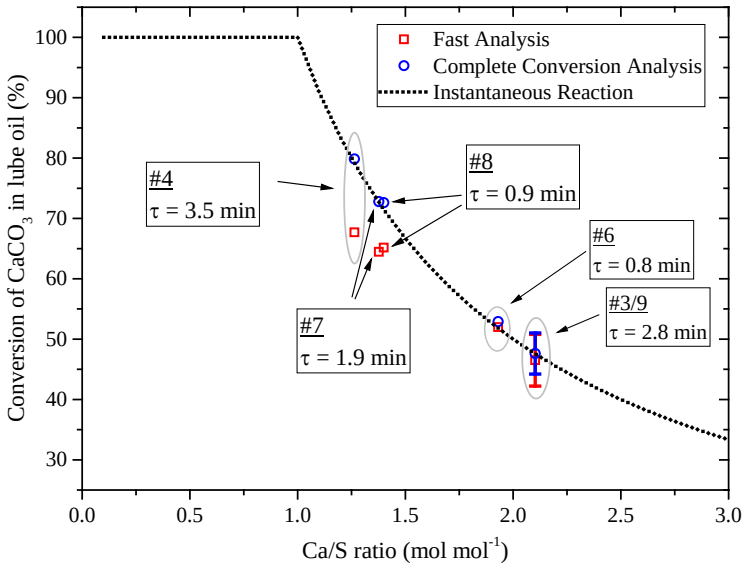

Figure 3.6. Effect of varying the residence time (τ) on the $CaCO_3$ conversion in the lube oil.

3.3.4 Stirrer speed

The results of varying the stirrer speed and inlet H_2SO_4 concentration are presented in Figure 3.7. Stirrer speeds ranging from 120 rpm to 1200 rpm at a residence time of 2.5 min are investigated. Reducing the stirrer speed by a factor of three (settings 1200 rpm, 600 rpm, and 360 rpm) has only a minor impact on the conversion, both for the fast analysis and complete analysis measurement. However, when reducing the stirrer speed down to 120 rpm (a factor of 10), the conversion of $CaCO_3$ in the lube oil decreases roughly from 50% to 40%, with similar conversions observed for the fast and complete analysis, respectively. This is attributed to insufficient mixing between H_2SO_4 droplets and lube oil, augmented by sedimentation of the heavier H_2SO_4. Still, most of the added H_2SO_4 droplets do react with the $CaCO_3$ (around 80%). This implies again that the reaction between H_2SO_4 droplets and $CaCO_3$ reverse micelles is very fast. An experiment without mixing was also carried out. Lube oil and H_2SO_4 were dosed in a beaker without applying any

stirring, but with an excess of H_2SO_4 compared to $CaCO_3$, on a molar basis. FTIR spectra were obtained approximately one week after, showing that no reaction had occurred in the bulk lube oil. Lube oil samples were collected at different locations in the beaker. This implies that some degree of stirring is needed in order to create the contact between H_2SO_4 and the $CaCO_3$ micelles to initiate the neutralization reaction. The Brownian motion of the micelles alone is apparently not sufficient to react with H_2SO_4 in a measurable degree over the lube oil-acid boundary. Wu et al.[16,17] found that a H_2SO_4 droplet reacts immediately after injection into the lube oil. However, they injected single, µm-sized acid droplets, whereas, in the present experiments, where much larger amounts of acid are introduced, H_2SO_4 sediment and reaction can only take place over the lube oil-acid boundary. The Ca/S ratio in the lube oil-acid boundary may be significantly smaller than the Ca/S ratio for a small droplet in lube oil. Therefore, the adsorption is significantly lower in the lube oil-acid interface, thus no reaction is observed in the bulk lube oil.

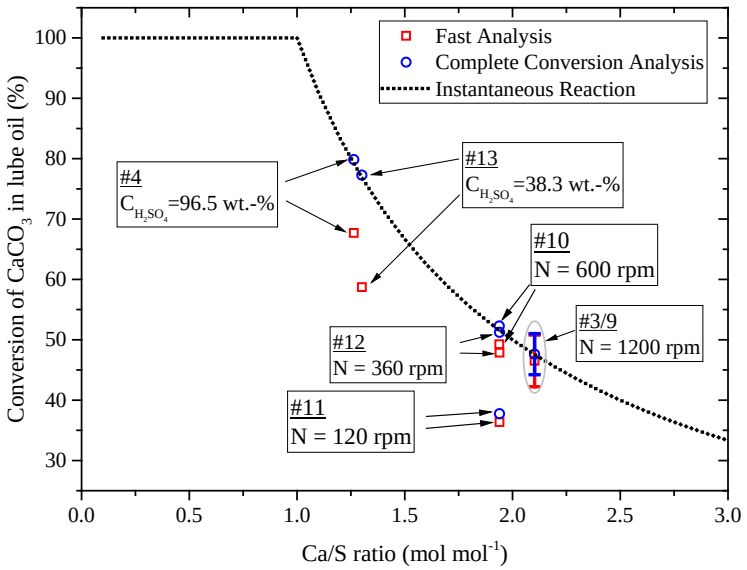

Figure 3.7. Effect of varying the inlet concentration of H_2SO_4 and stirrer speed (N) on the $CaCO_3$ conversion in the lube oil.

3.3.5 H_2SO_4 inlet concentration

In a large two-stroke marine diesel engine, almost pure H_2SO_4 condenses just below the top dead center position (TDC), whereas the concentration is lower in the lower part of the cylinder liner,[27] due to the higher temperature at TDC.[20] Therefore, experiments were carried out with two different H_2SO_4 concentrations: 96.5 wt.% and 38.3 wt.% at a Ca/S molar ratio of around 1.3. The results are presented in Figure 3.7. The results show that the complete conversion samples are in accordance with the dotted curve. It is observed that less $CaCO_3$ has reacted in the MFR in experiment 13 (38.3 wt.% H_2SO_4) compared to experiment 4 (96.5 wt.% H_2SO_4). This indicates that a lower concentration of H_2SO_4 droplets yields a lower conversion of $CaCO_3$ in the lube oil. However, the use of a diluted H_2SO_4 also introduces more water to the lube oil, and a new calibration curve was constructed. The new calibration curve did only consist of two calibration points at 72% and 82% conversion of $CaCO_3$ respectively but is used to predict a conversion around 60% which is outside the calibration interval. The effect of this is investigated for the calibration curve in Figure 3.3, predicting a conversion in the range of 50%. This yields only a deviation of ± 0.5 BN, compared to using the full calibration curve. Therefore, the difference in $CaCO_3$ conversion of experiment 4 and 13 is probably not

due to less data point in the calibration curve constructed for the 38.3 wt.% H_2SO_4 experiment. The reason could be that the increase in water content decreases the contact between H_2SO_4 and $CaCO_3$ micelles in the MFR setup, further inhibiting the neutralization reaction. Taking the uncertainties into account and a slightly different Ca/S molar ratio, the difference between the two experiments is not significant.

3.3.6 Implications for large two-stroke diesel engines

When the $CaCO_3$-H_2SO_4 reaction approaches stoichiometry (Ca/S = 1), the H_2SO_4 conversion was reduced significantly and it was not possible to reach complete conversion in the MFR setup. This observation was independent of residence time within the range investigated. It was further noted, when starting to add H_2SO_4 droplets into the lube oil, an initiation time of approximately 10 seconds should elapse, before reaction was observed (sudden change in color, due to the heavy formation of CO_2 bubbles from the neutralization reaction). Even with a reduced stirrer speed, complete conversion of the H_2SO_4 droplets and $CaCO_3$ reverse micelles could be observed (experiment 11). It was also found that no reaction takes place when no stirring was applied. This implies that the reaction between H_2SO_4 droplets and $CaCO_3$ reverse micelles is instantaneous in the lube oil when contact has been established by some degree of stirring.

In a large two-stroke marine diesel engine, the role of the piston rings is to spread and remove excess lube oil from the cylinder liners. This fast movement will cause some degree of mixing/stirring of the lube oil at the top of the piston, justifying that the conditions, for the mixing of H_2SO_4 and lube oil films in a large two-stroke marine diesel engine, can be approximated in the MFR setup, but this has not yet been confirmed. It is unknown whether the conclusions also apply when only having film-film interaction in an engine. By varying the stirrer speed it was seen that even at lower stirrer speeds, the reaction between H_2SO_4 droplets and $CaCO_3$ micelles was fast. The stirring from cycle to cycle of the lube oil inside an engine does not necessarily need to be well-mixed in order to reach complete conversion of all the condensed H_2SO_4, but a certain degree is needed, however. We conclude based on this study that the neutralization of H_2SO_4 droplets by the $CaCO_3$ micelles in the lube oil is very fast. However, corrosion of the cylinder liners is still an issue, presumably because of other factors.

Local molar excess of condensed H_2SO_4 compared to $CaCO_3$ in the lube oil film could be one situation of concern. Here all the $CaCO_3$ would be consumed locally and H_2SO_4 can then interact with the cylinder liner directly. This may happen if a local cold spot is occurring, accelerating the condensation of H_2SO_4 on the cylinder liner. A large portion of water could also condense, breaking apart the lube oil film. The results showed that the H_2SO_4 conversion was reduced when Ca/S approached 1, therefore, even stoichiometric amounts of H_2SO_4 and $CaCO_3$ locally in the lube oil film could result in corrosion issues. According to the results, a Ca/S molar ratio larger than 2 is required to obtain complete conversion of the added H_2SO_4 droplets within the residence time range investigated. This can be achieved by increasing the feeding rate of the lube oil into the cylinder liner or increase BN in the lube oil. Incomplete mixing/stirring from stroke to stroke of the lube oil-H_2SO_4 by the piston may also result in acid-steel interaction since the experiments showed that this decreases the contact between H_2SO_4 droplets and $CaCO_3$ micelles. A significant part of the dosed lube oil into the cylinder liners can combust, losing $CaCO_3$ to the combustion air. In this study, it is assumed that only a negligible amount of lube oil is lost to the combustion air.

The most severe cylinder liner corrosion wear is seen near the TDC. An explanation could be that the upward motion of the piston collects the condensed acid above the top piston ring, and the acid cannot be neutralized quickly enough to prevent their corrosive action.[21] The lacking ability to neutralize the H_2SO_4 may be

explained by the findings outlined above, namely lack of proper mixing and excess of H_2SO_4 compared to $CaCO_3$ at local locations on the cylinder liners.

In practice, other issues than cold corrosion occur in the combustion chambers in large two-stroke diesel engines. These issues could be related to lacquering (film formed from the lube oil on cylinder liners and piston rings), scuffing (large metal-metal welding), etc. However, this was not covered in this work.

The MFR setup is scaled based on an approximate residence time in a large two-stroke marine diesel engine, which is calculated to be less than 4 minutes for a cylinder liner with a height of 3.45 m, diameter of 0.8 m, a lube oil thickness of 10 µm, and a lube oil flow rate of 23 ml/min. However, some of the lube oil stays in the engine for much shorter or longer time.[2,28] The experiments were carried out at room temperature and atmospheric pressure, which are different from real conditions in a large two-stroke marine diesel engine. An increase in temperature dramatically increases the total reaction rate,[2,15,19] and a faster reaction between H_2SO_4 droplets and $CaCO_3$ micelles is expected in a real application. This may decrease the effect of the observed limitation of the $CaCO_3$-H_2SO_4 reaction at lower Ca/S molar ratios. Only a minor difference is expected for the variation in pressure. The size of the H_2SO_4 droplets added to the MFR is in the millimeter-size range and the effect of varying droplet size is not investigated in the present study. The size of the acid droplets could have an effect on the neutralization reaction if H_2SO_4 is condensing on the lube oil film as a mist (aerosols). However, the most pronounced corrosion may be encountered, when larger H_2SO_4 droplets condense on the cylinder liner.[14]

3.4 Conclusions

The focus of this study has been to investigate the reaction between H_2SO_4 droplets and $CaCO_3$ micelles present in lube oil in a MFR at different conditions such as stirrer speed, H_2SO_4 concentration, residence time, and Ca/S molar ratio. The results show that the H_2SO_4-$CaCO_3$ reaction is not dependent on the investigated residence times. Furthermore, the H_2SO_4 conversion was reduced, when the Ca/S molar ratio approached unity, which may be explained by a significant reduction of the adsorption rate of $CaCO_3$ micelles on the H_2SO_4 droplets and insufficient macromixing, but this has not yet been confirmed. A certain degree of stirring is required in order to establish contact between H_2SO_4 droplets and $CaCO_3$ reverse micelles to initiate and maintain the reaction. The present study only investigated the $CaCO_3$ consumption from H_2SO_4 droplets, but $CaCO_3$ may also be consumed directly or indirectly by other species, e.g. SO_2.

The observations found here suggest that the neutralization reaction between H_2SO_4 droplets and $CaCO_3$ micelles in the lube oil is very fast and instantaneous in a real engine application if the cylinder liner is well-wetted, the oil-film is well-mixed, and contains an excess of $CaCO_3$ compared to the condensed H_2SO_4 (Ca/S > 2). Unfortunately, these ideal conditions may not be present in a large two-stroke marine diesel engine. This advocate that the workload of reducing the corrosion wear issue not necessarily should only lie in the optimization of the lube oil itself, but also the way lube oil is introduced into the engine and how it is spread out on the cylinder liner and perhaps other factors.

Acknowledgments

This work is part of the Combustion and Harmful Emission Control (CHEC) research center at the Department of Chemical and Biochemical Engineering at Technical University of Denmark. The project is funded by the Innovation Fund Denmark and co-sponsored by MAN Energy Solutions and Technical University of Denmark through the SULCOR project under grant 4106-00028B.

References

(1) MAN Diesel & Turbo. Service Letter SL2014-587/JAP. 2014.

(2) García, L.; Gehle, S.; Schakel, J. Impact of Low Load Operation in Modern Low Speed 2-Stroke Diesel Engines on Cylinder Liner Wear Caused by Increased Acid Condensation. *J. JIME* **2014**, *49* (1), 100–106.

(3) Adamkiewicz, A.; Drzewieniecki, J. Operational Evaluation of Piston Ring Wear in Large Marine Diesel Engines. *J. Polish CIMAC* **2012**.

(4) Amblard, C. New Chemistry to Protect against Cold Corrosion in Marine Cylinder Lubricants. *J. Japan Inst. Mar. Eng.* **2015**, *50* (6), 54–62.

(5) Golothan, D. W. Review of the Causes of Cylinder Wear in Marine Diesel Engines. *Inst. Mar. Eng. Trans.* **1978**, *90*, 137–163.

(6) Cordtz, R. L.; Schramm, J.; Rabe, R. Investigating SO_3 Formation from the Combustion of Heavy Fuel Oil in a Four-Stroke Medium Speed Test Engine. *Energy Fuels* **2013**, *27* (10), 6279–6286.

(7) Cordtz, R.; Schramm, J.; Andreasen, A.; Eskildsen, S. S.; Mayer, S. Modeling the Distribution of Sulfur Compounds in a Large Two Stroke Diesel Engine. *Energy Fuels* **2013**, *27* (3), 1652–1660.

(8) Naegeli, D. W.; Marbach, H. W. Role of Sulfur Oxides in Wear and Deposit Formation in Army Diesel Engines. Interim Report BFLRF No. 248, Contract No. DAAK70-87-C-0043. Southwest Research Institute: San Antonio, Texas, 1988.

(9) Nagaki, H.; Korematsu, K. Relation Between Diffusion Process of Sulfur Oxides in Exhaust Gas into Oil Film and Wear of Cylinder Liner and Piston Rings in Diesel Engines. *SAE Pap.* **1991**.

(10) Nagaki, H.; Korematsu, K. Effect of Sulfur Dioxide in Recirculated Exhaust Gas on Wear within Diesel Engines - (Relationship between Wear and Amount of SO_2 Absorbed by Lubricating Oil Film). *JSME Int. J. Ser. B-Fluids Therm. Eng.* **1995**, *38* (3), 465–474.

(11) Nagaki, H.; Korematsu, K. Effect of SO_2 in Recirculated Exhaust Gas on Wear in Diesel Engine - (Effect of SO_2 Added to Intake Air on Wear). *JSME Int. J. Ser. B-Fluids Therm. Eng.* **1996**, *39*, 193–201.

(12) Mortier, R. M.; Fox, M. F.; Orszulik, S. T. *Chemistry and Technology of Lubricants*, 3rd ed.; Springer Netherlands: Dordrecht, 2010.

(13) Wu, R. C.; Campbell, C. B.; Papadopoulos, K. D. Acid-Neutralizing of Marine Cylinder Lubricants: Effects of Nonionic Surfactants. *Ind. Eng. Chem. Res.* **2000**, *39* (10), 3926–3931.

(14) Hosonuma, K.; Tamura, K. Acid Neutralization of Overbased Detergents (Part 2) Neutralization with Sulfuric Acid Emulsion. *J. Japan Pet. Inst.* **1984**, *27* (2), 108–113.

(15) Hone, D. C.; Robinson, B. H.; Steytler, D. C.; Glyde, R. W.; Galsworthy, J. R. Mechanism of Acid Neutralization by Overbased Colloidal Additives in Hydrocarbon Media. *Langmuir* **2000**, *16* (2), 340–346.

(16) Wu, R. C.; Papadopoulos, K. D.; Campbell, C. B. Visualization Test for Neutralization of Acids by

Marine Cylinder Lubricants. *AIChE J.* **1999**, *45* (9), 2011–2017.

(17) Wu, R. C.; Papadopoulos, K. D.; Campbell, C. B. Acid-Neutralizing of Marine Cylinder Lubricants: Measurements and Effects of Dispersants. *AIChE J.* **2000**, *46* (7), 1471–1477.

(18) Fu, J.; Lu, Y.; Campbell, C. B.; Papadopoulos, K. D. Optical Microscopy inside a Heating Capillary. *Ind. Eng. Chem. Res.* **2005**, *44* (5), 1199–1203.

(19) Fu, J.; Lu, Y.; Campbell, C. B.; Papadopoulos, K. D. Temperature and Acid Droplet Size Effects in Acid Neutralization of Marine Cylinder Lubricants. *Tribol. Lett.* **2006**, *22* (3), 221–225.

(20) Fu, J.; Lu, Y.; Campbell, C. B.; Papadopoulos, K. D. Acid Neutralization by Marine Cylinder Lubricants Inside a Heating Capillary: Strong/Weak-Stick Collision Mechanisms. *Ind. Eng. Chem. Res.* **2006**, *45* (16), 5619–5627.

(21) Fu, J.; Papadopoulos, K. D.; Lu, Y.; Campbell, C. B. Ostwald Ripening: A Decisive Cause of Cylinder Corrosive Wear. *Tribol. Lett.* **2007**, *27* (1), 21–24.

(22) Garcia-Bermudes, M.; Rausa, R.; Papadopoulos, K. Formation of Colloidal Shells on Acidic Droplets Undergoing Neutralization in Marine Diesel Engine Cylinder Oils. *Tribol. Lett.* **2013**, *51* (1), 85–92.

(23) Duan, Y.; Rausa, R.; Zhao, Q.; Papadopoulos, K. D. Neutralization Mechanism of Acetic Acid by Overbased Colloidal Nanoparticles. *Tribol. Lett.* **2016**, *64* (8), 1–11.

(24) ASTM International. ASTM 2896-11. Standard Test Method for Base Number of Petroleum Products by Potentiometric Perchloric Acid Titration. 2011.

(25) Fogler, H. S. *Elements of Chemical Reaction Engineering*; Prentice Hall PTR: New Jersey, 2006.

(26) Kontogeorgis, G. M.; Kiil, S. *Introduction to Applied Colloid and Surface Chemistry*; John Wiley & Sons, Ltd: Chichester, UK, 2016.

(27) Stott, F. H.; Macdonald, A. G. The Influence of Acid Strength on the Corrosive Wear of Grey Cast Irons in Oil-Sulphuric Acid Mixtures. *Wear* **1988**, *122* (3), 343–361.

(28) Doyen, V.; Drijfholt, R. K.; Delvigne, T. PAPER NO .: 61 Advanced Applied Research Unravelling the Fundamentals of 2-Stroke Engine Cylinder Lubrication – an Innovative on-Line Measurement Method Based on the Use of Radioactive Tracers-. *CIMAC Congr. 2007, Vienna* **2007**.

4 | Mixed flow reactor experiments and modeling of sulfuric acid neutralization in lube oil for large two-stroke diesel engines

Preceding work of this chapter can be found in Appendix A (lube oil analyses to determine and quantify the alkaline core of the overbased detergent) and Appendix B (investigation of the well-mixed lube oil film assumption by use of computational fluid dynamics simulations).

This chapter is based on the published article “Mixed flow reactor experiments and modeling of sulfuric acid neutralization in lube oil for large two-stroke diesel engines”, published in Industrial & Engineering Chemistry Research. The article was published in print January 9, 2019, and is available under the following DOI: 10.1021/acs.iecr.8b05808. The supporting information for this chapter can be found in Appendix C and D.

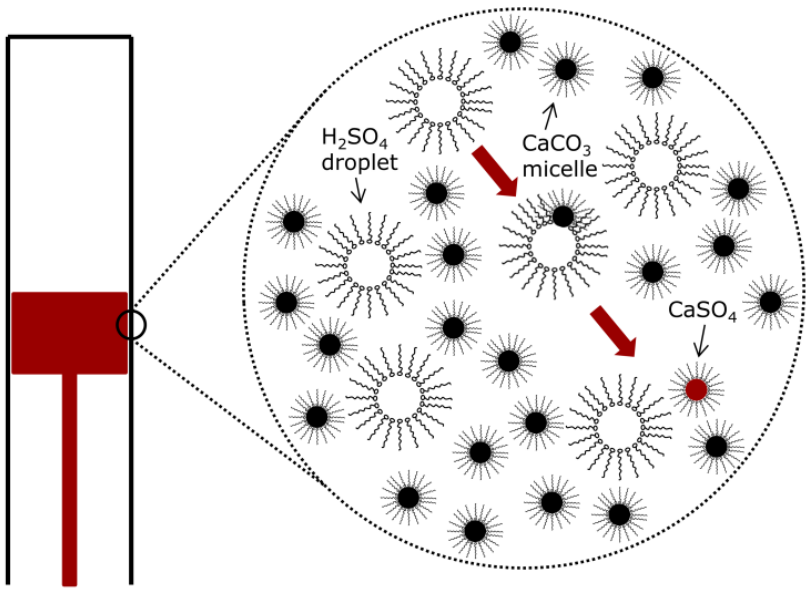

Abstract

Lubrication oil for marine diesel engines contains additives in the form of $CaCO_3$-based reverse micelles, which can neutralize condensing H_2SO_4, and thereby limit uncontrolled corrosive wear of the piston rings and cylinder liner. In the present work, the neutralization mechanism was studied experimentally and through modeling. Using a mixed flow reactor (MFR), the rate of the acid-base reaction was measured as a function of relevant process parameters. In addition, the competition between $CaCO_3$ reverse micelles and NaOH droplets for a reaction with H_2SO_4 droplets in a lube oil emulsion was explored in a batch reactor. For the residence times investigated, the results show that $CaCO_3$ conversion is significantly reduced when reaching a critically low Ca/S ratio. Furthermore, a mathematical model for the neutralization of H_2SO_4 droplets by $CaCO_3$ reverse micelles in lube oil under well-mixed conditions was developed. Using the video-microscopy experiments of Fu et al. [*Tribol. Lett.* **2006**, *22* (3), 221–225], it was possible to estimate kinetic parameters for the reaction. The model was used to predict conversion of H_2SO_4 in a lube oil film at the cylinder liner surface for conditions relevant for a full-scale application. Calculations indicated that H_2SO_4 may reach the liner surface regardless of how well-wetted the surface is.

4.1 Introduction

As a result of the economic crisis of 2008 and the abundance of ships in the shipping market, the slow-steaming operation principle for large two-stroke diesel engines emerged as a measure for increasing fuel efficiency. Use of slow-steaming, combined with new engine designs and tunings for further fuel savings, led to increased operating cylinder pressure and lower liner surface temperature.[1] These changes in operating conditions result in increased water and acid condensation on the cylinder lubrication (lube) oil film on the cast iron liner surfaces,[2–4] promoting a combination of corrosion and wear (cold corrosion) of the cylinder liners and piston rings and significantly reducing their lifetimes.[1,5–7] The condensing acid is mainly aqueous sulfuric acid (H_2SO_4), originating from the oxidation of the sulfur-rich fuel oil burned in marine diesel engines.[8,9] Commercial lube oils are typically formulated with calcium carbonate ($CaCO_3$) overbased detergent additives, present as nanometer-sized reverse micelles, which neutralize condensed H_2SO_4 in the lube oil film.[10–16] To counteract the increased condensation rate of H_2SO_4, it is necessary to increase the amount of $CaCO_3$ being fed to the cylinder liners, which is preferably done by increasing the concentration of $CaCO_3$ in the lube oil rather than by increasing the oil feed rate.[1,2,17] Under-lubrication may result in cold corrosion, which can occur within hours,[18] whereas overlubrication is cost-intensive and may lead to bore-polish (creating a mirrorlike cylinder liner surface), which prevents formation of a coherent lube oil film. Both may eventually result in scuffing (direct metal-to-metal contact).[6,19] Actually, a certain degree of controlled corrosion is beneficial; if the cylinder liners are a little rough, they can better maintain a protective lube oil film.[6,11] Therefore, to limit and control cold corrosion in engines, the lubrication strategy must be optimized. This is a challenge, especially when trying to set up general recommendations.[3] The situation gets even more complicated when switching fuel during service to comply with the new, stricter sulfur regulations.[18] An understanding of what affects and limits the reaction between the condensing H_2SO_4 and the neutralizing additives, $CaCO_3$ reverse micelles, in the lube oil can provide greater insight into how to optimize the lubrication strategy to limit cold corrosion.

The reaction between (sulfuric) acid droplets and $CaCO_3$ reverse micelles in lube oil has been investigated in laboratory experiments over a wide range of conditions. Data in batch mode were obtained using a video-

microscopy technique,[20–29] a stopped-flow method,[30–32] and by monitoring the CO_2 formed.[33–36] The video-microscopy experiments employed placing single acid droplets (70-200 µm in diameter) in a batch of lube oil, followed by measuring the subsequent shrinkage of the acid droplets. These studies indicate that the controlling step of the neutralization reaction is adsorption of a reverse micelle onto the acid droplet. In the capillary video-microscopy technique investigations, $CaCO_3$ reverse micelles were present in great excess on a molar basis compared with H_2SO_4,[25] whereas an excess of concentrated H_2SO_4 was used in the closed vessel experiments.[35,37]

Within an engine, the reaction taking place in the lube oil occurs in a system with continuous feeding of fresh lube oil and condensation of H_2SO_4, followed by the removal of lube oil to the drain. Presumably, the lube oil film is effectively mixed by the motion of the piston rings. In order to provide a better approximation of the reaction conditions in the lube oil at the cylinder liners in a full-scale marine diesel engine, Lejre et al.[38] used a mixed flow reactor (MFR) to study the reaction. They found that a certain intensity of stirring was required to initiate and maintain the reaction. Upon formation and stabilization of the H_2SO_4 into micrometer-sized droplets by the excess emulsifier molecules, a fast reaction occurred, as indicated by a sudden color change of the oil due to the formation of CO_2. The H_2SO_4-$CaCO_3$ reaction at steady-state was significantly reduced when a critically low Ca/S molar ratio was reached, in agreement with the observations of Roman.[35] Lejre et al. suggested that macromixing or micelle adsorption or desorption could be the controlling step under their conditions.

Models for the neutralization reaction are scarce. Schramm et al.[39] and Van Helden et al.[40,41] modeled cylinder liner corrosion, assuming that the neutralization of H_2SO_4 by $CaCO_3$ reverse micelles was acid diffusion-controlled. However, this assumption is contradicted by more recent investigations. Hone et al.[31] determined an activation energy, E_a, for the reaction of 54±2 kJ mol^{-1}, concluding that the neutralization reaction is not diffusion-controlled, because diffusion-controlled reactions usually have activation energies of less than ca. 20 kJ mol^{-1}. The work of Hone et al. is supported by data from Fu et al.,[24] who reported a 1000-fold increase in the neutralization rate when increasing the temperature from 25 to 170 ^{o}C, which corresponds to an activation energy of 52.8 kJ mol^{-1}.

The scope of the present work is to identify the rate-influencing steps (potentially a single rate-controlling one) in the neutralization reaction between H_2SO_4 droplets and $CaCO_3$ reverse micelles and to set up a mathematical model for the reaction system in a mixed flow reactor. The first part investigates the mechanism of the reaction and identifies the possible rate-limiting steps. Batch reactor experiments are conducted, comparing the reaction rates of $CaCO_3$ reverse micelles and NaOH droplets with H_2SO_4 in lube oil in order to assess the possibility of the reaction between $CaCO_3$ and H_2SO_4 being diffusion-controlled. Next, a mathematical model for the reaction system in a mixed flow reactor is set up, and kinetic data for the reaction are extracted from the video-microscopy experiments performed by Fu et al.[24] Simulations are validated against experimental data from the MFR experiments in our previous[38] and present work. Finally, the H_2SO_4-$CaCO_3$ neutralization reaction is explored under conditions representative of a marine diesel engine.

4.2 Experimental work

Experiments involving the reaction between H_2SO_4 droplets and $CaCO_3$-containing micelles in a lube oil were conducted in a reactor that could be operated in both batch and mixed-flow modes. The experimental procedure is described in detail in our previous work[38] and is therefore only touched upon briefly here.

4.2.1 Materials

The commercial lube oil used for the experiments was from Infineum and had a stated base number value (BN) of 100. The BN is defined as the quantity of acid, expressed in terms of the equivalent number of milligrams of KOH required to neutralize all alkaline constituents in a 1 g sample.[42] The H_2SO_4 was obtained from Sigma-Aldrich with a concentration of 95-98 wt.%. The NaOH solution used was 50 wt.% in water and also from Sigma-Aldrich.

4.2.2 Reactor

Operation in mixed flow reactor (MFR) mode is described elsewhere.[38] In short, H_2SO_4(aq) and lube oil were dosed separately to the reactor and mixed by a motor-driven stirrer. In MFR mode, the feeding was continuous, and the level of oil emulsion in the reactor was kept constant by an outlet pump. By taking measurements of the inlet flow rate and reactor volume, the residence time in the reactor could then be calculated.

The reactor was also operated in batch mode to study the competition between NaOH and $CaCO_3$ reacting in the lube oil. Specific amounts of lube oil and NaOH were mixed for 30 min at a maximum stirrer speed of 1200 rpm in order to ensure solubilization of the NaOH droplets into the lube oil. Maintaining 1200 rpm, concentrated H_2SO_4 was added dropwise by use of a syringe into the well-mixed lube oil emulsion, thus keeping a constant lube oil temperature of around 50 ^oC. A molar ratio between NaOH and $CaCO_3$ of 2 was chosen because NaOH and H_2SO_4 react 2:1, whereas $CaCO_3$ and H_2SO_4 react 1:1. $CaCO_3$-H_2SO_4 (Ca/S) molar ratios of 0.8 and 1.0 were also investigated. After the addition of H_2SO_4, mixing continued for 20 min to ensure complete conversion of H_2SO_4 by reaction with $CaCO_3$ reverse micelles and/or NaOH droplets.

4.2.3 Analysis method

The oil samples were analyzed by FTIR, and a calibration curve was used to convert the peak height of the $CaCO_3$ peak to the base number in the lube oil sample.[38] Selected infrared spectra (wavenumber range from 900 to 1700 cm^{-1}) are presented in Figure 4.1 for four different contents of BN in the lube oil after reaction with added H_2SO_4. The $CaCO_3$ concentrations were between 98.6 BN (in fresh lube oil) and 21.5 BN (around 80% conversion of the $CaCO_3$). When increasing the amount of H_2SO_4 added, more $CaCO_3$ is converted. This is shown as a decrease in the $CaCO_3$ band in Figure 4.1 and vice versa for the $CaSO_4$ band. For the MFR experiments, an outlet sample was sampled at steady state and analyzed immediately to estimate the conversion of $CaCO_3$ (this conversion is denoted as *Fast Analysis*). Afterward, the sample was stirred to ensure complete conversion of remaining H_2SO_4, if any. The sample was then analyzed again by FTIR and denoted *Complete Conversion Analysis*. Comparing the two conversions revealed if complete conversion of the added H_2SO_4 was achieved in the MFR within the specified residence time.

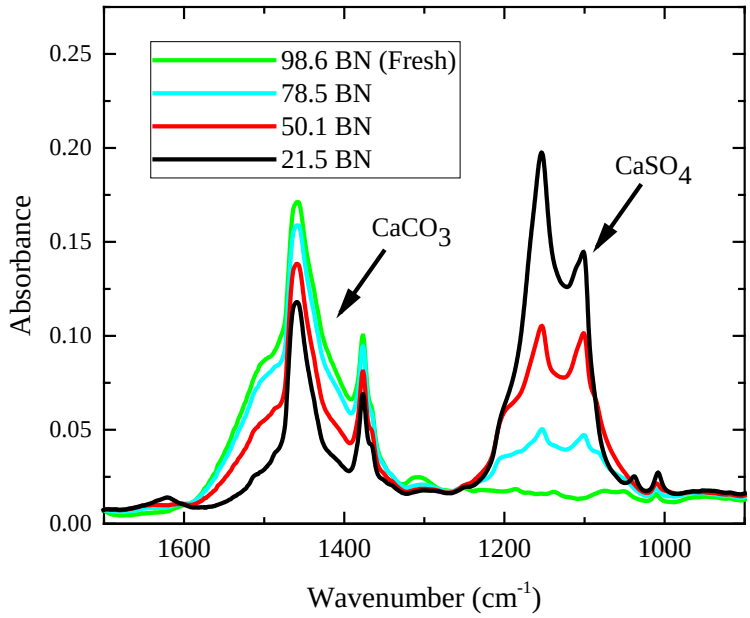

Figure 4.1. Selected segment of infrared spectra showing the $CaCO_3$ and $CaSO_4$ peaks of four different lube oil blends with different amounts of added H_2SO_4, giving $CaCO_3$ concentrations in the range of 98.6-21.5 BN. When more H_2SO_4 is added, the $CaCO_3$ peak decreases and the $CaSO_4$ increases. The spectrum of the 98.6 BN lube oil is that of a fresh lube oil without the addition of H_2SO_4.

The reacted lube oil from the batch reactor experiments was analyzed by FTIR after complete conversion of the added H_2SO_4. A two-point calibration curve was constructed, adding 50 wt.% NaOH to the lube oil sample prior to analysis on the FTIR, in order to match the NaOH-$CaCO_3$ molar ratio used in the batch reactor experiments. It was then possible to estimate the conversion of $CaCO_3$ in the lube oil and consequently the conversion of NaOH by the added H_2SO_4.

4.3 Neutralization mechanism and rate-limiting steps

The reaction between acid (H_2SO_4) droplets and alkaline ($CaCO_3$) reverse micelles (RM) is thought to proceed through the mechanism presented in Figure 4.2.[20,21]

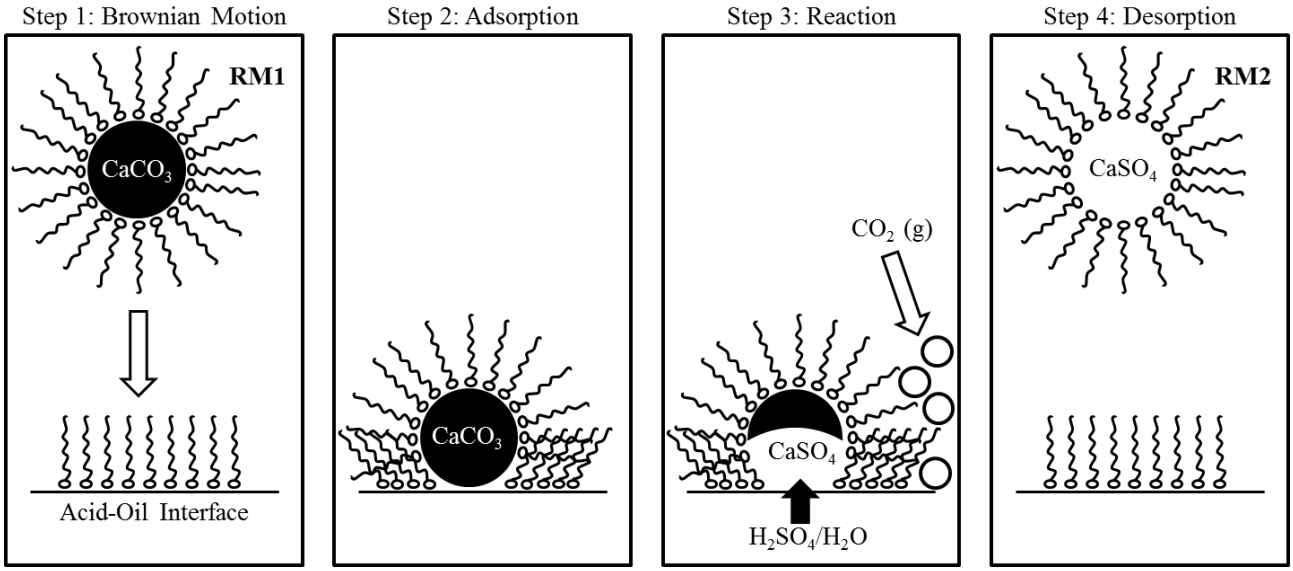

Figure 4.2. Neutralization mechanism between an acid droplet and $CaCO_3$ reverse micelle (Adapted with permission from ref 21. Copyright 2000 Wiley.).

The first step (Step 1 in Figure 4.2) is a collision between the reverse micelle (RM1) and the acid droplet interface by Brownian motion. A successful collision leads to adsorption of the reverse micelle to the acid interface (Step 2 in Figure 4.2). Next, a channel forms and H_2SO_4 and $CaCO_3$ react by the transferring of the acid into the reverse micelles (Step 3 in Figure 4.2). After the reaction, the reaction products are located in the reverse micelle (now called RM2), which desorbs from the acid droplet and back into the bulk oil (Step 4 in Figure 4.2). However, different locations for the reaction products have been noted in the literature.[21,25,31,34] Fu et al.[25] observed four different reaction behaviors in different lube oil formulations within a temperature range of 25-170 ^oC and attributed these differences to different lube oil formulations, temperatures, and overbased detergents. The observed reaction behaviors were explained by a strong/weak-stick collision mechanism, in which the neutralization rate is enhanced by formulating lube oils with a high frequency of strong-stick collisions. On the basis of these studies and the work by Lejre et al.,[38] possible rate-limiting steps in the neutralization mechanism between H_2SO_4 and $CaCO_3$ reverse micelles in lube oil formulations include: micelle diffusion, micelle adsorption, surface reaction, micelle desorption, and macromixing. For micelle diffusion to be rate-limiting, the rate at which the micelles diffuse must be comparable to the overall rate of reaction. If the limiting step is adsorption of a micelle onto a H_2SO_4 droplet, the reaction is controlled by the occurrence of a successful "sticky" collision. This is in contrast to a diffusion-controlled reaction, where the reaction is taking place at every collision. If the $CaCO_3$ reverse micelles have a strong adhesion to the H_2SO_4 droplet surface, occupying the surface of the droplet and preventing unreacted $CaCO_3$ reverse micelles from adsorbing, desorption may become the rate-limiting step in the neutralization mechanism. If the surface reaction is the rate-controlling step, the reaction rate will be limited by the rate of the surface reaction between H_2SO_4 and $CaCO_3$. However, the reaction is an acid-base reaction occurring irreversibly. Because of the small size of the $CaCO_3$ particles in lube oil (8-18 nm in diameter[22]) and the fact that the reaction rate increases with decreasing $CaCO_3$ particle size in acid,[43] it is presumed that the surface reaction between $CaCO_3$ and H_2SO_4 happens instantaneously, and the surface reaction is therefore not the rate-limiting step in the neutralization mechanism.[21] Finally, the reaction can also be controlled by the rate at which H_2SO_4 droplets and $CaCO_3$ reverse micelles are mixed in the reactor. In the following, possible rate-limiting steps are investigated and evaluated from batch reactor and mixed flow reactor experiments.

4.3.1 Batch reactor experiments – diffusion limitation

To evaluate whether or not the $CaCO_3$-H_2SO_4 reaction is diffusion-controlled, the relative rates of the H_2SO_4-$CaCO_3$ and H_2SO_4-NaOH reactions were investigated in batch reactor experiments:

$$H_2SO_4\ (aq) + CaCO_3\ (s) \rightarrow CaSO_4\ (s) + CO_2\ (g) + H_2O\ (l) \quad (4.1)$$

$$H_2SO_4\ (aq) + 2NaOH\ (aq) \rightarrow Na_2SO_4\ (s) + 2H_2O\ (l) \quad (4.2)$$

The reaction between H_2SO_4 and NaOH is diffusion-controlled,[44] as it can be considered instantaneous upon contact. If the reaction between $CaCO_3$ and H_2SO_4 is also diffusion-controlled, it would be expected that H_2SO_4 would react to a larger degree with $CaCO_3$ than with NaOH. A smaller particle size leads to a higher diffusion coefficient, thereby increasing the diffusion-controlled reaction rate on a molar basis,[44] and the NaOH droplets are much larger than the nanometer-sized micelles. In the experiments, the NaOH was solubilized into the lube oil by the excess dispersant and detergent molecules already present in the oil.[35] Common emulsions have a particle size distribution with a radius in the range of 1-10 μm,[45] which may be a representative size range for the emulsified NaOH droplets in the lube oil.

It is not expected that the controlling step for the NaOH-H_2SO_4 reaction would be changed when NaOH is solubilized into the lube oil emulsion. When the equal-sized H_2SO_4 and NaOH droplets (micrometer) collide, they are much larger than the nanometer-sized surfactants that may surround the droplets. It is therefore presumed that the surfactants do not constitute any hindrance for the NaOH-H_2SO_4 reaction. The reaction is further enhanced by the high stirring intensity used.

The batch reactor experiments were performed with a fixed molar ratio between NaOH and $CaCO_3$ of 2, corresponding to the stoichiometry of the reactions with H_2SO_4. Care was taken to provide equal mixing conditions for the NaOH and $CaCO_3$ to react with the added H_2SO_4 in the well-mixed reactor. Upon mixing of the lube oil and NaOH solution, concentrated H_2SO_4 was added dropwise. Two different Ca/S molar ratios were then investigated. At a Ca/S = 1, the neutralization ability of H_2SO_4 is 100%, meaning that the added H_2SO_4 has the ability to either convert all the $CaCO_3$, all the NaOH, or a mixture thereof. If all of the H_2SO_4 reacts first with the $CaCO_3$, 100% conversion of the $CaCO_3$ and 0% conversion of the NaOH would be found at complete conversion of the H_2SO_4. At Ca/S = 0.8, the H_2SO_4 is in excess compared with the $CaCO_3$ in the lube oil. Moreover, if all of the $CaCO_3$ is converted first, 25% conversion of the NaOH would be found at complete conversion of the H_2SO_4. The percentage conversions of $CaCO_3$ and NaOH with H_2SO_4 from the batch reactor experiments are shown in Figure 4.3.

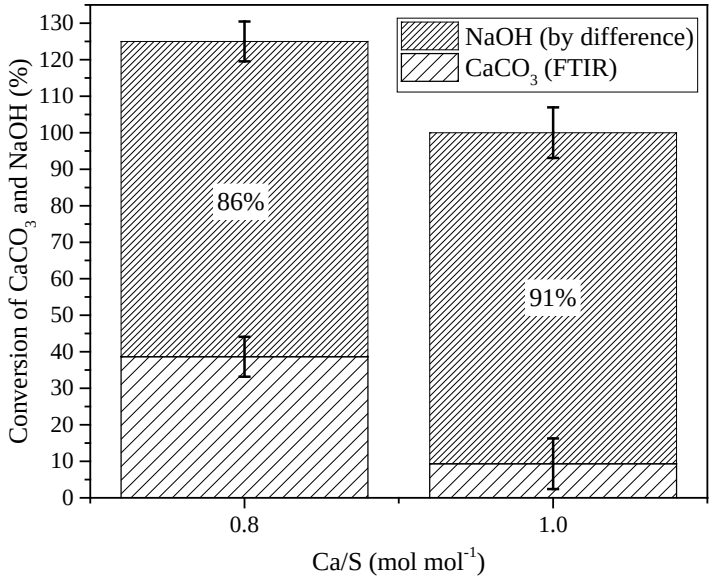

Figure 4.3. Results from the NaOH-H_2SO_4-lube oil batch reactor experiments, showing the accumulative percentage conversions of NaOH and $CaCO_3$ at two different Ca/S values. Error bars represent 2 times the sample standard deviations based on two repetitions.

At Ca/S = 1, 91% conversion of the NaOH was found, whereas only 9% of the $CaCO_3$ was converted. At Ca/S = 0.8, 86% conversion of the NaOH and 39% conversion of the $CaCO_3$ were observed. For both Ca/S molar ratios, most of the H_2SO_4 reacted with the NaOH, whereas only a minor fraction reacted with the $CaCO_3$ reverse micelles. From these results, it can be concluded that the H_2SO_4-$CaCO_3$ reaction is significantly slower than the H_2SO_4-NaOH reaction and is thus too slow to be diffusion-controlled.

Wu et al.[22] found that increasing the concentration of nonionic surfactant in a model oil increased the particle size of the reverse micelles (though they were still in the nanometer range), consequently increasing the neutralization rate of the H_2SO_4 droplet. They attributed this to the enlarged reverse micelles having space to accommodate more water and H_2SO_4 upon sticking to the oil-acid interface. However, they also suggested that the addition of nonionic surfactants may make the tails of the surfactants more flexible and thus the access of H_2SO_4 to the $CaCO_3$-core more feasible. This may facilitate the transport of H_2SO_4 into the reverse micelles, thereby increasing the neutralization rate when adding nonionic surfactants. However, it is difficult to directly compare the experiments performed by Wu et al. with the experiments performed in the batch reactor, because larger NaOH droplets were used in the present work and the effect of the $CaCO_3$ reverse micelle size on the neutralization rate was not isolated.

In conclusion, the batch reactor experiments support the findings of Hone et al.,[31] that the neutralization reaction between H_2SO_4 droplets and $CaCO_3$ reverse micelles cannot be diffusion-controlled. The mixed flow reactor experiments described next, serve to investigate the possible remaining rate-limiting steps.

4.3.2 Mixed flow reactor experiments

The MFR experiments serve both to partly provide information on the rate-limiting steps in the neutralization and partly as data for modeling validation. The data obtained in our previous work[38] were complemented in the present work with additional experiments in order to increase the number of repetitions as well as to obtain data at a Ca/S molar ratio approaching unity at varying stirrer speeds (to clarify the effect of

macromixing). The experimental conditions of the expanded work for each experimental number are supplied in Appendix C, which also contains data on the effects of residence time and inlet H_2SO_4 concentration on the $CaCO_3$ conversion.

4.3.2.1 Stirrer speed

The neutralization reaction could conceivably be limited by the rate of macromixing. Even when maximum stirrer speed is applied, perfect mixing might not be achieved in the MFR. Therefore, insufficient contact between H_2SO_4 droplets and $CaCO_3$ micelles may arise, resulting in local regions with an excess of H_2SO_4 droplets in the lube oil compared with $CaCO_3$, and consequently incomplete reaction of the added H_2SO_4.
Figure 4.4 shows the effect of stirrer speed, *N* (1200, 600, and 360 rpm), on the $CaCO_3$ conversion in the lube oil. The dotted line presents the theoretical conversion when the reaction between $CaCO_3$ and H_2SO_4 droplets is complete (i.e., complete conversion of the limiting reactant). The effect of reducing the stirrer speed by a factor of around 3 is negligible, both for the *Fast Analysis* and *Complete Conversion Analysis* conversions, as well as for both Ca/S molar ratios.

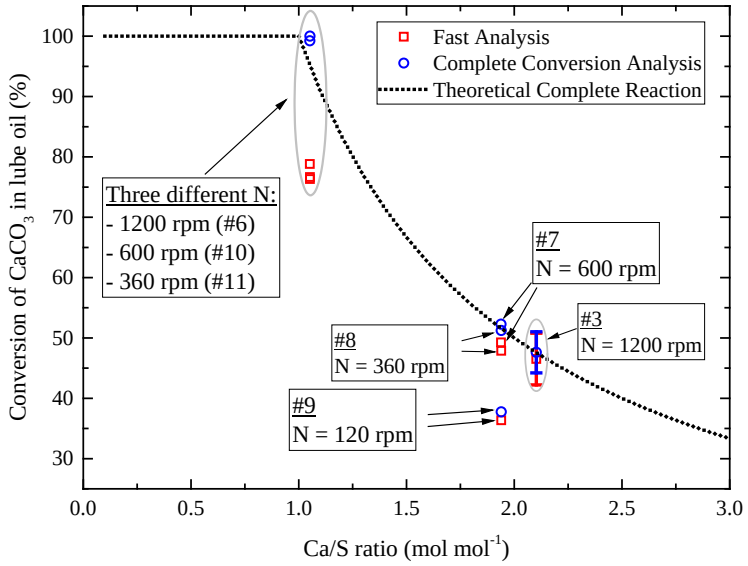

Figure 4.4. Effect of varying the stirrer speed (*N*) on the $CaCO_3$ conversion in the lube oil. Error bars represent 2 times the sample standard deviations. The experimental conditions were as follows: stirrer speed = 120-1200 rpm, inlet H_2SO_4 concentration = 96.5 wt.%, residence time (for *Fast Analysis*) = 2.1-2.8 min (see Table C.1 in Appendix C for more information on each experimental number).

The stirrer speed affects the macromixing in the reactor, as well as the solubilization of H_2SO_4 into the lube oil. If the H_2SO_4-$CaCO_3$ reaction had been macromixing-controlled, an effect on the conversion of $CaCO_3$ by decreasing the stirring intensity in the MFR would be expected. This was not the case, and it is concluded that the reaction is not controlled by macromixing when a certain degree of stirring is applied. Further, a reduced conversion of $CaCO_3$ at reduced Ca/S values would not be expected for a macromixing-controlled reaction at the same stirring speed. When the stirrer speed is decreased, the solubilization of H_2SO_4 into the lube oil may also be reduced, leading to an increased size of the H_2SO_4 droplets in the lube oil emulsion. Assuming that the reaction is limited by adsorption, this decreases the adsorption rate because the total surface area of the H_2SO_4 droplets also decreases. Reducing the stirrer speed by a factor of 10 (120 rpm), yields a conversion of only around 80% of the added H_2SO_4 in the MFR (similar conversions were observed

for the fast and complete analysis). The incomplete conversion of H_2SO_4 at this low stirrer intensity is attributable to insufficient mixing between H_2SO_4 droplets and lube oil, because sedimentation of the heavier H_2SO_4 was observed. This implies that most of the H_2SO_4 droplets are readily solubilized into the lube oil emulsion upon a minor degree of stirring.

4.3.2.2 Ca/S molar ratio

The effects of varying the Ca/S molar ratio on the $CaCO_3$ and H_2SO_4 conversions are presented in Figure 4.5 and Figure 4.6.

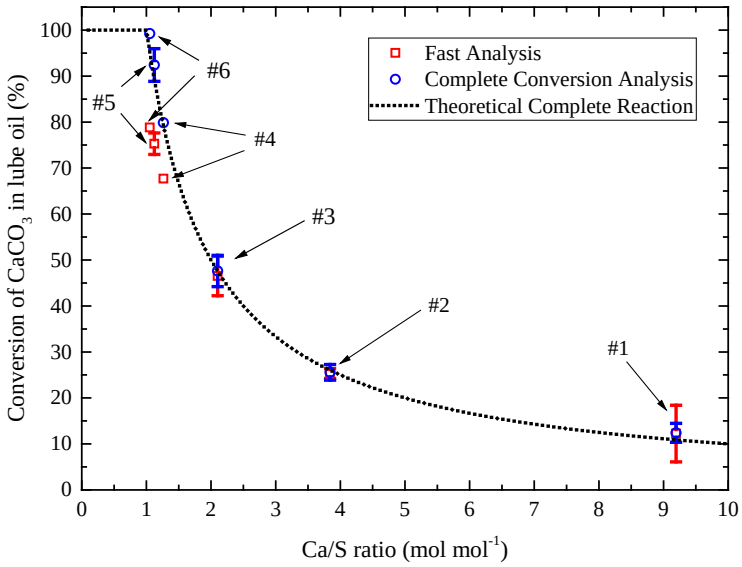

Figure 4.5. Effect of varying the Ca/S molar ratio on $CaCO_3$ conversion in lube oil. Error bars represent 2 times the sample standard deviations. The experimental conditions were the following: stirrer speed = 1200 rpm, inlet H_2SO_4 concentration = 96.5 wt.%, residence time (for *Fast Analysis*) = 2.1-3.5 min (see Table C.1 in Appendix C for more information on each experimental number).

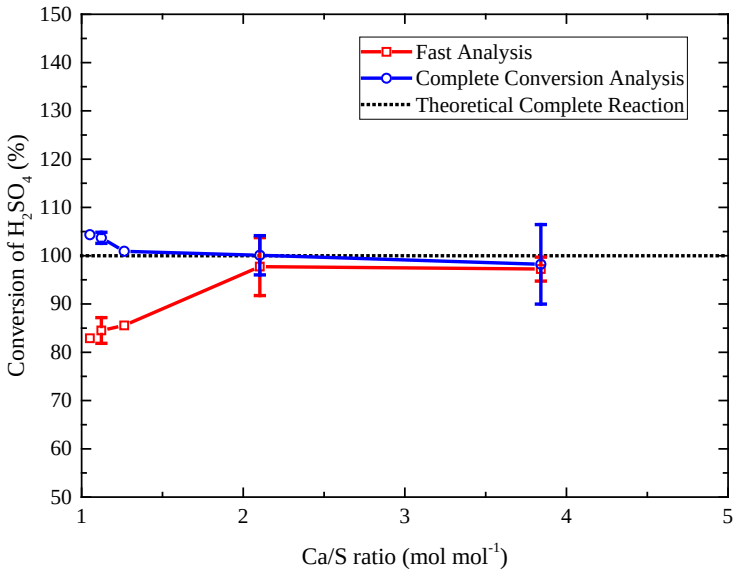

Figure 4.6. Effect of varying the Ca/S molar ratio on H_2SO_4 conversion. Error bars represent 2 times the sample standard deviations. The experimental conditions were the same as in Figure 4.5.

When the Ca/S ratio was larger than 2, complete conversion of H_2SO_4 was found in the MFR.[38] The H_2SO_4 conversion was observed to decrease when reaching a critically low Ca/S ratio of between 1.26 and 2.10. This is attributable to the reaction being adsorption or desorption controlled. At decreasing Ca/S ratios, significantly fewer $CaCO_3$ reverse micelles encircle each H_2SO_4 droplet. The reduced conversion of H_2SO_4 at lower Ca/S ratios can therefore be explained by a decrease in the adsorption rate of the $CaCO_3$ micelles on the H_2SO_4 droplet,[46] thus reducing the total reaction rate of $CaCO_3$ micelles. It is expected that a high bulk concentration of the adsorbate (in this work, $CaCO_3$ reverse micelles) leads to a high coverage of sites on a surface (H_2SO_4 droplet surface),[44] thereby increasing the likelihood of the reaction mechanism being controlled by desorption. This situation corresponds to a high Ca/S, where no apparent limitation is found (Ca/S ratio > 2 in, e.g., Figure 4.5). When fewer micelles are surrounding each droplet (corresponding to a low Ca/S value), the driving force from bulk to the surface is also decreased, thereby approaching adsorption-control.

Wu et al.[20] observed the formation of crystals ($CaSO_4$ from the neutralization reaction), which may deposit on the surface of the H_2SO_4 droplet, inhibiting further reaction (i.e., desorption-control). However, the occurrence of crystal formation depends on the lube oil formulation;[25] the reaction products may be solubilized into the lube oil if the lube oil is formulated with the suitable dispersants. Assuming that a stable emulsion is formed when H_2SO_4 is introduced into the lube oil (droplet radii in the range of 1-10 µm[45]), it is expected that inhibition by $CaSO_4$ crystal formation is not a concern. Wu et al.[21] further suggested that the adsorption of $CaCO_3$ micelles on the acid droplet micrometer-sized interface is the controlling step in the neutralization reaction mechanism. The arguments and experimental results presented in this section support this conclusion.

4.4 Mathematical modeling

4.4.1 Reaction rate expressions

The simulated degree of conversion of the H_2SO_4 droplets by the $CaCO_3$ reverse micelles is determined by the reaction rate expression. In Section 4.3, we concluded that reverse micelle adsorption onto the H_2SO_4 droplets is most likely the limiting step in the neutralization mechanism at well-mixed conditions, in line with the literature investigations.[21] However, early modeling studies[39–41] indicated that the neutralization reaction may be acid diffusion-controlled. In this study, a reaction rate expression that accounts for both micelle diffusion- and adsorption-resistance will be set up for comparison, and the rate-limiting step will be identified.

4.4.1.1 Diffusion-controlled reaction rate expression

Under diffusion-control, a reaction occurs instantaneously upon collision. The $CaCO_3$ reverse micelles move by Brownian motion,[20,22] and because of their small size, a high collision rate with the H_2SO_4 droplets is expected. An expression for the reaction rate was derived following Laidler,[44] assuming that the H_2SO_4 droplets are immobile compared with the much smaller $CaCO_3$ reverse micelles. This assumption is justified because the radius of the H_2SO_4 droplets is in the micrometer range,[45,47,48] whereas the radius of the $CaCO_3$ reverse micelles is in the nanometer range.[12,20,21,49–52] The diffusion-controlled reaction rate constant, k_{diff}, is given as:[44]

$$k_{diff} = 4\pi D_L d_c N_A \tag{4.3}$$

N_A is Avogadro's constant, and d_c, the critical distance from a droplet where a $CaCO_3$ reverse micelle immediately reacts under diffusion control, is assumed to be equal to the radius of the H_2SO_4 droplet, R_{SA} (at $R = R_{SA}, C_L = 0$). The diffusion coefficient of the $CaCO_3$ reverse micelles, D_L, is given as:[44]

$$D_L = \frac{k_B T}{6\pi\eta R_L} \tag{4.4}$$

Here, k_B is the Boltzmann constant, T is the temperature of the lube oil volume, R_L is the radius of the $CaCO_3$ reverse micelles, and η is the viscosity of the lube oil. The diffusion coefficient of the $CaCO_3$ reverse micelles increases with decreasing lube oil viscosity. The dependency on temperature is affected by that of the viscosity, which is typically a strong function of temperature.[47]

The micelle diffusion-controlled reaction rate is first order with respect to each reactant (H_2SO_4 droplet and $CaCO_3$ micelle, respectively), and is given by:[39–41]

$$\left(-r_{A,diff}\right) = k_{diff} C_d C_L \tag{4.5}$$

C_d is the concentration of sulfuric acid droplets and C_L is the molar concentration of the limestone, given as:

$$C_d = \frac{N_{SA}}{N_A} \tag{4.6}$$

$$C_L = N_L n_{L,M} = N_L \frac{V_L f_L \rho_L}{M_L} \tag{4.7}$$

N_{SA} is the number of H_2SO_4 droplets per unit volume of lube oil, N_L is the number of micelles in the lube oil volume, $n_{L,M}$ is the moles of $CaCO_3$ in one micelle, V_L is the volume of one micelle, f_L is the volume fraction of $CaCO_3$ in a micelle, $\rho_L$is the density of $CaCO_3$, and M_L is the molar weight of $CaCO_3$. The diffusion-controlled reaction rate constant only contains physical parameters and can therefore be calculated directly from the expressions given in Eqs. (4.3) and (4.4).

4.4.1.2 Adsorption-controlled reaction rate expression

Different reaction behaviors are reported in literature for an H_2SO_4 droplet in oil (both model and commercial oils); however, when a droplet was placed in an optimized commercial lube oil, shrinkage over time of the droplet was observed.[53] The droplet shrinkage experiments performed by Fu et al.[24] are used in this work to derive a reaction rate constant, because a comparable lube oil formulation was used in this study. According to Fu et al.,[24] the reaction of a sulfuric acid droplet in a commercial marine cylinder oil, containing $CaCO_3$-based additives, is adsorption-controlled. Their droplet shrinkage experiments (reported as radius versus time graphs) at temperatures in the range 298-443 K are here used to extract the adsorption-

controlled reaction rate constant by formulating molar rate balances of H_2SO_4 droplets and $CaCO_3$ reverse micelles. The molar H_2SO_4 consumption rate of one droplet is:

$$-\frac{dn_{SA}}{dt} = -\frac{d\left(V_{SA}C_{SA,d}\right)}{dt} = 4\pi R_{SA}^2 C_{SA,d}\left(-\frac{dR_{SA}}{dt}\right) \tag{4.8}$$

V_{SA} is the volume of one droplet and $C_{SA,d}$ is the concentration of H_2SO_4 in the droplets. The molar adsorption rate of $CaCO_3$ reverse micelles to the surface of a H_2SO_4 droplet is expressed as:[44]

$$-\frac{dn_L}{dt} = \mathrm{A}_{SA}k_{ads}C_L(1-\theta) \tag{4.9}$$

Here, k_{ads} is the adsorption-controlled reaction rate constant (m s^{-1}), θ is the fraction of the H_2SO_4 droplet surface that is covered by micelles, and A_{SA} is the surface area of the H_2SO_4 droplet. For an adsorption-controlled process, it is assumed that $\theta = 0$.[24] This means that immediately after a successful collision (adsorption) of a micelle onto the droplet surface, reaction occurs, followed by immediate desorption of the product back into the bulk. According to Eq. (4.9), the reaction rate depends on the concentration of $CaCO_3$ reverse micelles (or BN), which is in agreement with previous investigations.[21,35] The molar consumption rate of H_2SO_4, Eq. (4.8), can be set equal to the molar adsorption rate of $CaCO_3$ reverse micelles onto the H_2SO_4 droplets, Eq. (4.9). Solving for k_{ads} gives:

$$k_{ads} = \left(-\frac{dR_{SA}}{dt}\right)\frac{C_{SA,d}}{C_L} \tag{4.10}$$

The overall adsorption-controlled reaction rate is derived by multiplying Eq. (4.9) with N_{SA} and introducing the molar concentration of H_2SO_4 in the lube oil, $C_{SA} = N_{SA}V_{SA}C_{SA,d}$:

$$\left(-r_{A,ads}\right) = \frac{A_{SA}}{V_{SA}}\frac{1}{C_{SA,d}}k_{ads}C_{SA}C_L \tag{4.11}$$

4.4.1.3 Estimation of adsorption-controlled reaction rate constant

As said, values for the H_2SO_4 droplet shrinking rate, $(-dR_{SA}/dt)$, were determined from the video-microscopy experiments by Fu et al.[24] in the temperature range of 298-443 K for H_2SO_4 droplets in fully formulated lube oil. A strong dependence on temperature was found; by increasing the temperature from 298 to 443 K, the shrinking rate increased by a factor of more than 1000. A linear relation between $\ln(-dR_{SA}/dt)$ and $1/T$ was also found, and a modified Arrhenius type plot was constructed. The relation between shrinking rate and temperature can be established as:

$$-\frac{dR_{SA}}{dt} = 11.3\frac{m}{s}\exp\left(-\frac{52.8\frac{kJ}{mol}}{RT}\right) \tag{4.12}$$

Here, R is the ideal gas constant. The derived activation energy, E_a, of 52.8 kJ mol^{-1}, is in excellent agreement with the value of 54±2 kJ mol^{-1} found by Hone et al.[31] Duan et al.[54] reported activation energies in the range of 27.0-30.7 kJ mol^{-1} for the neutralization of acetic acid droplets in passenger-car lube oil, but this reaction involved a different mechanism compared with that of a H_2SO_4 droplet in marine lube oil.

Fu et al. used a lube oil with a base number of 70 and 50 vol.% H_2SO_4 droplets, corresponding to a concentration of $CaCO_3$ of C_L = 586.5 mol m^{-3} and an acid concentration of $C_{SA,d}$ = 9.4·10^3 mol m^{-3}. By substituting Eq. (4.12) into Eq. (4.10) and inserting the concentrations, the following expression for k_{ads} can be calculated:

$$k_{ads} = 180.6\frac{m}{s}\exp\left(-\frac{52.8\frac{kJ}{mol}}{RT}\right) \tag{4.13}$$

Equation (4.11), with k_{ads} from Eq. (4.13), provides a quantitative expression for the neutralization reaction under adsorption control.

4.4.1.4 The functional reaction rate expression

A functional reaction rate expression can now be derived to have the following layout:

$$(-r_A) = k_i' C_{SA} C_L \tag{4.14}$$

Where k_i' is either the diffusion- or adsorption-controlled reaction rate constant. To have the derived expressions, given in Eqs. (4.5) and (4.11), as presented as Eq. (4.14), k_{ads}' and k_{diff}' are given as:

$$k_{ads}' = \frac{3k_{ads}}{R_{SA}C_{SA,d}} \tag{4.15}$$

$$k_{diff}' = \frac{k_{diff}}{V_{SA}C_{SA,d}N_A} \tag{4.16}$$

Note that the micelle-diffusion and micelle-adsorption rate equations (based on Eq. (4.14)) are thereby identical, and only the rate constants (Eqs. (4.15) and (4.16)) are different.

4.4.2 Reactor System

A schematic illustration of the H_2SO_4 droplets-lube oil system in the mixed flow reactor setup is shown in Figure 4.7. The reactor has inlet flows for lube oil and H_2SO_4 droplets. The outlet flow serves to maintain a specific oil volume, V_{oil}. The lube oil volume is well-mixed, and the H_2SO_4 droplets are therefore mixed immediately into the oil, forming a stable water-in-oil emulsion. The well-mixed conditions in the MFR resemble those of an actual engine cylinder, where the high velocity of the piston conceivably leads to a well-mixed region in front of the piston. The H_2SO_4 droplets with a uniform droplet radius of R_{SA} and a concentration of $C_{SA,d}$ are fed to the mixed flow reactor with a flow rate of F_{SA}. The lube oil dosage is continuous, with a flow rate of $v_{oil,f}$, containing $CaCO_3$ reverse micelles in a concentration of $N_{L,f}$. The lube

oil outlet flow, v_o, contains unreacted $CaCO_3$ reverse micelles in the concentration, N_L, and the H_2SO_4 droplet concentration is N_{SA} (if any).

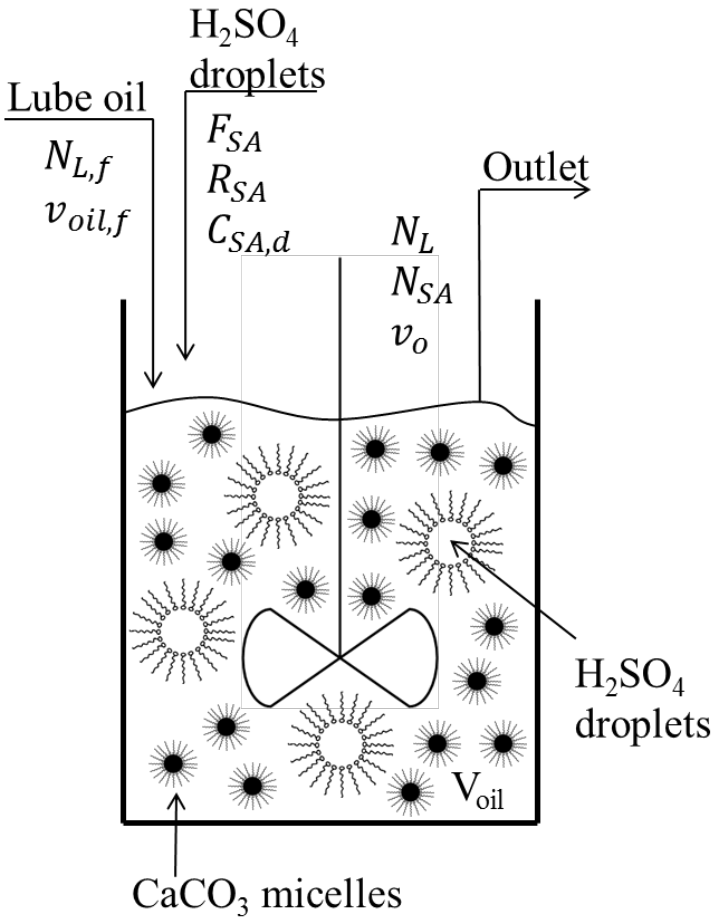

Figure 4.7. Schematic illustration of the neutralization of H_2SO_4 droplets in a lube oil by $CaCO_3$ reverse micelles under mixed flow reactor conditions. Lube oil volume and inlet and outlet conditions are indicated in the figure.

4.4.3 Mathematical Model

The present model describes the neutralization of H_2SO_4 droplets in a stirred lube oil volume containing $CaCO_3$ reverse micelles. The assumptions underlying the model are the following:

- The lube oil volume is well-mixed (no radial or axial concentration or temperature gradients) and in steady state with continuous, uniform feeding of lube oil and H_2SO_4 droplets.
- The outlet flow of lube oil, v_o, is equal to the sum of the inlet flows of lube oil, $v_{oil,f}$, and the droplets, $v_{SA,f}$. The reduction in outlet lube oil flow due to CO_2 (g) formation is not taken into account.
- The H_2SO_4 droplets are readily solubilized into the lube oil by excess surfactants as a water-in-oil emulsion.
- The only reaction considered in the lube oil is $CaCO_3$ (s) + H_2SO_4 (aq) → $CaSO_4$ (s) + CO_2 (g) + H_2O (l) with a reaction rate of $(-r_A)$.
- The $CaSO_4$ formation does not limit the neutralization reaction.

- The $CaCO_3$ micelles and H_2SO_4 droplets are spherical and uniform in size.
- Shrinking over time of $CaCO_3$ micelles and H_2SO_4 droplets is not taken into account; only consumption of entire droplets and micelles is considered.

4.4.3.1 H_2SO_4 number balance over a mixed flow reactor

The number balance for H_2SO_4 droplets is given as:

$$\underbrace{F_{SA}}_{In} - \underbrace{\frac{(-r_A)V_{oil}M_{SA}}{\rho_{\mathrm{SA}}\left(V_{SA}-V_{SA,o}\right)\frac{C_{SA,d}M_{SA}}{\rho_{\mathrm{SA}}}}}_{Produced} = \underbrace{N_{SA}v_o}_{Out} \tag{4.17}$$

Here, F_{SA} is the inlet H_2SO_4 droplet number flow, V_{oil} is the volume of lube oil in the reactor, M_{SA} is the molar weight of H_2SO_4, ρ_{SA} is the density of H_2SO_4, and v_o is the volumetric outflow. The term $C_{SA,d}M_{SA}/\rho_{SA}$ is the volume fraction of H_2SO_4 in the droplets. The term $\left(V_{SA}-V_{SA,o}\right)$ accounts for the volume change of a H_2SO_4 droplet. V_{SA} is the initial volume of a H_2SO_4 droplet, and $V_{SA,o}$ is the volume of a reacted H_2SO_4 droplet in the outlet. The latter is equal to 0, corresponding to a situation where a reacted H_2SO_4 droplet is entirely consumed. The volumetric outflow rate of lube oil emulsion, v_o, is equal to the sum of the volumetric inlet flow rates of lube oil, $v_{oil,f}$, and H_2SO_4 droplets, $v_{SA,f}$:

$$v_o = v_{oil,f} + v_{SA,f} = v_{oil,f} + F_{SA}V_{SA} \tag{4.18}$$

4.4.3.2 Reverse micelle number balance over mixed flow reactor

A number balance for the reverse micelles in the lube oil volume reads:

$$\underbrace{N_{L,f}v_{oil,f}}_{In} - \underbrace{\frac{(-r_A)V_{oil}M_L}{\rho_L\left(V_Lf_L - V_{L,o}f_{L,o}\right)}}_{Produced} = \underbrace{N_Lv_o}_{Out} \tag{4.19}$$

Again, the term $V_{L,o}f_{L,o}$ is equal to 0 because only consumption of entire $CaCO_3$ reverse micelles is considered. $N_{L,f}$ is the number of $CaCO_3$ reverse micelles per volume of lube oil in the inlet feed, given as:

$$N_{L,f} = \frac{f_{L,oil,w}\rho_{oil}}{\rho_LV_Lf_L} \tag{4.20}$$

Here, $f_{L,oil,w}$ is the weight fraction of $CaCO_3$ in the fresh lube oil, and ρ_{oil} is the density of the lube oil.

4.4.3.3 Ca/S molar ratio

It is of interest to investigate how the H_2SO_4 droplet flow into the lube oil volume affects the conversion of the H_2SO_4 droplets and $CaCO_3$ reverse micelles in the lube oil film. This is done by introducing the molar ratio of $CaCO_3$ to H_2SO_4 in the inlet feed, Ca/S, defined from the molar balance:

$$Ca/S = \frac{v_{oil,f}\rho_{oil}f_{L,oil,w}}{M_L F_{SA} V_{SA} C_{SA,d}} \tag{4.21}$$

Solving for F_{SA} gives:

$$F_{SA} = \frac{v_{oil,f}\rho_{oil}f_{L,oil,w}}{M_L V_{SA} C_{SA,d}\, Ca/S} \tag{4.22}$$

By substituting Eq. (4.22) into Eq. (4.17), the parameter Ca/S is now the independent variable. When Ca/S is equal to 1, then H_2SO_4 and $CaCO_3$ are present in stoichiometric amounts.

4.4.3.4 Estimation of model parameters

The chemical and physical properties for the H_2SO_4 droplets and $CaCO_3$ reverse micelles are shown in Table 4.1, together with typical operating conditions.

Table 4.1. Chemical and physical parameters for the H_2SO_4 droplets, $CaCO_3$ reverse micelles, and lube oil.

Parameter	**Parameter Value**	**Reference**
R_L	$5\cdot10^{-9}$ m	12,20,21,49–52
f_L	0.3 m^3 m^{-3}	12,20,21,49–52
$f_{L,oil,w}$	0.088 kg kg^{-1} (98.55 BN)	Measured[42]
ρ_{oil}	940 kg m^{-3}	Measured
ρ_L	2710 kg m^{-3}	55
ρ_{SA}	1840 kg m^{-3} (pure)	56
M_{SA}	$98.1\cdot10^{-3}$ kg mol^{-1}	Calculated
M_L	$100.1\cdot10^{-3}$ kg mol^{-1}	Calculated
$C_{SA,d}$	$18\cdot10^3$ mol m^{-3} (96.5 wt.%)	Calculated
τ	126 s	Measured
V_{oil}	$1.2\cdot10^{-4}$ m^3	Measured
T	327 K	Measured
η (327 K)	$6.2\cdot10^{-2}$ kg m^{-1} s^{-1}	Calculated[47]

Tobias and Klein[20] reported that a typical reverse micelle is roughly spherical, with an average diameter of the $CaCO_3$ core of 2.3 nm and a surfactant layer thickness of 0.9 nm. This gives a total diameter of the reverse micelle of 4.1 nm. Hudson et al.[49] reported core diameters in the range 1-10 nm, and a surfactant layer thickness in the range 1-5 nm, yielding total diameters in the range 3-20 nm. Lewis[21] reported an overall diameter in the range 8-18 nm, with core diameters between 4 and 14 nm. On the basis of these results, which are generally in accordance with other reported studies,[12,50–52] an average reverse micelle diameter of 10 nm is chosen, and a volume fraction of $CaCO_3$ in a reverse micelle, f_L, is estimated to be 0.3. The radius of the H_2SO_4 droplets will be discussed in Section 4.5.

The average base number (BN) of the lube oil used in the MFR experiments[38] was 98.55, corresponding to a weight fraction of $CaCO_3$ in the lube oil of 0.088 kg kg^{-1}. The density of $CaCO_3$ was taken from CRC,[55]

density of H_2SO_4 was from Perry[56] (96.5 wt.% H_2SO_4 solution corresponding to a density of approximately 1840 kg m^{-3}), and the density of the lube oil was measured using a scale and measuring glass.

The lube oil temperature in the MFR experiments was around 327 K. The lube oil viscosity was drawn from Sautermeister and Priest,[47] who measured the dynamic viscosity for a base oil at different temperatures. For the reference conditions, an average lube oil residence time in the reactor is taken as 126 s on the basis of the volumetric feed rate of lube oil, $v_{oil,f}$, and the average volume of lube oil, V_{oil}, used in the MFR experiments. The two output variables, N_L and N_{SA}, can be expressed as the conversion of $CaCO_3$, X_L, and H_2SO_4, X_{SA}, respectively:

$$X_{\mathrm{L}} = 1 - \frac{N_L v_o}{N_{L,f} v_{oil,f}} \tag{4.23}$$

$$X_{\mathrm{SA}} = 1 - \frac{N_{SA} v_o}{F_{SA}} \tag{4.24}$$

In summary, the model consists of two coupled algebraic equations, Eq. (4.17) and Eq. (4.19), which are solved for N_L and N_{SA} by use of Matlab, with the parameter Ca/S as the independent variable. The model parameters presented in this section have been used for the calculations that follow in the next section, unless otherwise stated.

4.5 Validation of mathematical model against MFR results

To validate the model and investigate the rate-controlling step of the neutralization reaction between H_2SO_4 droplets and $CaCO_3$ reverse micelles, model simulations are compared to experimental data from the MFR, by applying diffusion- and adsorption-controlled reaction rate expressions.

The only parameter not available and required for the analysis is the radius of the H_2SO_4 droplets, R_{SA}. R_{SA} was fitted to match the experimental data of $CaCO_3$ conversion from the MFR experiments (Figure 4.5), by use of a "least squares" approach. For the conditions given in Table 4.1, a value of R_{SA} equal to 0.5 µm was calculated by using the adsorption-controlled reaction rate expression given in Eq. (4.11) and a value of 0.7 µm for the diffusion-controlled reaction rate expression from Eq. (4.5). Goodwin[45] states that most common emulsions have a particle radius in the range of 1-10 µm. Typical acid and water droplet radii from used engine lube oils are found to be in the range of 2.5-15 µm.[48] This is for a stable emulsion after drainage of the lube oil. Sautermeister and Priest[47] measured H_2SO_4 droplet sizes in a stable base oil emulsion, measuring radii in the range of 0.25-1.6 µm depending on the H_2SO_4 droplet concentration. Consequently, it is expected that these droplet sizes were instantly formed in the MFR experiments, where large excesses of dispersant and detergent molecules are present in the used lube oil. On the basis of these values from the literature, it is concluded that the radii of 0.5 and 0.7 µm, respectively, fitted from the modeling, are both realistic values. Consequently, it is not possible from the MFR analysis to decide whether the limiting step of the reaction is adsorption or diffusion.

To investigate this in greater detail, the diffusion-controlled reaction rate expression was applied to describe the experimental H_2SO_4 droplet shrinkage data from Fu et al.,[24] who visually observed the shrinkage of H_2SO_4 droplets surrounding in a lube oil emulsion. At temperatures in the range 25-170 °C, they monitored

the radius-versus-time behavior. The diffusion-controlled reaction rate expression was used to calculate the molar diffusion of $CaCO_3$ reverse micelles from the bulk oil to the droplet surface. This value was then compared to the actual molar conversion rate of the H_2SO_4. If comparable, this could indicate diffusion control, whereas an excessive molar diffusion of $CaCO_3$ reverse micelle to the droplet, compared to the molar conversion rate of H_2SO_4, would indicate that diffusion is not the controlling step of the reaction. This scenario is investigated and described in Appendix D. Interestingly, the analysis shows that the molar diffusion of $CaCO_3$ reverse micelles is lower than the actual molar conversion rate of the H_2SO_4 droplet (a factor of 28.4 at 25 ^oC and factors of 134-165 at temperatures in the range 100-170 ^oC). This observation is unexpected, since a diffusion-limited value presumably is the upper limit for the reaction rate. The discrepancy may be due to one of the following two possible explanations: 1) that the calculated diffusion-controlled reaction rate constant (from Eq. (4.3)) underestimates the actual value for the present system (up to a factor 165, see Appendix D); or 2) that an alternative mechanism is occurring that enhances conversion of an H_2SO_4 droplet in a commercial lube oil.

The first explanation is investigated by implementing the factor of 165 into the diffusion-controlled reaction rate expression for the MFR modeling (with parameters from Table 4.1), and subsequently solving for R_{SA} gives an average radius of the H_2SO_4 droplets of 9.6 µm, which is still within the range of typical, realistic values.[45,47,48] This means that, even though the calculated diffusion-controlled reaction rate constant is increased by a factor of 165, a realistic averaged droplet radius is still found. It is therefore difficult to rule out diffusion as the controlling step for the reaction, at least from a computational point of view. Nevertheless, the batch reactor experiments with NaOH, as described in Section 4.3.1, indicated that the droplet-micelle reaction is not diffusion-controlled. In addition, Fu et al.[24] and Hone et al.[31] determined activation energies in the range of 54±2 kJ mol^{-1} (see Section 4.1). This magnitude of the temperature-dependency of the reaction rate constant is larger than the temperature-dependency calculated by Eq. (4.3) (if translated to an activation energy, it is equal to 35 kJ mol^{-1} by using the temperature-dependent viscosity measured by Sautermeister and Priest[47]). Based on these arguments, it seems that the reaction between H_2SO_4 droplets and $CaCO_3$ reverse micelles in lube oil is not controlled by diffusion.

With respect to the second explanation, it is possible that another reaction mechanism is occurring. Duan et al.[29] showed that an H_2SO_4 droplet is not soluble in oil without additives. However, in a commercial marine lube oil, surfactants are present in great excess, having the task of solubilizing various products into the lube oil that would otherwise precipitate and possibly have adverse consequences for the lubrication of the engine.[57] It is conceivable that these surfactants may also solubilize the H_2SO_4 droplet into the bulk lube oil (the empty reverse micelles pulls out the H_2SO_4 to the bulk oil), wherein, presumably, the H_2SO_4 is immediately converted due to its resulting very small size in the bulk oil. When a micelle adsorbs onto the droplet, it may also be that $H_2SO_4(aq)$ is transferred into the micelle in a degree that exceeds the molar amount of $CaCO_3$ in a micelle. This may also be the reason why the droplets vanished completely in the experiments by Fu et al.[24] The H_2SO_4 is then subsequently converted quickly in the bulk oil. Both of these mechanisms, if active, would contribute to an increased shrinkage rate.

To sum up, from a computational point of view, it is difficult to settle whether the reaction is diffusion- or adsorption-controlled (or if another mechanism is limiting). However, from determined activation energies from literature[24,31] and the batch reactor experiments with NaOH contained in this work, it is advocated that the reaction is not (entirely) controlled by diffusion. Whether the reaction is then adsorption-controlled or controlled by another mechanism (or a mixture) is difficult to determine. However, either way the reaction rate expression given in Eq. (4.11) provides a quantitative description of the reaction rate and its

temperature-dependency of the droplet-micelle reaction, with a fitted R_{SA} of 0.5 µm, which is based on actual, experimentally determined H_2SO_4 droplet conversion data from Fu et al.[24] Based on this, Eq. (4.11) is used to describe the apparent reaction rate expression for the droplet-micelle reaction in the remaining part of this work. The corresponding reaction rate constant is likewise denoted as an apparent reaction rate constant, k_{app}, in the remaining work.

Modeling predictions for R_{SA} = 0.5 µm are compared with the MFR data (Figure 4.5 and Figure 4.6) in Figure 4.8, along with simulations increasing R_{SA} by factors of 5 and 10, respectively. Modeling predictions with R_{SA} = 0.5 µm are in good agreement with experimental data, whereas larger droplet sizes lead to an underprediction of the degree of reaction. The predicted conversion of $CaCO_3$ and H_2SO_4 decreases significantly with increasing droplet radius. At Ca/S = 1, the conversions of H_2SO_4 and $CaCO_3$ are equal to each other. Here, the conversion decreases by 24 and 37% when the radius increases to 2.5 and 5.0 µm, respectively, relative to the reference conversion (for R_{SA} = 0.5 µm). This indicates that larger H_2SO_4 droplets present in the lube oil film may increase the risk of corrosive wear significantly,[25] because of the surface to volume ratio of the droplets decreasing when the radius increases (i.e., fewer but bigger droplets).

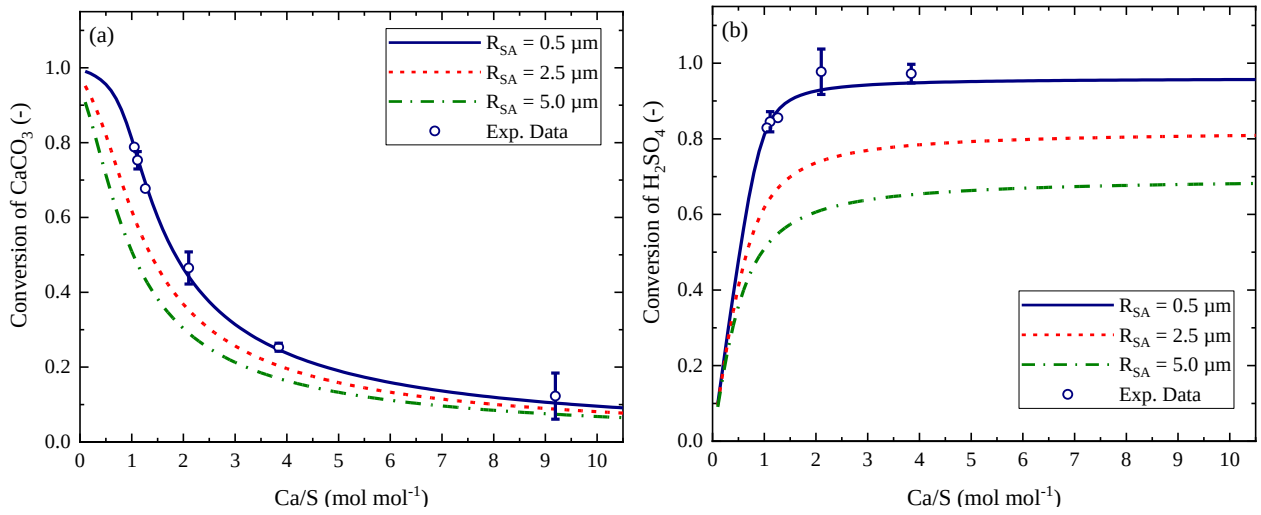

Figure 4.8. Model simulations showing conversion of (a) $CaCO_3$ reverse micelles and (b) H_2SO_4 droplets as functions of Ca/S by using the reaction rate constant given in Eq. (4.11) at three values of H_2SO_4 radius, R_{SA}. Circles represent MFR experimental data from Figure 4.5 and Figure 4.6. Model parameters are presented in Table 4.1.

4.5.1 Evaluation of model assumptions

The reaction rate constant expression used in the model simulations, Eq. (4.13), is based on the video-microscopy single droplet experiments performed by Fu et al.,[24] who reported a shrinking rate. The present model considers only consumption of entire droplets. A model describing the reaction of partly consumed H_2SO_4 droplets in the lube oil emulsion would have to take into account a size distribution. However, because the droplets are very small in size (~1 µm in radius), and the size distribution mimics a normal distribution with a low standard deviation,[47] one would argue that it is fair to assume that whole droplets are immediately consumed upon reactive contact.

Another difference is the size of the droplets. Fu et al. used initial droplet sizes in the range of 43.6-76.5 µm, reporting that a constant shrinking rate was found up until a certain radius was reached. After this point, the shrinking rate increases. This ‘change point’ was found to occur at around 28 µm at 403 K. Because even

smaller H_2SO_4 droplets are found in the MFR experiments, the derived reaction rate constant in Eq. (4.13) may underestimate the actual adsorption reaction rate. Further, Wu et al.[21] reported significantly different shrinking rates for different lube oil formulations having the same BN value. It is not known whether the lube oil used in the study by Fu et al. matches the lube oil used in the MFR experiments.

4.6 Application of the MFR model to conditions in a large two-stroke marine diesel engine

The mixed flow reactor model was developed to interpret the laboratory MFR experiments, while allowing for a validation of the reaction rate expression for the neutralization reaction, which can be used in more complex models. A full simulation of the neutralization reaction at the cylinder liner in a large two-stroke marine diesel engine would require a computational fluid dynamics approach. However, as discussed in the following, the mixed flow reactor model offers a useful approximation to conditions in the lube oil film and can be used to assess the importance of different process parameters. In a large two-stroke marine diesel engine, the lube oil-H_2SO_4 interactions depend on the piston movement (see Figure 4.9).

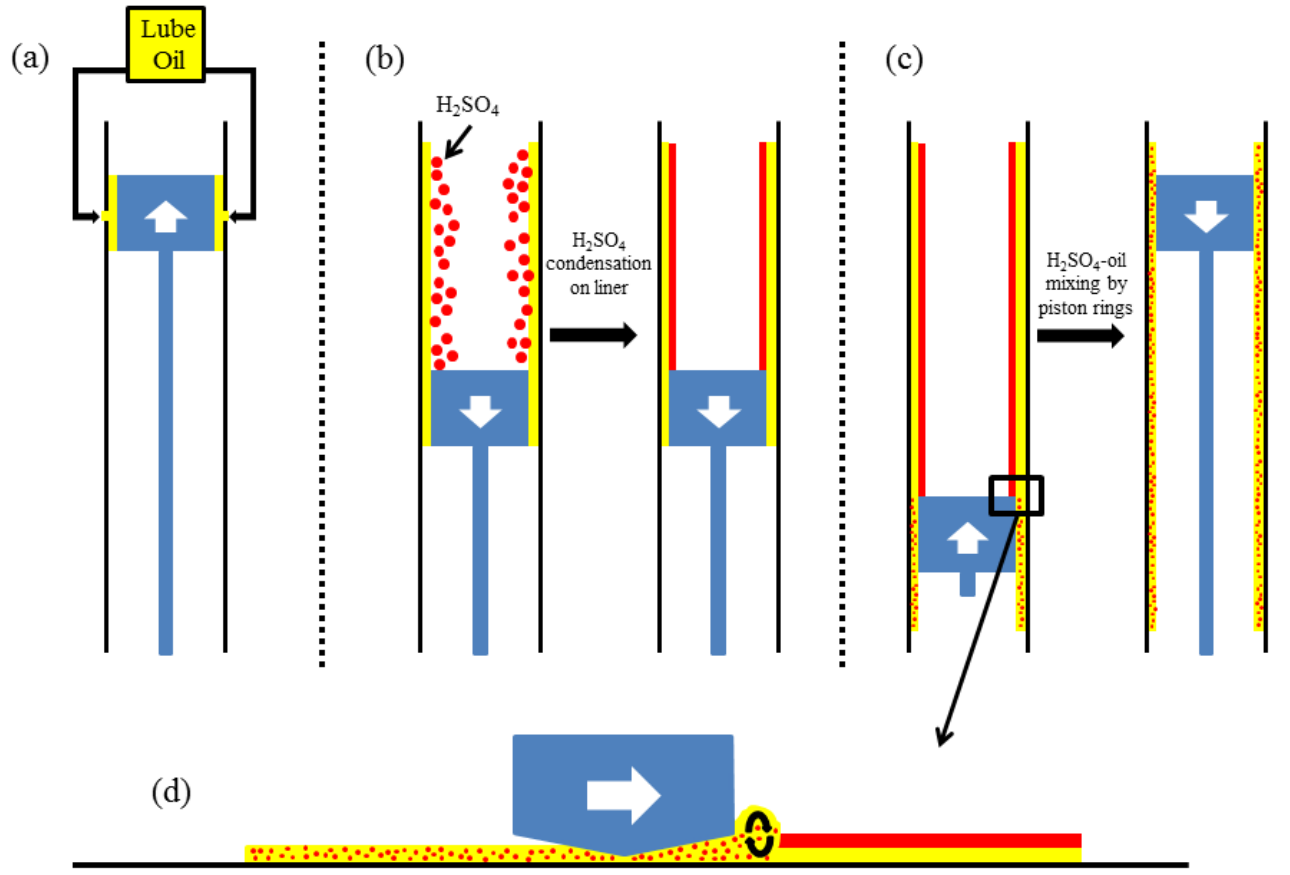

Figure 4.9. Illustration of lube oil dosage, H_2SO_4 droplet condensation, and mixing in an engine: (a) piston approaching top dead center (TDC), when fresh lube oil is dosed onto the piston ring pack[59] (the injection frequency of fresh lube oil is typically once every third to eighth engine revolution); (b) H_2SO_4 condensing onto the lube oil film when the piston moves toward the bottom dead center (BDC); (c) piston moving toward TDC again, contributing to a well-mixed lube oil film where the H_2SO_4 droplets are emulsified in the lube oil; and (d) horizontal close-up of a piston ring-lube oil film, where a moving front may develop where the lube oil and H_2SO_4 droplets are effectively mixed.

Dosing of the lube oil into the piston ring pack occurs during the piston's upward stroke (Figure 4.9(a)). When the piston is at the top dead center (TDC) and moves downward (expansion stroke, Figure 4.9(b)), H_2SO_4 condensates as droplets (either dilute or pure) onto the distributed lube oil film on the cylinder liner surface. It is believed that condensed H_2SO_4 forms a thin film on top of the layer of lube oil film.[7,39] The condensation of H_2SO_4 occurs in the gas phase just before reaching the lube oil film, where the temperature is lower than in the bulk gas phase.[6,47,48,58] Because no mixing is occurring, transport of $CaCO_3$ micelles to the H_2SO_4 happens by diffusion. However, when the piston moves toward TDC (compression stroke, Figure 4.9(c)), the piston rings act to spread and remove excess lube oil from the cylinder liner. The high velocity of the piston may lead to effective mixing of the condensed H_2SO_4 and lube oil at the moving front, in front of the piston ring, thereby emulsifying the H_2SO_4 droplets into the lube oil (Figure 4.9(d)). After the piston has passed a specific point, the local lube oil film may be left stagnant, allowing the H_2SO_4 to react with the cast iron liner until the next time the piston passes by, when it once again mixes the lube oil film emulsion. The cycle is repeated roughly every 0.5 s, which is the time for one stroke. However, fresh lube oil is not injected in every cycle but instead typically at every third to eighth engine revolution. The cast iron wall temperature would be in the range 373-533 K, and highest in the upper part of the cylinder, whereas the lube oil film is expected to attain the same temperature because of the high heat capacity and thermal conductivity of the cast iron.[3,7]

From an idealized perspective, two lube oil-H_2SO_4 interaction scenarios may take place. The first scenario involves condensation of H_2SO_4 onto the lube oil film during the expansion stroke, followed by diffusion of the H_2SO_4 through the lube oil film to the cylinder liner (Figure 4.9(b)). In the second scenario, the H_2SO_4 droplets are fully mixed with the lube oil by the action of the piston (Figure 4.9(d)). In scenario 1, transport of H_2SO_4 through the lube oil film toward the cylinder liner takes place by droplet diffusion. The diffusion coefficient, D_{SA}, can be estimated by the Stokes-Einstein relation given in Eq. (4.4). Taking the lube oil dynamic viscosity from Sautermeister and Priest[47] and assuming that the radius of the diffusing H_2SO_4 droplets is similar to that of the MFR experiments (0.5 µm), the diffusion coefficient is on the order of 10^{-12} m^2 s^{-1} at 533 K, decreasing to about 10^{-14} m^2 s^{-1} at 373 K. The mean Brownian displacement, $\bar{x}$, of a droplet after a specific time, t, can then be calculated by:[46]

$$\bar{x} = \sqrt{2D_{SA}t} \tag{4.25}$$

In the diffusion scenario, the H_2SO_4 droplet has 0.5 s to reach the cylinder liner before the piston returns and mixes the H_2SO_4 film with the lube oil film. Within 0.5 s, the H_2SO_4 droplet moves 1 µm at 533 K and 0.1 µm at 373 K, according to Eq. (4.25). The minimum lube oil film thickness, which is in the upper part of the cylinder, is between 2 and 5 µm in a full-scale application.[48,60] Unless the diffusing H_2SO_4 droplets are significantly smaller than the assumed value of 0.5 µm, it appears that little H_2SO_4 penetrates through the lube oil film on the cylinder liners in a film-film situation (Figure 4.9(b)). This finding is further supported by the fact that the lube oil is hydrophobic and the H_2SO_4 droplets hydrophilic.

The second lube oil-H_2SO_4 interaction scenario involves mixing between the H_2SO_4 film and the lube oil film by the piston rings at the moving front in front of the piston ring (Figure 4.9(d)). Presumably, this corresponds to a situation where the H_2SO_4-lube oil film is well-mixed. In this scenario, H_2SO_4 will be present on the wall and able to interact with the cylinder liner material. Every cycle serves to mix and replenish the lube oil and H_2SO_4 locally. The residence time of a H_2SO_4 droplet on the cylinder liner is

assumed to be low because of the well-mixed situation. Even though the average residence time of a lube oil film in a cylinder liner is estimated to be a couple of minutes,[61] the neutralization of H_2SO_4 has to be significantly faster to avoid reaction with the cylinder liner material. In a two-stroke marine diesel engine, the piston passes by a specific point on the cylinder liner twice per revolution. If rated at 70 rpm, the time for each stroke is around 0.5 s. The contact time for H_2SO_4 and lube oil may vary, however, depending on the vertical position on the cylinder liner. In the upper part, the gas phase contact time with the lube oil is the longest, allowing more time for the H_2SO_4 to condense. The temperature is higher, counteracting condensation, but the pressure is also higher, thereby increasing the dew point temperature. Thus, 0.5 s is an important time scale for the lube oil to neutralize H_2SO_4 and prevent it from reacting with the liner material.

With these considerations, scenario 2 appears most relevant because of the extent of interaction of H_2SO_4 with the cylinder liner material. Presumably, upon mixing with the lube oil film, H_2SO_4 becomes readily emulsified because of the large excess of detergents and dispersants in the lube oil, forming a stable emulsion. Thereby, conditions locally at the liner resemble those described by the MFR model: a well-mixed lube oil volume with a constant initial Ca/S molar ratio.

An average lube oil flow feed rate to the cylinder liner can be estimated to be $3.9 \cdot 10^{-7}$ m^3 s^{-1} on the basis of the assumption that a 30 MW engine with eight cylinders at 50% load consumes 0.7 g kWh^{-1}. For typical dimensions of the cylinder liner and a lube oil thickness of 10 µm, an average lube oil residence time of 220 s is estimated, which is a value in accordance with the residence time applied in the MFR experiments. However, despite the efficient mixing caused by the piston, the full lube oil volume in a cylinder cannot be approximated as a single mixed flow reactor. In the full-scale application, the lube oil film thickness varies vertically,[60] as does the H_2SO_4 condensation rate,[58] because varying amounts of H_2SO_4 may condense locally on the cylinder liners. Moreover, the mathematical model can provide estimates of the degree of conversion of the condensing H_2SO_4 at confined, local points in a large two-stroke marine diesel engine. This corresponds to the discretizing of the vertical direction of the lube oil film into smaller volumes, assuming that each volume has the behavior as a mixed flow reactor. The model can then be used to predict the conversion of H_2SO_4 at specific local initial conditions, such as Ca/S and temperature.

4.6.1 Parametric study

In the following, a parametric study is presented with the aim of investigating the neutralization reaction at conditions representative for a large two-stroke marine diesel engine. This gives an indication of how the reaction would progress in a realistic application. For this purpose, reference case simulation parameters are defined as T = 423 K, τ = 0.5 s, $f_{L,oil,w}$ = 0.089 kg kg^{-1} (100 BN), and $C_{SA,d}$ = $18 \cdot 10^3$ mol m^{-3}. The remaining parameters used in the model simulations are based on the ones presented in Table 4.1. The effect of lube oil temperature is investigated in the range of 373 to 533 K, corresponding to the cylinder liner temperature range in a two-stroke marine diesel engine.[3,7] Lube oils with different BN values are used in service, depending on the sulfur content in the burned fuel;[18] therefore, the effects of using 70 and 140 BN are also investigated. Depending on the operating conditions, different concentrations of H_2SO_4 droplets can condense onto the lube oil film in a real engine application.[58] The range from concentrated ($18 \cdot 10^3$ mol m^{-3}) to very dilute H_2SO_4 droplets ($1.8 \cdot 10^3$ mol m^{-3}) is therefore examined. Wu et al.[21] found that the shrinking rate of acid droplets depends on the lube oil formulation (i.e., different lube oils may not have identical reaction rate constants). Therefore, the effect of varying the reaction rate constant is studied.

4.6.1.1 Lube oil formulation

Figure 4.10 shows the effects of the apparent reaction rate constant and H_2SO_4 droplet radius on the conversion, with the reference case value varying by a factor of 5. Increasing k_{app} by a factor of 5 corresponds to decreasing R_{SA} by a factor of 5.

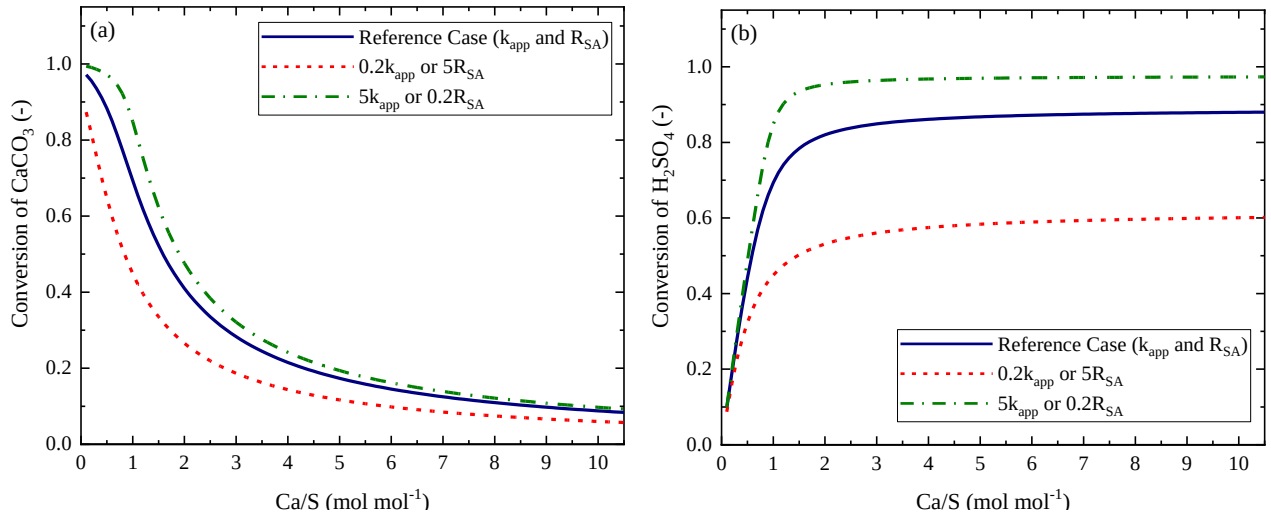

Figure 4.10. Model simulations showing conversion of (a) $CaCO_3$ reverse micelles and (b) H_2SO_4 droplets as functions of Ca/S at three values of k_{app} and R_{SA}. The model parameters are T = 423 K, τ = 0.5 s, $f_{L,oil,w}$ = 0.089 kg kg^{-1} (100 BN), and $C_{SA,d}$ = 18·10^3 mol m^{-3}, as well as those in Table 4.1.

A significant adverse effect is observed when decreasing the reaction rate constant (increasing R_{SA}). It shows that in order to enhance the performance of a specific lube oil with respect to neutralization, the oil should be formulated to increase the reaction rate constant. The simulations also suggest that the lube oil should be formulated with surfactants capable of emulsifying the H_2SO_4 sufficiently. If H_2SO_4 is poorly emulsified in the lube oil, resulting in enlarged droplets, significant amounts of H_2SO_4 may reach the cylinder liner material.

4.6.1.2 Base number

An important property of the lube oil is the base number (BN, i.e., $CaCO_3$ concentration). The effect of varying the BN in the lube oil is shown in Figure 4.11. The volumetric inlet flow rate, $v_{oil,f}$, is kept unchanged when the BN of the lube oil is altered. The weight fraction of $CaCO_3$ in the lube oil, $f_{L,oil,w}$, is changed, affecting the number of micelles in the inlet lube oil (Eq. (4.20)), $N_{L,f}$, and also the H_2SO_4 droplet flow to the lube oil volume (Eq. (4.22)), F_{SA}. Figure 4.11 shows that the conversion of H_2SO_4 increases slightly with the BN of the lube oil at a constant Ca/S molar ratio. For a Ca/S equal to 1, the conversion increases by 5% when the lube oil BN increases from 100 to 140 BN, and it decreases by 6% when a 100 BN lube oil is switched to a 70 BN lube oil. This is due to the higher concentrations of $CaCO_3$ and H_2SO_4, resulting in an increase in the reaction rate. The results indicate that it could be beneficial to use a higher BN lube oil in combination with a decreased lube oil feed rate (maintained Ca/S value). However, there is a tradeoff because a reduced oil feed rate may lead to exposure of the liner surface and insufficient lubrication leading to scuffing, for example.

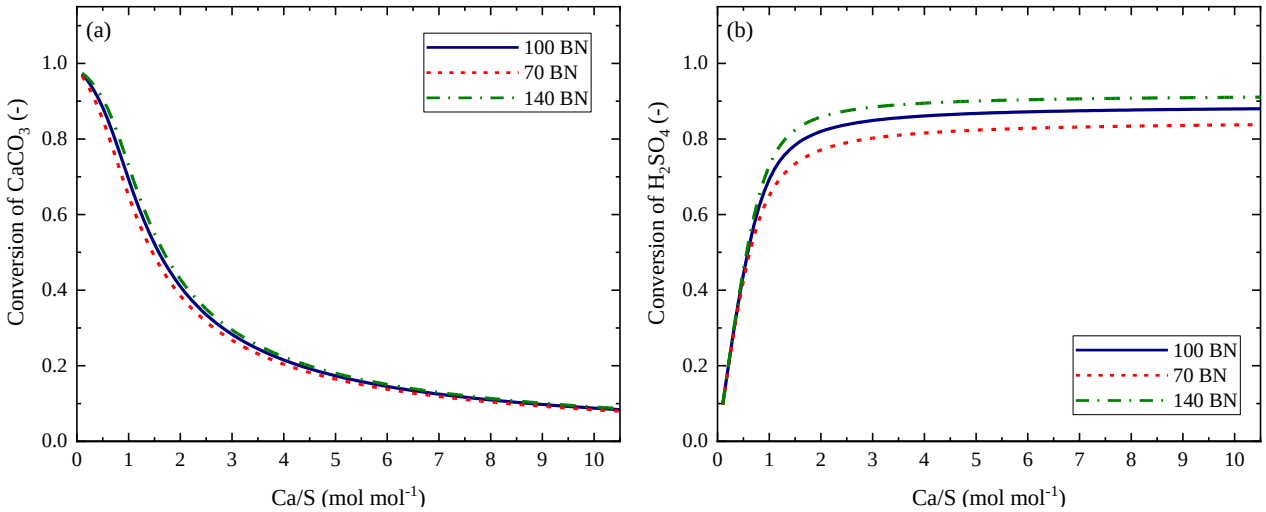

Figure 4.11. Model simulations showing conversion of (a) $CaCO_3$ reverse micelles and (b) H_2SO_4 droplets as functions of Ca/S at three values of the base number of the lube oil. The model parameters are R_{SA} = 0.5 µm, T = 423 K, τ = 0.5 s, and $C_{SA,d}$ = 18·10^3 mol m^{-3}, as well as those in Table 4.1.

4.6.1.3 Concentration of H_2SO_4 droplets

The effect of varying the concentration of the H_2SO_4 droplets is investigated in Figure 4.12. At a Ca/S molar ratio equal to 1, the conversion of H_2SO_4 increases by 10 and 23%, respectively, when the H_2SO_4 droplet concentration is diluted by factors of 5 and 10 compared with the reference value. When the H_2SO_4 droplet concentration decreases, the H_2SO_4 droplet flow, F_{SA}, is increased to maintain a constant Ca/S molar ratio. The number of H_2SO_4 droplets emulsified into the lube oil film is thereby increased, but they are more dilute. This leads to an increase in the reaction rate according to Eq. (4.11), and consequently a higher conversion is found for decreasing H_2SO_4 droplet concentration. However, the effect is minor compared with that of changing k_{app} and R_{SA} (Figure 4.10).

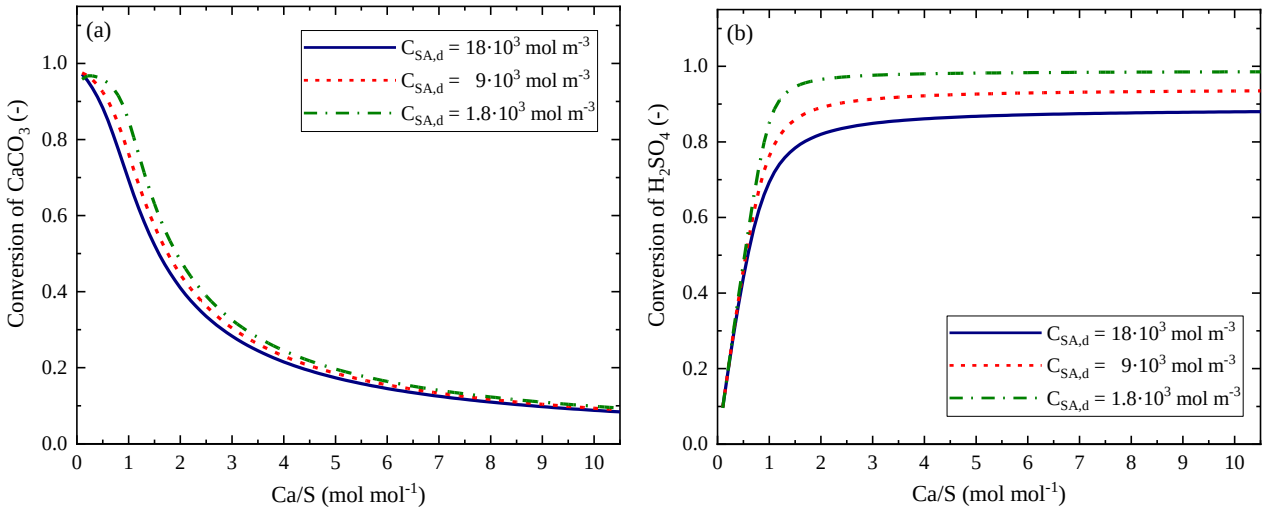

Figure 4.12. Model simulations showing conversion of (a) $CaCO_3$ reverse micelles and (b) H_2SO_4 droplets as functions of Ca/S at three values of H_2SO_4 droplet concentration. The model parameters are R_{SA} = 0.5 µm, T = 423 K, τ = 0.5 s, and $f_{L,oil,w}$ = 0.089 kg kg^{-1} (100 BN), as well as those in Table 4.1.

The simulations in Figure 4.12 show an opposite effect from decreased H_2SO_4 concentration as compared with that in the MFR experiments, where a decrease in H_2SO_4 concentration from $18 \cdot 10^3$ to $5 \cdot 10^3$ mol m^{-3} led to a small reduction in conversion.[38] However, significantly more water was introduced in the MFR experiments when decreasing the H_2SO_4 concentration and maintaining the Ca/S molar ratio. This may have reduced the solubilization of the H_2SO_4 droplets because of the limited amount of excess of dispersants and detergents in the lube oil, resulting in enlarged droplets. As shown in Figure 4.8, larger H_2SO_4 droplets result in a reduction in the conversion. The isolated effect of changing the H_2SO_4 droplet concentration may therefore be difficult to assess experimentally. Another explanation for the difference between the experimental and modeling results could lie in the assumption of the model that the used reaction rate constant does not depend on the H_2SO_4 droplet concentration. Duan et al.[54] show that the shrinking rate (dR_{SA}/dt) of acetic acid droplets in fully formulated passenger-car lube oil decreases when the acetic acid droplet concentration is decreased. Also, Fu et al.[26] report that the shrinking rate of a droplet of pure water is about 1 magnitude lower than that of a H_2SO_4 droplet. This suggests that the shrinking rate depends on the nature, chemical interactions, and concentration of the droplets. Local condensation of strongly diluted H_2SO_4 droplets will increase the water content of the lube oil emulsion. This could possibly lead to disruption of the lube oil film and direct H_2SO_4-metal contact, causing accelerated corrosion of the cylinder liner material,[62,63] especially at a low Ca/S molar ratio (Figure C.1 in Appendix C).

4.6.1.4 Residence time

The effect of reaction time is investigated in Figure 4.13. It is done by fixing the volume of the lube oil film and only changing the volumetric inlet lube oil flow rate, $v_{oil,f}$. The conversion increases with residence time, as expected. At a Ca/S equal to 1, the conversion decreases by 35% when the residence time is decreased from 0.5 to 0.1 s, and increases 22% when the residence time is increased from 0.5 to 2.5 s. In the MFR experiments, no effect of residence time in the range from 48 to 210 s at Ca/S molar ratios around 1.4 and 2.0 was found.[38] However, the model predicts an increase in the conversion of $CaCO_3$ by 17% at Ca/S = 1.4 when the residence time is increased from 48 to 210 s in the MFR (Figure C.2 in Appendix C).

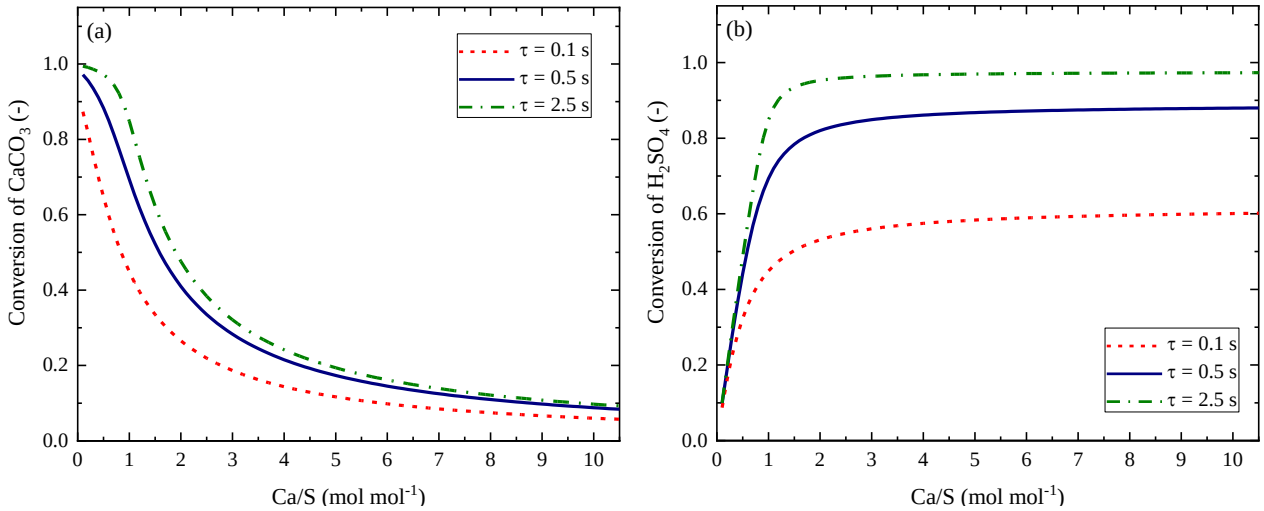

Figure 4.13. Model simulations showing conversion of (a) $CaCO_3$ reverse micelles and (b) H_2SO_4 droplets as functions of Ca/S at three values of lube oil film residence time. The model parameters are R_{SA} = 0.5 µm, T = 423 K, $f_{L,oil,w}$ = 0.089 kg kg^{-1} (100 BN), and $C_{SA,d}$ = $18 \cdot 10^3$ mol m^{-3}, as well as those in Table 4.1.

In Figure 4.14, the conversion of $CaCO_3$ (Figure 4.14(a)) and H_2SO_4 (Figure 4.14(b)) is shown as a function of residence time for three different Ca/S molar ratios. According to the predictions, the neutralization is initially very fast at engine conditions. This is in agreement with the findings of Roman,[35] who performed stirred thin lube oil film batch reactor experiments with a Ca/S molar ratio of around 0.5, a 100 BN lube oil, and a temperature of 373 K. He concluded that the reaction is extremely rapid and takes place within only a few seconds before reaching a plateau with a significantly reduced reaction rate. Modeling simulations for the same conditions as those of Roman indicate a 50% conversion of $CaCO_3$ within 0.4 s, whereas 90% conversion is achieved for a residence time of 5 s. These values are roughly in agreement with the ones given by Roman.[35]

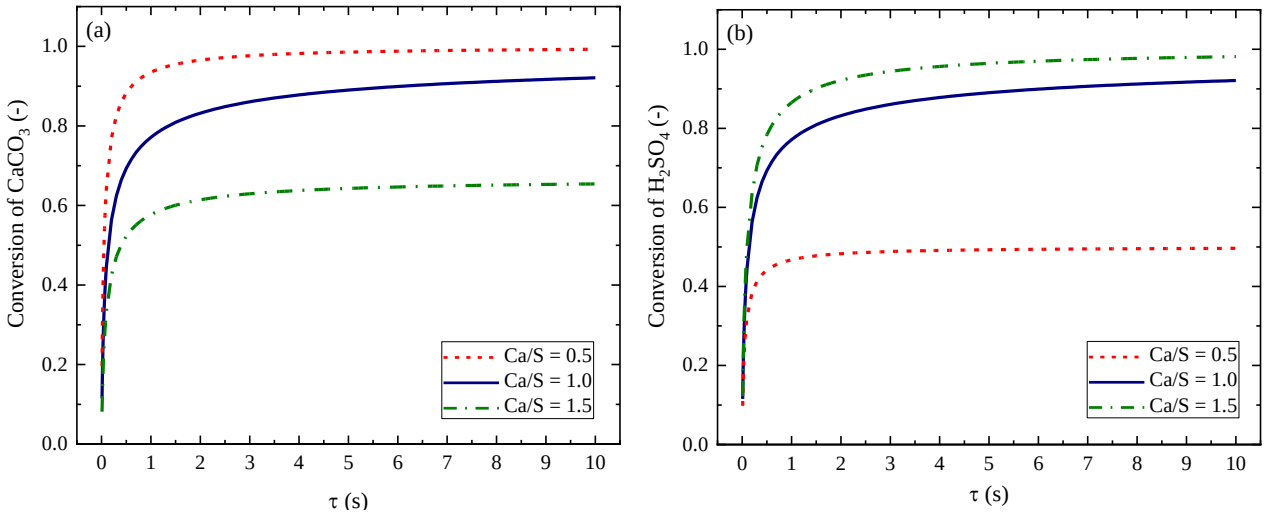

Figure 4.14. Model simulations showing conversion of (a) $CaCO_3$ reverse micelles and (b) H_2SO_4 droplets as functions of residence time at three values of Ca/S. The model parameters are R_{SA} = 0.5 µm, T = 423 K, $f_{L,oil,w}$ = 0.089 kg kg^{-1} (100 BN), and $C_{SA,d}$ = 18·10^3 mol m^{-3}, as well as those in Table 4.1.

4.6.1.5 Lube oil temperature

The effect of the lube oil temperature in the range 373 to 533 K is investigated in Figure 4.15. The model predicts a significant effect of temperature on conversion. The H_2SO_4 is almost fully neutralized after 0.5 s when the temperature is higher than 473 K and Ca/S>1 (Figure 4.15(b)). For instance, 92.5% H_2SO_4 is neutralized after 0.5 s at 533 K at Ca/S = 1. When H_2SO_4 is in great excess (e.g. Ca/S = 0.1), the $CaCO_3$ is almost completely depleted locally at these temperatures.

At 373 K (i.e., the lower end of the liner temperature in a two-stroke marine diesel engine),[7] a significant fraction of the H_2SO_4 is not neutralized, and the H_2SO_4 has the potential of interacting with the cylinder liner surface during the stagnant period until the next mixing stroke.

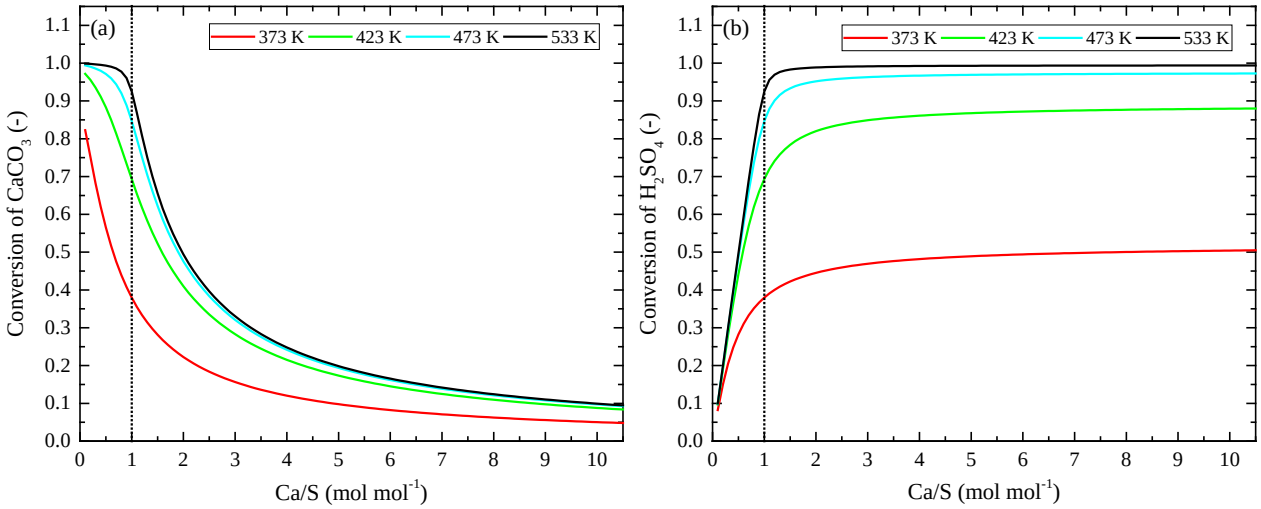

Figure 4.15. Model simulations showing conversion of (a) $CaCO_3$ reverse micelles and (b) H_2SO_4 droplets as functions of Ca/S at varying temperatures between 373 and 533 K. The model parameters are R_{SA} = 0.5 µm, τ = 0.5 s, $f_{L,oil,w}$ = 0.089 kg kg^{-1} (100 BN), and $C_{SA,d}$ = 18·10^3 mol m^{-3}, as well as those in Table 4.1. The vertical dotted line represents Ca/S = 1.

By use of Eq. (4.6), it is possible to calculate the average concentration of H_2SO_4 in the lube oil film emulsion after 0.5 s of reaction time after mixing by the passing piston rings and thereby also at the cylinder liner surface during the stagnant time period (see Figure 4.16). The H_2SO_4 concentration increases dramatically for Ca/S<1, showing that it is important to avoid a local excess of H_2SO_4 compared with $CaCO_3$ on the cylinder liner surface, in order to minimize corrosion and wear of the cylinder liner and piston rings. The concentration of H_2SO_4 decreases with increasing lube oil temperature, as expected from Figure 4.15.

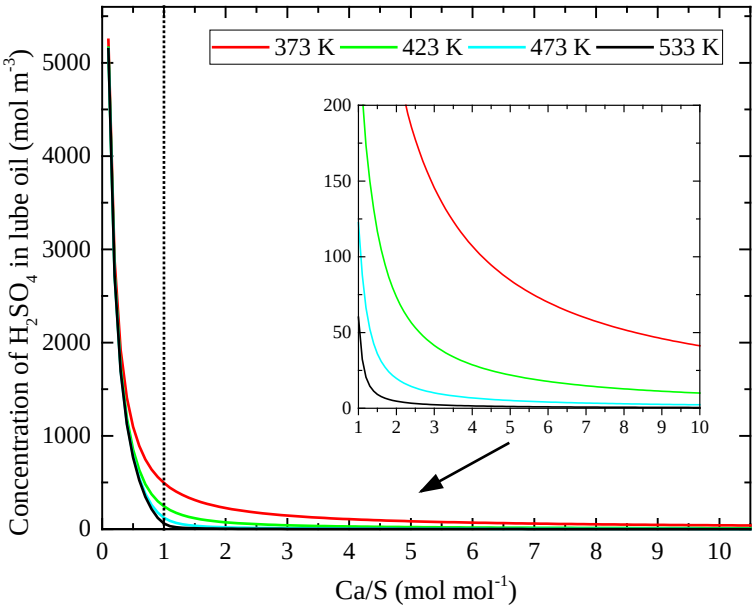

Figure 4.16. Model simulations showing the average concentration of H_2SO_4 in the lube oil film as a function of Ca/S at varying temperatures between 373 and 533 K. The model parameters are R_{SA} = 0.5 µm, τ = 0.5 s, $f_{L,oil,w}$ = 0.089 kg kg^{-1} (100 BN), and $C_{SA,d}$ = 18·10^3 mol m^{-3}, as well as those in Table 4.1. The vertical dotted line represents Ca/S = 1.

The results of Figure 4.15 and Figure 4.16 indicate that the H_2SO_4 is likely to reach the cylinder liner surface no matter how well lubricated the surface is. However, a certain degree of corrosion may be beneficial in order to maintain a rough cylinder liner surface for supporting a lube oil film.[11]

4.6.2 Practical implications

The parametric study indicates that the neutralization of H_2SO_4 and the interaction of H_2SO_4 with the liner surface is a complex function of lube oil formulation; the flow pattern at the cylinder liner (mixing behavior); and the vertical, local position at the cylinder liner (which affects the lube oil temperature, the residence time, and the concentration of condensing H_2SO_4). The upper part of the cylinder liner is the segment where the most severe wear is found.[3,64] In this section, possible factors affecting the presence of H_2SO_4 at the liner surface in the upper region are discussed.

The cylinder liner temperature in the upper part is high.[1] Consequently, a decrease in H_2SO_4 condensation rate would be expected,[58] and the neutralization reaction would be fast (Figure 4.16), both ultimately contributing to a reduction in wear.[1,3] However, the pressure in the cylinder liner is highest when the piston is near top dead center (TDC) upon combustion (thus SO_3/H_2SO_4 partial pressures are highest near TDC), resulting in a high dew point temperature of H_2SO_4(aq) in this area.[3] Furthermore, the upper part of the cylinder is exposed to the combustion gas for the longest length of time.[7] Despite the higher temperature, most of the H_2SO_4 formed from oxidation of the fuel sulfur may thus condense on the upper part of the cylinder liner segment, as reported.[7,58] A high load of H_2SO_4 in the lube oil in this region could also be facilitated by the upward motion of the piston, collecting the condensed H_2SO_4 above the top piston ring.[26] The upper part of the cylinder is also the area where the piston speed is the lowest,[1] decreasing the degree of mixing of the lube oil film, and the lube oil film thickness is at its minimum.[60] A local excess of H_2SO_4 compared with $CaCO_3$ in the upper part of the cylinder liner would explain the corrosive wear that has been observed. In addition, more water is known to condense in the upper part of the cylinder,[7] increasing the risk of direct H_2SO_4-liner contact through disruption of the lube oil film.[62,63]

One method to reduce the wear would be to increase the flow rate of lube oil and thereby the local Ca/S molar ratio in the upper segment. For a constant thickness of the lube oil film, the average residence time depends on the engine load and the feed rate of lube oil. When increasing the feed rate and the engine load, the average residence time decreases.[3,65] However, at the same time, more $CaCO_3$ is introduced, increasing the Ca/S molar ratio. The effect of increasing Ca/S is considerable when Ca/S<1.5, according to Figure 4.15. A lower engine load leads to a lower piston velocity, thus increasing the exposure time between lube oil and H_2SO_4. This gives more time for the neutralization reaction to occur, but it also gives more time for non-neutralized H_2SO_4 in the lube oil emulsion to react with the cylinder liner material at stagnant conditions. The Ca/S molar ratio can also be increased by using higher BN lube oil. According to the present work, increasing the BN of the lube oil at maintained Ca/S molar ratio, would lead to a slightly faster neutralization of H_2SO_4, thereby decreasing the contact between H_2SO_4 and the liner and consequently the corrosion. This is in accordance with experiences from service.[1]

The above analysis shows that the prevention of cold corrosion is a complex challenge. H_2SO_4 will be present at the cylinder liner surface to some degree regardless of how well-lubricated the surface is. It is therefore more a matter of how much H_2SO_4 can be neutralized in the shortest period of time, in order to prevent undesired corrosion in large two-stroke marine diesel engines.

4.7 Conclusions

The reaction between H_2SO_4 droplets and $CaCO_3$ micelles in lube oil has been studied in a well-mixed flow reactor and a batch reactor at Ca/S molar ratios, relevant for a real engine application. The purpose was to isolate the rate-limiting steps of the neutralization mechanism, potentially a single one. For the residence times investigated, the results showed that the reactant conversion was significantly reduced when the Ca/S molar ratio approached unity. It was also found, that a certain degree of stirring is required to establish contact between H_2SO_4 droplets and $CaCO_3$ reverse micelles in order to initiate and maintain the reaction, probably to effectively emulsify H_2SO_4 into the lube oil.

A mathematical model for the neutralization of H_2SO_4 droplets by $CaCO_3$ reverse micelles in lube oil under mixed-flow conditions has been developed and verified by using mixed flow reactor experimental data obtained by the authors. It was difficult to identify conclusively the limiting step of the neutralization reaction, however, a quantitative description of the reaction rate and its temperature-dependency was determined. The mixed flow reactor model offers a useful approximation of conditions in the lube oil film on the cylinder liner and can be used to assess the importance of different process parameters. The neutralization reaction rate increases significantly with the lube oil temperature, whereas the lube oil base number and the H_2SO_4 droplet concentration have only a minor impact at a maintained Ca/S molar ratio. Modeling predictions indicate that H_2SO_4 will be present to some degree on the cylinder liner surface, independent of how well-wetted the liner is. The concentration of H_2SO_4 in the lube oil film is significantly increased for conditions with a local molar excess of H_2SO_4 compared with $CaCO_3$ micelles (Ca/S<1). To control the corrosion rate, it is important to ensure that sufficient lube oil is provided in critical regions, particularly at the upper part of the cylinder liner where the most pronounced wear is most often found.

Both the derived reaction kinetics, which can be used in computational fluid dynamics (CFD) models, and the mathematical model are expected to facilitate further studies to understand and control corrosion and wear in large two-stroke marine diesel engines. By connecting the knowledge of where H_2SO_4 is condensing[58,66] with how it is neutralized (the present article), it may be possible to optimize the spatial lube oil dosage onto the cylinders to counteract severe corrosive wear.

Acknowledgments

This work is part of the Combustion and Harmful Emission Control (CHEC) research center at the Department of Chemical and Biochemical Engineering at the Technical University of Denmark. The project is funded by the Innovation Fund Denmark and cosponsored by MAN Energy Solutions and the Technical University of Denmark through the SULCOR project under grant 4106-00028B.

Nomenclature

A_i = Surface area of component i ($4\pi R_i^2$) [m^2]
BN = Base number [(mg KOH) (g oil)$^{-1}$]
Ca/S = Molar ratio of $CaCO_3$ to H_2SO_4 in inlet feed [mol mol^{-1}]
C_i = Concentration of component i [mol m^{-3}]

$C_{SA,d}$ = Concentration of H_2SO_4 in droplets [mol m^{-3}]
d_c = Critical distance where immediate reaction occurs [m]
D_i = Diffusion coefficient of component i [m^2 s^{-1}]
E_a = Activation energy [J mol^{-1}]
F_{SA} = H_2SO_4 droplet number flow [(number of droplets) s^{-1}]
f_{L} = Volume fraction of $CaCO_3$ in reverse micelle [m^3 m^{-3}]
$f_{\mathrm{L},oil,w}$ = Weight fraction of $CaCO_3$ in lube oil [kg kg^{-1}]
i = Component i [-]
k_{ads} = Adsorption-controlled reaction rate constant [m s^{-1}]
k'_{ads} = Adsorption-controlled reaction rate constant [m^3 mol^{-1} s^{-1}]
k_{app} = Apparent reaction rate constant [m s^{-1}]
k_B = Boltzmann constant, $1.38 \cdot 10^{-23}$ [kg m^2 s^{-2} K^{-1}]
k_{diff}/k'_{diff} = Diffusion-controlled reaction rate constant [m^3 mol^{-1} s^{-1}]
k_{res} = Resulting reaction rate constant [m^3 mol^{-1} s^{-1}]
M_i = Molar weight of component i [kg mol^{-1}]
N = Stirrer speed [rpm]
N_A = Avogadro's constant, $6.022 \cdot 10^{23}$ [molecules mol^{-1}]
n_i = Moles of component i [mol]
N_i = Number of component i per volume [number m^{-3}]
$N_{i,f}$ = Number of component i per volume in inlet feed [number m^{-3}]
$n_{\mathrm{L,M}}$ = Moles of $CaCO_3$ per reverse micelle [mol]
$-r_{A,i}$ = Reaction rate [mol m^{-3} s^{-1}]
R = Ideal gas constant, 8.314 [J mol^{-1} K^{-1}]
R_i = Radius of component i [m]
t = Time [s]
T = Temperature in lube oil volume [K]
V_i = Average volume of component i ($4/3\,\pi R_i^3$) [m^3]
$v_{i,f}$ = Volumetric feed rate of component i [m^3 s^{-1}]
v_o = Volumetric outflow of lube oil emulsion [m^3 s^{-1}]
V_{oil} = Volume of lube oil in mixed flow reactor [m^3]
$\bar{x}$ = Mean Brownian displacement of a particle [m]
X_{i} = Conversion of component i [-]

Greek Letters
η = Lube oil dynamic viscosity [kg m^{-1} s^{-1}]
θ = Fraction of surface that is occupied [-]
ρ_i = Density of component i [kg m^{-3}]
τ = Residence time [s]

Subscripts
ads = Adsorption-controlled
app = Apparent
diff = Diffusion-controlled
d = Droplet

f = Inlet feed
L = Limestone, $CaCO_3$ or $CaCO_3$ reverse micelle
o = Outlet
Oil = Lube oil
SA = Sulfuric acid, H_2SO_4 or H_2SO_4 droplet
w = weight

References

(1) CIMAC Working Group 8 “Marine Lubricants.” CIMAC Guideline Cold Corrosion in Marine Two Stroke Engines. 2017.

(2) MAN Diesel & Turbo. Service Letter SL2014-587/JAP. 2014.

(3) García, L.; Gehle, S.; Schakel, J. Impact of Low Load Operation in Modern Low Speed 2-Stroke Diesel Engines on Cylinder Liner Wear Caused by Increased Acid Condensation. *J. JIME* **2014**, *49* (1), 100–106.

(4) Cordtz, R. L.; Schramm, J.; Rabe, R. Investigating SO_3 Formation from the Combustion of Heavy Fuel Oil in a Four-Stroke Medium Speed Test Engine. *Energy Fuels* **2013**, *27* (10), 6279–6286.

(5) Adamkiewicz, A.; Drzewieniecki, J. Operational Evaluation of Piston Ring Wear in Large Marine Diesel Engines. *J. Polish CIMAC* **2012**.

(6) Cordtz, R. The Influence of Fuel Sulfur on the Operation of Large Two-Stroke Marine Diesel Engines. Ph.D. Dissertation, Technical University of Denmark, Kgs. Lyngby, 2015.

(7) Cordtz, R.; Mayer, S.; Eskildsen, S. S.; Schramm, J. Modeling the Condensation of Sulfuric Acid and Water on the Cylinder Liner of a Large Two-Stroke Marine Diesel Engine. *J. Mar. Sci. Technol.* **2018**, *23* (1), 178–187.

(8) Amblard, C. New Chemistry to Protect against Cold Corrosion in Marine Cylinder Lubricants. *J. Japan Inst. Mar. Eng.* **2015**, *50* (6), 54–62.

(9) Golothan, D. W. Review of the Causes of Cylinder Wear in Marine Diesel Engines. *Inst. Mar. Eng. Trans.* **1978**, *90*, 137–163.

(10) Bovington, C. H. Friction, Wear and the Role of Additives in Controlling Them. In *Chemistry and Technology of Lubricants*; Mortier, R. M., Fox, M. F., Orszulik, S. T., Eds.; Springer Netherlands: Dordrecht, 2010; pp 77–105.

(11) Atkinson, D. Onboard Condition Monitoring of Cold Corrosion in Two-Stroke Marine Diesel Engines. *11th Int. Conf. Cond. Monit. Mach. Fail. Prev. Technol. C. 2014 / MFPT 2014* **2014**, *5* (2), 17–22.

(12) Marković, I.; Ottewill, R. H.; Cebula, D. J.; Field, I.; Marsh, J. F. Small Angle Neutron Scattering Studies on Non-Aqueous Dispersions of Calcium Carbonate - Part I. The Guinier Approach. *Colloid Polym. Sci.* **1984**, *262* (8), 648–656.

(13) Seddon, E. J.; Friend, C. L.; Roski, J. P. Detergents and Dispersants. In *Chemistry and Technology of Lubricants*; Mortier, R. M., Fox, M. F., Orszulik, S. T., Eds.; Springer Netherlands: Dordrecht, 2010; pp 213–236.

(14) Bodnarchuk, M. S.; Heyes, D. M.; Breakspear, A.; Chahine, S.; Edwards, S.; Dini, D. Response of Calcium Carbonate Nanoparticles in Hydrophobic Solvent to Pressure, Temperature, and Water. *J. Phys. Chem. C* **2015**, *119* (29), 16879–16888.

(15) Bodnarchuk, M. S.; Heyes, D. M.; Breakspear, A.; Chahine, S.; Dini, D. A Molecular Dynamics Study of $CaCO_3$ Nanoparticles in a Hydrophobic Solvent with a Stearate Co-Surfactant. *Phys. Chem.*

Chem. Phys. **2015**, *17* (20), 13575–13581.

(16) Bodnarchuk, M. S.; Dini, D.; Heyes, D. M.; Breakspear, A.; Chahine, S. Molecular Dynamics Studies of Overbased Detergents on a Water Surface. *Langmuir* **2017**, *33* (29), 7263–7270.

(17) Jakobsen, S. B. Service Experience of MAN B&W Two Stroke Diesel Engines. In *28th CIMAC World Congress*; Helsinki, 2016.

(18) Jacobsen, D. M. S.; Pedersen, J. M.; Svensson, J.; Mayer, S. Cylinder Lube Oil Experiences and New Development for the MAN B&W Two-Stroke Engines. In *28th CIMAC World Congress*; Helsinki, 2016.

(19) Christensen, O. Cylinder Lubrication of Two-Stroke Crosshead Marine Diesel Engines. *Wärtsilä Tech. J.* **2010**, 39–48.

(20) Wu, R. C.; Papadopoulos, K. D.; Campbell, C. B. Visualization Test for Neutralization of Acids by Marine Cylinder Lubricants. *AIChE J.* **1999**, *45* (9), 2011–2017.

(21) Wu, R. C.; Papadopoulos, K. D.; Campbell, C. B. Acid-Neutralizing of Marine Cylinder Lubricants: Measurements and Effects of Dispersants. *AIChE J.* **2000**, *46* (7), 1471–1477.

(22) Wu, R. C.; Campbell, C. B.; Papadopoulos, K. D. Acid-Neutralizing of Marine Cylinder Lubricants: Effects of Nonionic Surfactants. *Ind. Eng. Chem. Res.* **2000**, *39* (10), 3926–3931.

(23) Fu, J.; Lu, Y.; Campbell, C. B.; Papadopoulos, K. D. Optical Microscopy inside a Heating Capillary. *Ind. Eng. Chem. Res.* **2005**, *44* (5), 1199–1203.

(24) Fu, J.; Lu, Y.; Campbell, C. B.; Papadopoulos, K. D. Temperature and Acid Droplet Size Effects in Acid Neutralization of Marine Cylinder Lubricants. *Tribol. Lett.* **2006**, *22* (3), 221–225.

(25) Fu, J.; Lu, Y.; Campbell, C. B.; Papadopoulos, K. D. Acid Neutralization by Marine Cylinder Lubricants Inside a Heating Capillary: Strong/Weak-Stick Collision Mechanisms. *Ind. Eng. Chem. Res.* **2006**, *45* (16), 5619–5627.

(26) Fu, J.; Papadopoulos, K. D.; Lu, Y.; Campbell, C. B. Ostwald Ripening: A Decisive Cause of Cylinder Corrosive Wear. *Tribol. Lett.* **2007**, *27* (1), 21–24.

(27) Garcia-Bermudes, M.; Rausa, R.; Papadopoulos, K. Vertically-Oriented-Capillary Video-Microscopy: Drops Levitated by a (Reacting) Fluid. *Ind. Eng. Chem. Res.* **2011**, *50* (24), 14142–14147.

(28) Garcia-Bermudes, M.; Rausa, R.; Papadopoulos, K. Formation of Colloidal Shells on Acidic Droplets Undergoing Neutralization in Marine Diesel Engine Cylinder Oils. *Tribol. Lett.* **2013**, *51* (1), 85–92.

(29) Duan, Y.; Rausa, R.; Zhao, Q.; Papadopoulos, K. D. Neutralization Mechanism of Acetic Acid by Overbased Colloidal Nanoparticles. *Tribol. Lett.* **2016**, *64* (8), 1–11.

(30) Hone, D. C.; Robinson, B. H.; Steytler, D. C.; Glyde, R. W.; Cleverley, J. A. Acid-Base Chemistry in High-Performance Lubricating Oils. *Can. J. Chem.* **1999**, *77*, 842–848.

(31) Hone, D. C.; Robinson, B. H.; Steytler, D. C.; Glyde, R. W.; Galsworthy, J. R. Mechanism of Acid Neutralization by Overbased Colloidal Additives in Hydrocarbon Media. *Langmuir* **2000**, *16* (2), 340–346.

(32) Hone, D.; Robinson, B.; Galsworthy, J.; Glyde, R. Colloidal Chemistry of Lubricating Oils. In *Reactions And Synthesis In Surfactant Systems*; Texter, J., Ed.; Surfactant Science; CRC Press, 2001; pp 385–394.

(33) Hosonuma, K.; Tamura, K. Acid Neutralization of Overbased Detergents (Part 1) Neutralization in the Test Methods of ASTM Base Number. *J. Japan Pet. Inst.* **1984**, *27* (2), 101–107.

(34) Hosonuma, K.; Tamura, K. Acid Neutralization of Overbased Detergents (Part 2) Neutralization with Sulfuric Acid Emulsion. *J. Japan Pet. Inst.* **1984**, *27* (2), 108–113.

(35) Roman, J.-P. New Method of Measurement in Thin Film of the Neutralization of Marine Lubricants for Low-Speed and Medium-Speed Diesel Engines. In *CIMAC Congress 1998, Copenhagen*;

Copenhagen, 1998; pp 913–926.
(36) Akiyama, K.; Masunaga, K.; Kado, K.; Yoshioka, T. Cylinder Wear Mechanism in an EGR-Equipped Diesel Engine and Wear Protection by the Engine Oil. Paper 872158. *SAE Int.* **1987**, 1–7.
(37) Roman, J.-P.; Foin, C.; Hosonuma, K.; Naganuma, N. Study of the Impact of Marine Lubricants Additive Chemistry on Adhesive Wear, Scuffing and Corrosive Wear - Relationship between Neutralization Speed Measured by NAMO and Corrosive Wear. In *CIMAC Congress*; Hamburg, 2001; pp 1284–1298.
(38) Lejre, K. H.; Kiil, S.; Glarborg, P.; Christensen, H.; Mayer, S. Reaction of Sulfuric Acid in Lube Oil: Implications for Large Two-Stroke Diesel Engines. In *Proceedings of the ASME 2017 Internal Combustion Engine Division Fall Technical Conference*; ASME: Seattle, United States, 2017; Vol. 1, pp 1–10.
(39) Schramm, J.; Henningsen, S.; Sorenson, S. C. Modelling of Corrosion of Cylinder Liner in Diesel Engines Caused by Sulphur in the Diesel Fuel. In *SAE Technical Paper*; SAE International, 1994; pp 1–10.
(40) van Helden, A. K. A Physico-Chemical Model of Corrosive Wear in Low Speed Diesel Engines, Report D-9. 1987, pp 1–16.
(41) van Helden, A. K.; Valentijn, M. C.; van Doornt, H. M. J. Corrosive Wear in Crosshead Diesel Engines. *Tribol. Int.* **1989**, *22* (3), 189–193.
(42) ASTM International. ASTM 2896-11. Standard Test Method for Base Number of Petroleum Products by Potentiometric Perchloric Acid Titration. 2011.
(43) Kiil, S. Experimental and Theoretical Investigations of Wet Flue Gas Desulphurisation. Ph.D. Dissertation, Technical University of Denmark, Kgs. Lyngby, 1998.
(44) Laidler, K. J. *Chemical Kinetics*; Harper & Row: New York, 1987.
(45) Goodwin, J. W. *Colloids and Interfaces with Surfactants and Polymers*; John Wiley & Sons, Ltd: Chichester, UK, 2009.
(46) Kontogeorgis, G. M.; Kiil, S. *Introduction to Applied Colloid and Surface Chemistry*; John Wiley & Sons, Ltd: Chichester, UK, 2016.
(47) Sautermeister, F. A.; Priest, M. Physical and Chemical Impact of Sulphuric Acid on Cylinder Lubrication for Large 2-Stroke Marine Diesel Engines. *Tribol. Lett.* **2012**, *47* (2), 261–271.
(48) Sautermeister, F. A.; Priest, M.; Lee, P. M.; Fox, M. F. Impact of Sulphuric Acid on Cylinder Lubrication for Large 2-Stroke Marine Diesel Engines: Contact Angle, Interfacial Tension and Chemical Interaction. *Tribol. Int.* **2013**, *59*, 47–56.
(49) Hudson, L. K.; Eastoe, J.; Dowding, P. J. Nanotechnology in Action: Overbased Nanodetergents as Lubricant Oil Additives. *Adv. Colloid Interface Sci.* **2006**, *123-126* (SPEC. ISS.), 425–431.
(50) Roman, J.-P.; Hoornaert, P.; Faure, D.; Biver, C.; Jacquet, F.; Martin, J.-M. Formation and Structure of Carbonate Particles in Reverse Microemulsions. *J. Colloid Interface Sci.* **1991**, *144* (2), 324–339.
(51) Marković, I.; Ottewill, R. H. Small Angle Neutron Scattering Studies on Non-Aqueous Dispersions of Calcium Carbonate. Part III. Concentrated Dispersions. *Colloid Polym. Sci.* **1986**, *264* (5), 454–462.
(52) Marković, I.; Ottewill, R. H. Small Angle Neutron Scattering Studies on Nonaqueous Dispersions of Calcium Carbonate Part 2. Determination of the Form Factor for Concentric Spheres. *Colloid Polym. Sci.* **1986**, *264* (1), 65–76.
(53) Papadopoulos, K. D. Personal Communication, March 13, 2019.
(54) Duan, Y.; Rausa, R.; Fiaschi, P.; Papadopoulos, K. D. Neutralization of Acetic Acid by Automobile Motor Oil. *Tribol. Int.* **2016**, *98*, 94–99.
(55) John R. Rumble. CRC Handbook of Chemistry and Physics http://hbcponline.com (accessed May 1, 2018).

(56) Perry, R. H. *Perry's Chemical Engineers' Handbook*, 7th ed.; Green, D. W., Maloney, J. O., Eds.; McGraw-Hill: New York, 1997.
(57) Mortier, R. M.; Fox, M. F.; Orszulik, S. T. *Chemistry and Technology of Lubricants*, 3rd ed.; Springer Netherlands: Dordrecht, 2010.
(58) Karvounis, N.; Pang, K. M.; Mayer, S.; Walther, J. H. Numerical Simulation of Condensation of Sulfuric Acid and Water in a Large Two-Stroke Marine Diesel Engine. *Appl. Energy* **2018**, *211*, 1009–1020.
(59) CIMAC Working Group 8 "Marine Lubricants." CIMAC Recommendation 31: The Lubrication of Two-Stroke Crosshead Diesel Engines. 2017.
(60) Christiansen, J.; Klit, P.; Volund, A.; Hwang, J.-H. Calculation of Oil Film Thickness from Damping Coefficients for a Piston Ring in an Internal Combustion Engine. In *Proceedings of the International Conference BALTTRIB'2007*; Kaunas, 2007; pp 162–167.
(61) Doyen, V.; Drijfholt, R. K.; Delvigne, T. PAPER NO .: 61 Advanced Applied Research Unravelling the Fundamentals of 2-Stroke Engine Cylinder Lubrication – an Innovative on-Line Measurement Method Based on the Use of Radioactive Tracers-. *CIMAC Congr. 2007, Vienna* **2007**.
(62) Stott, F. H.; Macdonald, A. G. The Influence of Acid Strength on the Corrosive Wear of Grey Cast Irons in Oil-Sulphuric Acid Mixtures. *Wear* **1988**, *122* (3), 343–361.
(63) Macdonald, A. G.; Stott, F. H. The Corrosive Wear of Cast Iron in Oil-Sulphuric Acid Mixtures. *Corros. Sci.* **1988**, *28* (5), 485–501.
(64) Cordtz, R.; Schramm, J.; Andreasen, A.; Eskildsen, S. S.; Mayer, S. Modeling the Distribution of Sulfur Compounds in a Large Two Stroke Diesel Engine. *Energy Fuels* **2013**, *27* (3), 1652–1660.
(65) Hammett, J. Utilising the Latest Findings Engine Oil Stress from Field & Laboratory Engine Testing. *J. JIME* **2014**, *49* (3), 6–13.
(66) Pang, K. M.; Karvounis, N.; Walther, J. H.; Schramm, J.; Glarborg, P.; Mayer, S. Modelling of Temporal and Spatial Evolution of Sulphur Oxides and Sulphuric Acid under Large, Two-Stroke Marine Engine-like Conditions Using Integrated CFD-Chemical Kinetics. *Appl. Energy* **2017**, *193*, 60–73.

5 | Experimental investigation and mathematical modeling of the reaction between SO_2(g) and $CaCO_3$(s)-containing micelles in lube oil for large two-stroke marine diesel engines

This chapter is a manuscript in preparation for submission. The supporting information for this chapter can be found in Appendix E.

Abstract

When sulfur-rich fuel is burned in diesel engines, SO_2 is formed, which may oxidize and react with water to form corrosive H_2SO_4. However, the gaseous SO_2 may also consume $CaCO_3$-containing reverse micelles present in lube oil. This study investigates the reaction in a batch reactor setup. The SO_2-$CaCO_3$ reaction exhibits a weak temperature dependence because the absorption of SO_2 in the lube oil emulsion decreases at increased temperature. Further, due to increased SO_2 absorbance, the reaction shows high dependence on the initial water concentration. The conversion of $CaCO_3$ is quantified and the resulting products are determined by Fourier Transform Infrared Spectroscopy (FTIR). Initially, $CaSO_3$ is formed, but $CaSO_4$ is also observed at extended residence times and increased temperature. A mathematical model is set up and kinetic parameters are determined by fitting the model to the experimental data. The batch reactor model is then used to predict $CaCO_3$ conversions in lube oil from SO_2 for worst-case conditions relevant for a full-scale engine application. Simulations show that consumption of $CaCO_3$ from SO_2 is insignificant in a two-stroke marine diesel engine application and that the H_2SO_4-$CaCO_3$ reaction is far more important than the SO_2-$CaCO_3$ reaction.

5.1 Introduction

Due to introduction of the so-called slow-steaming approach, where large vessels began to operate at a lower load (speed), and new engine designs and tunings, the maritime sector has experienced increased sulfuric acid (H_2SO_4) condensation, originating from the fuel sulfur, leading to abnormal corrosive wear of the cylinder liner and piston rings.[1–4] To control corrosion, lubrication (lube) oils are formulated with base additives, commonly present as nanometer-sized $CaCO_3$ micelles.[5–7] At present, in some specific control areas, it is allowed to operate with a high sulfur content in the fuel if using an exhaust cleaning technology capable of reducing the emissions to a level equivalent to that of burning low-sulfur fuel.[8,9] Depending on price and availability, it may therefore be cost-effective to burn high sulfur fuels in the future, and even burning fuels with a sulfur content higher than today's limit of 3.5 wt.%. As the fuel burned switches and new engine designs are introduced, the lube oil dosing has to conform to maintain its satisfactory performance.

A defective dosing of lube oil has severe consequences, such as scuffing (direct metal to metal contact).[10,11] It is therefore crucial to have general guidelines on how lube oil should be dosed onto the cylinder liners in order to limit corrosion at a minimal cost. To achieve this, understanding of the formation of the relevant acids in the gas phase,[10,12–14] the transport to the lube oil film,[15–17] the neutralization mechanism by the base additives,[17–34] and the corrosion of the liner material[1,4,35–43] is pivotal. Information about how base additives ($CaCO_3$ micelles) are consumed is essential because this assists determination of the lube oil flow rate to the cylinder liners and its base additive concentration. In line with this, the neutralization mechanism between $CaCO_3$ micelles and H_2SO_4 droplets has been investigated and the corresponding reaction rate was determined.[19,21] Research has mainly been focused on H_2SO_4 which is thought to be the main cause for the observed corrosive wear and $CaCO_3$ consumption.[4,36] However, some studies claim that SO_2 can also contribute directly to corrosive wear and $CaCO_3$ consumption.[44–48] If this is the case, determination of reaction kinetics of the $CaCO_3$-SO_2 reaction, and the relative importance to the $CaCO_3$-H_2SO_4 reaction would allow for an assessment of what consumes the $CaCO_3$ reverse micelles. Nagaki and Korematsu[46,47] advocate that SO_2 absorbs into the lube oil film in an engine and forms H_2SO_4, which subsequently reacts with the cylinder liner and/or $CaCO_3$. Naegeli and Marbach[48] likewise found an increased wear rate for increasing SO_2 addition to the intake air through the formation of sulfurous acid (H_2SO_3). The formation of H_2SO_3 in lube oil may also contribute to consumption of $CaCO_3$. However, both research groups added the SO_2 to the intake air and one may speculate if this contributed to increased SO_3(g) formation upon the compression stroke and thereby increased the condensation rate of H_2SO_4. The isolated effect of SO_2 on consumption of $CaCO_3$ in lube oil is therefore not clear. Nevertheless, it is known from other research fields that SO_2 does indeed react with $CaCO_3$ e.g., in wet flue gas desulfurization (FGD) plants.[49,50] Here, SO_2 is removed (scrubbed) from flue gas by reacting with $CaCO_3$ in an aqueous slurry:[49]

$$SO_2 + H_2O \rightarrow H^+ + HSO_3^- \quad (5.1)$$

$$HSO_3^- \rightarrow H^+ + SO_3^{2-} \quad (5.2)$$

$$2HSO_3^- + O_2 \rightarrow 2H^+ + 2SO_4^{2-} \quad (5.3)$$

$$Ca^{2+} + SO_4^{2-} + 2H_2O \rightarrow CaSO_4 \cdot 2H_2O(s) \quad (5.4)$$

This means that SO_2 reacts with $CaCO_3$ to form $CaSO_4$, which is the same product when $CaCO_3$ is reacting with H_2SO_4.[18,19] However, if the system is not saturated with O_2, the following may happen:[49]

$$Ca^{2+} + SO_3^{2-} + \frac{1}{2}H_2O \rightarrow CaSO_3 \cdot \frac{1}{2}H_2O(s) \quad (5.5)$$

The above illustrates that, besides $CaCO_3$ and SO_2, water and O_2 have to be present in the reaction system. The reactions only happen when water is present because SO_2 is absorbed into the water according to Eq. (5.1). The process is usually carried out at a temperature in the range 40-60 ^oC, at a pH in the range 5-6, and at atmospheric pressure.[49–51] Furthermore, the reaction between gaseous SO_2, in a humid simulated flue gas, and $CaCO_3$ particles has been investigated in a sand bed reactor.[52] Here, it was found that the oxygen content in the simulated flue gas (0-9%) had a minor effect on the initial reaction rate, whereas the relative humidity (0.24-0.92) and particle diameter (4-100 µm) had significant effects. Also, the temperature dependency of the reaction indicated a weak dependency (investigated in the range 40-80 ^oC). At 23 ^oC in another study, both in presence and absence of water, the reaction between gaseous SO_2 and $CaCO_3$ particles was investigated, finding that both $CaSO_3$ and $CaSO_4$ were formed and that the reaction was significantly enhanced when water was present.[53,54] However, dissimilarities exist between the reaction conditions of the above-mentioned examples and the conditions prevailing in a lube oil film; the most crucial one being the presence of the lube oil phase itself. However, precursors for a successful reaction may be present in a lube oil film in an engine: plenty of condensing water, plenty of SO_2 and O_2 in the combustion chamber, reactive $CaCO_3$ reverse micelles, and that SO_2 absorbs in oil.[12,15,16,19,55]

The scope of the present work is to investigate the reaction between gaseous SO_2 and $CaCO_3$ reverse micelles in lube oil in the presence of water and O_2, and more specifically to decide if SO_2 is able to consume any of the $CaCO_3$ in the lube oil. The components are pressurized in a batch reactor setup at specific conditions such as residence time, Ca/S molar ratio, pressure, temperature, and water content. Upon an experiment, the lube oil is analyzed and the conversion of $CaCO_3$ and the products are determined. Reaction kinetics is derived by setting up a model of the batch reactor setup, followed by fitting of the model to the experimental data. The mathematical model is then used to investigate the importance of the SO_2-$CaCO_3$ reaction at specific marine diesel engine conditions.

5.2 Experimental section

5.2.1 Materials

Lube oil from Infineum, with a base number (BN) value of 100±2, which corresponds to 8.9±0.18 wt.% $CaCO_3$, was used. The BN is defined as the quantity of acid, expressed in terms of the equivalent number of milligrams of KOH, required to neutralize all alkaline constituents in a 1 g sample.[56] The two gas mixtures (technical air and 1 mol% SO_2 in air) were obtained from AGA A/S. For the Karl Fischer titration method, Hydranal Solvent-Oil, Hydranal Titrant 2, and Toluene were applied, all obtained from Sigma-Aldrich. The $CaSO_3 \cdot 0.5H_2O$ and $CaSO_4 \cdot 2H_2O$ powders were from Wako and Sigma-Aldrich, respectively, and the $CaCO_3$ powder was Faxe Bryozo limestone from Faxe, Denmark.

5.2.2 Batch reactor setup

The reaction was investigated in a stirred batch reactor (Parr 4575) at temperatures and pressures similar to a full-scale marine diesel engine application. The batch reactor setup is illustrated in Figure 5.1.

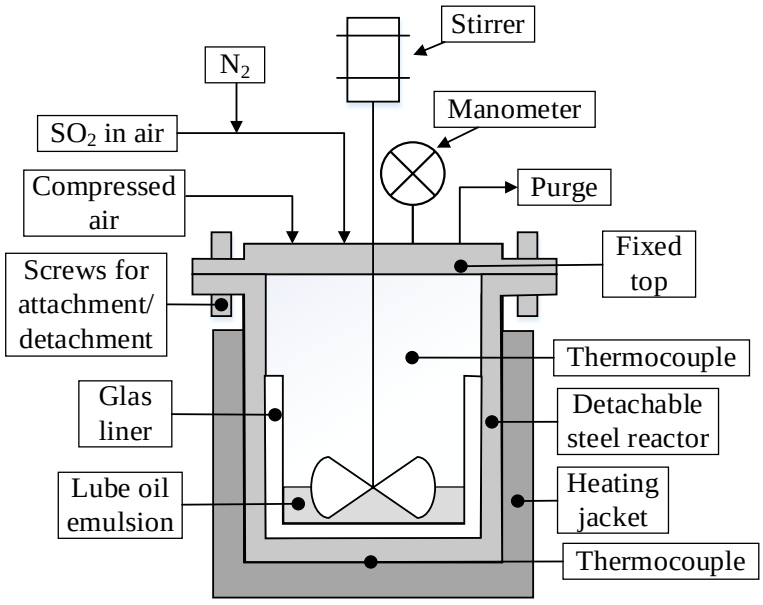

Figure 5.1. Illustration of the high-pressure and high-temperature batch reactor setup.

Lube oil and water were weighed prior to an experiment in a glass beaker (liner) to achieve specific water and $CaCO_3$ contents in the lube oil emulsion. Typical values were 9 g of lube oil and 0.5 g of demineralized water. The beaker was then placed inside the reactor. It was possible to achieve a maximum pressure of around 200 bar and a maximum temperature of around 350 ^{o}C in the reactor. The reactor was pressurized with technical air and/or with 1 mol% SO_2 in air. The lube oil was stirred during an experiment. The heating profile of the batch reactor is presented in Figure 5.2.

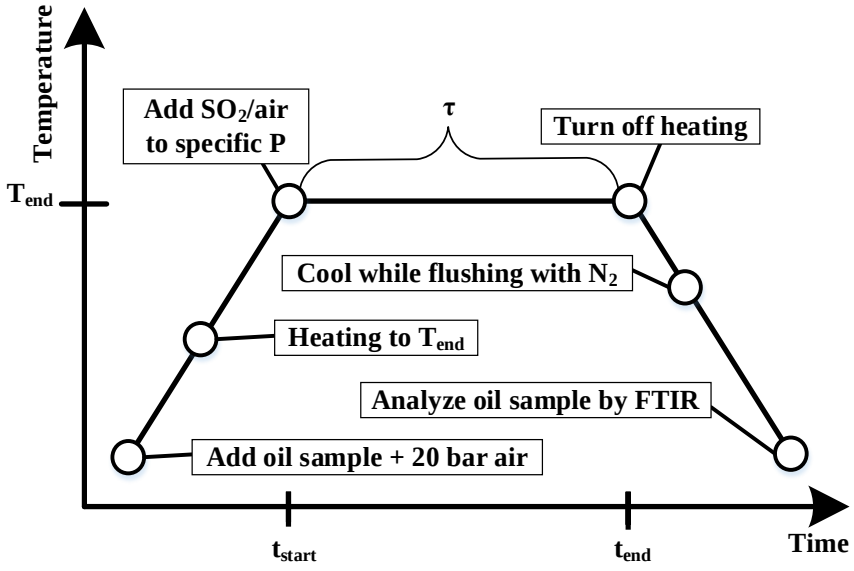

Figure 5.2. The temperature profile of the batch reactor setup during an experiment.

After the lube oil emulsion was placed inside the batch reactor, the latter was assembled, flushed three times with air, and a pressure leak test was carried out with air at 20 bar. The batch reactor was then gradually

heated to a specific temperature and the heating was conducted under pressure (20 bar at room temperature) to keep as much of the added water in the liquid phase as possible. Two temperature sensors were used: one inside the reactor and another just below the bottom of the reactor. The temperature in the reactor was difficult to control because the reactor had thick steel walls and was heated by an outer heating jacket. Less than 10 ^{o}C in difference between these two measurement points was generally observed. The temperature used for data treatment was an average of these two measurement points. When a specific temperature was reached, a mixture of 1 mol% SO_2 in air was introduced to the batch reactor till a specific pressure. After a specific residence time (τ), the gas phase was ventilated and the reactor was immediately flushed with N_2, while the reactor was cooled. During this flushing/cooling stage, the major part of the added water evaporated. The SO_2 was introduced after heating to a specific temperature in order to control the residence time and temperature. Using this procedure, all the water was kept inside the batch reactor during an experiment, limiting the evaporation of water from the lube oil.

5.2.3 Analysis methods

The lube oil samples were analyzed by a Thermo Scientific Nicolet iS50 ATR-FTIR (Attenuated Total Reflectance Fourier Transform Infrared Spectroscopy) spectrometer to obtain an infrared spectrum. The resulting base number (BN) was calculated by a calibration curve relating the height of the $CaCO_3$ band from an infrared spectrum to the base number. The latter was determined by titration following a standard test method, ASTM D-2896.[56] The procedure is described by Lejre et al.[18] Applying this method made it possible to determine the degree of conversion of $CaCO_3$ after reaction with SO_2. The water content in the fresh lube oil was measured by Karl Fischer titration using a 701 KF Titrino autotitrator from Metrohm. Toluene was used to assist the Hydranal-Solvent Oil in dissolving the lube oil sample sufficiently. The water content in the fresh 100 BN lube oil was determined to 1.1 wt.% with a sample standard deviation of 0.3 wt.%, based on four measurements. The water contents given in this work are overall initial water content values taking into account both the already present water in the lube oil (taken as the averaged value, 1.1 wt.%) and the added demineralized water.

5.2.3.1 Spectra of products from the reaction between SO_2 and $CaCO_3$

Upon an experiment, the lube oil was analyzed by FTIR-ATR[18] to investigate the degree of reaction of $CaCO_3$, but also to determine the reaction products. The use of FTIR allowed distinction between $CaCO_3$, $CaSO_3$, and $CaSO_4$. This is illustrated in Figure E.1 in Appendix E, where infrared spectra of the pure powder components are shown.

5.2.3.2 Blank experiments

Blank experiments were conducted according to the experimental procedure described, but without SO_2 in the gas phase. The results revealed that all the added demineralized water evaporated during the cooling stage and that no effect of the experimental procedure on the resulting lube oil infrared spectra was found. Consequently, the observed change in $CaCO_3$ band, when SO_2 is present in the gas phase, is the isolated effect of reaction with SO_2. The calibration curves determined earlier[18] are therefore useful in quantifying the $CaCO_3$ in a lube oil sample for the SO_2 experiments. The resulting infrared spectra together with an unused 100 BN lube oil spectrum are shown in Figure E.2 in Appendix E.

5.2.3.3 Spectrum of drain oil

To get an idea of which products to expect, an infrared spectrum of a drain oil sample was obtained (presented in Figure E.3 in Appendix E). From titration results, the base number was around 20. Only $CaSO_4$ and $CaCO_3$ are contained in the drain oil sample, because $CaSO_3$ has a band in the range 800-1000 cm^{-1} that is absent in the spectrum. However, this is only one randomly analyzed lube oil sample from practice. Further, no information in the literature about the observation of $CaSO_3$ in an engine application has been found. This does therefore not necessarily mean that $CaSO_3$ is not formed in an engine followed by oxidation to $CaSO_4$.

5.3 Results and discussion

5.3.1 Batch reactor experiments

The batch reactor experiments seek to clarify if SO_2 and $CaCO_3$ reverse micelles react in a lube oil emulsion and if reaction is observed, which products that are formed. The reaction is investigated at conditions relevant for an engine application. Further, the effect of temperature, residence time, and initial water concentration on the product distribution and $CaCO_3$ conversion are also studied.

5.3.1.1 Product determination and effect of temperature

An experiment at room temperature was carried out with a Ca/S ratio of around unity and a total pressure in the batch reactor of 50 bar of 1 mol% SO_2 in air. The Ca/S molar ratio is defined as the initial molar ratio between $CaCO_3$ in the oil phase to SO_2 in the gas phase. 6.2 wt.% of water was initially present in the lube oil sample. The residence time was 60 minutes. Figure 5.3 compares the resulting infrared spectrum with an infrared spectrum of the fresh 100 BN lube oil and the pure $CaSO_3$ spectrum (from Figure E.1).

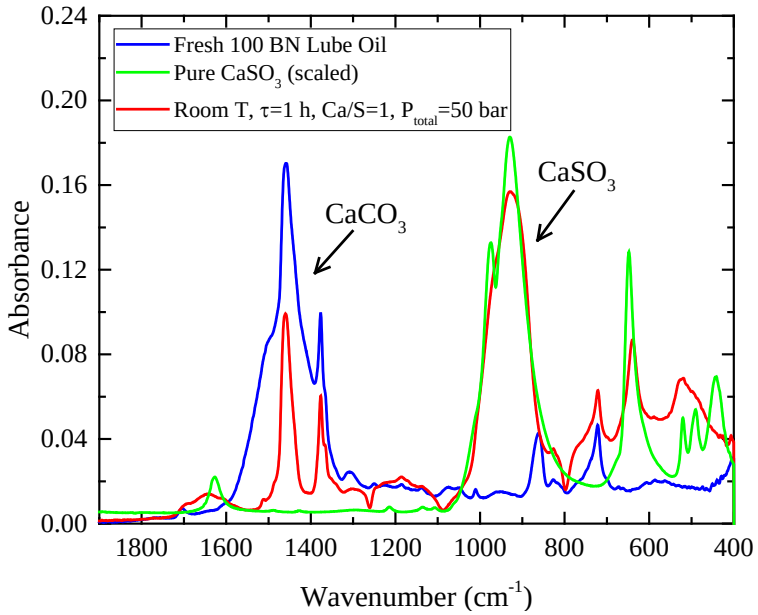

Figure 5.3. Infrared spectra from room temperature experiment (red), unused 100 BN lube oil (blue), and pure $CaSO_3$ (green). Experimental conditions: Ca/S=1, P_{total}=50 bar, 6.2 wt.% water in lube oil, and τ=60 min. Note, that a shift in baseline due to water is found in the range 400-1000 cm^{-1} and 1600-1700 cm^{-1} for the room temperature experiment spectrum (red).

By using calibration curve data for the $CaCO_3$ band,[18] it was found that no $CaCO_3$ was left in the lube oil sample. The results in Figure 5.3 also show that no or very little $CaSO_4$ was formed, i.e., all $CaCO_3$ reacted to $CaSO_3$. Figure 5.4(a) shows spectra obtained as a function of temperature and in Figure 5.4(b), the resulting conversions of $CaCO_3$ together with the Ca/S molar ratios are shown. It is observed that the conversion increases slightly with temperature (with exception of the 27 °C experiment), while it decreases slightly with Ca/S molar ratio (see Figure 5.4(b)). When the temperature is increased, the absorption of SO_2 to the lube oil emulsion decreases. Therefore, it is expected that the reaction rate constant will have a more significant dependence on the temperature than depicted in Figure 5.4. The significantly higher conversion observed for the room temperature experiment (27 °C) may therefore be linked to a larger absorption of SO_2 into the lube oil emulsion. Another explanation could be that the SO_2 had an increased reaction time at lower temperatures, because the desorption time of SO_2 after an experiment may be increased at decreased temperature.

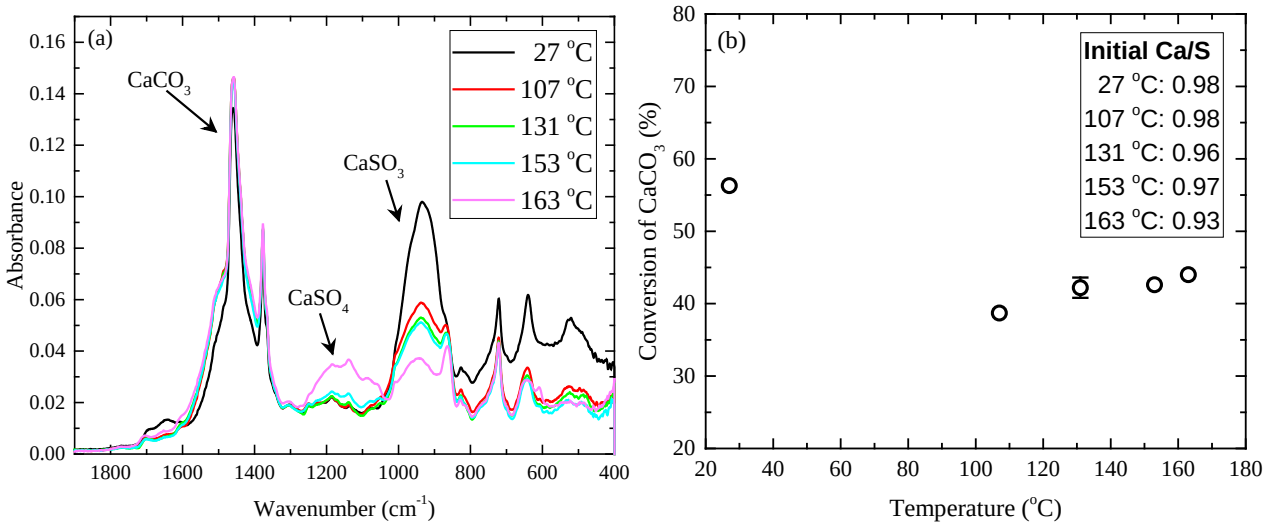

Figure 5.4. (a) Spectra of lube oil samples after being exposed to different temperatures for 10 minutes in the range 27-163 °C according to the procedure presented in Figure 5.2. Experimental conditions: P_{total}=90-105 bar, 6.6 wt.% overall initial water in lube oil, τ=10 min. (b) The effect of temperature on the conversion of $CaCO_3$ and the Ca/S molar ratio at the specific temperature. The error bars represent lower and upper conversions determined from two similar experiments and the data point is the averaged conversion. The theoretically maximum degree of $CaCO_3$ conversion is 100% because the Ca/S molar ratio is lower than 1.

To investigate if the reaction between SO_2 and $CaCO_3$ is limited by equilibrium, an experiment with a residence time of 24 hours was carried out with the following conditions: T=120 °C, Ca/S=0.90, P_{total}=90 bar, and 6.8 wt.% water in the lube oil emulsion. The resulting infrared spectrum revealed that complete conversion of $CaCO_3$ was found, i.e., the conversions of $CaCO_3$ shown in Figure 5.4 are not limited by equilibrium in the system. According to the resulting spectrum (shown in Figure E.4 in Appendix E), an observable fraction of the $CaCO_3$ was converted to $CaSO_4$. No $CaSO_4$ was found for temperatures up to 153 °C for a residence time of 10 minutes, Figure 5.4(a), indicating that $CaSO_3$ is formed first followed by a change in the reaction mechanism. It was not possible to investigate the effect of temperature above 163 °C with the present experimental configuration because the oil would ignite.

5.3.1.2 Effect of residence time

The effect of residence time on the reaction of $CaCO_3$ with SO_2 was investigated at temperatures of 131 °C and 153 °C, depicted in Figure 5.5. Apparently, the reaction is fast initially and then slows down significantly with time. For the experiments carried out at 153 °C, more $CaSO_4$ was observed at increased residence time, but the amount of $CaSO_3$ was more or less constant. This supports that $CaSO_3$ is formed initially followed by either oxidation of $CaSO_3$ to $CaSO_4$ or formation of $CaSO_4$ directly from the SO_2-$CaCO_3$ reaction. The spectra can be found in Figure E.5 in Appendix E.

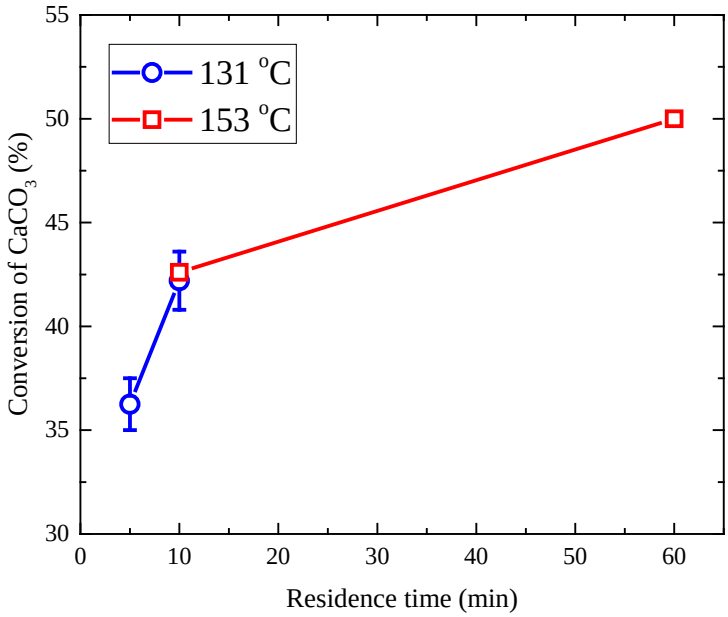

Figure 5.5. The effect of varying the residence time on the degree of conversion of $CaCO_3$ at two temperatures, 131 °C and 153 °C. Experimental conditions. P_{total}=90-105 bar, 6.6 wt.% water in the lube oil emulsion, and Ca/S around 1. The error bars represent lower and upper conversions determined from two experiments and the data points are the averaged conversions.

5.3.1.3 Effect of water concentration

The effect of initial water concentration (1.1-12%) in the lube oil emulsion on the $CaCO_3$ conversion at 131 °C is shown in Figure 5.6. The conversion of $CaCO_3$ increases linearly with the initial water content in the lube oil. The water content in the fresh lube oil was measured by Karl Fischer titration to around 1.1 wt.%, and the low water content experiment was carried out without addition of demineralized water. The water contents presented in Figure 5.6 are therefore overall water content values, both taking into account the already present water and the added demineralized water. The increased conversion at increased water content in the lube oil emulsion may be attributed partly to an increased SO_2 absorption in the lube oil emulsion because the solubility of SO_2 is higher in water than in lube oil.[55,57] However, also the reaction rate may depend on the water concentration. An experiment at room temperature, without any added water to the lube oil, was also carried out with conditions similar to the room temperature experiment shown in Figure 5.3. Instead of reaching complete conversion of $CaCO_3$, a conversion of only 25.6% was observed. The initial molar ratio between water and $CaCO_3$ was calculated to 0.7, meaning that enough water was present assuming that $CaSO_3 \cdot ½H_2O$ is formed from the reaction. A reason for not observing this could be due to some of the water not being available to participate in the reaction; the Karl Fischer titration gives only the

total amount of water in a sample, or that a different hydrated $CaSO_3$ product is formed. Nevertheless, the effect of water content on the conversion of $CaCO_3$ is significant and apparently, the reaction between SO_2 and $CaCO_3$ only proceeds when water is present.

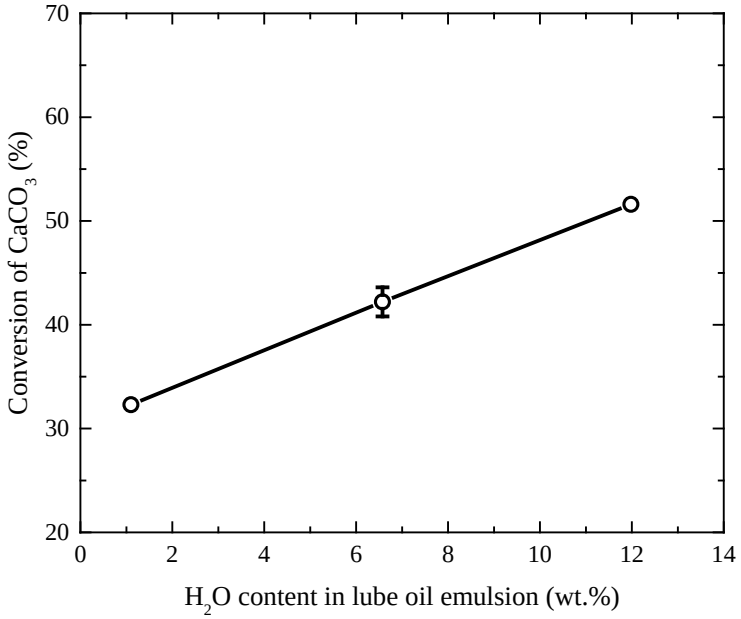

Figure 5.6. The effect of varying the initial water content in the lube oil emulsion on the degree of conversion of $CaCO_3$. Experimental conditions: P_{total}=90bar, T=131 ^oC, τ=10 min, and Ca/S around 1. The error bars represent lower and upper conversions determined from two experiments and the data point is the averaged conversion.

5.3.1.4 Stability of $CaSO_3$

As shown previously, the main product formed between SO_2 and $CaCO_3$ was $CaSO_3$. However, at increased temperature (see Figure 5.4(a)) and residence time (see Figure E.4 and Figure E.5 in Appendix E) also $CaSO_4$ was formed. This may imply that $CaSO_3$ oxidizes to $CaSO_4$ at elevated pressure and temperature. However, heating a $CaSO_3$ containing lube oil sample in an oven at atmospheric pressure at 150 ^oC did not lead to the formation of $CaSO_4$, showing that $CaSO_3$ is stable over time. Pressurizing the lube oil sample, containing $CaSO_3$, to 80 bar at 150 ^oC for 1 hour indicated that a small fraction of the $CaSO_3$ had oxidized to $CaSO_4$; however, this observation was not conclusive because the loss of water from the sample resulted in a shift in baseline. The associated infrared spectra (Figure E.6 and Figure E.7) and a detailed description are found in Appendix E. The above indicates that $CaSO_3$ is stable when first formed. The formed $CaSO_4$ found at increased residence time and temperature is therefore attributed to that, at some point, when the concentration of $CaSO_3$ reaches a certain point, the $CaCO_3$ starts to be converted into $CaSO_4$ and the formation rate of $CaSO_3$ is significantly reduced (or even stopped).

5.3.1.5 Neutralization ability of $CaSO_3$

The neutralization ability of $CaSO_3$ was investigated by converting all initial $CaCO_3$ to $CaSO_3$ followed by addition of 96 wt.% H_2SO_4. A lube oil emulsion with 6.2 wt.% water was pressurized to 50 bar of 1 mol% SO_2 in air at room temperature. An FTIR spectrum recorded after one hour of residence time confirmed that all $CaCO_3$ had converted to $CaSO_3$. Then, 96 wt.% H_2SO_4 was added to the lube oil sample, making sure that

$CaSO_3$ was in molar excess compared to H_2SO_4 at complete conversion of the H_2SO_4. The resulting infrared spectra revealed that the $CaSO_3$ was converted to $CaSO_4$. This reaction proceeds in the following way:

$$CaSO_3 + H_2SO_4 \rightarrow CaSO_4 + SO_2 + H_2O \quad (5.6)$$

The release of SO_2 from the sample after addition of H_2SO_4 was verified by a gas detector. The observation that $CaSO_3$ reacts with H_2SO_4 shows that the neutralization ability is retained when $CaCO_3$ reacts with SO_2 to form $CaSO_3$. Whether the $CaSO_3$-H_2SO_4 has a similar reaction rate as the $CaCO_3$-H_2SO_4 reaction is unknown. In addition, the existence of $CaSO_3$ in the lube oil prevented accurate determination of the BN by the titration method. The resulting spectra are depicted in Figure E.8 in Appendix E.

5.3.2 Mathematical modeling of lube oil batch reactor

A mathematical model for the reaction in the batch reactor setup is developed with the aim of extracting a kinetic expression for the $CaCO_3$-SO_2 reaction. The model is fitted to the experimental data to extract a reaction rate constant for the reaction. The rate expression is then used to investigate the relative importance of the $CaCO_3$-SO_2 and $CaCO_3$-H_2SO_4 reactions at engine conditions.

The assumptions underlying the batch reactor model are:

- The lube oil emulsion volume is well-mixed (no radial or axial concentration or temperature gradients).
- The only reaction considered in the lube oil is $CaCO_3$ (s) + SO_2 (aq) → $CaSO_3$ (s) + CO_2 (g) with a reaction rate of $(-r_A)$.
- SO_2 from the gas phase absorbs both in the lube oil and in the water. A combined expression for Henry's constant, H_L, dependent on the water concentration in the lube oil emulsion, is used.
- Even though it is thought that SO_2 only reacts with $CaCO_3$ in the presence of water, SO_2 is also present in the lube oil itself. This SO_2 is assumed to be available for reaction, because water may be present in/near the $CaCO_3$ reverse micelles.
- The effect of the initial water concentration on the conversion of $CaCO_3$ is reflected in the combined Henry's constant only.
- The effect of O_2 is not considered, because a large excess of O_2, on a molar basis compared to SO_2/$CaCO_3$, was present in the batch reactor experiments.
- Formation of $CaSO_3$ does not limit the $CaCO_3$-SO_2 reaction.
- The ideal gas law is used to calculate the concentration of SO_2 in the gas phase.
- Only the transfer of SO_2 from the gas phase to the liquid phase is considered, i.e., the release of SO_2 from the liquid phase to the gas phase is not taken into account.

5.3.2.1 Reaction rate expression

The reaction rate expression is based on the reaction between SO_2 and $CaCO_3$ forming $CaSO_3$ because it was found that $CaSO_3$ was the main product in the temperature range from room temperature to 163 °C for a residence time of 10 min. Therefore, the simple overall reaction rate expression is assumed to be given as:

$$(-r_A) = kC^L_{SO_2}C^L_{CaCO_3} \quad (5.7)$$

Here, $C_{SO_2}^L$ is the bulk concentration of SO_2 in the lube oil emulsion and $C_{CaCO_3}^L$ is the bulk concentration of $CaCO_3$ in the lube oil emulsion (proportional to the base number, BN). The concentrations are with respect to the lube oil emulsion, which consists of the lube oil and the added demineralized water. The bulk concentration of SO_2 in the lube oil emulsion is estimated from the absorption of gaseous SO_2 into the emulsion. The model takes into account the uptake of SO_2 from the gas phase to the lube oil emulsion followed by reaction between SO_2(aq) and $CaCO_3$(s). It includes mass balances for SO_2 in the gas phase and oil phase, respectively, and for $CaCO_3$ in the oil phase. An illustration of the system is shown in Figure 5.7. For now, the reaction order of the water concentration in the lube oil emulsion is assumed to be zero, even though a dependence on conversion from the water concentration was found (Figure 5.6). This dependence is assumed to be due to an increased SO_2 uptake from the gas phase and is reflected by the combined Henry's constant depending on the initial water concentration.

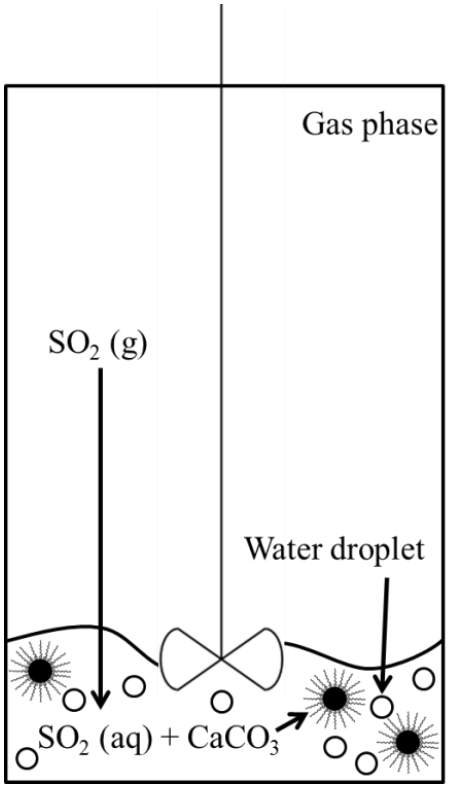

Figure 5.7. An illustration of the batch reactor setup: SO_2(g) has to be absorbed by the lube oil emulsion (oil and/or water) before it can react with the $CaCO_3$(s) in the lube oil.

5.3.2.2 Mass balance of SO_2 in the gas phase

A mass balance for the SO_2 in the gas phase is set up:

$$\frac{dC_{SO_2}^G}{dt} = -N_{SO_2}\frac{V_L}{V_G} \tag{5.8}$$

Here, N_{SO_2} (mol m^{-3} s^{-1}) is the absorption rate of SO_2 from the gas phase to the lube oil emulsion, which is assumed to be given as:[49]

$$N_{SO_2} = K_G a\left(p^G_{SO_2} - p^*_{SO_2}\right) \tag{5.9}$$

K_G (mol m^{-2} bar^{-1} s^{-1}) is the overall mass transfer coefficient of SO_2 on gas basis, a (m^2 m^{-3}) is the specific gas-liquid interfacial area, $p^G_{SO_2}$ is the bulk partial pressure of SO_2 in the gas phase, and $p^*_{SO_2}$ is the partial pressure of gas-phase SO_2 in equilibrium with the bulk lube oil concentration $C^L_{SO_2}$. The equilibrium relationship is given by Henry's law by introducing Henry's constant of the lube oil emulsion, H_L:

$$p^*_{SO_2} = H_L C^L_{SO_2} \tag{5.10}$$

The partial pressure of SO_2 in the gas phase, $p^G_{SO_2}$, is linked to the concentration of SO_2 in the gas phase by the ideal gas law:

$$p^G_{SO_2} = C^G_{SO_2} RT \tag{5.11}$$

The overall gas-side mass transfer coefficient, K_G, is given as:[58]

$$K_G = \frac{1}{\frac{1}{k_G} + \frac{H_L}{k_L}} \tag{5.12}$$

Here, k_G (mol m^{-2} s^{-1} bar^{-1}) is the gas film mass transfer coefficient and k_L (m s^{-1}) is the liquid film mass transfer coefficient.

5.3.2.3 Mass balance of SO_2 in the lube oil emulsion

In the lube oil emulsion, SO_2 enters from the gas phase and is consumed by the $CaCO_3$ reverse micelles. The mass balance of SO_2 in the lube oil emulsion is formulated as:

$$\frac{dC^L_{SO_2}}{dt} = N_{SO_2} - (-r_A) \tag{5.13}$$

Here, Eq. (5.7) describes $(-r_A)$ and Eq. (5.9) describes N_{SO_2}.

5.3.2.4 Mass balance of $CaCO_3$ in the lube oil emulsion

The $CaCO_3$ is consumed by reaction with SO_2, which gives the following mass balance:

$$\frac{dC^L_{CaCO_3}}{dt} = -(-r_A) \tag{5.14}$$

Three differential equations are thereby derived describing the concentration change over time in the batch reactor of SO_2 in the gas phase, Eq. (5.8), SO_2 in the lube oil emulsion, Eq. (5.13), and $CaCO_3$ in the lube oil emulsion, Eq. (5.14). The aim is to derive the reaction rate constant, k, given in Eq. (5.7), by fitting the model to the experimental data.

5.3.2.5 Initial conditions

Three initial conditions are needed: one for the $CaCO_3$ concentration in the lube oil, one for the SO_2 concentration in the gas phase, and one for the SO_2 concentration in the lube oil emulsion. The fresh lube oil was measured to have an average base number (BN) of 98.55 BN,[18] which corresponds to a $CaCO_3$ concentration of 825.6 mol m^{-3}. Because the fresh lube oil contains 1.1 wt.% water, the water-free lube oil has a $CaCO_3$ concentration of 834.8 mol m^{-3}. The concentrations and reaction rates are based on the volume of the lube oil emulsion (lube oil + water), thus the water-free concentration of $CaCO_3$ is multiplied by the ratio of lube oil volume to lube oil emulsion. The initial concentration of SO_2 in the total gas phase is calculated by the ideal gas law using the partial pressure of SO_2 in the gas phase and the temperature. Lastly, it is assumed that the initial concentration of SO_2 in the lube oil emulsion is zero. The Ca/S molar ratio is defined as the initial molar ratio between $CaCO_3$ in the emulsion and SO_2 in the gas phase, calculated as:

$$\frac{Ca}{S} = \frac{C^L_{CaCO_3,0} V_L}{C^G_{SO_2,0} V_G} \tag{5.15}$$

If equal to e.g. 0.5, 50% conversion of the gaseous SO_2 is expected for complete conversion of the $CaCO_3$ reverse micelles in the lube oil emulsion.

5.3.2.6 Estimation of input parameters

The input parameters to the model include experimental conditions and estimation of K_G, a, H_L, and k. The experimental conditions are found in Table E.1 in Appendix E for the experiments from Figure 5.4. The volumes of the water and lube oil in the emulsion were calculated by scaling the weighted values with the densities (940 kg m^{-3} for lube oil[18,19] and 1000 kg m^{-3} for demineralized water). The water content of the lube oil itself (1.1 wt.%) was also taken into account.

It is unknown whether the SO_2(g) is absorbed into the water droplets, which are emulsified in the lube oil, the lube oil itself, or a mixture thereof. For the present purpose, Henry's constant for SO_2 in both water and lube oil were estimated. The temperature dependent Henry's constant for SO_2 in water was estimated from NIST.[57] Henry's constant for SO_2 in a fully formulated lube oil is more challenging to assess. The experimental results showed that SO_2 reacts with the $CaCO_3$ in the lube oil; this makes the determination of only solubility in the lube oil difficult. Costa and Underhill,[55] who studied uptake of SO_2 in different lube oil formulations at 25 °C, also observed that SO_2 reacted with the base content in the lube oil, resulting in an overestimation of the 'solubility'. For the present study, Henry's constant at 25 °C was calculated from the study of Costa and Underhill,[55] based on a lube oil not containing base additives reacting with the SO_2. The resulting Henry's constant indicates that SO_2 is more soluble in water than in lube oil. A combined Henry's constant is derived based on the amount of water present initially in a lube oil sample in the following way, using a scaled resistance-like expression:

$$H_L = \frac{1}{\frac{1}{H_{oil}}\left(\frac{V_{oil}}{V_L}\right) + \frac{1}{H_{water}}\left(\frac{V_{water}}{V_L}\right)} \tag{5.16}$$

Here, H_{oil} and H_{water} are Henry's constants for lube oil and water, respectively, and V_{oil}, V_{water}, and V_L are the volumes of lube oil, water, and lube oil emulsion ($V_L = V_{oil} + V_{water}$). A detailed assessment of the derivation of the Henry's constants can be found in Appendix E.

The collected parameter $K_G a$ is then estimated. The specific gas-liquid interfacial area, a, represents the area between the gas phase and the liquid phase where the mass transfer takes place. It is assumed that the mass transfer happened at the gas-oil interface. The specific interfacial area for the gas-oil interface is calculated as:

$$a = \frac{A_L}{V_L} = \frac{\pi R_{reactor}^2}{V_L} \tag{5.17}$$

Because the radius of the batch reactor is 3.15 cm, and a typical amount of the lube oil emulsion was 10.1 ml, a = 308.7 m^2 m^{-3}. This is for a stagnant lube oil volume.

Further, an evaluation of the resistance of the mass transfer of SO_2 from the gas phase to the liquid phase was carried out, revealing that mass transfer is controlled by the liquid-side resistance, viz, $K_G = k_L/H_L$. The calculations can be found in Appendix E. A crude estimate of the liquid film mass transfer coefficient, k_L, is given as:[58]

$$k_L = \frac{D_L}{\delta_L} \tag{5.18}$$

D_L is the diffusion coefficient of SO_2 in the liquid phase and δ_L is the liquid film thickness. The calculation of k_L is likewise found in Appendix E.

The only unknown in the model is thereby k, which is fitted to match the modeling results to the experimental data (conversion of $CaCO_3$ at specific τ, Figure 5.4). However, implementing and solving the above described model revealed that only an insignificant degree of conversion of $CaCO_3$ can be achieved irrespectively of the magnitude of k, which is in disagreement with the experimental results. The reason for this discrepancy between simulation and experimental results is attributed to an underestimation of the overall film mass transport coefficient of SO_2, K_G, and specific gas-liquid interfacial area, a, because the estimated K_G and a, based on Eqs. (5.17) and (5.18), are based on a stagnant lube oil film and pure surface diffusion. Therefore, $K_G a$ for the present system was estimated by use of the work from Meille et al.,[59] who measured $k_L a$ ($K_G a = k_L a/H_L$) values as a function of stirrer speeds for different batch reactor dimension, finding that stirring of a liquid in a batch reactor contributed to an increased value of $k_L a$. Based on their work, a factor of 120 between $k_L a$ for a stagnant case (based on Eqs. (5.17) and (5.18) and the experimental parameters from Meille et al.) and an agitated case (stirrer speed of 600 rpm which was the stirrer speed applied in this work) was found and was used in the subsequent modeling. The justifications and calculations are found in Appendix E.

5.3.2.7 Arrhenius plot

Based on the fitting of k, an Arrhenius expression, which takes the temperature dependence into account, was then constructed, by Eq. (5.19), and is shown in Figure 5.8 for the temperature range 107-163 ^oC.

$$\ln(k) = \ln(A) - \frac{E_a}{R}\frac{1}{T} \tag{5.19}$$

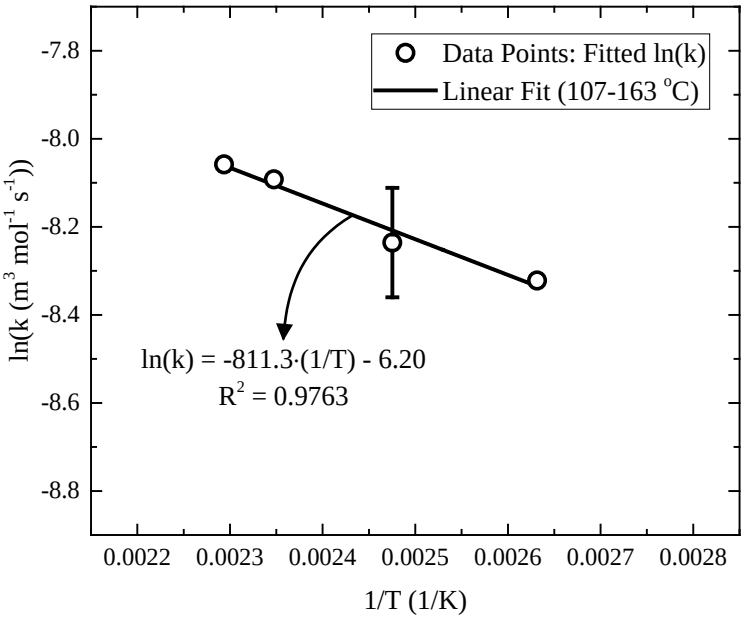

Figure 5.8. Arrhenius plot of the determined reaction rate constants at temperatures in the range from 107 °C to 163 °C. The linear fit, corresponding equation, and R^2 value are also shown. The error bars represent lower and upper $\ln(k)$ values determined from two similar experiments and the data point is the averaged value. From the trendline, the activation energy is determined to 6.7 kJ mol^{-1} and the pre-exponential factor to $2.03 \cdot 10^{-3}$ m^3 mol^{-1} s^{-1}.

A satisfactory linear fit is observed between $\ln(k)$ and $1/T$ from which an activation energy (E_a) of 6.7 kJ mol^{-1} and a pre-exponential factor (A) of $2.03 \cdot 10^{-3}$ m^3 mol^{-1} s^{-1} are determined by use of Eq. (5.19) and the linear fit of Figure 5.8. The determined E_a reveals that the temperature dependence of the reaction rate constant is weak, in accordance with literature.[52] Figure 5.8 also shows a rather high uncertainty on the determination of the fitted k.

A maximum simulated $CaCO_3$ conversion of 19.6% could be achieved for the room temperature experiment conditions (assuming infinite fast reaction, i.e., completely mass-transfer controlled), which is far from the experimentally determined conversion (56.3%). The reason for this may be due to a viscosity effect because the viscosity highly affects $K_G a$ and the viscosity of lube oil drastically changes with temperature,[60,61] thus it may be difficult to estimate an exact value of $K_G a$ at room temperature. Another explanation may be that another limitation/mechanism exists at room temperature than for the higher temperature experiments or that the SO_2 is better maintained in the lube oil emulsion during the desorption stage of the experimental procedure. This may lead to an extended reaction time of the SO_2 in the lube oil emulsion, leading to an increased conversion of $CaCO_3$. If increasing the calculated $K_G a$ at stagnant conditions by a factor of 600, it was now possible to simulate the experimentally determined conversion of $CaCO_3$ at room temperature, however, the resulting fitted k is not in line with the ones determined at higher temperatures (see Figure E.9 in Appendix E). Lastly, the value of $K_G a$ may still be underestimated even though a factor of 120 between stagnant and stirred conditions was determined previously and used in the fitting procedure. Nevertheless, the room temperature case was excluded in the process of extracting a reaction rate constant, because this temperature is not relevant for an engine application. It was found that the SO_2 from the gas phase is readily

absorbed into the lube oil, illustrated by a steep increase in the concentration curve for the SO_2 in the lube oil emulsion. This can be seen in Figure E.10 in Appendix E which shows the concentration profiles of $CaCO_3$ in the lube oil emulsion, SO_2 in the oil film emulsion, and SO_2 in the gas phase for the 131 ^oC simulation.

5.3.2.8 Comparison between model and experimental data for varying residence time

The model was used to compare with the experimental data from Figure 5.5, as shown in Figure 5.9. The differences between modeling predictions and experimental data may be due to SO_2 not desorbing immediately after ventilation of the SO_2 gas phase and flushing with N_2, resulting in an extended reaction time. The effect of prolonged reaction time may be more pronounced for the shorter residence time experiment. Another explanation could be that the reaction reaches a plateau where no more $CaSO_3$ is formed, but instead, $CaCO_3$ is converted to $CaSO_4$, but at a much lower reaction rate, possibly because O_2 also has to participate in the reaction. The above was indicated from the experiments, see e.g. Figure E.5 in Appendix E, and may explain the mismatch between the model and simulation trends.

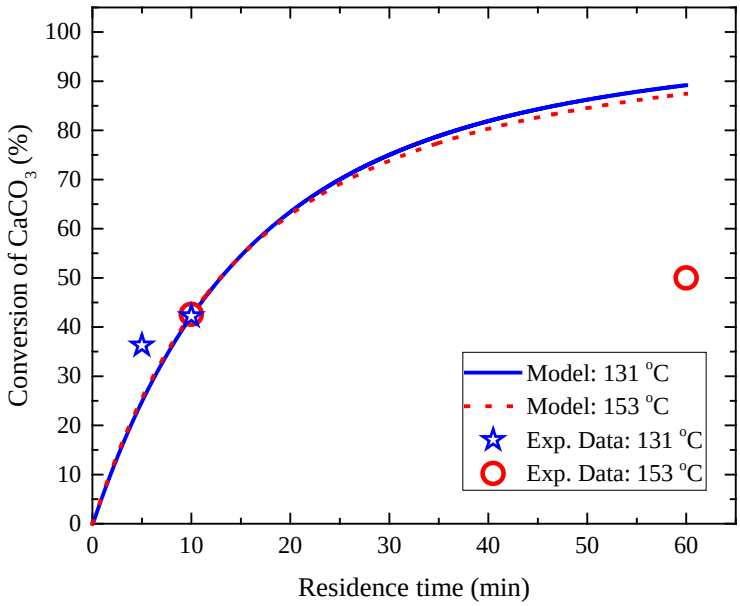

Figure 5.9. The effect of varying the residence time on the degree of conversion of $CaCO_3$ at two temperatures, 131 and 153 ^oC. The figure compares the model predictions with the experimental data from Figure 5.5.

5.3.2.9 Comparison between model and experimental data for varying initial water concentration

The effect of varying initial water concentration on the conversion of $CaCO_3$ was predicted by the model and compared with the experimental data from Figure 5.6. The result of this is shown in Figure 5.10. This figure shows that the model captures the experimentally determined conversions sufficiently within the uncertainty of the analysis technique. This means that the combined Henry's constant expression, Eq. (5.16), describes the water dependence sufficiently. The effect of water concentration is minor relative to the change because increasing the initial water concentration by a factor of 11 increases the conversion of $CaCO_3$ by a factor of around 1.5.

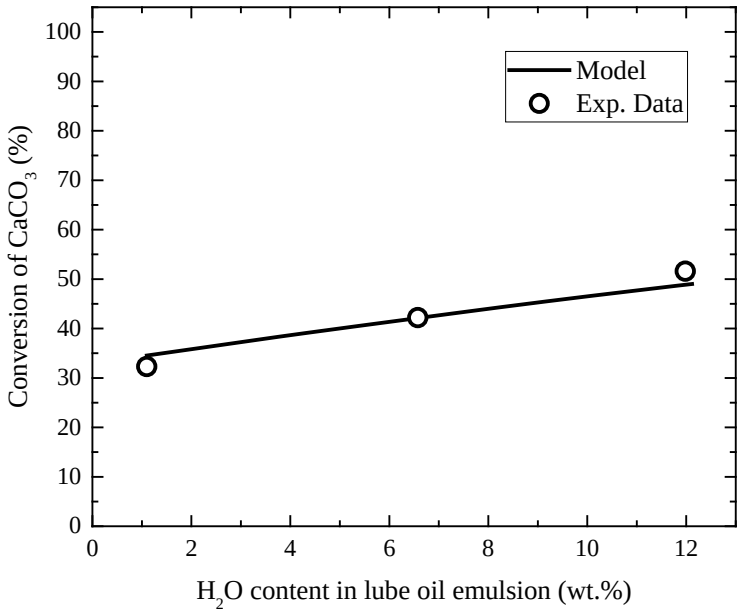

Figure 5.10. The effect of varying the initial water content in the lube oil emulsion on the degree of conversion of $CaCO_3$ at 131 ^oC. The figure compares the model predictions with the experimental data from Figure 5.6.

The lube oil emulsion was gradually heated under pressure prior to introducing the SO_2 in air gas mixture to keep as much of the water in the liquid phase. However, a fraction of the water may evaporate during an experiment and the exact concentration of water in the lube oil emulsion may not equal the initial water concentration in the emulsion. The vapor pressure of water at 131 ^oC was calculated to 2.7 bar,[57] and comparing this value with the pressure prior to introducing the SO_2 gas mixture (around 30 bar at 131 ^oC), it is advocated that most of the water was present in the liquid phase during an experiment. This, together with the minor effect of changing the water concentration on the conversion of $CaCO_3$ (relative to the change) suggests that the initial water concentration can be used for estimation of the combined Henry's constant from Eq. (5.16).

5.3.2.10 Discussion on model simulations

The above sections emphasize that accurate estimation of the correlated parameters $K_G a$ and k are required in order to predict the conversion of $CaCO_3$ by reaction with SO_2 precisely. Therefore, $K_G a$ was estimated by use of data from the literature,[59] and Figure 5.8 was constructed. Whether these two parameters are estimated correctly is unknown, however, the estimated values of $K_G a$ and k are one pair of parameters to the model which simulates the conversions of $CaCO_3$ in accordance with the experimentally determined conversions. To verify if the determined parameters are true, one solution could be to measure the parameter $K_G a$ independently as done in the work of Meille et al.[59] The effects of $K_G a$ and k on the conversion of $CaCO_3$ are simulated in Figure 5.11 for the experimental conditions of the 131 ^oC experiment.

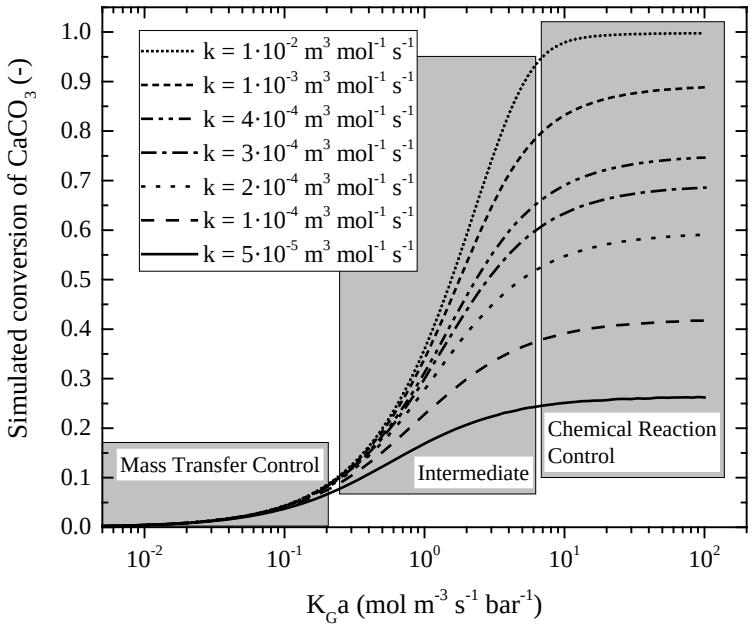

Figure 5.11. Simulation results showing the simulated conversion of $CaCO_3$ as a function of $K_G a$ for seven different reaction rate constant values. The following parameters were used for the simulations: T=131 °C, τ=10 min, P_{total}=90 bar, $C^G_{SO_2,0}$=17.26 mol m^{-3}, 6.6 wt.% water in lube oil, and Ca/S = 0.96.

Three different regions are illustrated in Figure 5.11. At low $K_G a$ values, the reaction between SO_2 and $CaCO_3$ is mass transfer controlled, i.e., no effect of reaction rate is found. However, the mass transfer of SO_2 from the gas phase to the liquid phase is too low in order to achieve an observable degree of conversion of $CaCO_3$ (for the specific residence time available, i.e., 10 min), or at least a degree comparable to the experimental degree of conversion. At high $K_G a$ values, only a minor effect of increasing $K_G a$ even further is found, however, the effect of increasing k is large relative to the increase. In-between, an intermediate region is found. At stagnant conditions, $K_G a$ was calculated to $1.62 \cdot 10^{-2}$ mol m^{-3} s^{-1} bar^{-1}, which explains the insignificant degree of reaction of $CaCO_3$ if comparing this value with Figure 5.11. Multiplying $K_G a$ by 120 gives 1.95 mol m^{-3} s^{-1} bar^{-1}, which translates to being in the intermediate region of Figure 5.11 where both mass transfer and reaction control. Knowing the conversion of $CaCO_3$ (e.g. 42.2% at 131 °C) and $K_G a$, k was calculated to $2.65 \cdot 10^{-4}$ m^3 mol^{-1} s^{-1}, in accordance with Figure 5.11. In the intermediate region, a large change in k only lead to a relative minor effect on the conversion of $CaCO_3$. Because analysis uncertainties may be in the order of ±2 BN, this has a large effect on the uncertainty of k as shown in Figure 5.8. However, at increasing $K_G a$ the resistance to the conversion of $CaCO_3$ goes toward chemical reaction. This means that a small change in k has a large impact on the conversion, which would decrease the corresponding uncertainty in an Arrhenius plot. Further, the temperature dependency on k increases for increasing $K_G a$. If applying a factor of 600 instead of the estimated 120 used to construct Figure 5.8, the activation energy becomes 23.5 kJ mol^{-1} and the uncertainty of the 131 °C data point in the Arrhenius plot was significantly decreased due to the stronger temperature effect (see Figure E.9 in Appendix E).

For the mathematical model, an overall reaction rate expression was set up only considering the overall reaction between SO_2 and $CaCO_3$. The mechanistic details of the reaction mechanism were thereby collected in the overall reaction rate constant, k. In reality, SO_2 may further react to HSO_3^- or SO_3^{2-} after entering the

water in the lube oil emulsion. These reactions are not taken into account in the modeling and further studies are required to map the exact reaction mechanism between SO_2, water, lube oil, and $CaCO_3$ reverse micelles.

5.3.3 Application of the batch reactor model to conditions in a large two-stroke diesel engine

The batch reactor model developed in this work was used to interpret the experiments carried out at varying conditions in a batch reactor for determination of absorption and reaction rate expressions for the SO_2-$CaCO_3$ reaction. These expressions are intended to be used in e.g. computational fluid dynamics simulations to provide a full overview of the effect of SO_2 on the consumption of $CaCO_3$ and accumulation of SO_2 in the lube oil at the cylinder liner in a large two-stroke marine diesel engine. As will be discussed in the following, the batch reactor model derived in this work offers a useful approximation to local conditions prevailing in a marine diesel engine and can be used to assess the importance of the SO_2-$CaCO_3$ reaction as well.

The entire combustion chamber in an engine can be considered as one batch reactor, where the gas volume is much larger than the lube oil volume, as in the case of the batch reactor experiments. However, the size of the combustion chamber changes as a stroke progresses. Assuming stagnation at different piston positions, each volume can therefore be considered as a batch reactor with associated partial pressure of SO_2 in the gas phase and lube oil emulsion volume. Under this circumstance, the batch reactor model of this work can assist in determining the absorption of SO_2 and subsequent degree of reaction between SO_2 and $CaCO_3$.

Assuming that all fuel-S is instantaneously converted to SO_2 prior to the expansion stroke, the partial pressure of SO_2 will be highest at the very top of the cylinder (at top dead center, TDC). As the expansion stroke progresses, the partial pressure of SO_2 in the gas phase decreases as the combustion chamber volume increases, the combustion gas is exhausted, and later further diluted by the intake air. Ideally, this leads to desorption of SO_2 from the lube oil emulsion due to the changed SO_2 concentration gradient across the gas-liquid interface. Due to the fast passage of the piston, it may be fair to assume that the desorption rate of SO_2 is too slow to actually come into force. That desorption of SO_2 from the lube oil emulsion is not an instantaneous process, was also observed in the batch reactor experiments. However, this means that the absorption rate of SO_2 decreases as the expansion stroke progresses and may be stopped during the compression stroke where all the exhaust gas has been ventilated and replaced by fresh intake air. This means that at a local, discretized volume section of the cylinder liner, the partial pressure of SO_2 is constantly changing. To keep it simple, the partial pressure of SO_2 in the gas phase is assumed to be constant for each piston position, which also serves as a worst-case scenario. Further, the residence time has to be chosen. Because the gas phase is constantly renewed, the residence time for the simulations is chosen as the residence time for the lube oil in the engine. This is augmented by the fact that the lube oil is in contact with the SO_2 throughout this time either through the gas phase or in the oil. Assuming, in the following simulations, that the partial pressure of SO_2 is constant throughout the residence time may ultimately overestimate the degree of conversion of $CaCO_3$ from SO_2. Average lube oil residence times of up to 4 min in an engine have been calculated.[1,18,62]

5.3.3.1 Engine simulation: SO_2-$CaCO_3$ reaction

The modeling of the SO_2-$CaCO_3$ reaction in discretized combustion chamber volumes by the batch reactor model underlies the following assumptions, besides the ones given previously:

- The cylinder liner is discretized into smaller volumes, where each subvolume assumes constant gaseous SO_2 concentration, lube oil temperature, and lube oil thickness throughout the specified residence time. The change in gaseous SO_2 concentration at a specific subvolume during the expansion stroke is thereby neglected.
- Desorption of SO_2 from the lube oil film is neglected.
- The lube oil temperature and thickness are constant throughout the vertical length.
- The dilution of gaseous SO_2 during the expansion stroke by exhaustion of the combustion gas and intake air is not taken into account. The gaseous SO_2 concentration profile varies along the vertical direction, but only by the volume expansion, i.e., when the gas volume doubles, the gaseous SO_2 concentration halves. This means that the gaseous SO_2 concentration is highest at top dead center, TDC, and lowest at bottom dead center, BDC.
- All the injected fuel-S is instantaneously converted to gaseous SO_2.
- Oxidation of SO_2 to SO_3 is not considered, i.e., no H_2SO_4 is present in the system.
- The gas and liquid volumes are well-mixed (no radial or axial concentration or temperature gradients).

An illustration of the discretized volumes with corresponding gaseous SO_2 concentrations are presented in Figure 5.12, where each subvolume assumes the behavior of a batch reactor.

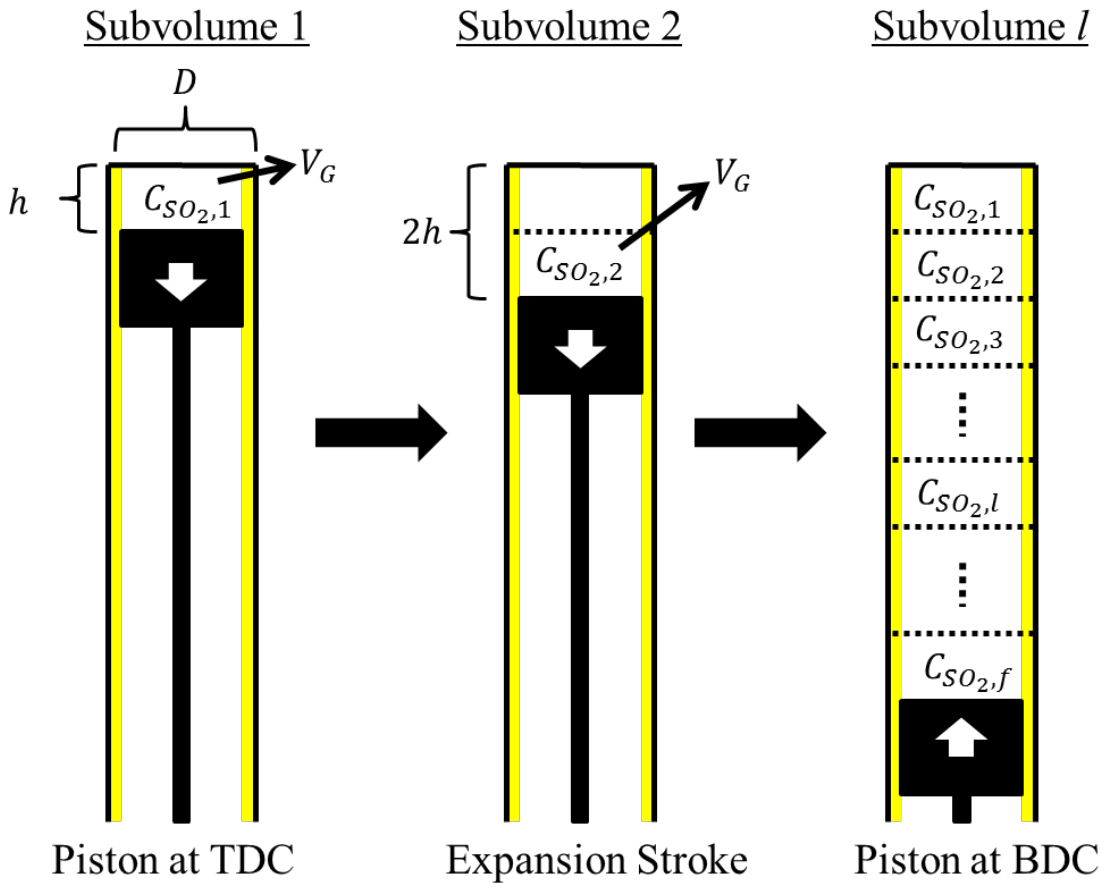

Figure 5.12. An illustration of a cylinder showing the discretized subvolumes, where h is the height of a subvolume, D is the diameter of the cylinder, V_G is the gas volume of a subvolume, l is the subvolume number, $C_{SO_2,l}$ is the gaseous concentration of SO_2 in subvolume l, and f is the last subvolume number.

During expansion, the pressure decreases (volume increases). This leads to a reduced concentration of SO_2 in the gas phase and thereby in the lube oil emulsion (the absorption rate is decreased). Therefore, it is expected that the degree of reaction between SO_2 and $CaCO_3$ is reduced as the expansion in the engine progresses. Input parameters used for the engine simulations are found in Table 5.1.

Table 5.1. Input parameters used for the engine simulations. The engine dimensions are based on an 8S80ME-C9.5 engine from MAN Energy Solutions.

Parameter	**Parameter Value**	**Reference**
Cylinder diameter, D	0.8 m	
Cylinder height, H	3.45 m	
Gas volume of a subvolume, V_G	0.08 m^3	
Vertical height of a subvolume, h	0.16 m	
Number of cylinders	8	
Specific fuel oil consumption	175 g kWh^{-1}	63,64
Engine power	30 MW (at 100% load)	64
Sulfur content in fuel	4.5 wt.%	Assumed
Engine speed	60 rpm	Assumed
Temperature	100 ^oC	Assumed[15]
Lube oil film thickness	1 µm	Assumed
Specific gas-liquid interface, a	10^6 m^2 m^{-3}	Eq. (5.17)
Water content in lube oil film	5 wt.%	Assumed
Residence time, τ	10 min	Based on 1,62,65

The concentration of SO_2 in the gas phase in each subvolume was based on the first subvolume concentration, $C_{SO_2,1}$. When the pressure is highest in the engine, it is assumed that all the fuel has just been burned and thereby all the fuel sulfur is present as SO_2. This was assumed to happen when the piston is at TDC. At TDC, the compression volume of the gas is around 80 liters (typical value of a two-stroke marine diesel engine), corresponding to h being equal to 16 cm. The dimensions of the cylinder liner were based on typical values from a two-stroke marine diesel engine, having a diameter, D, of 0.8 meter. The concentration of SO_2 in the gas phase was based on a typical fuel flow (assuming that all fuel-sulfur is immediately converted to SO_2) and the gas volume. The fuel flow was found to be 175 g kWh^{-1},[63] and when having 8 cylinders rated at 30 MW (at 100% load), 4.5 wt.% sulfur in the fuel (a high, worst-case value), and that new fuel was injected every second (corresponding to 60 rpm), 0.2559 mol SO_2 was present in the uppermost cylinder subvolume at complete combustion. Dividing by 80 liters, yields $C_{SO_2,1}$ = 3.2 mol m^{-3}. The fuel flow rate was also calculated by MAN's CEAS Engine Calculator[64] for the specific engine (but with 73.1 rpm), confirming that an approximate fuel flow rate is 175 g kWh^{-1}. It was assumed that SO_2 is not exhausted during the expansion stroke, therefore: $C_{SO_2,i} = C_{SO_2,1}/i$. This means that the SO_2 concentration rapidly decreases in the subsequent subvolumes as the expansion stroke progresses. This behavior was also modeled by Nagaki and Korematsu.[46]

It should be emphasized, even though the concentration of SO_2 decreases in the whole volume between the top of the cylinder and the piston during the expansion stroke, that the SO_2 concentration of the preceding

subvolume is unaffected of the present subvolume. In other words, it was assumed that $C_{SO_2,1}$ kept the value of 3.2 mol m^{-3} throughout the whole simulation even though the SO_2 gas concentration decreases to 1.6 mol m^{-3} when the piston has moved 16 cm further downwards and so forth for the remaining subvolumes. The temperature also varies along the stroke length, being highest near TDC and lowest near BDC and depends on the load. Preliminary simulations carried out under engine conditions revealed that conversion of $CaCO_3$ increased at decreasing temperature. The reason for this behavior is that the absorption of SO_2 from the gas phase to the lube oil film happens almost instantaneously and the SO_2 concentration in the lube oil film reaches therefore equilibrium instantaneously. This is attributable to the large amount of SO_2 in the gas phase compared to $CaCO_3$ in the lube oil film (on a molar basis) and that a is large. Further, the temperature dependence of k is weak (Figure 5.8) which cannot completely counteract the stronger temperature dependency of the Henry's constant: more SO_2 is absorbed at decreasing temperature (increasing $C_{SO_2}^L$), which increases the overall conversion because k is more or less unaffected by the temperature. Therefore, a lower temperature of 100 °C was chosen for the simulations. The results of the simulations are found in Figure 5.13, where the conversions of $CaCO_3$ in each subvolume are presented.

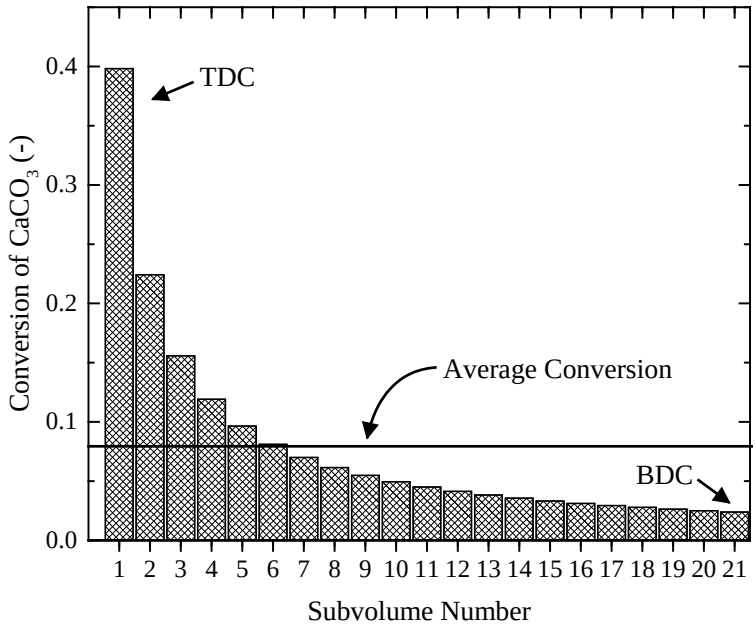

Figure 5.13. The simulated conversion of $CaCO_3$ in each subvolume (Figure 5.12) for the conditions given in Table 5.1. The average $CaCO_3$ conversion (7.9%) is also provided in the figure by the horizontal line.

When sampling a lube oil off-shore, it is an averaged $CaCO_3$ conversion throughout the whole vertical direction of the cylinder liner that is sampled. The average $CaCO_3$ conversion throughout the vertical direction of the cylinder is therefore also given in Figure 5.13 (7.9%). A typical recommendation is to achieve between 50-75% conversion of $CaCO_3$ in practice,[4] which means that SO_2 cannot solely be accounted guilty for the observed consumption of $CaCO_3$ in practice. Further, the inputs to the model presented in Table 5.1 are chosen in order to enhance the conversion of $CaCO_3$, e.g., the chosen temperature, load, sulfur content in the fuel, residence time, etc. That means, under a worst-case scenario, maximum 7.9% of the available $CaCO_3$ in lube oil can be neutralized by reaction with SO_2.

5.3.3.2 Engine simulation: Competition between SO_2-$CaCO_3$ and H_2SO_4-$CaCO_3$ reactions

The previous section showed that around 40% of the $CaCO_3$ could potentially be consumed by SO_2 in the lube oil at worst-case conditions near TDC (Figure 5.13, for a residence time of 10 min). However, if H_2SO_4 is present in the lube oil emulsion, the effect of SO_2 on the consumption of $CaCO_3$ may be even smaller if the reactivity of the H_2SO_4-$CaCO_3$ reaction outmatches the SO_2-$CaCO_3$ reaction. The H_2SO_4-$CaCO_3$ reaction has been investigated by the authors previously,[19] simulating that 38% of the $CaCO_3$ is consumed after a residence time of 0.5 s, for a temperature of 100 ^oC and for a Ca/S molar ratio equal to 1 (remaining parameters: radius of H_2SO_4 droplets: 0.5 µm, 100 BN lube oil, and concentration of H_2SO_4 droplets: $18 \cdot 10^3$ mol m^{-3}). Comparing this conversion degree to the one determined in this work reveals that the rate of the H_2SO_4-$CaCO_3$ reaction is superior compared to the SO_2-$CaCO_3$ reaction. This means, if both SO_2 and H_2SO_4 are present in the lube oil film, the $CaCO_3$ would rather react with H_2SO_4 than with SO_2. If H_2SO_4 is limited compared to $CaCO_3$, on a molar basis, then $CaCO_3$ would first consume the majority of the H_2SO_4, followed by reaction with SO_2. However, H_2SO_4 gradually condenses onto the cylinder liner (during each expansion stroke), which means that H_2SO_4 may be available for reaction with $CaCO_3$ continually. That the H_2SO_4-$CaCO_3$ reaction outmatches the SO_2-$CaCO_3$ reaction adds to the argument that the significance of SO_2, as consumption source of $CaCO_3$ reverse micelles, is negligible in a marine diesel engine application. This is further augmented by the possibility of formation of $CaSO_3$ as the product from the SO_2-$CaCO_3$ reaction, which also can react with H_2SO_4 forming $CaSO_4$.

It is also possible to directly compare the H_2SO_4-$CaCO_3$ and SO_2-$CaCO_3$ reaction in an engine application through the present batch reactor model. This can be implemented by extending the reaction mechanism as described in Appendix E. However, the competition between the two reactions highly depends on the initial concentration of H_2SO_4 in the lube oil emulsion. It was found (simulations are not shown here) that the H_2SO_4-$CaCO_3$ reaction is generally dominant over the SO_2-$CaCO_3$ reaction. The dominance increases for increasing temperature, decreasing SO_2 partial pressure, and increasing initial H_2SO_4 concentration. Near TDC, the temperature is highest and most H_2SO_4 is condensing,[1,4,15,16] and toward the bottom of the cylinder liner, the partial pressure of SO_2 in the gas phase is rapidly declining. This yet again reinforces that H_2SO_4 is responsible for consuming the vast majority of the $CaCO_3$ in the lube oil in an engine application.

Nagaki and Korematsu[47] even concluded that increased absorption of SO_2 in the lube oil film by EGR (Exhaust Gas Recirculation), increased the wear, however, the consumption of base additives remained unchanged. This contradicts their postulate that H_2SO_4 is formed from SO_2 in the lube oil film,[45–47] unless H_2SO_4 readily reacts with the cylinder liner surface upon formation, preventing interaction with $CaCO_3$. Yet, this seems to be unlikely, taking into account the reactivity of the $CaCO_3$ reverse micelles and the magnitude of the reaction rate of the H_2SO_4-$CaCO_3$ reaction.[19] Instead, this may again point in the direction of SO_2 not being responsible for consuming $CaCO_3$, but still, in combination with water, have a corrosive effect on the cylinder liner surface.
As shown by this study, SO_2 is absorbed into the lube oil film and interaction with the liner is thereby possible. If local conditions allow a large amount of water to condense,[15] SO_2(aq) may have direct access to the liner material, possibly promoting corrosive wear.

5.4 Conclusions

The reaction between gaseous SO_2 and $CaCO_3$ reverse micelles in lube oil has been studied using a batch reactor setup, and a mathematical model was set up in order to extract kinetic parameters of the reaction. The model was then used to predict the significance of the SO_2-$CaCO_3$ reaction at worst-case conditions similar to the ones prevailing in a large two-stroke marine diesel engine.

The experimental work in a batch reactor revealed that SO_2 and $CaCO_3$ do react in lube oil, initially forming $CaSO_3$, but at increased residence times and temperatures, $CaSO_4$ was also formed. Further, water had a significant effect on the degree of conversion of $CaCO_3$, which was attributed to an increased absorption rate of SO_2 in the lube oil emulsion. The effect of temperature was minor because the absorption of SO_2 decreases at increased temperature and the temperature dependence on the reaction rate constant was found to be weak. Modeling of the experimental data showed that the mass transfer coefficient, K_G, and reaction rate constant, k, are highly correlated and multiple solutions can be found when fitting the model to the experimental data. Therefore, K_G was estimated by use of experiments from literature,[59] and a resulting Arrhenius plot was constructed from which kinetic parameters were determined.

The batch reactor model was then used to predict $CaCO_3$ conversions by reaction with SO_2 at worst-case conditions similar to the ones prevailing in a large diesel engine by discretizing the vertical direction of the cylinder liner. The simulations revealed that the $CaCO_3$ conversion highly depended on the SO_2 concentration in the gas phase and the highest conversion of $CaCO_3$ was therefore at TDC. However, the SO_2 concentration in the gas phase readily decreases as the expansion stroke progresses and the averaged worst-case $CaCO_3$ conversion determined (7.9%) cannot explain the $CaCO_3$ conversions found in practice. The present study also showed that, when H_2SO_4 is present in the lube oil film, it will be converting the major part of the $CaCO_3$.

Therefore, it is concluded that the reaction SO_2-$CaCO_3$ is not playing any significance in a two-stroke marine diesel engine with respect to consumption of $CaCO_3$ reverse micelles in the lube oil. If SO_2(aq) can react with the cylinder liner material and contribute to corrosion is unknown, however. This study, together with earlier work on the H_2SO_4-$CaCO_3$ reaction from the present authors,[19] are expected to facilitate and support further studies on how to control corrosive wear in large two-stroke marine diesel engines at a minimal lube oil consumption.

Acknowledgments

This work is part of the Combustion and Harmful Emission Control (CHEC) research center at the Department of Chemical and Biochemical Engineering at the Technical University of Denmark. The project is funded by the Innovation Fund Denmark and cosponsored by MAN Energy Solutions and the Technical University of Denmark through the SULCOR project under grant 4106-00028B.

Nomenclature

a = Specific gas-liquid interfacial area [m^2 m^{-3}]
A = Pre-exponential factor [m^3 mol^{-1} s^{-1}]
A_L = Stagnant area of lube oil emulsion [m^2]
BN = Base number [(mg KOH) (g oil)$^{-1}$]

Ca/S = Initial molar ratio of $CaCO_3$ in lube oil to SO_2 in gas phase [mol mol^{-1}]
C_i^j = Concentration of component i in component j [mol m^{-3}]
D = Diameter of the cylinder [m]
D_i = Diffusion coefficient of SO_2 in component i [m^2 s^{-1}]
E_a = Activation energy [J mol^{-1}]
f = Last subvolume number [-]
h = Height of a subvolume [m]
H = Height of cylinder liner [m]
H_i = Henry's constant of SO_2 in component i [bar m^3 mol^{-1}]
i = Component i [-]
j = Component j [-]
k = Reaction rate constant [m^3 mol^{-1} s^{-1}]
k_G = Gas film mass transfer coefficient [mol m^{-2} s^{-1} bar^{-1}]
K_G = Overall gas-side mass transfer coefficient of SO_2 [mol m^{-2} bar^{-1} s^{-1}]
k_L = Liquid film mass transfer coefficient [m s^{-1}]
l = Subvolume numer [-]
N_i = Absorption rate of component i from the gas phase to the lube oil emulsion [mol m^{-3} s^{-1}]
p_i^j = Bulk partial pressure of component i in component j [bar]
P = Pressure in batch reactor [bar]
R = Ideal gas constant, 8.314 [J mol^{-1} K^{-1}]
$(-r_A)$ = Reaction rate [mol m^{-3} s^{-1}]
$R_{reactor}$ = Radius of batch reactor [m]
t = Time [s]
T = Temperature [^{o}C or K]
V_i = Volume of component i [m^3]

Greek Letters
δ_L = Liquid film thickness [m]
τ = Residence time [s]

Superscripts and subscripts
G = Gas phase
L = Lube oil emulsion (lube oil + water)
oil = Lube oil

References

(1) García, L.; Gehle, S.; Schakel, J. Impact of Low Load Operation in Modern Low Speed 2-Stroke Diesel Engines on Cylinder Liner Wear Caused by Increased Acid Condensation. *J. JIME* **2014**, *49* (1), 100–106.
(2) MAN Diesel & Turbo. Service Letter SL2014-587/JAP. 2014.
(3) Adamkiewicz, A.; Drzewieniecki, J. Operational Evaluation of Piston Ring Wear in Large Marine Diesel Engines. *J. Polish CIMAC* **2012**.

(4) CIMAC Working Group 8 “Marine Lubricants.” CIMAC Guideline Cold Corrosion in Marine Two Stroke Engines. 2017.

(5) Bovington, C. H. Friction, Wear and the Role of Additives in Controlling Them. In *Chemistry and Technology of Lubricants*; Mortier, R. M., Fox, M. F., Orszulik, S. T., Eds.; Springer Netherlands: Dordrecht, 2010; pp 77–105.

(6) Atkinson, D. Onboard Condition Monitoring of Cold Corrosion in Two-Stroke Marine Diesel Engines. *11th Int. Conf. Cond. Monit. Mach. Fail. Prev. Technol. C. 2014 / MFPT 2014* **2014**, *5* (2), 17–22.

(7) Marković, I.; Ottewill, R. H.; Cebula, D. J.; Field, I.; Marsh, J. F. Small Angle Neutron Scattering Studies on Non-Aqueous Dispersions of Calcium Carbonate - Part I. The Guinier Approach. *Colloid Polym. Sci.* **1984**, *262* (8), 648–656.

(8) International Maritime Organization (IMO). Sulphur oxides (SOx) and Particulate Matter (PM) – Regulation 14. http://www.imo.org/en/OurWork/Environment/PollutionPrevention/AirPollution/Pages/Sulphur-oxides-(SOx)-%E2%80%93-Regulation-14.aspx (accessed Oct 22, 2018).

(9) Jacobsen, D. M. S.; Pedersen, J. M.; Svensson, J.; Mayer, S. Cylinder Lube Oil Experiences and New Development for the MAN B&W Two-Stroke Engines. In *28th CIMAC World Congress*; Helsinki, 2016.

(10) Cordtz, R. The Influence of Fuel Sulfur on the Operation of Large Two-Stroke Marine Diesel Engines. Ph.D. Dissertation, Technical University of Denmark, Kgs. Lyngby, 2015.

(11) Christensen, O. Cylinder Lubrication of Two-Stroke Crosshead Marine Diesel Engines. *Wärtsilä Tech. J.* **2010**, 39–48.

(12) Pang, K. M.; Karvounis, N.; Walther, J. H.; Schramm, J.; Glarborg, P.; Mayer, S. Modelling of Temporal and Spatial Evolution of Sulphur Oxides and Sulphuric Acid under Large, Two-Stroke Marine Engine-like Conditions Using Integrated CFD-Chemical Kinetics. *Appl. Energy* **2017**, *193*, 60–73.

(13) Cordtz, R. L.; Schramm, J.; Rabe, R. Investigating SO_3 Formation from the Combustion of Heavy Fuel Oil in a Four-Stroke Medium Speed Test Engine. *Energy Fuels* **2013**, *27* (10), 6279–6286.

(14) Cordtz, R.; Schramm, J.; Andreasen, A.; Eskildsen, S. S.; Mayer, S. Modeling the Distribution of Sulfur Compounds in a Large Two Stroke Diesel Engine. *Energy Fuels* **2013**, *27* (3), 1652–1660.

(15) Cordtz, R.; Mayer, S.; Eskildsen, S. S.; Schramm, J. Modeling the Condensation of Sulfuric Acid and Water on the Cylinder Liner of a Large Two-Stroke Marine Diesel Engine. *J. Mar. Sci. Technol.* **2017**, 1–10.

(16) Karvounis, N.; Pang, K. M.; Mayer, S.; Walther, J. H. Numerical Simulation of Condensation of Sulfuric Acid and Water in a Large Two-Stroke Marine Diesel Engine. *Appl. Energy* **2018**, *211*, 1009–1020.

(17) Schramm, J.; Henningsen, S.; Sorenson, S. C. Modelling of Corrosion of Cylinder Liner in Diesel Engines Caused by Sulphur in the Diesel Fuel. In *SAE Technical Paper*; SAE International, 1994; pp 1–10.

(18) Lejre, K. H.; Kiil, S.; Glarborg, P.; Christensen, H.; Mayer, S. Reaction of Sulfuric Acid in Lube Oil: Implications for Large Two-Stroke Diesel Engines. In *Proceedings of the ASME 2017 Internal Combustion Engine Division Fall Technical Conference*; ASME: Seattle, United States, 2017; Vol. 1, pp 1–10.

(19) Lejre, K. H.; Glarborg, P.; Christensen, H.; Mayer, S.; Kiil, S. Mixed Flow Reactor Experiments and Modeling of Sulfuric Acid Neutralization in Lube Oil for Large Two-Stroke Diesel Engines. *Ind. Eng. Chem. Res.* **2019**, *58* (1), 138–155.

(20) Wu, R. C.; Papadopoulos, K. D.; Campbell, C. B. Visualization Test for Neutralization of Acids by Marine Cylinder Lubricants. *AIChE J.* **1999**, *45* (9), 2011–2017.
(21) Wu, R. C.; Papadopoulos, K. D.; Campbell, C. B. Acid-Neutralizing of Marine Cylinder Lubricants: Measurements and Effects of Dispersants. *AIChE J.* **2000**, *46* (7), 1471–1477.
(22) Wu, R. C.; Campbell, C. B.; Papadopoulos, K. D. Acid-Neutralizing of Marine Cylinder Lubricants: Effects of Nonionic Surfactants. *Ind. Eng. Chem. Res.* **2000**, *39* (10), 3926–3931.
(23) Fu, J.; Lu, Y.; Campbell, C. B.; Papadopoulos, K. D. Temperature and Acid Droplet Size Effects in Acid Neutralization of Marine Cylinder Lubricants. *Tribol. Lett.* **2006**, *22* (3), 221–225.
(24) Fu, J.; Lu, Y.; Campbell, C. B.; Papadopoulos, K. D. Acid Neutralization by Marine Cylinder Lubricants Inside a Heating Capillary: Strong/Weak-Stick Collision Mechanisms. *Ind. Eng. Chem. Res.* **2006**, *45* (16), 5619–5627.
(25) Fu, J.; Papadopoulos, K. D.; Lu, Y.; Campbell, C. B. Ostwald Ripening: A Decisive Cause of Cylinder Corrosive Wear. *Tribol. Lett.* **2007**, *27* (1), 21–24.
(26) Garcia-Bermudes, M.; Rausa, R.; Papadopoulos, K. Vertically-Oriented-Capillary Video-Microscopy: Drops Levitated by a (Reacting) Fluid. *Ind. Eng. Chem. Res.* **2011**, *50* (24), 14142–14147.
(27) Garcia-Bermudes, M.; Rausa, R.; Papadopoulos, K. Formation of Colloidal Shells on Acidic Droplets Undergoing Neutralization in Marine Diesel Engine Cylinder Oils. *Tribol. Lett.* **2013**, *51* (1), 85–92.
(28) Duan, Y.; Rausa, R.; Zhao, Q.; Papadopoulos, K. D. Neutralization Mechanism of Acetic Acid by Overbased Colloidal Nanoparticles. *Tribol. Lett.* **2016**, *64* (8), 1–11.
(29) Hone, D. C.; Robinson, B. H.; Steytler, D. C.; Glyde, R. W.; Cleverley, J. A. Acid-Base Chemistry in High-Performance Lubricating Oils. *Can. J. Chem.* **1999**, *77*, 842–848.
(30) Hone, D. C.; Robinson, B. H.; Steytler, D. C.; Glyde, R. W.; Galsworthy, J. R. Mechanism of Acid Neutralization by Overbased Colloidal Additives in Hydrocarbon Media. *Langmuir* **2000**, *16* (2), 340–346.
(31) Hone, D.; Robinson, B.; Galsworthy, J.; Glyde, R. Colloidal Chemistry of Lubricating Oils. In *Reactions And Synthesis In Surfactant Systems*; Texter, J., Ed.; Surfactant Science; CRC Press, 2001; pp 385–394.
(32) Hosonuma, K.; Tamura, K. Acid Neutralization of Overbased Detergents (Part 1) Neutralization in the Test Methods of ASTM Base Number. *J. Japan Pet. Inst.* **1984**, *27* (2), 101–107.
(33) Hosonuma, K.; Tamura, K. Acid Neutralization of Overbased Detergents (Part 2) Neutralization with Sulfuric Acid Emulsion. *J. Japan Pet. Inst.* **1984**, *27* (2), 108–113.
(34) Roman, J.-P. New Method of Measurement in Thin Film of the Neutralization of Marine Lubricants for Low-Speed and Medium-Speed Diesel Engines. In *CIMAC Congress 1998, Copenhagen*; Copenhagen, 1998; pp 913–926.
(35) Akiyama, K.; Masunaga, K.; Kado, K.; Yoshioka, T. Cylinder Wear Mechanism in an EGR-Equipped Diesel Engine and Wear Protection by the Engine Oil. Paper 872158. *SAE Int.* **1987**, 1–7.
(36) Amblard, C. New Chemistry to Protect against Cold Corrosion in Marine Cylinder Lubricants. *J. Japan Inst. Mar. Eng.* **2015**, *50* (6), 54–62.
(37) Buck, A. M.; Cattaneo, A. G.; Coit, R. A.; Edgar, J. A.; Isitt, A. R. Engine Lubricating Oils for the Reduction of Wear. In *3rd World Petroleum Congress, 28 May-6 June, The Hague, the Netherlands*; 1951; pp 405–412.
(38) Macdonald, A. G.; Stott, F. H. The Corrosive Wear of Cast Iron in Oil-Sulphuric Acid Mixtures. *Corros. Sci.* **1988**, *28* (5), 485–501.
(39) Golothan, D. W. Review of the Causes of Cylinder Wear in Marine Diesel Engines. *Inst. Mar. Eng. Trans.* **1978**, *90*, 137–163.

(40) McConnell, G.; Nathan, W. S. A Wear Theory for Low Speed Diesel Engines Burning Residual Fuel. *Wear* **1962**, *5* (1), 43–54.
(41) Stott, F. H.; Macdonald, A. G. The Influence of Acid Strength on the Corrosive Wear of Grey Cast Irons in Oil-Sulphuric Acid Mixtures. *Wear* **1988**, *122* (3), 343–361.
(42) van Helden, A. K.; Valentijn, M. C.; van Doornt, H. M. J. Corrosive Wear in Crosshead Diesel Engines. *Tribol. Int.* **1989**, *22* (3), 189–193.
(43) Yahagi, Y. Corrosive Wear of Diesel Engine Cylinder Bore. *Tribol. Int.* **1987**, *20* (6), 365–373.
(44) McGeehan, J. A.; Kulkarni, A. V. Mechanism of Wear Control by the Lubricant in Diesel Engines, No. 872029. In *SAE Technical Paper Series*; 1987; pp 1–14.
(45) Nagaki, H.; Korematsu, K. Relation Between Diffusion Process of Sulfur Oxides in Exhaust Gas into Oil Film and Wear of Cylinder Liner and Piston Rings in Diesel Engines. *SAE Pap.* **1991**.
(46) Nagaki, H.; Korematsu, K. Effect of Sulfur Dioxide in Recirculated Exhaust Gas on Wear within Diesel Engines - (Relationship between Wear and Amount of SO_2 Absorbed by Lubricating Oil Film). *JSME Int. J. Ser. B-Fluids Therm. Eng.* **1995**, *38* (3), 465–474.
(47) Nagaki, H.; Korematsu, K. Effect of SO_2 in Recirculated Exhaust Gas on Wear in Diesel Engine - (Effect of SO_2 Added to Intake Air on Wear). *JSME Int. J. Ser. B-Fluids Therm. Eng.* **1996**, *39*, 193–201.
(48) Naegeli, D. W.; Marbach, H. W. Role of Sulfur Oxides in Wear and Deposit Formation in Army Diesel Engines. Interim Report BFLRF No. 248, Contract No. DAAK70-87-C-0043. Southwest Research Institute: San Antonio, Texas, 1988.
(49) Kiil, S. Experimental and Theoretical Investigations of Wet Flue Gas Desulphurisation. Ph.D. Dissertation, Technical University of Denmark, Kgs. Lyngby, 1998.
(50) Córdoba, P. Status of Flue Gas Desulphurisation (FGD) Systems from Coal-Fired Power Plants: Overview of the Physic-Chemical Control Processes of Wet Limestone FGDs. *Fuel* **2015**, *144*, 274–286.
(51) Kiil, S.; Michelsen, M. L.; Dam-Johansen, K. Experimental Investigation and Modeling of a Wet Flue Gas Desulfurization Pilot Plant. *Ind. Eng. Chem. Res.* **1998**, *37* (7), 2792–2806.
(52) Klingspor, J.; Karlsson, H. T.; Bjerle, I. A Kinetic Study of the Dry SO_2-Limestone Reaction at Low Temperature. *Chem. Eng. Commun.* **1983**, *22*, 81–103.
(53) Baltrusaitis, J.; Usher, C. R.; Grassian, V. H. Reactions of Sulfur Dioxide on Calcium Carbonate Single Crystal and Particle Surfaces at the Adsorbed Water Carbonate Interface. *Phys. Chem. Chem. Phys.* **2007**, *9* (23), 3011–3024.
(54) Al-Hosney, H. A.; Grassian, V. H. Water, Sulfur Dioxide and Nitric Acid Adsorption on Calcium Carbonate: A Transmission and ATR-FTIR Study. *Phys. Chem. Chem. Phys.* **2005**, *7* (6), 1266.
(55) Costa, D. L.; Underhill, D. Solubility and Reactivity of Sulfur Dioxide in Various Oils. *Am. Ind. Hyg. Assoc. J.* **1976**, *37* (1), 46–51.
(56) ASTM International. ASTM 2896-11. Standard Test Method for Base Number of Petroleum Products by Potentiometric Perchloric Acid Titration. 2011.
(57) NIST Chemistry WebBook: https://webbook.nist.gov/chemistry.
(58) Smith, P. G. *Introduction to Food Process Engineering*; Food Science Text Series; Springer US: Boston, MA, 2011.
(59) Meille, V.; Pestre, N.; Fongarland, P.; de Bellefon, C. Gas/Liquid Mass Transfer in Small Laboratory Batch Reactors: Comparison of Methods. *Ind. Eng. Chem. Res.* **2004**, *43* (4), 924–927.
(60) Lee, J. H.; Foster, N. R. Measurement of Gas-Liquid Mass Transfer in Multi-Phase Reactors. *Appl. Catal.* **1990**, *63* (1), 1–36.
(61) Sautermeister, F. A.; Priest, M. Physical and Chemical Impact of Sulphuric Acid on Cylinder

Lubrication for Large 2-Stroke Marine Diesel Engines. *Tribol. Lett.* **2012**, *47* (2), 261–271.

(62) Hammett, J. Utilising the Latest Findings Engine Oil Stress from Field & Laboratory Engine Testing. *J. JIME* **2014**, *49* (3), 6–13.

(63) Lamas, M. I.; Rodríguez, C. G. Emissions from Marine Engines and NOx Reduction Methods. *J. Marit. Res.* **2012**, *9* (1), 77–82.

(64) MAN Energy Solutions. CEAS Engine Calculations https://marine.man-es.com/two-stroke/ceas (accessed Jul 12, 2018).

(65) Doyen, V.; Drijfholt, R. K.; Delvigne, T. PAPER NO .: 61 Advanced Applied Research Unravelling the Fundamentals of 2-Stroke Engine Cylinder Lubrication – an Innovative on-Line Measurement Method Based on the Use of Radioactive Tracers-. *CIMAC Congr. 2007, Vienna* **2007**.

6 | Revisiting the scientific hypotheses

This chapter revisits the hypotheses presented in Chapter 1 in order to clarify whether each of the hypotheses was true or false.

Hypothesis 1 *The neutralization reaction between H_2SO_4 and the alkaline additives (present as micelles) in lube oil is limited by a single rate-limiting step; micelle diffusion, micelle adsorption, chemical reaction, micelle desorption, or macromixing.*

The mathematical modeling in Chapter 4 could not distinguish between the potential limiting-steps outlined; however, the experimental batch reactor data together with data from literature indicate, that the neutralization reaction is presumably adsorption-controlled. In addition, a reaction rate expression with associated kinetic parameters was derived and determined.

Therefore, hypothesis 1 was found to be partly clarified. More investigations are needed to truly confirm that the rate of adsorption is the rate-controlling step.

Hypothesis 2 *The H_2SO_4 droplets get into the bulk of the lube oil film, eventually reaching the cylinder liner surface, by either:*

- *Diffusion, or*
- *Mixing by the piston rings*

The MFR experiments revealed that decreasing the stirring rate to a very low intensity (120 rpm), led to sedimentation of the H_2SO_4 and thereby prevented emulsification of the H_2SO_4. Also, an experiment with no stirring was carried out (large excess of H_2SO_4 compared to $CaCO_3$ on a molar basis was present), yielding that H_2SO_4 sedimented. Subsequent analysis of the bulk lube oil revealed that no conversion of the $CaCO_3$ had happened. This indicates that a certain degree of stirring is needed in order to solubilize the H_2SO_4 into the lube oil. Further, the diffusion of the H_2SO_4 droplets depends very much on the size of the droplets.

Calculations of the mean Brownian displacement under engine conditions (Chapter 4) revealed that the diffusion of the H_2SO_4 droplets is too slow to reach the cylinder liner upon condensation onto the lube oil film within the time frame available. Lastly, the lube oil is hydrophobic and H_2SO_4 is hydrophilic, which advocates that H_2SO_4 would just deposit on top of the lube oil film in an engine application. In conclusion, for the H_2SO_4 to be emulsified (formation of tiny H_2SO_4 droplets) and eventually reach the cylinder liner wall, the lube oil film has to be mixed, which happens by the piston rings.

Therefore, hypothesis 2 was found to be partly true.

Hypothesis 3 *The specific engine conditions will have a significant impact on the conversion rate of the acidic sulfur components.*

From the H_2SO_4 experiments and modeling, it was found that the resulting droplet size of the emulsified H_2SO_4 is crucial for the conversion rate of H_2SO_4, i.e., the smaller the droplets, the faster the neutralization. The resulting droplet size may depend on the lube oil formulation, but may also be highly affected by the mixing of the piston rings (affected by for instance piston speed and design). The lube oil film temperature was also showed to exhibit a significant effect on the conversion rate. In addition, a low Ca/S molar ratio was found to significantly reduce the reactant conversions (depends for instance on the conditions in the gas phase and the lube oil dosage strategy). The available reaction time was also showed to impact the resulting conversion degree (affected by factors such as load and piston speed). An increased base number (BN) value at a maintained Ca/S molar ratio would also increase the conversion rate, but the effect is not that pronounced.

With respect to SO_2, the simulations at engine conditions and the batch reactor experiments revealed that the lube oil temperature, the partial pressure of SO_2 in the gas phase, and the water concentration in the lube oil impact the conversion degree (which is affected by operating temperature in gas phase, pressure, sulfur content in fuel, engine speed, etc.).

Therefore, hypothesis 3 was found to be true.

Hypothesis 4 *Different experimental setups can be used to individually investigate the sub-processes happening in a lube oil film.*

From the literature review (Chapter 2), it was found that H_2SO_4 and SO_2 are the main contributors with respect to consumption of the alkaline additives and corrosive wear of the cylinder liners. To isolate the effect of each component, the reactions between H_2SO_4-$CaCO_3$ and SO_2-$CaCO_3$ were studied individually in separate experimental setups. Modeling tools were used to extract kinetics and the relative importance of the two reactions was assessed. Furthermore, the MFR setup was used to investigate how H_2SO_4 emulsifies and reacts in the lube oil film and a batch reactor setup was used to investigate how gaseous SO_2 reacts in the lube oil.

Therefore, hypothesis 4 was found to be true.

Hypothesis 5 *The SO_2 reacts with the alkaline additives in the lube oil in an engine due to the high partial pressure of SO_2 prevailing in the combustion chamber.*

SO_2 is in molar excess in the engine compared to H_2SO_4, because only up to 10% of the SO_2 is converted to SO_3 (and eventually H_2SO_4). It was therefore thought that the large concentration gradient of SO_2, between the combustion gas and the lube oil film, would lead to rapid absorption and reaction with the alkaline additives. However, the SO_2 is rapidly diluted in the combustion chamber as the expansion stroke progresses and is eventually exhausted and ventilated. Simulations carried out at worst-case large engine conditions revealed that the consumption of $CaCO_3$ reverse micelles in the lube oil film from SO_2 is insignificant compared to the conversion from H_2SO_4. Nevertheless, if SO_2 consumes $CaCO_3$ in an engine, it will likely happen in the upper part of the cylinder liner, where the partial pressure of SO_2 in the combustion gas is highest.

Therefore, hypothesis 5 was found to be partly true, because SO_2 do react with $CaCO_3$, but the reaction is insignificant in a marine diesel engine application.

Hypothesis 6 *Different analysis equipment can be used to accurately measure the BN and determine the reaction products in the lube oil.*

It was found that the titration approach is a reliable and accurate analysis method for determining the BN of lube oils. However, for the purpose of quantifying the BN rapidly upon sampling (for determining if unreacted H_2SO_4 was present in a lube oil sample), the titration method was not applicable. Also, when $CaSO_3$ was present in a lube oil sample (after reaction with SO_2), the titration method had difficulties in analyzing the lube oil samples. Different analysis methods were explored, such as gas analysis, ED-XRF, TGA, and FTIR (described in Appendix A). TGA proved to be applicable for determining the BN of fresh lube oils accurately. ED-XRF was useful in determining the BN from the calcium content, but also for determining the conversion by the sulfur uptake in the lube oil from SO_2 and H_2SO_4. However, FTIR was mainly used for analyzing the lube oil samples (after reaction with H_2SO_4 and SO_2), due to having various advantages compared to the other analysis techniques. Firstly, the analysis method is accurate and reliable, reflected by the low standard deviations on the resulting spectra. Secondly, it was possible to analyze the lube oil samples from the outlet of the MFR rapidly, making it possible to investigate whether complete conversion of the H_2SO_4 had been achieved within the MFR. Thirdly, with the use of FTIR, it was possible to investigate which reaction products that were formed from the reactions between H_2SO_4 and SO_2 with $CaCO_3$ reverse micelles.

Therefore, hypothesis 6 was found to be true.

Hypothesis 7 *Modeling results can be used to estimate the acid concentration on the cylinder liner surface, which can be used in a model concerning the corrosive wear of the surface material.*

The mathematical model derived in Chapter 4 was used to estimate the average H_2SO_4 concentration in the lube oil film. Because the lube oil film was assumed to be well-mixed, the concentration of H_2SO_4 at the cylinder liner surface is equal to the bulk concentration of H_2SO_4 in the lube oil emulsion. If a corrosive wear model is derived, having the average H_2SO_4 concentration as an input parameter, it may be possible to predict the resulting wear rate. The mathematical model regarding SO_2 in Chapter 5, could also predict the SO_2 concentration in the lube oil film emulsion. However, a refined overall mass transfer coefficient or the validation of the model by performing laboratory scale engine experiments may be needed to improve the accuracy of the model predictions. The kinetic expressions derived in Chapters 4 and 5 may also be used in computational fluid dynamics (CFD) models to predict the temporal and spatial concentrations of H_2SO_4 and SO_2 at the cylinder liner surface.

Therefore, hypothesis 7 was found to be true.

7 | Conclusions and future work

This chapter consists of two parts. First, the results of the work presented in the preceding chapters are summarized. Then follow suggestions for further work.

7.1 Conclusions

In this thesis, the potential sulfur-related neutralization reactions, which may take place in a lubrication (lube) oil film present on a cylinder liner in large two-stroke marine diesel engines, were investigated. More specifically, the chemistry includes SO_2(g)/H_2SO_4(aq) reactions with $CaCO_3$(s) in reverse micelles, formulated into commercial lube oils with the purpose of protecting the cast iron cylinder liner wall and piston rings. The reactions were investigated separately using experiments and mathematical modeling.

A literature review of the two-stroke engine principle and the sulfur-related processes occurring during the combustion cycle were outlined. This included formation of SO_2 and H_2SO_4 in the combustion chamber, condensation of H_2SO_4 onto the cylinder liner surface, the reaction between H_2SO_4 and $CaCO_3$ reverse micelles in the lube oil, the reaction between H_2SO_4 and cast iron both with and without wear and base oil, and finally the reaction mechanism between SO_2 and $CaCO_3$/cast iron. Also, ways to control corrosion were described. The literature study revealed the complexity of the cold corrosion phenomenon and why it is important to develop predictive tools of the sub-processes to improve the ability to predict cold corrosion in the large two-stroke marine diesel engines, namely to accelerate and support the development process of new engine designs with improved engine efficiency.

The reaction between aqueous H_2SO_4 droplets and $CaCO_3$ reverse micelles in lube oil was investigated in a mixed flow reactor (MFR) setup. Lube oil samples were collected at steady state and were immediately analyzed by Fourier Transform Infrared Spectroscopy (FTIR) to determine the $CaCO_3$ conversion. For the residence times investigated in the MFR, it was found that the H_2SO_4-$CaCO_3$ reaction was significantly reduced when the Ca/S molar ratio approached unity. In addition, a certain degree of stirring was needed in order to maintain and initiate the reaction, probably due to the necessity of achieving a sufficient degree of emulsification of the H_2SO_4 into the lube oil emulsion. While the investigated range of residence times

showed no effect on the $CaCO_3$ conversion, dilution of the inlet H_2SO_4 concentration resulted in a slight decrease in $CaCO_3$ conversion. A mathematical model of the MFR setup was developed and the only unknown parameter in the model was the average radius of the H_2SO_4 droplets. This parameter was fitted by matching simulations with experimental MFR data and values in the range 0.5-9.6 µm were estimated. From the mathematical modeling, an apparent reaction rate expression, including kinetic parameters, was presented. The mathematical modeling could not distinguish between the potential limiting-steps outlined; however, the experimental batch reactor data together with data from literature indicate, that the neutralization reaction is presumably adsorption-controlled. Because the MFR model offers a useful approximation to the conditions in the lube oil film on the cylinder liner wall, the model could be used to predict the influence of different process parameters on the H_2SO_4 conversion at conditions relevant for a full-scale application. It was found that the lube oil temperature significantly affects the H_2SO_4 conversion, while the base number (BN) of the lube oil and the H_2SO_4 droplet concentration have only a minor impact at a maintained Ca/S molar ratio. The H_2SO_4 concentration in a well-mixed lube oil film was also simulated and it was concluded that H_2SO_4 may be in contact with the cylinder liner wall regardless of how well-wetted the liner is. The H_2SO_4 concentration at the cylinder liner wall was pronounced when having a low Ca/S molar ratio (even worse when having a molar excess of H_2SO_4 compared to $CaCO_3$). This situation may correspond to the situation prevailing near TDC, where the most severe corrosive wear is found in practice. One way of reducing the wear here would thereby be to increase the amount of lube oil supplied in this upper region. To combat uncontrolled corrosive wear of the cylinder liner, it may therefore be a matter of optimizing the vertical distribution of the lube oil, having sufficient lube oil (i.e., $CaCO_3$) at the critical regions.

The reaction between gaseous SO_2 and $CaCO_3$ in lube oil was investigated in a stirred high-pressure high-temperature batch reactor setup. The reacted lube oil samples were analyzed by FTIR-ATR. It was observed that SO_2 does react with $CaCO_3$ reverse micelles in lube oil. The reaction products were found to be a mixture of $CaSO_3$ and $CaSO_4$, however, $CaSO_4$ was formed at increased residence times and temperatures. The initial concentration of water in the lube oil emulsion had a significant effect on the $CaCO_3$ conversion, while the effect of temperature was minor. These observations were explained by a change in SO_2 absorption in the lube oil emulsion because the absorption increases at increased water concentration and decreases at increasing temperatures. The formed $CaSO_3$ was found to react with H_2SO_4 in a similar way as the $CaCO_3$. This means that the conversion from $CaCO_3$ to $CaSO_3$ may not reduce the neutralization ability of the lube oil emulsion in terms of BN. In addition, a mathematical model was derived to describe the experimental batch reactor data in order to extract a kinetic expression for the SO_2-$CaCO_3$ neutralization reaction, The modeling showed a strong correlation between the mass transfer coefficient and the reaction rate constant. To cope with this, the mass transfer coefficient was estimated by the use of experimental results from the literature, and it was then possible to determine kinetic parameters for the reaction. The derived model was used to predict $CaCO_3$ conversions from SO_2 at conditions relevant for a full-scale marine diesel engine application. The modeling showed that $CaCO_3$ conversion is dependent on the SO_2 concentration in the gas phase, and the conversion of $CaCO_3$ was therefore most pronounced near TDC. Simulations carried out at worst-case conditions revealed that less than 8% of the total $CaCO_3$ in the lube oil would react with SO_2. The study also showed that the H_2SO_4-$CaCO_3$ reaction is much faster than the SO_2-$CaCO_3$ reaction at relevant full-scale conditions. This means that SO_2 is only expected to consume a negligible fraction of the $CaCO_3$ in the lube oil film in a marine diesel engine application. However, simulations revealed that SO_2 absorbs readily into the lube oil emulsion and aqueous SO_2 may therefore be present in the lube oil emulsion and at the cast iron cylinder liner wall in a significant amount. Even though SO_2 is not expected to consume any significant amount of BN, it may contribute to corrosive wear in a similar way as the H_2SO_4.

Overall, the models developed in this thesis could be used as part of a larger diesel engine model that considers the entire cylinder. This could include gas phase modeling and H_2SO_4 condensation modeling, presented in Chapter 2, which can serve as boundary conditions for the lube oil emulsion modeling. The output from the lube oil emulsion modeling would be the H_2SO_4 concentration in the lube oil emulsion, which would serve as an input to a corrosive wear model for modeling of the corresponding wear rate. It may eventually be possible to calculate the wear rate from specific engine conditions and designs, with the aim of determining optimal lubrication strategies.

7.2 Future work

Suggestions for future work are divided into four main parts: H_2SO_4 experiments and modeling, SO_2 experiments and modeling, analysis methods, and overall outlook.

7.2.1 H_2SO_4 experiments and modeling

For the investigated residence times, it was observed that the H_2SO_4 neutralization reaction was significantly reduced at low Ca/S ratios, making an investigation of the limiting step possible. However, it would be interesting to investigate the reaction at even lower residence times (<48 seconds). This has been done in the literature,[1–3] but without any success in quantifying the conversion of H_2SO_4 as a function of time and for different reaction systems. The FTIR proved to be a reliable and fast analysis method, which may be useful in achieving the above. The progress of the reaction could be investigated in a reciprocating pin-on-disc laboratory apparatus, which would take into account the actual mixing of the lube oil and realistic residence times.

Exploring the reaction of an H_2SO_4 droplet in commercial lube oil formulations is also recommended, in order to settle how H_2SO_4 is consumed in lube oil. This could include use of model oils and different commercial lube oils in order to map the influence of various formulations. It was suggested that the H_2SO_4 droplet may be solubilized by the excess surfactant, leading to an increased shrinking rate. It would be interesting to investigate this hypothesis in greater detail, eventually by use of the video-microscopy setup by Fu et al.[4]

It would be useful with an experimentally determined average H_2SO_4 droplet size in a fully formulated lube oil emulsion, if possible. This would also allow for the implementation of a size distribution of the H_2SO_4 droplets into the model. The literature values are based on typical emulsions, stable base oils, and stable drain oils.[5–7] The H_2SO_4 droplet size may be significantly smaller than the found values due to the large amount of detergents and dispersants present in a fully formulated lube oil. In addition, the shrinkage of the H_2SO_4 droplets (instead of the assumption about a droplet is consumed at once) could also be implemented.

Mixed flow reactor experiments with different commercial or model lube oils could be carried out to assess the importance of different formulations on the kinetics, with the aim of improving the lube oil formulation. However, it was found in literature[3,4,8] that the higher the lube oil temperature, the lower the difference between lube oils of various formulations. It would also be of interest to determine and quantify the effect of H_2SO_4 droplet concentration on the reaction rate constant.

Performing CFD simulations may be useful to verify the assumed well-mixed situation occurring in a full-scale marine diesel engine. Initial CFD simulations of a reciprocating piston ring sliding over a lube oil film were performed (a short description is given in Appendix B), but various issues arose due to the very dynamic and complex environment of the lube oil-piston ring environment. Refinement of the CFD model is highly needed.

Full-scale measurements would be interesting to perform to investigate the lube oil coverage on the cylinder liner and to investigate the hypothesis that corrosive wear is most pronounced near TDC due to an insufficient amount of lube oil containing the necessary amount of $CaCO_3$ reverse micelles. By use of FTIR immediately after sampling, it would allow for assessment of the reaction products, and thereby if $CaSO_3$ can be observed in practice. Investigation of different lube oil dosage strategies practically could provide new insight into how to improve the lube oil coverage in the critical locations where corrosive wear is pronounced without using more lube oil. It would also be useful to estimate the fraction of lube oil which is lost due to for example evaporation and combustion. This knowledge is important to optimize the lube oil feed rate by model simulations.

7.2.2 SO_2 experiments and modeling

As shown in Chapter 5, it is crucial to estimate the accurate value of the overall mass transfer coefficient K_G in order to get an accurate estimate of the reaction rate constant. Therefore, carrying out experiments which measure K_G would be useful. It would also be beneficial to measure the temperature dependency of Henry's constant for SO_2 in lube oil. These measurement campaigns may be challenging, because measurements have to be done with a lube oil containing all the emulsifying agents, but not containing the $CaCO_3$ reverse micelles.

From literature, it is indicated that SO_2 has a corrosive effect on cast iron.[9–11] If this is the case in an engine application, a model simulating the SO_2 concentration in the lube oil film at specific engine conditions is required for determination of the corresponding corrosion (and thereby wear rate). In the light of this, it is therefore crucial to verify the SO_2 absorption model derived in Chapter 5. The simulated absorption concentrations of SO_2 in the lube oil emulsion at engine conditions could be validated against laboratory scale engine experiments capable of measuring the SO_2 accumulation or $CaCO_3$ conversion in the lube oil.[12]

Further investigations of the reaction mechanism between aqueous SO_2 and $CaCO_3$ reverse micelles could also be of interest. Interestingly, $CaSO_4$ was only observed in the lube oil samples at extended residence times and higher temperatures. This would clarify if $CaSO_4$ is formed by oxidation from $CaSO_3$ or directly from the reaction between $CaCO_3$-H_2O-SO_2-O_2. This would also be useful in improving the existing SO_2 model to better predict the effect of residence time on the $CaCO_3$ conversion.

7.2.3 Analysis methods

FTIR-ATR was mainly used to analyze the lube oil samples after reaction with H_2SO_4 and SO_2. Off-shore, the BN of a lube oil sample is mainly determined by a 'BN shaker'. However, this analysis method is not that accurate, consumes solvents, breaks easily, is time-demanding, and needs a relatively large sample size. In this PhD, the FTIR-ATR analysis method proved to be reliable, accurate, easy to use, fast, and uses a little

sample size. However, a handheld FTIR-ATR apparatus for use on-board vessels is pricy and reliable calibration models are needed for accurate BN determination. The learnings from using the FTIR-ATR apparatus in this PhD can be used in further development of a handheld FTIR apparatus which can be used on-board the large vessels for lube oil analysis. This would include the development of reliable chemometric models.

7.2.4 Overall outlook

The work presented in this thesis is expected to be combined with the remaining work carried out within the SULCOR umbrella (described in Chapter 1) in order to map the influence of modified engine designs or operating conditions on the corrosive wear rate, thus providing knowledge about how to minimize lube oil and fuel consumptions without sacrificing component lifetime and reliability of the marine diesel engines.
The kinetics of this work can, for instance, be used in more complex models such as 3D CFD models and coupled with gas phase[13] and condensation[14] models, the combined model can be used to predict the local H_2SO_4 and SO_2 concentrations prevailing at the liner surface. These concentration profiles at the cylinder liner surface can then be used as an input for a wear/corrosion model, which can predict the expected wear rate. Ultimately, it would be possible to estimate the wear rate of a cylinder liner at specific operating conditions and engine design and predict how different operating conditions and engine designs affect the wear rate. This would allow for optimization of the lube oil and fuel consumptions with respect to achieving low levels of cold corrosion. This would be a valuable predictive tool because engine experiments carried out in practice are often expensive, difficult, time-consuming, and non-representative.

References

(1) Wu, R. C.; Papadopoulos, K. D.; Campbell, C. B. Visualization Test for Neutralization of Acids by Marine Cylinder Lubricants. *AIChE J.* **1999**, *45* (9), 2011–2017.

(2) Hone, D. C.; Robinson, B. H.; Steytler, D. C.; Glyde, R. W.; Galsworthy, J. R. Mechanism of Acid Neutralization by Overbased Colloidal Additives in Hydrocarbon Media. *Langmuir* **2000**, *16* (2), 340–346.

(3) Roman, J.-P. New Method of Measurement in Thin Film of the Neutralization of Marine Lubricants for Low-Speed and Medium-Speed Diesel Engines. In *CIMAC Congress 1998, Copenhagen*; Copenhagen, 1998; pp 913–926.

(4) Fu, J.; Lu, Y.; Campbell, C. B.; Papadopoulos, K. D. Temperature and Acid Droplet Size Effects in Acid Neutralization of Marine Cylinder Lubricants. *Tribol. Lett.* **2006**, *22* (3), 221–225.

(5) Goodwin, J. W. *Colloids and Interfaces with Surfactants and Polymers*; John Wiley & Sons, Ltd: Chichester, UK, 2009.

(6) Sautermeister, F. A.; Priest, M. Physical and Chemical Impact of Sulphuric Acid on Cylinder Lubrication for Large 2-Stroke Marine Diesel Engines. *Tribol. Lett.* **2012**, *47* (2), 261–271.

(7) Sautermeister, F. A.; Priest, M.; Lee, P. M.; Fox, M. F. Impact of Sulphuric Acid on Cylinder Lubrication for Large 2-Stroke Marine Diesel Engines: Contact Angle, Interfacial Tension and Chemical Interaction. *Tribol. Int.* **2013**, *59*, 47–56.

(8) Wu, R. C.; Campbell, C. B.; Papadopoulos, K. D. Acid-Neutralizing of Marine Cylinder Lubricants: Effects of Nonionic Surfactants. *Ind. Eng. Chem. Res.* **2000**, *39* (10), 3926–3931.

(9) Xiang, Y.; Wang, Z.; Xu, C.; Zhou, C.; Li, Z.; Ni, W. Impact of SO_2 Concentration on the Corrosion Rate of X70 Steel and Iron in Water-Saturated Supercritical CO_2 Mixed with SO_2. *J. Supercrit. Fluids*

2011, *58* (2), 286–294.

(10) Johansson, L.-G.; Vannerberg, N.-G. The Corrosion of Unprotected Steel in an Inert-Gas Atmosphere Containing Water Vapour, Oxygen, Nitrogen and Different Amounts of Sulphur Dioxide and Carbon Dioxide. *Corros. Sci.* **1981**, *21* (12), 863–876.

(11) Allam, I. M.; Arlow, J. S.; Saricimen, H. Initial Stages of Atmospheric Corrosion of Steel in the Arabian Gulf. *Corros. Sci.* **1991**, *32* (4), 417–432.

(12) Kjemtrup, L.; Cordtz, R. F.; Meyer, M.; Schramm, J. Experimental Investigation of Sulfuric Acid Condensation and Corrosion Rate in Motored BUKH DV24 Diesel Engine. In *Proceedings of the ASME 2017 Internal Combustion Engine Division Fall Technical Conference*; ASME: Seattle, United States, 2017; pp 1–8.

(13) Pang, K. M.; Karvounis, N.; Walther, J. H.; Schramm, J.; Glarborg, P.; Mayer, S. Modelling of Temporal and Spatial Evolution of Sulphur Oxides and Sulphuric Acid under Large, Two-Stroke Marine Engine-like Conditions Using Integrated CFD-Chemical Kinetics. *Appl. Energy* **2017**, *193*, 60–73.

(14) Karvounis, N.; Pang, K. M.; Mayer, S.; Walther, J. H. Numerical Simulation of Condensation of Sulfuric Acid and Water in a Large Two-Stroke Marine Diesel Engine. *Appl. Energy* **2018**, *211*, 1009–1020.

Appendix A | Lube oil analyses to determine and quantify the alkaline core of the overbased detergents

The present chapter describes shortly the different analyses carried out to determine and quantify the alkaline component(s) of the overbased detergent core that is formulated into the lube oil used for the work described in the subsequent chapters. The lube oil was supplied from Infineum and had a stated base number (BN) value of 100. The unit of BN is defined as the quantity of acid, expressed in terms of the equivalent number of milligrams of KOH required to neutralize all alkaline constituents in a one gram sample (mg KOH (g oil sample)$^{-1}$).[1] It is important to know the component(s) of the alkaline additive core to determine the H_2SO_4 neutralization mechanism and which analysis methods that can be utilized for product analysis of the spent lube oils. Generally, it is reported that the core consists of either a metal carbonate or a mixture of metal carbonate and metal hydroxide. The metal cation can be Ca^{2+}, Na^{2+}, Mg^{2+}, or a mixture thereof.[2–5] The reactions between the metal carbonate/hydroxide with H_2SO_4 are shown in Eqs. (A.1) and (A.2), where M is the metal cation. The major difference between these two reactions is the formation of gaseous CO_2 in Eq. (A.1).

$$MCO_{3(s)} + H_2SO_{4(aq)} \rightarrow MSO_{4(s)} + H_2O_{(l)} + CO_{2(g)} \quad \text{(A.1)}$$

$$M(OH)_{2(s)} + H_2SO_{4(aq)} \rightarrow MSO_{4(s)} + 2H_2O_{(l)} \quad \text{(A.2)}$$

A.1 Titration

The standard test method of measuring BN is by titration using the method ASTM D2896.[1] This method was applied in this PhD project to determine the BN in the lube oil samples using a Mettler Toledo T50 potentiometric titrator. The BN determined by this method and apparatus was regarded as the ‘actual’ BN value. Therefore, the performance and reproducibility were tested by measuring different cylinder lube oils having BN in the range 6-100. The 6 BN lube oil was a system oil, however. The results of this analysis are presented in Table A.1. The table shows the mean BN value measured by five repetitions and the two times the sample standard deviation which was found to be less than 1 BN. This means that the titration method is a precise and robust analysis method to determine the BN of a lube oil sample. However, the method does not give any information about which kind of alkaline components that are present in the lube oil.

Table A.1. BN results from analyzing different lube oils with the ASTM D2896 method.

	Stated BN value of lube oil by the manufacturer				
#	**6 BN**	**25 BN**	**40 BN**	**70 BN**	**100 BN**
1	6.35	24.58	40.9	71.99	98.74
2	6.32	25.15	40.62	72.6	98.02
3	6.24	24.75	41.56	72.84	98.24
4	6.41	24.67	40.89	73.02	98.73
5	6.29	24.36	40.77	73.05	99.03
Mean, $\bar{x}$	**6.32**	**24.70**	**40.95**	**72.70**	**98.55**
Standard deviation, s	0.06	0.29	0.36	0.44	0.41
$2s$	0.13	0.58	0.72	0.87	0.82
$(2s/\bar{x}) \times 100\%$	**2.02**	**2.35**	**1.76**	**1.20**	**0.83**

A.2 Gas analysis

On-board, the analysis of drain oils are often carried out by a small pressure cell for the sake of simplicity, which relates the CO_2 evolution from the reaction between an acid and MCO_3, equivalent to the reaction given in Eq. (A.1), to the BN.[3] This method only has the opportunity of measuring the gas-generating reactions, thus it will not include the BN related to $M(OH)_2$ (Eq. (A.2)).

In relation to this, continuous analysis of the outlet gas from mixed flow reactor (MFR) experiments (the setup is described in detail in Chapter 3) by dosing H_2SO_4 and lube oil was carried out. The system was flushed continuously with nitrogen in order to only measure the CO_2 produced from the neutralization reaction, Eq. (A.1). It was found that CO_2 was produced, however, it was observed that the vast majority of the produced gaseous CO_2 was captured in the outlet lube oil stream and did thereby not go into the gas phase. Three experiences were made from these experiments: (1) gas analysis was not a suitable analysis method for detection of base number conversion in a continuous setup, (2) desorption of gaseous CO_2 from the lube oil is a slow process, and (3) CO_2 *is* formed from the reaction indicating that a part of the alkalinity is certainly from metal carbonate.

A.3 Energy Dispersive X-Ray Fluorescence (ED-XRF)

To determine the metal cation of the core of the overbased detergent, Energy Dispersive X-Ray Fluorescence (ED-XRF) measurements were carried out following the standard method ASTM D7751.[6] Measurements of the 100 BN lube oil from Table A.1 yielded that no sodium (Na) was present and only a negligible amount of magnesium (Mg), around 150 mg kg^{-1}. On the contrary, calcium (Ca) was highly present, around 35000 mg kg^{-1} (3.5%). Converting the Ca amount in the lube oil to BN (mg KOH (g oil sample)$^{-1}$) gives 99.24 BN, where two times the sample standard deviation of two repetitions was 1.35 BN. Doing the same with the Mg content gives less than 1 BN. It was therefore concluded that the metal cation of the core of the reverse micelles is Ca^{2+}. The ED-XRF measurements also revealed a sulfur content of around 1% in the 100 BN lube

oil. Whether it is only $CaCO_3$ or a mixture of $CaCO_3$ and $Ca(OH)_2$ that are formulated into the lube oil was then investigated.
Moreover, the ED-XRD method was also able to measure the conversion of $CaCO_3$, at complete reaction of the limiting reactant, by considering the sulfur uptake in the lube oil samples from reaction with SO_2 and H_2SO_4.

A.4 Thermogravimetric Analysis (TGA)

The thermogravimetric analysis (TGA) method measures the weight of a sample over time as the temperature changes. This may be used to distinguish between $CaCO_3$ and $Ca(OH)_2$ with the proposed method of Kim and Olek.[7] The products of thermal decomposition of $Ca(OH)_2$ are CaO and water and for $CaCO_3$, the products are CaO and CO_2. It is reported that $Ca(OH)_2$ decomposes in the temperature range 350-550 ^oC, whereas $CaCO_3$ decomposes in the temperature range 500-700 ^oC,[7] possibly making it possible to distinguish between the two components in the lube oil. The measurements were carried out having a heating rate of 10 ^oC min^{-1} and inert (nitrogen) atmosphere over the sample. By tracking the weight loss of a Faxe Bryozo limestone powder sample (96.9 wt.% $CaCO_3$ and 1.2 wt.% $MgCO_3$[8]), it was found that the limestone sample started to decompose around 520 ^oC and the decomposition is complete around 850 ^oC.

A typical TGA curve of a 100 BN lube oil is presented in Figure A.1.

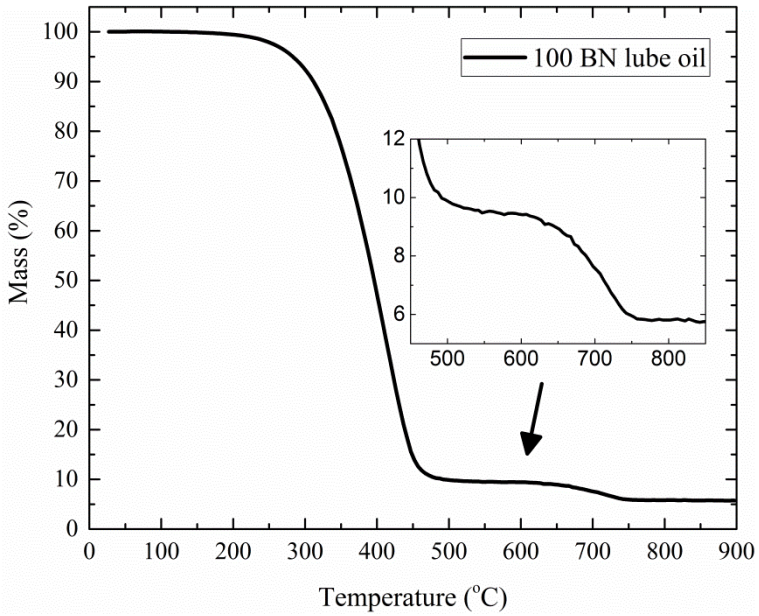

Figure A.1. TGA curve of a 100 BN lube oil sample carried out at a heating rate of 10 ^oC min^{-1} and inert (nitrogen) atmosphere over the sample.

It is shown that the lube oil already starts to lose weight at a temperature of 150 ^oC. The largest fraction of the lube oil evaporates in the temperature range 300-475 ^oC. This may be attributed to evaporation of the lube oil itself. Just after 500 ^oC, the mass of the lube oil sample stagnates shortly and then decreases again at increasing temperature, until around 800 ^oC. The mass loss in this temperature range may be ascribed to the decomposition of $CaCO_3$. Measuring the mass loss in the temperature range 520-850 ^oC (the approximate decomposition temperature range for the limestone powder sample, as described above) and assumes that

this is solely due to evaporation of CO_2 from the $CaCO_3$, the resulting BN value is calculated to 99.45, which is in agreement with the actual value (98.55 BN from titrator results, see Table A.1).

This procedure was then repeated for the different lube oil samples shown in Table A.1. The resulting base numbers, determined by the TGA procedure, are graphically illustrated in Figure A.2 as a function of the BN determined from the titrator. The analysis was repeated three times for each lube oil (except for the lube oil with around 6 BN, which was only repeated twice) and the BN determined by the TGA is thereby an averaged value with corresponding two times the sample standard deviation, presented as error bars in Figure A.2. The error is larger for the TGA method than for the titrator method. The diagonal is also shown with a scattering of ±2BN. An acceptable agreement between the two analysis methods is found. Taking this into account together with the reported decomposition ranges of $CaCO_3$ (500-700 ^oC) and $Ca(OH)_2$ (350-550 ^oC), respectively,[7] it is more than likely that the alkaline core of the overbased detergents consists solely of $CaCO_3$.

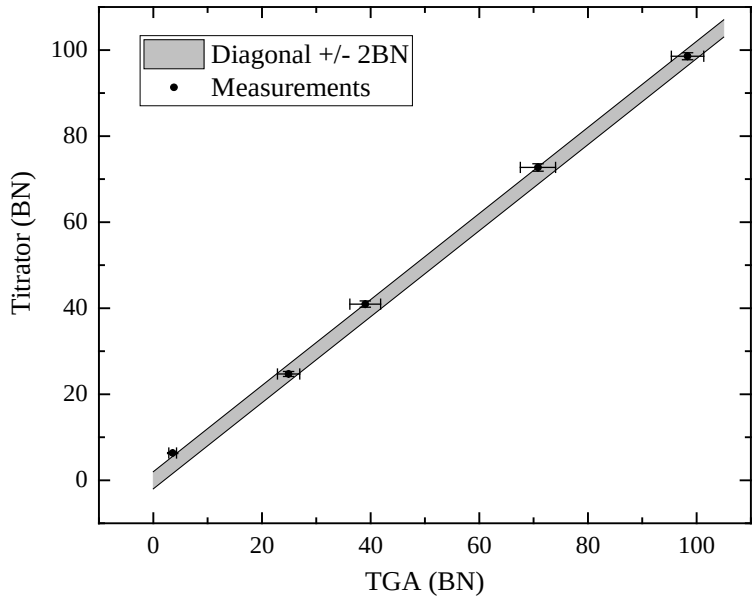

Figure A.2. The determined BN values from the titrator approach as a function of the BN determined from the TGA method. The error bars are two times the sample standard deviation. The grey area is the diagonal with a scattering of ±2BN.

A.5 Fourier Transform Infrared Spectroscopy (FTIR)

An analysis method capable of determining the conversion of $CaCO_3$ while the reaction with H_2SO_4 was in progress (at incomplete conversion of H_2SO_4) was needed for the study of the neutralization reaction (described in details in Chapters 3 and 4). The titration method was not capable of this, because the lube oil sample is first dissolved by a solvent, followed by stirring and titration with an acid, in the titration method. If unreacted H_2SO_4 was present in the lube oil prior to analysis with the titrator, it would have plenty of time and opportunity to further react with the $CaCO_3$. A possible analysis method measuring the immediate conversion degree of $CaCO_3$, regardless of the presence of H_2SO_4, was found to be Fourier Transform Infrared Spectroscopy (FTIR) with the accessory Attenuated Total Reflectance (ATR). How the FTIR-ATR could be used for this purpose is described in greater detail in Chapters 3 and 4.

The FTIR method was also able to distinguish between $Ca(OH)_2$ and $CaCO_3$, by obtaining an infrared spectrum of the pure components. The analyzed $CaCO_3$ is a Faxe Bryozo limestone (96.9 wt.% $CaCO_3$ and 1.2 wt.% $MgCO_3$[8]), whereas the $Ca(OH)_2$ powder was obtained from Sigma-Aldrich (>95 wt.% $Ca(OH)_2$ and <3 wt.% $CaCO_3$). The resulting infrared spectra are depicted in Figure A.3 together with the spectrum of the 100 BN lube oil. The spectrum of the $CaCO_3$ powder has been scaled for the sake of comparison with the intensity of the two other spectra.

The locations of the bands of the powders are in agreement with reported literature locations.[9,10] From the infrared spectra, it is observed that $Ca(OH)_2$ has a distinctive band around a wavenumber of 3640 cm^{-1}, whereas the $CaCO_3$ has several bands: at 710, 870, and 1390 cm^{-1}. The lube oil and $CaCO_3$ have three similar bands at the wavenumbers 710, 870, and 1400-1500 cm^{-1}. In addition, the lube oil spectrum has no observable band at 3640 cm^{-1}. Based on those observations, it is evident that no $Ca(OH)_2$ is present in the 100 BN lube oil (or at least a vanishingly small fraction, which is within the detection limit of the FTIR analysis method). It should also be noted that the very distinct band in the range 2750-3000 cm^{-1} for the 100 BN lube oil spectrum is a Carbon-Hydrogen (C-H) peak.

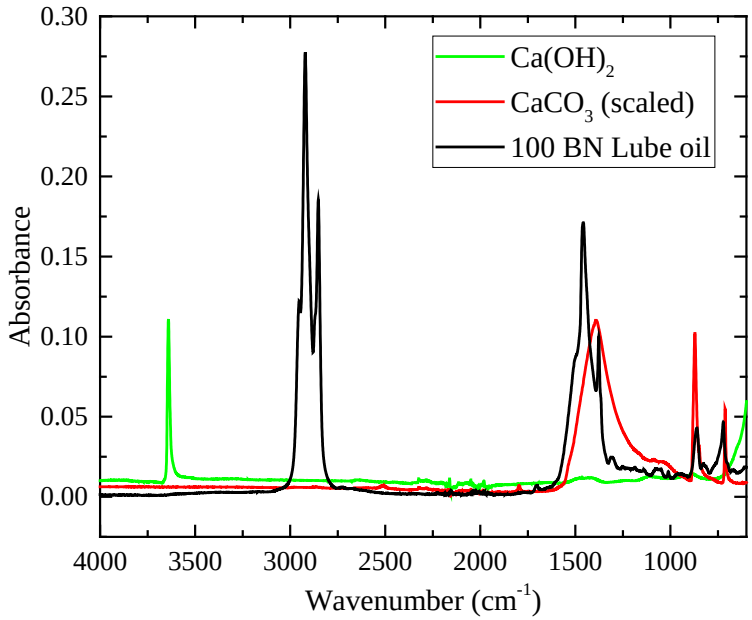

Figure A.3. The infrared spectra of $Ca(OH)_2$, $CaCO_3$, and the 100 BN lube oil.

A.6 Concluding remarks

Different analysis methods were employed to determine the composition of the alkaline additive core formulated in the 100 BN lube oil used in the work of this thesis. By use of titration, gas analysis, ED-XRF, TGA, and FTIR it was concluded that the core consists of $CaCO_3$. From the different analyses, it became obvious that FTIR is a very robust, reliable, and fast analysis method. To convert from an infrared spectrum of a lube oil sample to BN, the characteristic $CaCO_3$ band at 1400-1500 cm^{-1} may be useful. However, the band height/width has to be related to the BN by another technique, e.g. the titration approach, which is regarded as the most accurate analysis method for BN determination of lube oil samples. This is explored and described in greater detail in Chapters 3 and 4.

References

(1) ASTM International. ASTM 2896-11. Standard Test Method for Base Number of Petroleum Products by Potentiometric Perchloric Acid Titration. 2011.

(2) Hone, D. C.; Robinson, B. H.; Steytler, D. C.; Glyde, R. W.; Galsworthy, J. R. Mechanism of Acid Neutralization by Overbased Colloidal Additives in Hydrocarbon Media. *Langmuir* **2000**, *16* (2), 340–346.

(3) Atkinson, D. Onboard Condition Monitoring of Cold Corrosion in Two-Stroke Marine Diesel Engines. *11th Int. Conf. Cond. Monit. Mach. Fail. Prev. Technol. C. 2014 / MFPT 2014* **2014**, *5* (2), 17–22.

(4) Fu, J.; Lu, Y.; Campbell, C. B.; Papadopoulos, K. D. Acid Neutralization by Marine Cylinder Lubricants Inside a Heating Capillary: Strong/Weak-Stick Collision Mechanisms. *Ind. Eng. Chem. Res.* **2006**, *45* (16), 5619–5627.

(5) Mortier, R. M.; Fox, M. F.; Orszulik, S. T. *Chemistry and Technology of Lubricants*, 3rd ed.; Springer Netherlands: Dordrecht, 2010.

(6) ASTM International. ASTM 7751-16. Standard Test Method for Determination of Additive Elements in Lubricating Oils by EDXRF Analysis. 2017.

(7) Kim, T.; Olek, J. Effects of Sample Preparation and Interpretation of Thermogravimetric Curves on Calcium Hydroxide in Hydrated Pastes and Mortars. *Transp. Res. Rec. J. Transp. Res. Board* **2012**, *2290* (1), 10–18.

(8) Kiil, S. Experimental and Theoretical Investigations of Wet Flue Gas Desulphurisation. Ph.D. Dissertation, Technical University of Denmark, Kgs. Lyngby, 1998.

(9) Legodi, M. A.; de Waal, D.; Potgieter, J. H.; Potgieter, S. S. Rapid Determination of $CaCO_3$ in Mixtures Utilising FT—IR Spectroscopy. *Miner. Eng.* **2001**, *14* (9), 1107–1111.

(10) Böke, H.; Akkurt, S.; Özdemir, S.; Göktürk, E. H.; Caner Saltik, E. N. Quantification of $CaCO_3$-$CaSO_3 \cdot 0.5H_2O$–$CaSO_4 \cdot 2H_2O$ Mixtures by FTIR Analysis and Its ANN Model. *Mater. Lett.* **2004**, *58* (5), 723–726.

Appendix B | Short description of preliminary CFD simulations concerning the mixing of lube oil by a sliding piston ring

The mixing of the lube oil film between the cylinder liner surface and a piston ring was studied by use of CFD simulations. A report of the simulations was written by the authot with the title "*Mixing of Lubrication Oil at the Cylinder Liner in Marine Diesel Engines*". However, in the sake of simplicity, only a short summary of the main results from this preliminary study is provided here. The system investigated was a segment of a piston ring sliding over a cylinder liner with an initial thickness of the lube oil film of 60 µm (10 µm between piston ring tip and cylinder liner). The scope was to investigate the mixing of the lube oil accumulating in front of the moving piston ring. The system used for the simulations is shown in Figure B.1.

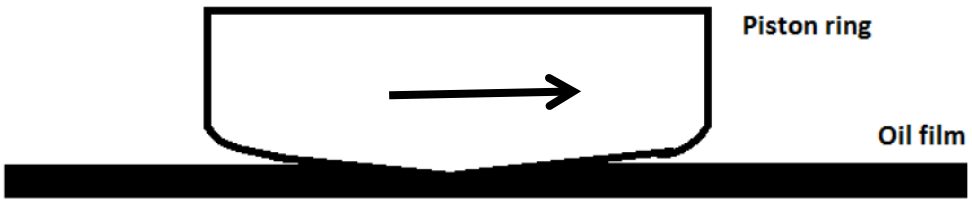

Figure B.1. A sketch of a slice of a piston ring and lube oil film. The lube oil film is located on top of the cylinder liner.

The simulations proved to be computationally expensive and a lot of different problems were encountered, mainly related to stability issues because of the very dynamic behavior of the piston ring-lube oil-cylinder liner system. However, it was possible to extract some indicative results when assuming no gravity. These results are shown in Figure B.2. As shown, the piston ring moves in the positive x-direction, scraping off the lube oil. Some lube oil is accumulated in front of the piston ring, making a curl. Due to the assumption of no gravity, nothing is forcing the curl downward, and the curl therefore increases in length with increasing time. One could argue that the implementation of gravity would have the effect of providing additional mixing between the curl and the lube oil film. The simulation snapshots given in Figure B.2 indicate that mixing will occur when the piston ring is moving, scraping off the lube oil film, thereby forming a curl, which eventually will mix with the stationary lube oil film phase. Taking into account the fast movement of the piston in practice, these simulations may translate to the lube oil curl in front of the moving piston ring being well-mixed. However, much more work needs to be done on this subject in order to increase the reliability of the simulations.

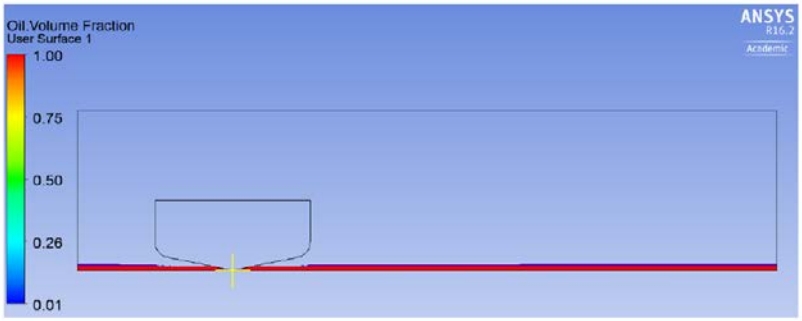

t = 0 s, L = 0 mm

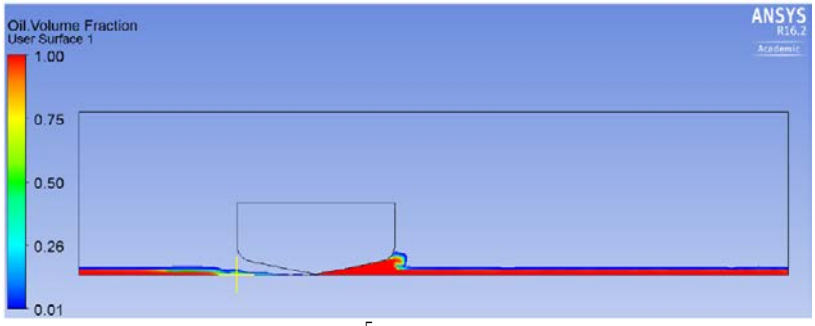

t = $40 \cdot 10^{-5}$ s, L = 1.05 mm

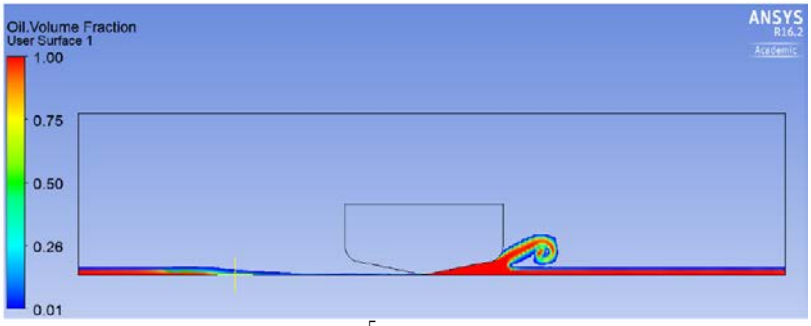

t = $100 \cdot 10^{-5}$ s, L = 2.62 mm

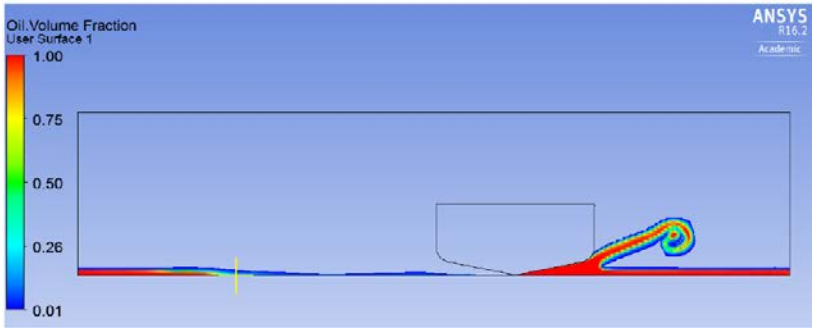

t = $160 \cdot 10^{-5}$ s, L = 4.19 mm

Figure B.2. The lube oil-piston ring simulations at different times (t) and moved piston ring lengths (L). The cross illustrates the initial position of the piston ring at t = 0 s. Main simulation parameters were: velocity of piston ring = 2.62 m s^{-1}, initial lube oil film thickness = 60 µm, distance between piston ring tip and cylinder liner = 10 µm, no gravity taking into account, temperature = 25 ^{o}C, pressure = 1 atm, density of lube oil = 870 kg m^{-3}, molar mass = 120 g mol^{-1}, dynamic viscosity = 0.05 Pa s, time step = 10^{-5} s.

Appendix C | Supporting information for Chapter 4: Mixed flow reactor experiments and modeling of sulfuric acid neutralization in lube oil for large two-stroke diesel engines

C.1 Experiments: MFR conditions

The dotted line in the experimental figures in the main text presents the theoretical conversion of $CaCO_3$ in lube oil and added H_2SO_4, when the reaction between $CaCO_3$ and H_2SO_4 droplets is complete, i.e. all added H_2SO_4 has reacted since Ca/S $\geq$ 1. For a Ca/S molar ratio of 4, 25% conversion of the $CaCO_3$ in the lube oil is expected, as the dotted curve predicts. The dotted line for complete conversion of H_2SO_4 is therefore 100%. The measured conversions of $CaCO_3$ in the MFR (denoted *Fast Analysis* in figures) at specific conditions are then compared to this curve. If the values match within the uncertainties, complete conversion of H_2SO_4 has been reached in the MFR setup. The measured conversions of $CaCO_3$ in the lube oil in the MFR are represented by the squared symbols in the figures. The circled symbols represent the measured conversion of $CaCO_3$ in the lube oil sample at complete conversion (after additional reaction time with stirring of the samples, denoted *Complete Conversion Analysis*). Ideally, the complete conversion measurements and the dotted curve should be equal to each other. When there is a difference between the complete conversion points and fast analysis point, e.g. when Ca/S approaches 1, complete conversion of H_2SO_4 droplets was not achieved in the MFR. The numbers in the figures identify each experiment according to Table C.1.

The total residence time is longer than specified since the time between sampling and obtaining an infrared spectrum was a couple of minutes. The effect of post-sampling time on the conversion is expected to be little due to the minor effect of residence time on the conversion. Also, no stirring in the lube oil sample took place after sampling, which may contribute to quenching of the neutralization reaction.

Table C.1. Experimental conditions for the lube oil-H_2SO_4 experiments in the MFR, varying $CaCO_3/H_2SO_4$ molar ratio (Ca/S), residence time (τ), stirrer speed (N), and H_2SO_4 concentration ($C_{H_2SO_4}$) in inlet stream. Experimental uncertainty for the determination of the Ca/S molar ratio is given as two times sample standard deviation for experiments 1-3 and 5.

Exp. #	Ca/S (mol mol^{-1})	No. of exp.	τ (min)	N (rpm)	$C_{H_2SO_4}$ (wt.%)
1	9.19 ± 0.17	2	2.9	1200	96.5
2	3.84 ± 0.07	2	2.8	1200	96.5
3	2.10 ± 0.06	2	2.8	1200	96.5
4	1.26	1	3.5	1200	96.5
5	1.12 ± 0.04	5	2.2	1200	96.5
6	1.05	1	2.1	1200	96.5
7	1.94	1	2.5	600	96.5
8	1.94	1	2.5	360	96.5
9	1.94	1	2.5	120	96.5
10	1.05	1	2.2	600	96.5
11	1.05	1	2.2	360	96.5

C.2 Residence time

Minor effect of the investigated residence times (0.8-3.5 min) on the conversions was found.[1] It was attributed to the reaction being very fast at well-mixed conditions until an unspecified point where the reaction is significantly reduced (or more or less stops). This behavior was also observed by others as described in Chapter 4.[2,3]

C.3 Inlet sulfuric acid concentration

Decreasing the inlet H_2SO_4 concentration by a factor of 2.5, decreased the $CaCO_3$ conversion around 10%.[1] This may be attributed to the introduction of large amount of water which alters the conditions in the MFR. For instance, when introducing dilute H_2SO_4 in the inlet, more droplets are needed in order to maintain a certain Ca/S molar ratio. When more water is present in the inlet and the amount of surfactants in the lube oil is limited, the dilute H_2SO_4 droplets may not be solubilized fully or fast enough. Thereby, some droplets may exist in bulk and are thereby enlarged, contributing to an increased neutralization time. In addition, fewer $CaCO_3$ reverse micelles encircle each H_2SO_4 droplet, also decreasing the adsorption rate. The trend of decreased reaction rate at decreased acid concentration is in accordance with the video-microscopy experiments performed by Duan et al.[4] with acetic acid droplets in a fully formulated passenger-car lube oil. A decrease in the acetic acid concentration led to a decrease in shrinking rate of the acetic acid droplet;[4] however, when decreasing the acid concentration, the Ca/S molar ratio increases and the isolated effect is thereby difficult to extract from the video-microscopy experiments.

C.4 Mathematical modeling: Ratio between outlet and inlet flow rates at varying H_2SO_4 droplet concentration

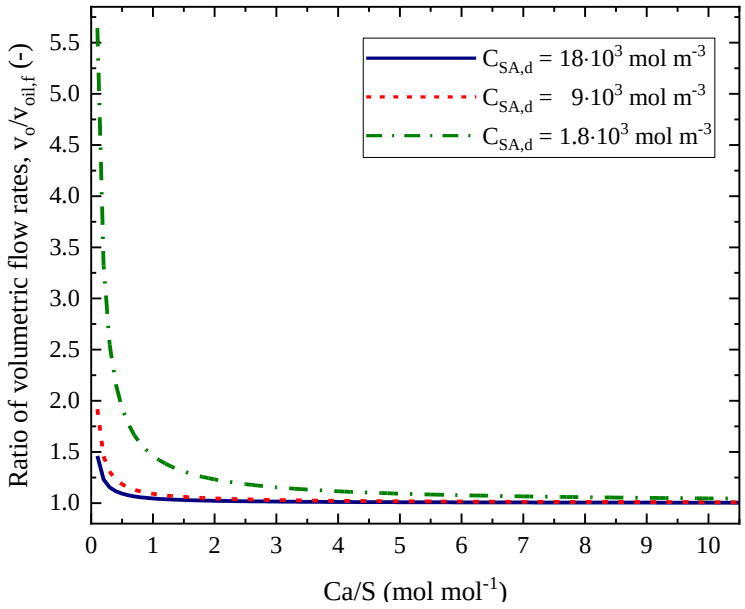

Figure C.1. Model simulations showing ratio of outlet volumetric flow rate to inlet volumetric flow rate of lube oil for three different H_2SO_4 droplet concentrations. Model parameters are: R_{SA} = 0.5 µm, T = 423 K, τ = 0.5 s, $f_{L,oil,w}$ = 0.089 kg kg^{-1} (100 BN), as well as those in Table 4.1 in Chapter 4.

C.5 Mathematical modeling: Residence time variation for MFR conditions

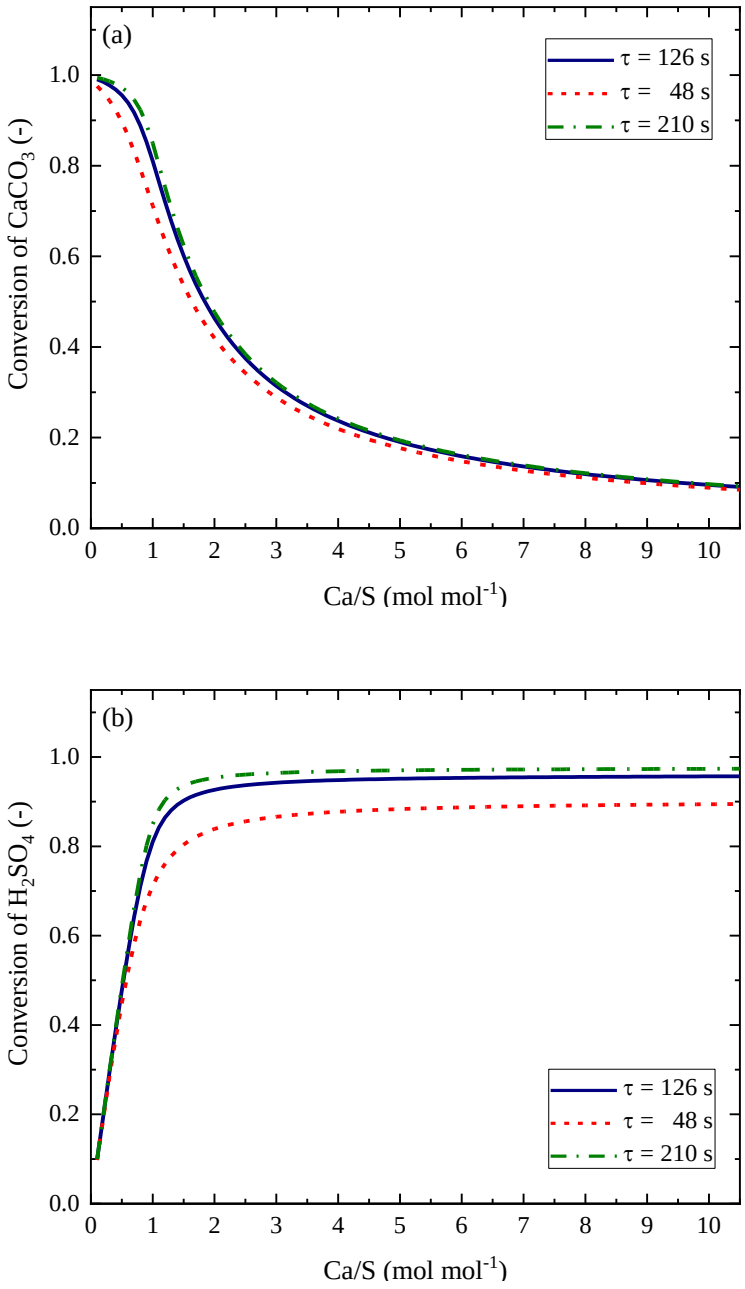

Figure C.2. Model simulations showing conversion of (a) $CaCO_3$ reverse micelles and (b) H_2SO_4 droplets as a function of Ca/S at three values of residence time. Model parameters are: R_{SA} = 0.5 μm as well as those in Table 4.1 in Chapter 4 (MFR conditions).

References

(1) Lejre, K. H.; Kiil, S.; Glarborg, P.; Christensen, H.; Mayer, S. Reaction of Sulfuric Acid in Lube Oil: Implications for Large Two-Stroke Diesel Engines. In *Proceedings of the ASME 2017 Internal Combustion Engine Division Fall Technical Conference*; ASME: Seattle, United States, 2017; Vol. 1, pp 1–10.

(2) Hone, D. C.; Robinson, B. H.; Steytler, D. C.; Glyde, R. W.; Galsworthy, J. R. Mechanism of Acid Neutralization by Overbased Colloidal Additives in Hydrocarbon Media. *Langmuir* **2000**, *16* (2), 340–346.

(3) Roman, J.-P. New Method of Measurement in Thin Film of the Neutralization of Marine Lubricants for Low-Speed and Medium-Speed Diesel Engines. In *CIMAC Congress 1998, Copenhagen*; Copenhagen, 1998; pp 913–926.

(4) Duan, Y.; Rausa, R.; Fiaschi, P.; Papadopoulos, K. D. Neutralization of Acetic Acid by Automobile Motor Oil. *Tribol. Int.* **2016**, *98*, 94–99.

Appendix D | Supporting information for Chapter 4: Modeling of the experimental data from the work by Fu et al.

The scope of this appendix is to model the experimental shrinkage data of Fu et al.,[1] concerning reaction of a H_2SO_4 droplet in lube oil by use of a diffusion-controlled reaction rate expression. The objective is to assess whether the reaction between an H_2SO_4 droplet and $CaCO_3$ reverse micelles is limited by diffusion.

As presented in Section 4.4.1, the work of Fu et al.[1] was used to calculate kinetic parameters (activation energy and pre-exponential factor) resulting in an adsorption-controlled reaction rate constant (Eq. (4.13)), since Fu et al.[1] concluded that the reaction between an H_2SO_4 droplet and $CaCO_3$ reverse micelles was adsorption-controlled. However, it was found that the model (containing the diffusion-controlled reaction rate expression) matches the experimental MFR data when R_{SA} = 0.7 µm (Section 4.5). This radius of the H_2SO_4 droplets is within the expected range,[2] as also discussed in Section 4.5 (a radius of 0.5 µm was calculated when using the kinetic parameters from Fu et al., see e.g. Figure 4.8). Therefore, to investigate whether the reaction is diffusion- or adsorption-controlled, the diffusion of $CaCO_3$ reverse micelles from bulk lube oil to the H_2SO_4 droplet is compared to the actual conversion rate of the H_2SO_4 droplet – for the experimental data given by Fu et al.[1]

First, the molar conversion of H_2SO_4 in the droplet is related to the change in radius ($-dR_{SA}/dt$), according to:

$$-\frac{dn_{SA}}{dt} = -\frac{d\left(V_{SA}C_{SA,d}\right)}{dt} = 4\pi R_{SA}(t)^2 C_{SA,d}\left(-\frac{dR_{SA}}{dt}\right) \tag{D.1}$$

Here, V_{SA} is the volume of the H_2SO_4 droplet (m^3), $C_{SA,d}$ is the concentration of the H_2SO_4 in the droplet (mol m^{-3}), and R_{SA} is the radius of the H_2SO_4 droplet (m).

The flux of $CaCO_3$ reverse micelles to the droplet is evaluated from Fick's first law of diffusion,[3] assuming that when $R = R_{SA}$, $C_L = 0$. Also, it is assumed that the H_2SO_4 droplet is immobile and much larger in size compared to the $CaCO_3$ reverse micelles, thus $D_{AB} = D_L$ and $R_{AB} = R_{SA}$. The flux is then given as:

$$\vec{J} = 4\pi R_{SA}(t) D_L(T) C_L \tag{D.2}$$

C_L is the bulk concentration of $CaCO_3$ in the lube oil (mol m^{-3}) and is assumed to be constant throughout the reaction, because $CaCO_3$ is in great molar excess compared to H_2SO_4 in the reaction system.[1] D_L is the diffusion coefficient of the reverse micelles (m^2 s^{-1}), which is given as:

$$D_L = \frac{k_B T}{6\pi\eta(T) R_L} \tag{D.3}$$

It is expected that $\vec{J} \geq -\frac{dn_{SA}}{dt}$, because reaction of the H_2SO_4 droplet only can progress if $CaCO_3$ is present in sufficient concentrations. If equal, this may indicate that the reaction is limited by diffusion. If the diffusive flux is much larger, it may indicate that the reaction is not controlled by diffusion. To investigate this further, the flux is put equal to $(-dn_{SA}/dt)$ and a factor, *F*, is introduced:

$$\vec{J}F = -\frac{dn_{SA}}{dt} \tag{D.4}$$

This factor describes the ratio between the molar conversion of H_2SO_4 and the flux of $CaCO_3$ reverse micelles to the droplet. If *F* is smaller than 1, the diffusive flux is larger than the molar consumption rate, and vice versa for a value of *F* larger than 1.

It is desirable to fit the parameter F by use of the experimental data given by Fu et al.,[1] thus the expression given in Eq. (D.4) is solved for dR_{SA}/dt:

$$\frac{dR_{SA}}{dt} = -F\frac{D_L(T)C_L}{R_{SA}(t)C_{SA,d}} \tag{D.5}$$

With the initial condition: $R_{SA} = R_{SA,0}$ at t = 0, where $R_{SA,0}$ is the initial radius of the non-reacted droplet (from the experiments performed by Fu et al.:[1] 71.4 µm at 25 °C, 76.45 µm at 100 °C, 58.3 µm at 130 °C, and 43.55 µm at 170 °C). The remaining parameters are given as (from Fu et al.[1]):

$$C_{SA,d} = 9400\,\frac{mol}{m^3}\ (= 50\ \text{vol.\%}\ H_2SO_4\ \text{in droplet})$$
$$C_L = 586.5\,\frac{mol}{m^3}\ (= 70\ \text{BN lube oil, assumed constant})$$
$$R_L = 5 \cdot 10^{-9} m$$

The temperature-dependent viscosity is calculated from the work of Sautermeister and Priest,[4] who measured dynamic viscosities for a base oil at different temperatures. An exponential fit of η versus T was used to describe the temperature variation of the viscosity, giving the viscosities presented in Table D.1.

Table D.1. Calculated viscosities at temperatures in the range 25-170 °C based on work of Sautermeister and Priest.[4]

Temperature, T [°C]	25	100	130	170
Viscosity, η [kg/(m s)]	0.195	0.014	0.0066	0.0028

The radius-time behavior is illustrated in Figure D.1 from solving Eq. (D.5) for F = 1, where the points are the experimental data from Fu et al.[1] and the curves are the modeling results.

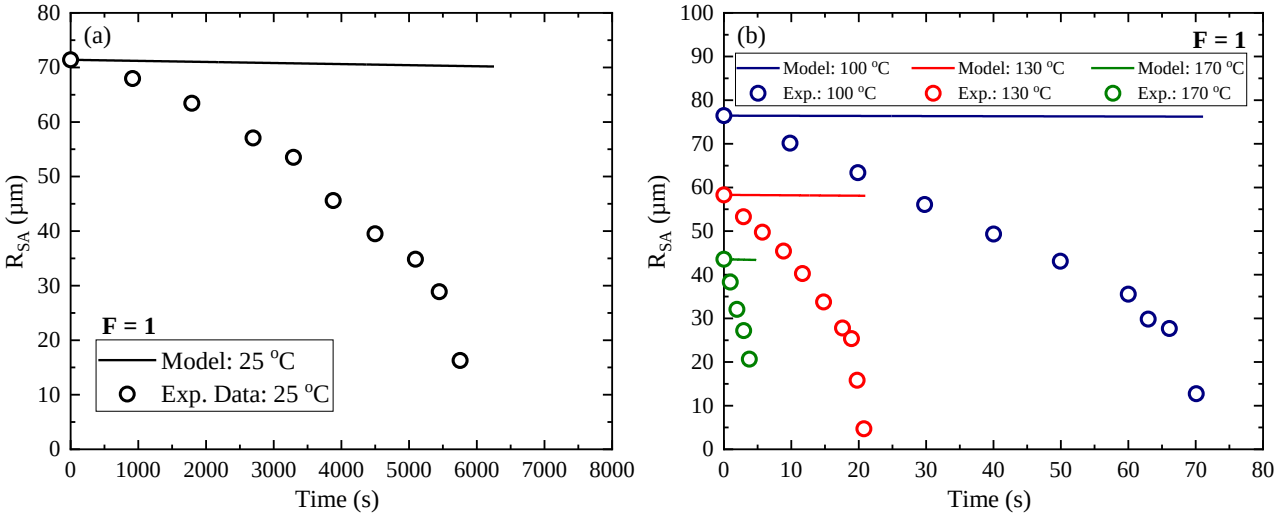

Figure D.1. Radius versus time: experimental data (points) and simulations (lines) at 25 °C (left figure) and 100, 130 and 170 °C (right figure) for F = 1.

As shown in Figure D.1, the model does not fit the experimental data; the predicted conversion is much lower than the observed value for F = 1. This means that the diffusion is much slower than the actual molar conversion rate of the H_2SO_4 droplet. How much slower is investigated next by fitting the model to the experimental data by fitting of the parameter F, see Figure D.2.

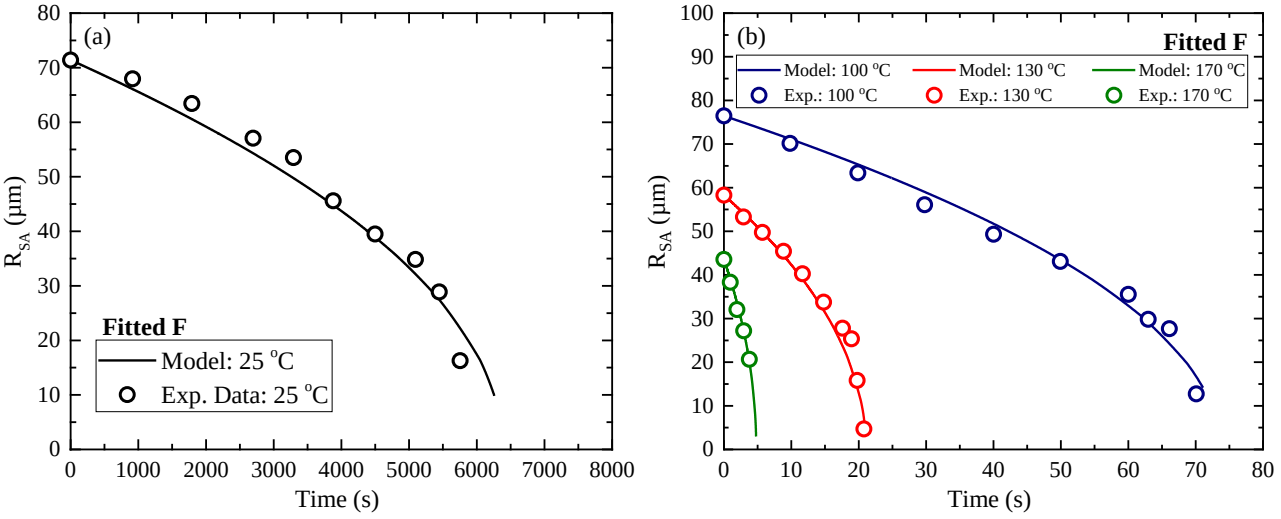

Figure D.2. Radius versus time: experimental data (points) and simulations (lines) at 25 °C (left figure) and 100, 130 and 170 °C (right figure) for fitted F (see Table D.2).

As shown in Figure D.2, the model simulations describe the data sufficiently when having the fitted values of F at each temperature. These values are shown in Table D.2.

Table D.2. The fitted parameter F at each temperature.

Temperature, T [°C]	25	100	130	170
***F* [-]**	28.4	165	143	134

This means that the diffusion is up to 165 times 'too slow' in order to describe the molar conversion of the H_2SO_4 droplet. This is counterintuitive, because the molar conversion rate of H_2SO_4 cannot be larger than the molar diffusive flow of $CaCO_3$ reverse micelles to the H_2SO_4 droplet, unless the H_2SO_4 droplet is consumed by another mechanism than the direct reaction between the droplet and reverse micelle.

A small analysis is carried out below to verify that the factor cannot be attributed to uncertainties in the parameter estimation.

Radius of the reverse micelles

The radius of the reverse micelles was chosen as 5 nm, however, radii between 1.5 and 10 nm are reported in literature.[5–10] When the radius of the reverse micelles gets lower, the diffusion increases, but only a factor of around 3 can be found here (1.5 nm versus the 5 nm used for the calculations given here).

Concentration of limestone in the lube oil

The parameter C_L is used to describe the concentration of limestone in the lube oil. It is assumed that this value is constant. It is assumed that this assumption is valid, since the lube oil is in great excess compared to the H_2SO_4 droplet.[1] If a lower C_L is used, this would decrease the diffusion of reverse micelles to the droplet (and thus the concentration gradient).

Viscosity of the lube oil

The viscosity of the lube oil was taken from Sautermeister and Priest;[4] it is based on a base oil. A temperature-dependent viscosity of an SAE50 cylinder lube oil was acquired from MAN Energy Solutions. Using this viscosity expression leads to the same conclusion, namely that the diffusion is much slower than the actual molar conversion rate of the H_2SO_4 droplet. The change in the fitted F-values, by using the changed viscosity expression, is within a factor of less than three at all temperatures.

Concentration of the H_2SO_4 droplet

The concentration of the H_2SO_4 droplet, $C_{SA,d}$ is equal to 9400 kg m^{-3}, which corresponds to a 50 vol.% H_2SO_4 solution – as used in the experiments from Fu et al. It is assumed that this value does not change during the experiments.

Temperature

It was assumed that the temperature is constant throughout the experiment. However, due to the heat of reaction ($\Delta H^\circ = -92.9$ kJ mol^{-1})[11] it may be that the temperature is increased locally around the droplet. If setting F = 1, and fitting the temperature in order to match the model to the experimental data, the temperatures in Table D.3 are found.

Table D.3. Fitted temperatures when setting F = 1.

Reported temperature, T [°C]	25	100	130	170
Fitted temperature, T [°C] (for F=1)	118	390	464	580

As shown, an extreme increase in temperature is required in the modeling in order to describe the experimental data for F = 1.

References

(1) Fu, J.; Lu, Y.; Campbell, C. B.; Papadopoulos, K. D. Temperature and Acid Droplet Size Effects in Acid Neutralization of Marine Cylinder Lubricants. *Tribol. Lett.* **2006**, *22* (3), 221–225.

(2) Goodwin, J. W. *Colloids and Interfaces with Surfactants and Polymers*; John Wiley & Sons, Ltd: Chichester, UK, 2009.

(3) Laidler, K. J. *Chemical Kinetics*; Harper & Row: New York, 1987.

(4) Sautermeister, F. A.; Priest, M. Physical and Chemical Impact of Sulphuric Acid on Cylinder Lubrication for Large 2-Stroke Marine Diesel Engines. *Tribol. Lett.* **2012**, *47* (2), 261–271.

(5) Wu, R. C.; Papadopoulos, K. D.; Campbell, C. B. Visualization Test for Neutralization of Acids by Marine Cylinder Lubricants. *AIChE J.* **1999**, *45* (9), 2011–2017.

(6) Hudson, L. K.; Eastoe, J.; Dowding, P. J. Nanotechnology in Action: Overbased Nanodetergents as Lubricant Oil Additives. *Adv. Colloid Interface Sci.* **2006**, *123-126* (SPEC. ISS.), 425–431.

(7) Roman, J.-P.; Hoornaert, P.; Faure, D.; Biver, C.; Jacquet, F.; Martin, J.-M. Formation and Structure of Carbonate Particles in Reverse Microemulsions. *J. Colloid Interface Sci.* **1991**, *144* (2), 324–339.

(8) Marković, I.; Ottewill, R. H.; Cebula, D. J.; Field, I.; Marsh, J. F. Small Angle Neutron Scattering Studies on Non-Aqueous Dispersions of Calcium Carbonate - Part I. The Guinier Approach. *Colloid Polym. Sci.* **1984**, *262* (8), 648–656.

(9) Marković, I.; Ottewill, R. H. Small Angle Neutron Scattering Studies on Nonaqueous Dispersions of Calcium Carbonate Part 2. Determination of the Form Factor for Concentric Spheres. *Colloid Polym. Sci.* **1986**, *264* (1), 65–76.

(10) Marković, I.; Ottewill, R. H. Small Angle Neutron Scattering Studies on Non-Aqueous Dispersions of Calcium Carbonate. Part III. Concentrated Dispersions. *Colloid Polym. Sci.* **1986**, *264* (5), 454–462.

(11) John R. Rumble. CRC Handbook of Chemistry and Physics http://hbcponline.com (accessed Mar 5, 2019).

Appendix E | Supporting information for Chapter 5: Experimental investigation and mathematical modeling of the reaction between SO_2(g) and $CaCO_3$(s)-containing micelles in lube oil for large two-stroke marine diesel engines

Nomenclature

a = Specific gas-liquid interfacial area [m^2 m^{-3}]
BN = Base number [(mg KOH) (g oil)$^{-1}$]
C = Temperature dependency constant [K]
Ca/S = Initial molar ratio of $CaCO_3$ in lube oil to SO_2 in gas phase [mol mol^{-1}]
C_i^j = Concentration of component i in component j [mol m^{-3}]
D_i = Diffusion coefficient of SO_2 in component i [m^2 s^{-1}]
E = Liquid enhancement factor [-]
H_i = Henry's constant of SO_2 in component i [bar m^3 mol^{-1}]
i = Component i [-]
j = Component j [-]
k_i = Reaction rate constant for reaction i [m^3 mol^{-1} s^{-1}]
k_B = Boltzmann constant, $1.38 \cdot 10^{-23}$ [kg m^2 s^{-2} K^{-1}]
k_G = Gas film mass transfer coefficient [mol m^{-2} s^{-1} bar^{-1}]
K_G = Overall gas-side mass transfer coefficient of SO_2 [mol m^{-2} bar^{-1} s^{-1}]
k_L = Liquid film mass transfer coefficient [m s^{-1}]
M_i = Molecular weight of component i [g mol^{-1}]
P = Pressure in batch reactor [bar]
R = Ideal gas constant, 8.314 [J mol^{-1} K^{-1}]
R_A = Radius of the solute [m]
t = Time [s]
T = Temperature [^{o}C or K]
V_i = Volume of component i [m^3]

Greek Letters
δ_i = Film thickness of component i [m]

η = Viscosity [kg m^{-1} s^{-1}]
Σ_v = Summation of atomic diffusion volumes [-]
τ = Residence time [s]

Superscripts and subscripts
G = Gas phase
L = Lube oil emulsion (lube oil + water)
oil = Lube oil

E.1 Spectra of possible products from the reaction between SO_2 and $CaCO_3$

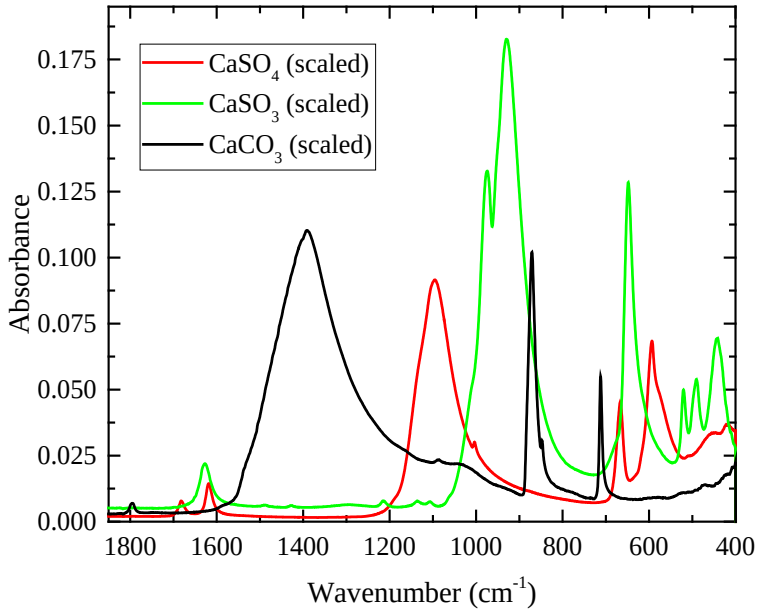

Figure E.1. Infrared spectra of pure $CaCO_3$ (black), $CaSO_3$ (green), and $CaSO_4$ (red).

E.2 Blank experiment

Both a room temperature and a 150 ^oC blank experiment were carried out by pressurizing the batch reactor to 90 bar of air for 60 minutes followed by flushing with N_2. The resulting infrared spectra are shown in Figure E.2 together with an infrared spectrum of a fresh 100 BN lube oil. A little effect is observed in Figure E.2 for the room temperature blank experiment for the $CaCO_3$ band, where water contributes to a shift in baseline, especially in the range 400-1000 cm^{-1} and 1600-1700 cm^{-1}. A negligible difference between unused lube oil and the 150 ^oC blank experiment is also found, meaning that only the majority of the added demineralized water in the lube oil sample had evaporated during the flushing/cooling stage of the experiment. Furthermore, this also proved that the experimental procedure does not affect the $CaCO_3$ band and more importantly that the observed change in $CaCO_3$ band, when SO_2 is present in the gas phase, is then due to reaction with SO_2 only.

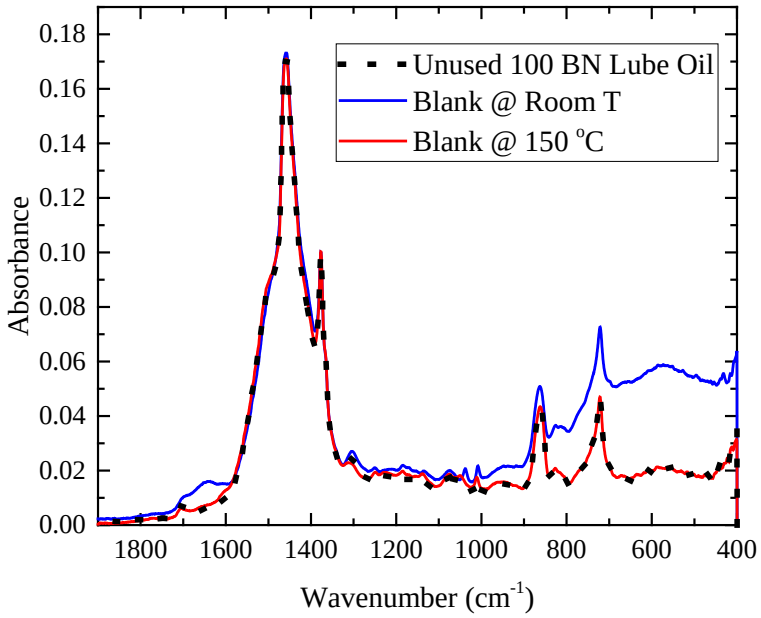

Figure E.2. Blank experiments at room temperature (blue) and 150 °C (red) together with a spectrum of a fresh 100 BN lube oil (black dots).

E.3 Spectrum of drain oil

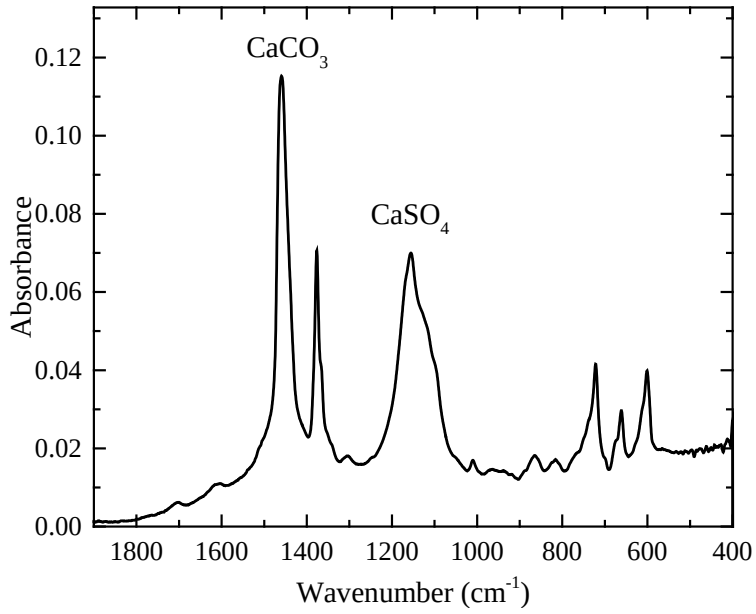

Figure E.3. Infrared spectrum of a drain oil from service, showing a $CaCO_3$ and a $CaSO_4$ band.

E.4 Effect of temperature

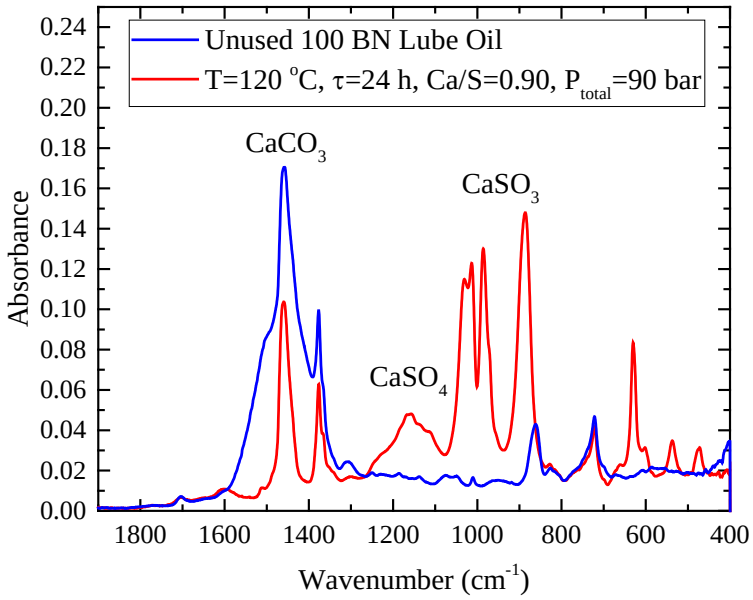

Figure E.4. Infrared spectrum of an unused 100 BN lube oil (blue) and a spectrum of a lube oil exposed for SO_2 (red) at the following conditions: P_{total}=90 bar, 6.8 wt.% initial water in lube oil, Ca/S=0.90, τ=24 hours, and T=120 °C. The locations of $CaCO_3$, $CaSO_3$, and $CaSO_4$ are also indicated in the figure.

E.5 Effect of residence time

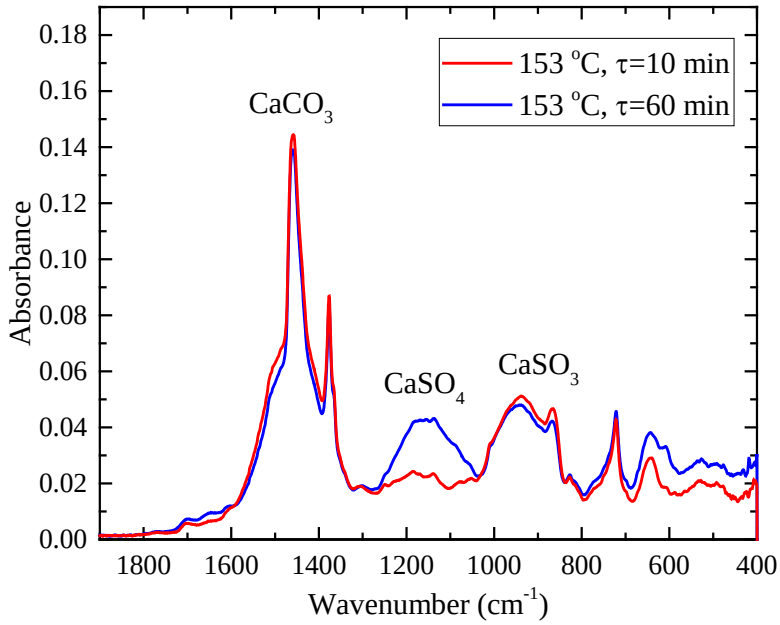

Figure E.5. Spectra of lube oil samples with two different residence times. Experimental conditions: T=153 °C, P_{total}=90 bar, 6.6 wt.% initial water in lube oil, and Ca/S around 1.

E.6 Stability of $CaSO_3$

A lube oil sample containing 6.4 wt.% of water was pressurized with 1 mol% SO_2 in air environment (initial Ca/S around 1.2) at room temperature. After one hour of reaction time, the obtained infrared spectrum revealed that almost all $CaCO_3$ had been converted to $CaSO_3$ (not all $CaCO_3$ was converted because Ca/S > 1); see Figure E.6. An infrared spectrum of the lube oil sample obtained the day after showed that no further reaction/oxidation had occurred. This means that the formed $CaSO_3$ is stable over time at room temperature and atmospheric pressure and surroundings (air). The sample was then heated in an oven for 2 hours at 150 ^oC. Figure E.6 shows that no $CaSO_4$ was formed; however, the $CaSO_3$ top has a different shape. The reason for this and the possibly formed product is unknown at the moment. Upon heating, most of the water evaporated. The difference in spectra before and after heating in the oven at around 1600-1700 cm^{-1} and 400-800 cm^{-1} is due to the removal of water (Figure E.6). This means that heating of the sample in an oven cannot oxidize the formed $CaSO_3$. The effect of increased air pressure and elevated temperature was then investigated, depicted in Figure E.7. No effect of pressurizing the lube oil sample at 90 bar for 2 hours at room temperature was found. A shift in baseline is found between the two spectra, which is due to an increased amount of water that was added between the two measurements prior to the experiment. Then, the sample was added to the reactor once again, pressurized with 80 bar of air (at 150 ^oC), and then heated to approximately 150 ^oC. After 1 hour at 150 ^oC, the reactor was cooled and a spectrum was recorded yet again. Figure E.7 reveals that the $CaSO_4$ band around 1060-1260 cm^{-1} had increased in intensity, indicating that some of the $CaSO_3$ had oxidized to $CaSO_4$, however, less water was present in the sample resulting in a shift in baseline, which hampers the conclusion. No matter what, the oxidation is minor taking into account the reaction time available.

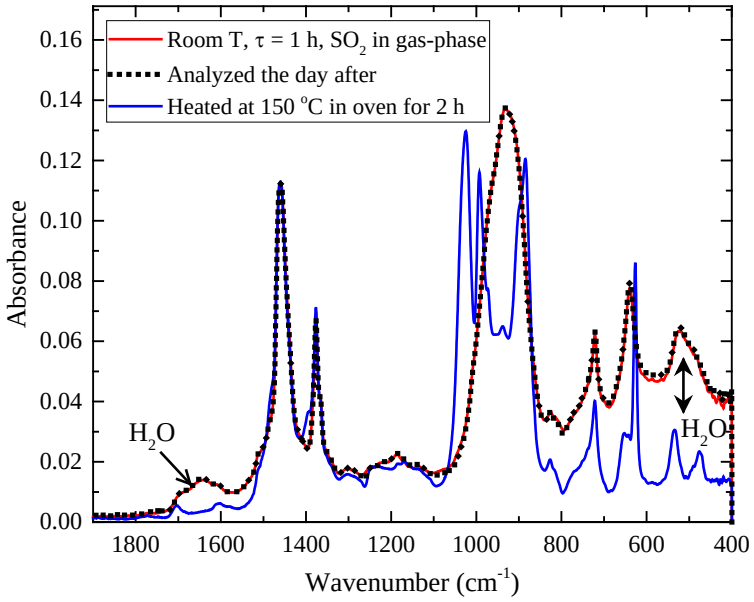

Figure E.6. Spectra of lube oil samples investigating the stability of $CaSO_3$: Room temperature lube oil sample with a residence time of 1 h and SO_2 in the gas phase (red), the spectrum of the lube oil sample analyzed the day after (black dotted), and a spectrum of the lube oil after heating at 150 ^oC in an oven for 2 h (blue).

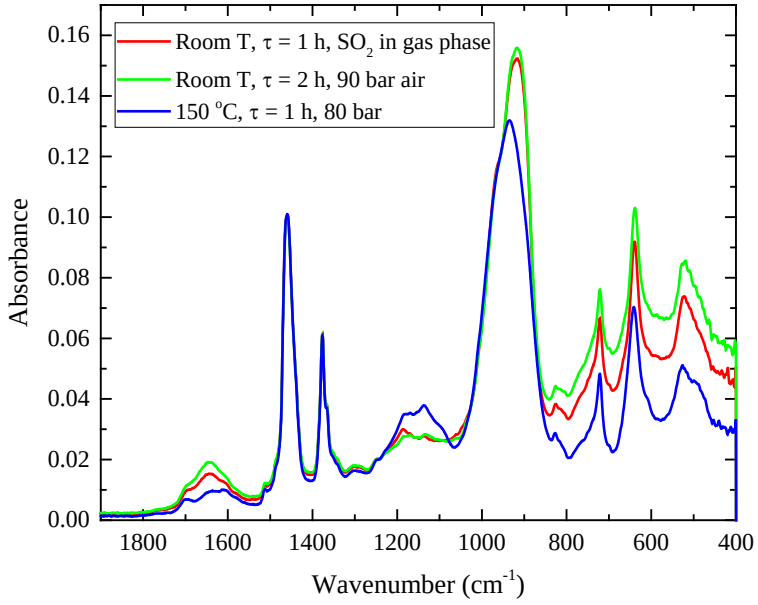

Figure E.7. Spectra of lube oil samples investigating the stability of $CaSO_3$: Room temperature lube oil sample with a residence time of 1 h and excess of SO_2 in the gas phase (Ca/S < 1) (red), followed by exposing the lube oil sample to 90 bar of air for 2 h at room temperature (green), and then exposing the lube oil sample to heating at 150 °C for 1 h at 80 bar (@150 °C) in air in the batch reactor (blue).

E.7 Neutralization ability of $CaSO_3$

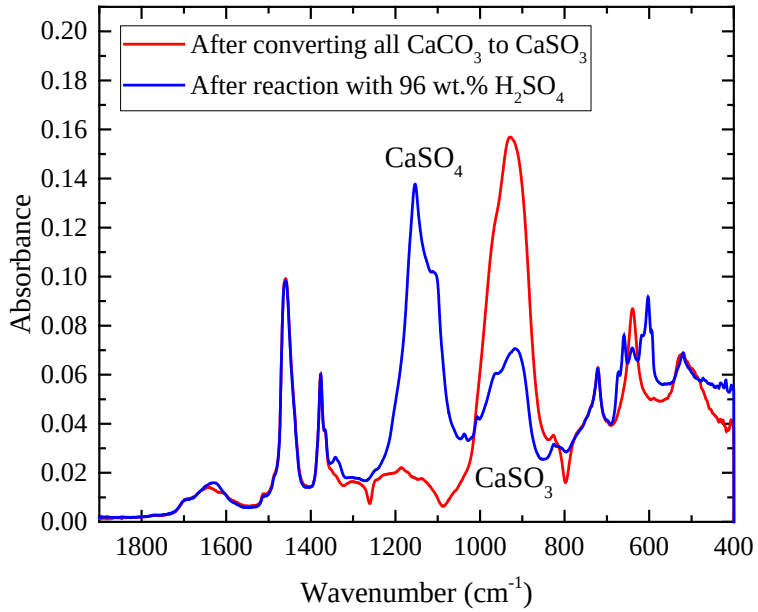

Figure E.8. Room temperature spectrum of a lube oil sample where all $CaCO_3$ has been converted to $CaSO_3$, before (red) and after (blue) adding a specific amount of H_2SO_4.

E.8 Experimental conditions for experiments at varying temperature

Table E.1. Experimental conditions for the experiments carried out at varying temperature. The conditions for the 131 °C experiment are average values based on two similar experiments.

Parameter	**#1**	**#2**	**#3**	**#4**	**#5**
Temperature (°C)	27	107	131	153	163
P_{total} **(bar)**	90	105	90	90	100
$C^G_{SO_2,0}$ **(mol m^{-3})**	16.83	16.77	17.26	16.93	17.65
$\left(\frac{V_{oil}}{V_L}\right)$ **(m^3 m^{-3})**	0.9388	0.9387	0.9373	0.9384	0.9377
$\left(\frac{V_{water}}{V_L}\right)$ **(m^3 m^{-3})**	0.0612	0.0613	0.0627	0.0616	0.0623
V_G **(m^3)**	$4.8\cdot10^{-4}$	$4.8\cdot10^{-4}$	$4.8\cdot10^{-4}$	$4.8\cdot10^{-4}$	$4.8\cdot10^{-4}$
τ **(min)**	10	10	10	10	10
Ca/S (mol mol^{-1})	0.98	0.98	0.96	0.97	0.93

E.9 Determination of Henry's constant for the lube oil emulsion

Henry's constant for SO_2 in water was estimated from NIST.[1] The temperature dependence was estimated from the van't Hoff equation:

$$H(T) = H^{\circ}\exp\left[C\left(\frac{1}{T} - \frac{1}{T^{\circ}}\right)\right] \quad \text{(E.1)}$$

Here, H° is Henry's constant at T° (1.4 mol kg^{-1} bar^{-1} at 25 °C) and C is a temperature dependency constant equal to 2900 K.[1]

Costa and Underhill[2] present the solubility of SO_2 in different lube oils obtained at 25 °C in terms of the Ostwald solubility coefficient (ml of dissolved gas at the partial pressure and temperature of the experiment dissolved in 1 ml of solvent). Observing that a specific mineral oil did not react with SO_2 ("Squibb Medical Mineral Oil"), the average Ostwald solubility coefficient was measured to 4.97 ml ml^{-1}. This is converted to a Henry's constant by use of the ideal gas law and stated density of the oil (885 kg m^{-3}), giving 0.227 mol kg^{-1} bar^{-1}. Also, the Henry's constant for SO_2 in a commercial lubricant (20W-40) was estimated by Nagaki and Korematsu[3] to 1.46±0.35 MPa $\text{mol}_{\text{oil}}\ \text{mol}^{-1}_{SO_2}$ (one standard deviation) at 19 °C. To convert it to mol kg^{-1} bar^{-1}, the molecular weight of the lube oil is needed. Because most of the lube oil may consist of mineral oil, the given molecular weight from Costa and Underhill for Squibb Medical Mineral Oil is used (250 g mol^{-1}). This gives a Henry's constant in the range 0.221-0.360 mol kg^{-1} bar^{-1}, which is in accordance to the value determined by Costa and Underhill.[2] To extrapolate Henry's constant to elevated temperatures, the enthalpy of solution is required. However, this value is unknown for oil, to the knowledge of the authors. Therefore, the temperature dependency constant, C, for water is used to extrapolate Henry's constant. Doing this gives an estimated Henry's constant for SO_2 in lube oil at 131 °C equal to 0.0177 mol kg^{-1} bar^{-1} if using Henry's constant determined by Costa and Underhill.

The Henry's constants given above have the unit of mol kg^{-1} bar^{-1}, however, the unit of Henry's constant in the modeling is bar m^3 mol^{-1}. In order to convert between these, the inverse of the Henry's constant is divided by the density of the water and lube oil, respectively. The density of lube oil is measured at room temperature to 940 kg m^{-3},[4] however, at elevated temperature the density decreases. The densities at higher temperatures are based on estimates.[5,6] At 131 °C, the density of lube oil and water are estimated to be 871 kg m^{-3} and 934 kg m^{-3}, respectively. The resulting Henry's constants with unit bar m^3 mol^{-1} are presented in Table E.2.

Table E.2. Henry's constants for water and lube oil at two temperatures (25 °C and 131 °C). Unit: bar m^3 mol^{-1}.

	25 °C	**131 °C**
Water	$7.14 \cdot 10^{-4}$	$9.80 \cdot 10^{-3}$
Lube oil	$4.69 \cdot 10^{-3}$	$6.50 \cdot 10^{-2}$

E.10 Evaluation of resistance of SO_2 from the gas phase to the liquid phase

The overall resistance to the transfer of SO_2 from the gas phase to the liquid phase is equal to the sum of the resistances within the individual phases, given as:[7]

$$\frac{1}{K_G} = \frac{1}{k_G} + \frac{H_L}{k_L} \tag{E.2}$$

Where the film gas mass transfer coefficient, k_G, is given as:[7]

$$k_G = \frac{D_G}{\delta_G RT} \tag{E.3}$$

And the film liquid mass transfer coefficient, k_L, is given as:[7]

$$k_L = \frac{D_L}{\delta_L} \tag{E.4}$$

D_G and D_L are the diffusion coefficients of SO_2 in the gas phase and liquid phase, respectively, and δ_G and δ_L are the thicknesses of the gas film and liquid film, respectively. D_G is calculated by:[8]

$$D_G = \frac{1.43 \cdot 10^{-7} T^{1.75}}{P M_{AB}^{1/2} \left[(\sum v)_A^{1/3} + (\sum v)_B^{1/3} \right]^2} \tag{E.5}$$

Here, T is the temperature in K, P is the pressure in bar, M_A is the molecular weight of SO_2 (64.1 g mol^{-1}), M_B is the molecular weight of air (29.0 g mol^{-1}), $M_{AB} = 2[(1/M_A) + (1/M_B)]^{-1}$ (equal to 39.9 g mol^{-1}), and $\sum v$ is summation of atomic diffusion volumes for each component (41.8 for SO_2 and 19.7 for air). D_L is calculated by:[9]

$$D_L = \frac{k_B T}{6\pi\eta R_A} \tag{E.6}$$

Here, k_B is Boltzmann's constant, η is the viscosity of the solvent, and R_A is the radius of the solute. The latter is assumed to equal half the collision diameter of the solute in the gas phase. The effect of temperature on the collision diameter is small (for nitrogen, argon, oxygen, and air);[10] the value at room temperature is therefore used. The viscosity is estimated from the data provided by Sautermeister and Priest,[11] who measured dynamic viscosities for a base oil at different temperatures. A linear fit of $\ln(\eta)$ versus $1/T$ was used to describe the temperature variation of the viscosity. It is assumed that pressure has a negligible effect on the diffusion coefficient in a liquid.

The combined Henry's constant for the lube oil emulsion, as described in Chapter 5 and in the previous section, is calculated as:

$$H_L = \frac{1}{\frac{1}{H_{oil}}\left(\frac{V_{oil}}{V_L}\right) + \frac{1}{H_{water}}\left(\frac{V_{water}}{V_L}\right)} \tag{E.7}$$

To evaluate the controlling resistance of the transfer of SO_2 from the gas phase to the liquid phase, two different temperatures are considered at a total pressure of 90 bar, 25 and 131 ^{o}C, respectively. The parameters are presented in Table E.3 and Henry's constants of lube oil and water at 25 and 131 ^{o}C are shown in Table E.2.

Table E.3. Input parameters used in the evaluation of resistance of SO_2 from the gas phase to the liquid phase.

Parameter	Value	Reference
δ_G	$1\cdot10^{-3}$ m	12
δ_L	$1\cdot10^{-4}$ m	12
R	$8.314\cdot10^{-5}$ m^3 bar K^{-1} mol^{-1}	-
M_{SO_2}	64.1 g mol^{-1}	Calculated
M_{air}	29.0 g mol^{-1}	Calculated
$M_{SO_2,air}$	39.9 g mol^{-1}	Calculated
$(\sum_v)_{SO_2}$	41.8	8
$(\sum_v)_{air}$	19.7	8
P	90 bar	Exp. value
k_B	$1.38\cdot10^{-23}$ m^2 kg s^{-2} K^{-1}	-
R_A	$1.8\cdot10^{-10}$ m	13
$\left(\frac{V_{oil}}{V_L}\right)$	0.9373	Exp. Value
$\left(\frac{V_{water}}{V_L}\right)$	0.0627	Exp. Value
T_1	25 ^{o}C	-
T_2	131 ^{o}C	-
$\eta@T_1$	0.197 kg m^{-1} s^{-1}	11
$\eta@T_2$	0.006 kg m^{-1} s^{-1}	11

The result of inserting the parameters, presented in Table E.2 and Table E.3, into the above equations is presented in Table E.4.

Table E.4. The calculated coefficients and constants from the equations given above: diffusion coefficients, Henry's constants, and mass transfer coefficients.

Parameter	Temperature	Calculated Value
D_G	T_1	$1.41 \cdot 10^{-7}$ m^2 s^{-1}
D_G	T_2	$2.40 \cdot 10^{-7}$ m^2 s^{-1}
D_L	T_1	$6.17 \cdot 10^{-12}$ m^2 s^{-1}
D_L	T_2	$2.55 \cdot 10^{-10}$ m^2 s^{-1}
H_L	T_1	$3.48 \cdot 10^{-3}$ bar m^3 mol^{-1}
H_L	T_2	$4.80 \cdot 10^{-2}$ bar m^3 mol^{-1}
k_G	T_1	$5.70 \cdot 10^{-3}$ mol m^{-2} s^{-1} bar^{-1}
k_G	T_2	$7.16 \cdot 10^{-3}$ mol m^{-2} s^{-1} bar^{-1}
k_L	T_1	$6.17 \cdot 10^{-8}$ m s^{-1}
k_L	T_2	$2.55 \cdot 10^{-6}$ m s^{-1}
k_L/H_L	T_1	$1.77 \cdot 10^{-5}$ mol m^{-2} s^{-1} bar^{-1}
k_L/H_L	T_2	$5.30 \cdot 10^{-5}$ mol m^{-2} s^{-1} bar^{-1}
K_G	T_1	$1.77 \cdot 10^{-5}$ mol m^{-2} s^{-1} bar^{-1}
K_G	T_2	$5.26 \cdot 10^{-5}$ mol m^{-2} s^{-1} bar^{-1}

The calculated values in Table E.4 reveal that $K_G \approx k_L/H_L$, viz, mass transfer is controlled by mass transfer on the liquid side. Calculating the resistances (inverse values) give that the mass transfer of SO_2 is 99.7% in the liquid phase at 25 ^{o}C and 99.3% at 131 ^{o}C. For the modeling in Chapter 5, it is therefore valid to assume that $K_G = k_L/H_L$.

E.11 Difference between stagnant and stirred batch reactor on $K_G a$

The scope of this section is to calculate the difference between a stagnant liquid film where mass transfer happens by surface diffusion and a stirred liquid volume where diffusion happens by surface convection.[14] The calculated product $k_L a$ based on Eqs. (5.17) and (5.18) in Chapter 5 is for a stagnant case. According to Meille et al., the stirring rate has a significant effect on $k_L a$ in a batch reactor setting.[15] They report $k_L a$ values as a function of stirring rate for four different batch reactor dimensions. The first step is to calculate $k_L a$ based on Eqs. (5.17) and (5.18) in Chapter 5, followed by comparing this value with the experimentally determined value from Meille et al. First, k_L is calculated by the procedure presented in the above section based on the conditions prevailing for reactor configuration 3 in the work of Meille et al., where the liquid was methanol and the gas phase was hydrogen.[15] The temperature applied was 35 ^{o}C. The viscosity of methanol at this temperature is equal to 0.000474 kg m^{-1} s^{-1}.[16] R_A is found to $1.45 \cdot 10^{-10}$ m which is half the collision diameter in the gas phase for hydrogen.[17] The specific gas-liquid interfacial area is calculated to 50.7 m^2 m^{-3} and $k_L a$ is then calculated to $1.66 \cdot 10^{-3}$ m s^{-1}. The stirring rate applied in the batch reactor of this work was 600 rpm. At this stirring rate, a $k_L a$ of 0.1 s^{-1} was measured in the work of Meille et al. (reactor 3 without baffles).[15] A factor of 60 is therefore found between the calculated, stagnant case and the measured,

stirred case for the conditions of Meille et al.

However, a fundamental difference is found between the present work and the work by Meille et al., viz, the liquid to reactor volume ratio. In the work of Meille et al,. liquid volumes in the range 35-50% were used, and the stirrer was submerged into the liquid leading to mass transfer happening through surface convection.[14] In the present work, the liquid volume was around 2% and the stirrer was not submerged completely into the lube oil, as illustrated in Figure 5.1 in Chapter 5. Here, the liquid surface break up and the gas entrains the liquid, called surface entrainment.[14] Because stirrer speed has a strong effect on $k_L a$, an extra factor of 2 is assumed between mass transfer achieved by surface convection and surface entrainment. This is also the factor between using baffles or not in the reactor configuration in the work of Meille et al.[15] It is thereby assumed that the effect of surface entrainment compared to surface convection corresponds to using baffles or not. Thereby, the calculated $k_L a$ determined by Eqs. (5.17) and (5.18) in Chapter 5 has to be multiplied by a factor of 120 to account for the actual stirring prevailing during the experiment.

So far, the liquid film enhancement factor, E, has taken the value 1. This factor is multiplied on $k_L a$ and describes the enhancement of absorption of SO_2 when the reaction occurs within the liquid film. By evaluating the Hatta modulus using the estimated k_L for a stirred case (assuming $k_L a$ is increased by a factor 120 compared to the stagnant case), it is found that $E \approx 1$ and reaction is therefore occurring in the bulk liquid and not in the liquid film.[18]

E.12 Arrhenius plot for a factor of 600 of $K_G a$ between a stagnant and a stirred batch reactor

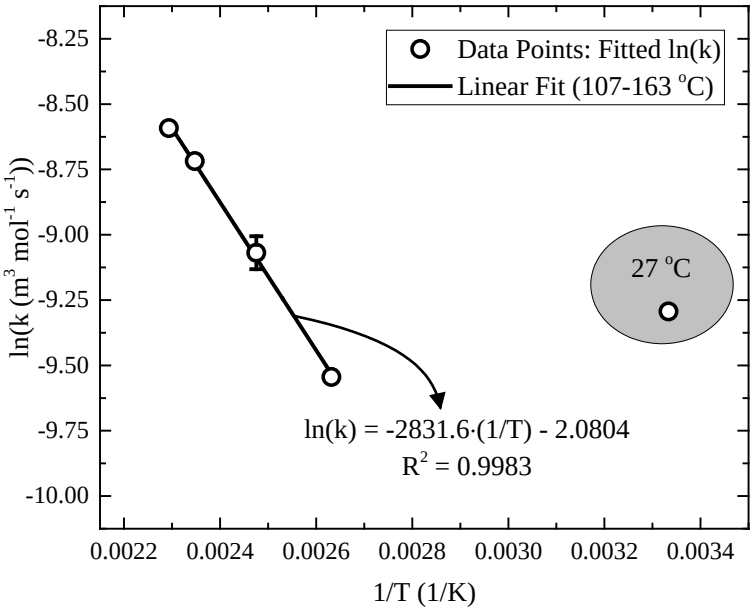

Figure E.9. Arrhenius plot of the determined reaction rate constants at temperatures in the range from 107 °C to 163 °C for using 600 times the calculated $K_G a$ at stagnant conditions. The linear fit, corresponding equation, and R^2 value are also shown. The error bars represent lower and upper $\ln(k)$ determined from two similar experiments and the data point is the average value. From the trendline, the activation energy is determined to 23.5 kJ mol^{-1} and the pre-exponential factor to $1.25 \cdot 10^{-1}$ m^3 mol^{-1} s^{-1}. The 27 °C data point is excluded from the linear fit.

E.13 Concentration profiles for 131 °C simulation using a factor of 120 of $K_G a$ between a stagnant and a stirred batch reactor

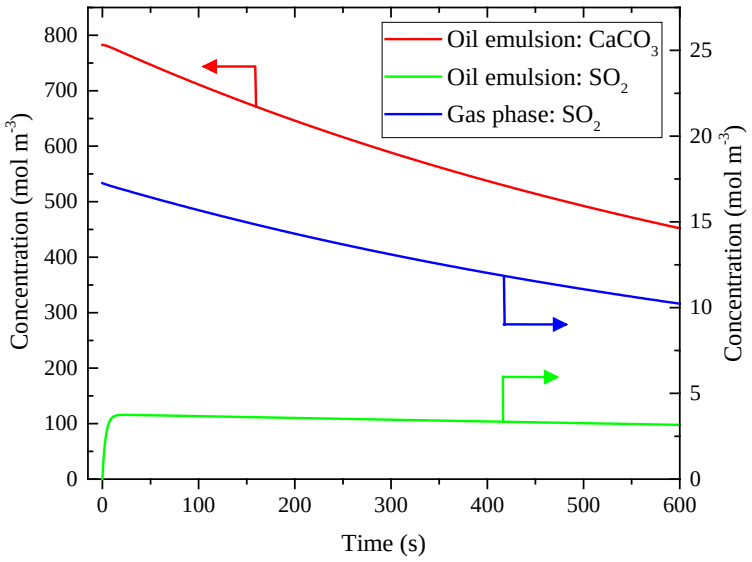

Figure E.10. Simulation results for a temperature of 131 °C showing the concentration profiles of the SO_2 in the gas phase, SO_2 in the lube oil emulsion, and $CaCO_3$ in the lube oil emulsion by fitting the reaction rate constant to achieve 42.2% conversion of $CaCO_3$ after 10 min. The following parameters were used for the simulations: T=131 °C, P_{total}=90 bar, $C^G_{SO_2,0}$=17.26 mol m^{-3}, 6.6 wt.% water, and Ca/S = 0.96.

E.14 Competition between SO_2-$CaCO_3$ and H_2SO_4-$CaCO_3$ reactions

To extend the reaction mechanism for the batch reactor model to include the H_2SO_4-$CaCO_3$ reaction, the following change to the $CaCO_3$ balance was implemented:

$$\frac{dC^L_{CaCO_3}}{dt} = -k_1 C^L_{CaCO_3} C^L_{SO_2} - k_2 C^L_{CaCO_3} C^L_{H_2SO_4} \tag{E.8}$$

The consumption of H_2SO_4 is formulated as:

$$\frac{dC^L_{H_2SO_4}}{dt} = -k_2 C^L_{CaCO_3} C^L_{H_2SO_4} \tag{E.9}$$

This assumes that the following two reactions are competing:

$$CaCO_3 + SO_2 \xrightarrow{k_1} CaSO_3 + CO_2 \tag{E.10}$$

$$CaCO_3 + H_2SO_4 \xrightarrow{k_2} CaSO_4 + CO_2 + H_2O \tag{E.11}$$

The temperature dependent reaction rate constant for the H_2SO_4–$CaCO_3$ reaction is taken from Lejre et al.,[4] by using that the concentration of the H_2SO_4 droplets is $18.1 \cdot 10^{-3}$ mol m^{-3} and that the average radius of the H_2SO_4 droplets is 0.5 µm, which is a typical value in emulsions.[19] There is a fundamental difference between how SO_2 and H_2SO_4 reach the bulk lube oil film. For the modeling, it was found that equilibrium occurred instantaneously between the SO_2 in the gas phase and lube oil emulsion film. This kept the SO_2 concentration in the lube oil constant (due to abundant excess of SO_2, on a molar basis, in the gas phase compared to the $CaCO_3$ in the lube oil) throughout the investigated residence time of 10 min. Considering H_2SO_4, it is believed that H_2SO_4 condenses during each expansion stroke on top of the lube oil film and is then mixed into emulsion during the compression stroke where it has the possibility of reacting with $CaCO_3$. This means that H_2SO_4 is gradually entering the lube oil emulsion during the residence time of the lube oil film. This is important to consider because the relative importance between the SO_2-$CaCO_3$ and H_2SO_4-$CaCO_3$ reactions is described by the fraction between their associated reaction rate expressions: $k_2 C^L_{CaCO_3} C^L_{H_2SO_4} / k_1 C^L_{CaCO_3} C^L_{SO_2}$. The relative significance of the competing reactions is then also determined by the initial concentrations present in the lube oil emulsion. When a large fraction of H_2SO_4 condenses, the fraction increases. Assuming that the initial concentration of H_2SO_4 is equal to the initial concentration of $CaCO_3$ divided by 600 (stoichiometric molar amount between H_2SO_4 and $CaCO_3$ over 10 minutes and all the H_2SO_4 is therefore introduced over 600 combustion cycles). For subvolume 1 conditions and having one second in residence time yielded that the conversion of $CaCO_3$ was in total 0.23% and the conversion of H_2SO_4 was 87.1%. This means that 63% of the $CaCO_3$ was converted from H_2SO_4, and the rest was from SO_2. However, when the initial concentration of H_2SO_4 gets larger, more $CaCO_3$ is consumed (percentage) by H_2SO_4 and the same is valid for increasing temperature and decreasing partial pressure of SO_2 in the gas phase.

References

(1) NIST Chemistry WebBook: https://webbook.nist.gov/chemistry.

(2) Costa, D. L.; Underhill, D. Solubility and Reactivity of Sulfur Dioxide in Various Oils. *Am. Ind. Hyg. Assoc. J.* **1976**, *37* (1), 46–51.

(3) Nagaki, H.; Korematsu, K. Effect of Sulfur Dioxide in Recirculated Exhaust Gas on Wear within Diesel Engines - (Relationship between Wear and Amount of SO_2 Absorbed by Lubricating Oil Film). *JSME Int. J. Ser. B-Fluids Therm. Eng.* **1995**, *38* (3), 465–474.

(4) Lejre, K. H.; Glarborg, P.; Christensen, H.; Mayer, S.; Kiil, S. Mixed Flow Reactor Experiments and Modeling of Sulfuric Acid Neutralization in Lube Oil for Large Two-Stroke Diesel Engines. *Ind. Eng. Chem. Res.* **2019**, *58* (1), 138–155.

(5) The Engineering ToolBox. Lubricating oil density versus temperature https://www.engineeringtoolbox.com/temperature-density-petroleum-lubricating-oil-lubricant-volume-correction-ASTM-D1250-d_1943.html (accessed Jun 25, 2018).

(6) The Engineering ToolBox. Water density calculator https://www.engineeringtoolbox.com/water-density-specific-weight-d_595.html (accessed Jun 25, 2018).

(7) Smith, P. G. *Introduction to Food Process Engineering*; Food Science Text Series; Springer US: Boston, MA, 2011.

(8) Poling, B. E.; Prausnitz, J. M.; O'Connell, J. P. *The Properties of Gases and Liquids*, 5th ed.; McGraw-Hill: New York, 2001.

(9) Laidler, K. J. *Chemical Kinetics*; Harper & Row: New York, 1987.

(10) Glassman, I.; Harris, B. L. Collision Diameters of Some Gases as a Function of Temperature. *J. Phys.*

Chem. **1952**, *56* (6), 797–799.
(11) Sautermeister, F. A.; Priest, M. Physical and Chemical Impact of Sulphuric Acid on Cylinder Lubrication for Large 2-Stroke Marine Diesel Engines. *Tribol. Lett.* **2012**, *47* (2), 261–271.
(12) Cussler, E. L. *Diffusion: Mass Transfer in Fluid Systems*; Cambridge University Press: New York, 2009.
(13) de Groot, P. A. *Handbook of Stable Isotope Analytical Techniques: Volume 1*, 1st ed.; Elsevier: Amsterdam, The Netherlands, 2004.
(14) Lee, J. H.; Foster, N. R. Measurement of Gas-Liquid Mass Transfer in Multi-Phase Reactors. *Appl. Catal.* **1990**, *63* (1), 1–36.
(15) Meille, V.; Pestre, N.; Fongarland, P.; de Bellefon, C. Gas/Liquid Mass Transfer in Small Laboratory Batch Reactors: Comparison of Methods. *Ind. Eng. Chem. Res.* **2004**, *43* (4), 924–927.
(16) Mikhail, S. Z.; Kimel, W. R. Densities and Viscosities of Methanol-Water Mixtures. *J. Chem. Eng. Data* **1961**, *6* (4), 533–537.
(17) Ismail, A. F.; Chandra Khulbe, K.; Matsuura, T. *Gas Separation Membranes: Polymeric and Inorganic*, 1st ed.; Springer International Publishing: Cham, Switzerland, 2015.
(18) Levenspiel, O. *The Chemical Reactor Omnibook*; OSU Book Stores, Inc.: Oregon, 1989.
(19) Goodwin, J. W. *Colloids and Interfaces with Surfactants and Polymers*; John Wiley & Sons, Ltd: Chichester, UK, 2009.